Actividad eléctrica cortical de alta frecuencia. Modulación por ritmos endógenos y sistema dopaminérgico

Tesis de Doctorado en Ciencias Biológicas

Opción Neurociencias

Pedeciba Biología

UdelaR.

Matías Cavelli

2019

Orientador: Dr. Pablo Torterolo Minetti (FMed)

Co-orientador: Dra. Giselle Prunell (IIBCE)

Laboratorio de Neurobiología del Sueño, Departamento de Fisiología, Facultad de Medicina, UdelaR.

Resumen

La actividad electrográfica cortical está generada principalmente por las neuronas piramidales de la corteza cerebral y regulada por otras neuronas corticales y subcorticales. Estas poblaciones interactúan de forma dinámica (secuencial y/o sincrónica) generando los diversos ritmos electro-corticales. Estos patrones varían según el estado comportamental y las distintas funciones cognitivas.

La actividad cortical se puede estudiar con distintas técnicas electrofisiológicas, como el registro de unidades, los potenciales de campo local (LFP), el electrocorticográma (ECoG), el magnetoencefalográma (MEG) o el electroencefalográma (EEG). Durante el posgrado (Maestría y Doctorado) me he dedicado a investigar cuáles son estos patrones de actividad cortical, cómo varían durante la vigilia, el sueño y durante la manipulación de los distintos sistemas que regulan el ciclo sueño-vigilia (sistemas activadores y somnogénicos).

En nuestro laboratorio nos hemos especializado en el análisis de la actividad del ECoG de alta frecuencia, actividad gamma (> 30 Hz), dado que estos patrones oscilatorios se encuentran fuertemente vinculados a la vigilia, las funciones cognitivas; entre ellas, la percepción. En este sentido y trabajando en diversos modelos animales (gato, rata, ratón) y humanos, encontramos que la actividad gamma es máxima durante la vigilia y que esta se pierde progresivamente durante las diferentes etapas del sueño lento. Por otra parte, cuando ingresamos al sueño REM (etapa donde ocurren preferentemente los ensueños o actividad onírica), la actividad gamma local aumenta mientras que la comunicación entre áreas alejadas del cerebro a esta frecuencia (coherencia gamma) cae hasta sus valores mínimos. Estos resultados fueron replicados en varios órdenes de mamíferos, lo que nos llevó a postular que este fenómeno se encuentra conservado en la evolución.

También encontramos que la coherencia de las bandas de alta frecuencia puede ser modulada por otros ritmos del cerebro, como la actividad theta (5-10 Hz) de la red hipocámpica (red vinculada a la formación de nuevas memorias) o los potenciales respiratorios generados por el pasaje de aire por las fosas nasales. Postulamos que dichas modulaciones son parte de procesos de comunicación neuronal de acople entre frecuencias, que se presentan fuertemente dependientes del estado comportamental de los individuos, y que podrían estar en la base del proceso de integración de la información neural distribuida.

Por último, nos encontramos indagando sobre que rol cumplen los sistemas de neuromodulación sobre la generación, mantenimiento y modulación de la actividad de alta frecuencia. Particularmente el sistema el

dopaminérgico. En este sentido mostramos como la lesión dopaminérgica de la Sustancia Nigra pars compacta (modelo animal de enfermedad de Parkinson) es capaz de disminuir la potencia y coherencia gamma a nivel de la neocorteza y el bulbo olfatorio. Por otra parte, observamos que la lesión dopaminérgica con 6-hidroxidopamina genera importantes alteraciones en el acople respiratorio de la actividad gamma cortical.

Tanto el sueño natural como las manipulaciones experimentales de los sistemas activadores o sus alteraciones durante diversas patologías han mostrado cursar con múltiples alteraciones en la capacidad de generar, modular y mantener la actividad gamma cortical. Por esto pensamos que varias alteraciones cognitivas y motoras que se observan en diversos trastornos psiquiátricos o neurológicos (por ejemplo, psicosis o Parkinson), podrían tener como base la imposibilidad de sincronizar y acoplar normalmente la actividad cerebral de alta frecuencia durante la vigilia.

Estrategia de investigación y organización de la Tesis

En nuestro laboratorio nos hemos especializado en el análisis de la actividad electro-cortical de alta frecuencia (actividad gamma > 30 Hz), dado que estos patrones oscilatorios se encuentran fuertemente vinculados a la vigilia y las funciones cognitivas. Varias técnicas de registro electrofisiológico son capaces de registrar la actividad eléctrica de poblaciones de neuronas en el cerebro. En particular, en esta Tesis utilizamos el electrocorticograma (ECoG) como principal herramienta de registro. Esta técnica consiste en el registro de la actividad eléctrica mediante la colocación de macro o meso-electrodos directamente sobre la corteza o la duramadre. Las señales obtenidas del ECoG se utilizaron para clasificar el estado comportamental de los animales de experimentación (principalmente gato y rata). También se utilizaron para medir los niveles de sincronía neuronal registrados en cada estado comportamental, y durante diversos abordajes y manipulaciones farmacológicas. Diferentes variaciones del análisis espectral de potencias fueron utilizadas como índices de sincronización local (actividad poblacional cercana al electrodo de registro). Además, empleamos diferentes índices de sincronización espectral entre áreas del cerebro, principalmente variaciones de los denominados análisis de coherencia espectral y correlaciones cruzadas (relaciones espectrales entre pares de electrodos). Por último, implementamos una serie de herramientas analíticas que permiten medir los niveles de acoplamiento entre actividad electrográfica de distintas frecuencias. Todos estos indicadores de sincronía espectral fueron utilizados durante las diferentes etapas del ciclo sueño y vigilia, como durante diversas manipulaciones experimentales. Los resultados de estos análisis se muestran en los distintos **Capítulos** de esta Tesis.

Esta Tesis se organiza en cuatro **Capítulos.** Cada **Capítulo** presenta una breve introducción al problema de investigación junto a un resumen de los resultados obtenidos en cada trabajo (Artículos publicados o en revisión, en revistas arbitradas). En cada **Capítulo**, los trabajos como primer autor serán referidos como **Artículos** mientras que los trabajos como coautor serán tratados como **Anexos.** En la parte final de la Tesis se podrán encontrar las **Conclusiones Generales** y la **Bibliografía** utilizada.

Índice:

Abreviaturas

BO: bulbo olfatorio

CA: cataplejía

CFC: “cross frequency coupling” o acoplamiento entre frecuencias

ECoG: electrocorticográma

EEG: electroencefalograma

EP: enfermedad de Parkinson

GABA: “gamma aminobutiric acid” o acido gamma aminobutírico

HFO: “high frequency oscillaltion” u oscilaciones de alta frecuencia

Hz: Hertz

LFP: “local field potential” o potencial de campo local

MEG: magnetoencefalográma

M2: corteza motora secundaria

NMDA: n-metil d-aspartato

NPO: nucleo pontis oralis

NREM: sueño no REM

PAC: “phase amplitude coupling” o acoplamiento fase amplitud

Pf: corteza prefrontal

REM: “rapid eyes movements” o movimientos oculares rápidos

REMc: REM carbacol

SNpc: Sustancia Nigra pars compacta

V2: corteza visual secundaria

6-OHDA: 6-hidroxidopamina

1. Capítulo 1. Actividad gamma durante la vigilia y el sueño

1.1. El problema de la integración y el acople por sincronía

Se puede considerar al cerebro como redes neuronales altamente distribuidas, en el que las operaciones se ejecutan de forma secuencial y/o sincrónica, careciendo de un único centro de coordinación (Singer, 2007, 2004). Este órgano integra eventos neuronales que se producen en diferentes momentos y áreas cerebrales, en una experiencia unificada. El intento por comprender los mecanismos que se encargan de esta unificación se conoce como “the binding problem” o “el problema de la integración” y es considerado uno de los retos más importantes que la neurociencia cognitiva tiene para resolver (Von der Malsburg, 1995; Von der Malsburg and Schneider, 1986).

Uno de los mecanismos de integración sería la sincronización de la actividad neuronal distribuida, visualizado como enganche de fase sobre las oscilaciones generadas por las redes neurales (Singer, 2007, 1999). La primera evidencia experimental que apoya el papel integrador de la sincronía fue observada en grupos de neuronas espacialmente segregadas y registradas simultáneamente, que sincronizaban su actividad sólo cuando eran activadas por un estímulo visual particular. La frecuencia a la que periódicamente se sincronizaban estos pares de neuronas era de aproximadamente 40 Hz (Gray et al., 1989; Gray and Singer, 1989). Este mecanismo fue llamado en primera instancia “binding-by-synchrony” o “integración por sincronía” y modificaciones puntuales de esta idea basadas en nuevas evidencias fueron formuladas más recientemente como “comunication through coherence” o “comunicación mediante coherencia” (Fries, 2015, 2005; Womelsdorf et al., 2007). Por otra parte, formulaciones teóricas de este mecanismo de integración fueron propuestos con anterioridad por Milner (Milner, 1974), Grossberg (Grossberg, 1976) y Von der Malsburg (Von der Malsburg and Schneider, 1986).

1.2. Banda gamma (30-100 Hz) de frecuencia

Fenómenos de sincronización se aprecian en los potenciales de campo locales (“local field potential” o LFP por sus siglas en inglés), el electrocorticograma (ECoG), el electroencefalograma (EEG) y el magnetoencefalograma (MEG), dado que estos reflejan la actividad sincrónica de grupos neuronales registrados localmente. El EEG presenta una señal compleja en la cual se pueden distinguir diferentes componentes. Muchos de estos son característicos de la vigilia y el sueño, por lo que su presencia o ausencia se utiliza para clasificar el estado comportamental en el que se encuentran los individuos (Cavelli, 2015).

A las oscilaciones del EEG que se observan en el rango de frecuencia de 30 a 100 Hz se le denomina actividad u oscilaciones gamma (Uhlhaas et al., 2009). Jasper y Andrews (1938) utilizaron por primera vez el término ondas gamma para designar a las ondas entre los 35 a 45 Hz (Buzsáki and Wang, 2012; Jasper and Andrews, 1938), y los LFP corticales se registraron por primera vez en el bulbo olfatorio de erizos por Adrian en 1942 (Adrian, 1942; Rojas-Líbano and Kay, 2008). La actividad gamma se ha observado no sólo en animales, sino también en humanos (Bouyer et al., 1981; Llinás and Ribary, 1993; Maloney et al., 1997; Steriade et al., 1996; Tiitinen et al., 1993). La aplicación de las técnicas de EEG y MEG ha mostrado que un aumento de la actividad o potencia gamma aparece durante los estados comportamentales activos; también se la ha vinculado con una variedad de funciones cognitivas tales como la percepción de estímulos externos, la integración poli-sensorial, el movimiento y la coordinación sensorio-motora, la atención, el mantenimiento de contenidos en la memoria a corto plazo, la formación de memorias asociativas, así como en pensamientos e imágenes internamente generadas (Rieder et al., 2011; Rojas-Líbano and Kay, 2008; Singer, 2007, 2004; Uhlhaas et al., 2011, 2009; Womelsdorf et al., 2007). La génesis de estos ritmos se produciría a nivel cortical y estaría ligada a la inhibición peri-somática GABAérgica, las sinapsis eléctricas (Buhl et al., 2003; Buzsáki and Wang, 2012), potenciada por la formación reticulada (Garcia-rill, 2017; Garcia-Rill et al., 2014; Luster et al., 2016) y el circuito tálamo-cortical que tiende a resonar a esta frecuencia (Llinás and Ribary, 2006).

1.3. Coherencia gamma en el EEG

La coherencia entre dos ondas es una medida de su similitud en contenido de frecuencias. Dos ondas son coherentes a determinada frecuencia cuando tienen una relación de fase constante a esa frecuencia y la relación entre las amplitudes a esa frecuencia también se mantiene constante. Se cree que el grado de coherencia gamma del EEG entre dos regiones corticales refleja la fuerza de las interconexiones funcionales (re-entradas) que se producen entre ellas (Bullock et al., 2003; Edelman and Tononi, 2000). Por otra parte, la sincronización gamma entre áreas alejadas de la corteza presenta desfasajes cercanos a cero, que pueden ser menores que las latencias de propagación de estímulos entre dichas áreas, lo que supone que las oscilaciones sincrónicas son una propiedad de las redes distribuidas que se autoorganizan (Buzsáki, 2006; Buzsáki and Wang, 2012; Singer, 2015; Wang, 2010). La actividad coherente del EEG en la banda gamma de frecuencias también aumenta durante diferentes comportamientos y diferentes funciones cognitivas tanto en animales como en seres humanos (Bouyer et al., 1981; Bressler et al., 1993; Härle et al., 2004).

A su vez, la coherencia gamma entre diferentes áreas del cerebro ha sido vista como un correlato neural de la consciencia (Joliot et al., 1994; Llinás et al., 1998) y es un factor crítico en la percepción de estímulos (Melloni et al., 2007; Rodriguez et al., 1999; Varela et al., 2001). En este sentido, la coherencia en la banda gamma de frecuencia se pierde durante la narcosis (inconsciencia) inducida por los anestésicos generales como los barbitúricos, isoflurano, etc., (John, 2002; Mashour, 2006). Esta también se altera seriamente durante varios trastornos psiquiátricos que afectan la cognición como la esquizofrenia (Uhlhaas et al., 2006; Uhlhaas and Singer, 2010, 2006). Por otra parte, el uso de antagonistas NMDA, producen importantes cambios en la actividad gamma del EEG (Lazarewicz et al., 2010; Pal et al., 2015), y por sus efectos conductuales, es considerado un modelo farmacológico válido para el estudio de las bases neurobiológicas de las enfermedades del espectro psicótico (Javitt and Zukin, 1991; Moghaddam and Jackson, 2003; Rung et al., 2005).

1.4. El sueño REM y ensoñaciones: un modelo natural de psicosis

La actividad cognitiva no sólo ocurre durante la vigilia, sino también durante el sueño REM, durante el cual se producen lo que llamamos ensueños o actividad onírica. A estos se les considera un tipo especial de actividad cognitiva o proto-conciencia (Hobson, 2009). Los ensueños se caracterizan por su riqueza y claridad sensorial, discontinuidades e incongruencias en el tiempo, en el espacio y en los personajes. También existe una distorsión de la realidad, se violan las leyes físicas y esto se acepta pasivamente. En estos hay una pérdida del control voluntario (el individuo no sabe lo que va a pasar a continuación, la atención es inestable y está dirigida en forma rígida), existe la falta de consciencia de estar soñando y la memoria de dichos eventos se vuelve lábil (Hobson, 2009; Nir and Tononi, 2010; Rechtschaffen, 1978).

Existen similitudes cualitativas y cuantitativas entre algunas de las características del sueño REM y el estado mental de la psicosis (Gottesmann, 2006; Gottesmann and Gottesman, 2007; Scarone et al., 2008). Actualmente, el sueño REM es considerado como un modelo natural de psicosis (Benson and Zarcone, 1985; Hobson, 1997; Scarone et al., 2008). Las alucinaciones de las enfermedades dentro del espectro psicótico tienen características similares a las experiencias oníricas del sueño REM. A su vez, en ambas condiciones disminuye la actividad de la corteza prefrontal junto a importantes cambios en la actividad de la vía dopaminérgica mesolímbica (Braun et al., 1997; Corsi-Cabrera et al., 2003; Gottesmann, 2006; Gottesmann and Gottesman, 2007). En contraste, durante el sueño de ondas lentas o sueño no-REM (NREM) profundo, hay ausencia o fuerte reducción en las funciones cognitivas (Hobson, 2009; Nir and Tononi, 2010).

1.5. Coherencia y potencia gamma durante la vigilia, el sueño y los estados alterados de conciencia

Durante los últimos años nos hemos centrado en el estudio de la actividad gamma durante la vigilia y el sueño, así como también durante los estados alterados de consciencia que pueden ser generados por maniobras experimentales o la administración de sustancias que alteran los sistemas normales de control del ciclo sueño-vigilia. En este sentido y partiendo del trabajo pionero de Santiago Castro-Zaballa (Castro-Zaballa et al., 2013), nos dedicamos a investigar que sucede con la actividad gamma durante los ciclos normales de sueño y vigilia .

Utilizando el análisis de coherencia como medida de sincronización entre áreas alejadas del cerebro, mostramos que, en gatos, la coherencia gamma es máxima durante la vigilia activa y que la misma cae progresivamente hasta llegar al sueño profundo para luego caer a sus mínimos valores durante el sueño REM (ver **Anexo 1** (Castro-Zaballa et al., 2014)). En estos trabajos, también observamos que aunque la coherencia gamma se perdía durante sueño REM, se podía observar un aumento la potencia gamma (índice de sincronización local) en alguno de los electrodos de registro (Castro-Zaballa et al., 2013; Maloney et al., 1997).

Basados en estos resultados iniciales, publicamos el **Artículo 1** (Cavelli et al., 2015) donde, utilizando a la rata como modelo animal, analizamos la potencia y la coherencia gamma durante la vigilia y el sueño, así como sus dinámicas durante los estados transicionales. Observamos que, al igual que lo previamente observado en gato, la actividad gamma es máxima durante la vigilia, cae progresivamente durante el sueño, pero interesantemente al ingresar al sueño REM esta caída de coherencia se da frente a un claro aumento de potencia gamma en todas las áreas registradas.

ARTICULO 1

(Cavelli et al., 2015)

Behavioural Brain Research 281 (2015) 318–325

Contents lists available at ScienceDirect

Behavioural Brain Research

journal homepage: www.elsevier.com/locate/bbr

Research report

Coherent neocortical gamma oscillations decrease during REM sleep in the rat

Matías Cavelli[a], Santiago Castro[a], Natalia Schwarzkopf[a], Michael H. Chase[b,c], Atilio Falconi[a], Pablo Torterolo[a,*]

[a] Laboratorio de Neurobiología del Sueño, Departamento de Fisiología, Facultad de Medicina, Universidad de la República, General Flores 2125, 11800 Montevideo, Uruguay
[b] WebSciences International, 1251 Westwood Blvd., Los Angeles, CA 90024, USA
[c] UCLA School of Medicine, Los Angeles, CA 90095, USA

HIGHLIGHTS

- The electroencephalogram of adult rats was recorded during sleep and wakefulness.
- The intra and inter-hemispheric coherence of the EEG gamma band was analyzed.
- The coherence was larger in W and almost absent during REM sleep.

ARTICLE INFO

Article history:
Received 8 October 2014
Received in revised form
19 December 2014
Accepted 23 December 2014
Available online 31 December 2014

Keywords:
Cortex
Consciousness
EEG
Synchronization
Coherence

ABSTRACT

Higher cognitive functions require the integration and coordination of large populations of neurons in cortical and subcortical regions. Oscillations in the high frequency band (30–100 Hz) of the electroencephalogram (EEG), that have been postulated to be a product of this interaction, are involved in the binding of spatially separated but temporally correlated neural events, which results in a unified perceptual experience. The extent of this functional connectivity can be examined by means of the mathematical algorithm called "coherence", which is correlated with the "strength" of functional interactions between cortical areas. As a continuation of previous studies in the cat [6,7], the present study was conducted to analyze EEG coherence in the gamma band of the rat during wakefulness (W), non-REM (NREM) sleep and REM sleep.

Rats were implanted with electrodes in different cortical areas to record EEG activity, and the magnitude squared coherence values within the gamma frequency band of EEG (30–48 and 52–100 Hz) were determined.

Coherence between all cortical regions in the low and high gamma frequency bands was greater during W compared with sleep. Remarkably, EEG coherence in the low and high gamma bands was smallest during REM sleep.

We conclude that high frequency interactions between cortical areas are radically different during sleep and wakefulness in the rat. Since this feature is conserved in other mammals, including humans, we suggest that the uncoupling of gamma frequency activity during REM sleep is a defining trait of REM sleep in mammals.

1. Introduction

Electroencephalographic (EEG) oscillations in the gamma frequency (30–100 Hz) band are involved in the integration or binding of spatially separated but temporally correlated neural events [1–3]. An increase in gamma power typically appears during states/behaviors that are characterized by the active cognitive processing of external percepts or internally generated thoughts and images in humans and during alert wakefulness in animals [4–7].

The degree of EEG coherence between two cortical regions is correlated with the strength of the functional interconnections

* Corresponding author. Tel.: +598 2924 34 14x3234.
E-mail address: ptortero@fmed.edu.uy (P. Torterolo).

http://dx.doi.org/10.1016/j.bbr.2014.12.050
0166-4328/

that occur between them [1,2,8,9]. Recently, Siegel et al. (2012) have proposed that frequency-specific correlated oscillations in distributed cortical networks provide indices, or 'fingerprints', of the network interactions that underlie cognitive processes [10].

Gamma coherence between different brain areas, which is greatest during wakefulness (W) has been viewed as a possible neural correlate of consciousness [11]. In effect, coherence in the gamma frequency band decreases during narcosis (unconsciousness) induced by anesthesia [12,13].

During deep non-REM (NREM) sleep there is an absence, or at least a strong reduction in cognitive functions. In contrast, dreams that occur more prominently during rapid eye movement (REM) sleep, are considered a special kind of cognitive activity or protoconsciousness [14]. Recently, we demonstrated in the cat that there is high level of neocortical intra and interhemispheric gamma coherence during alert wakefulness, it decreases during quiet W and NREM sleep, and is almost absent during REM sleep [6,7].

In the present report, we evaluated the extent of EEG 30–100 Hz coherence between intra and interhemispheric neocortical activity during naturally occurring sleep and W in the rat.

2. Materials and methods

2.1. Experimental animals

Twelve adult male Wistar rats (300–350 g) were used in this study. The animals were determined to be in good health by the Institutional Animal Care Facility. All of the animals were maintained on a 12:12-h light-dark cycle under controlled temperature (21–24 °C) conditions with free access to food and water. All of the experimental procedures were conducted in accord with the *Guide for the Care and Use of Laboratory Animals* (8th edition, National Academy Press, Washington, DC, 2010) and approved by the Institutional Animal Care Commission (protocol No. 071140-001931-12, Facultad de Medicina, Universidad de la República). Adequate measures were taken to minimize pain, discomfort or stress of the animals. In addition, all efforts were made in order to use the minimal number of animals necessary to produce reliable scientific data.

2.2. Surgical procedures

The surgical procedures employed were similar to those in our previous studies [15,16]. The animals were chronically implanted with electrodes to monitor the states of sleep and W. Anesthesia was induced with a mixture of ketamine-xylazine (90 mg/kg; 5 mg/kg i.p. respectively). The animal's head was positioned in a stereotaxic frame and the skull was exposed. In order to record the EEG, stainless steel screw electrodes were placed in the calvarium, overlying the parietal and occipital cortices and the cerebellum (Fig. 1). Bipolar electrodes were inserted into the neck muscle in order to record the electromyogram (EMG). The electrodes were connected to a plug that was bonded to the skull with acrylic cement.

At the end of the surgical procedures, an analgesic was administered. Incision margins were kept clean and a topical antibiotic was administered on a daily basis. After the animals had recovered from the preceding surgical procedures, they were adapted to the recording environment for a period of at least one week.

2.3. Experimental sessions

Experimental sessions of 6 h in duration were conducted during the light period, between 12 A.M. and 6 P.M, in a temperature controlled (21–24 °C) and sound attenuated chamber. All animals had free access to water and food. During these sessions (as well as during the adaptation sessions), the animals were able to move freely within the confines of the recording-chamber.

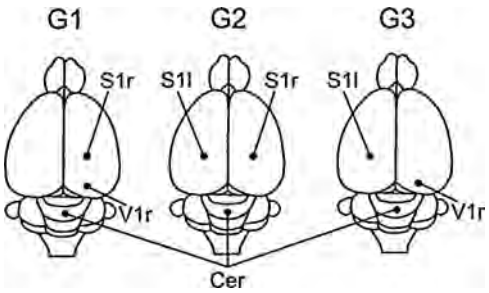

Fig. 1. Position of recording electrodes. The figure presents a summary of the position of the recording electrodes on the surface of the primary somatosensory and primary visual cortices (according to Ref. [31]). The electrodes were referred to a common electrode that was located over the cerebellum (Cer). G1–G3, are groups of animals with different electrode locations (four animals per group). S1, somatosensory primary cortex; V1, visual primary cortex; r, right; l, left.

EEG and EMG of each rat were recorded daily for a period of approximately 2 weeks in order to obtain a complete data set. The activity of two cortical areas was recorded simultaneously with monopolar electrodes. A common electrode reference montage was placed on the cerebellar surface; this montage is critical for the analysis of coherence [17–21]. For each pair of recordings, data were obtained during four recording sessions, and for every combination of electrodes, in three groups (G1–G3) of 4 rats (Fig. 1).

Bioelectric signals were amplified (×1000), filtered (0.1–200 Hz), sampled (512 Hz, 16 bits) and stored in a PC using Spike 2 software (Cambridge Electronic Design). Data were obtained during spontaneously occurring W, NREM and REM sleep. The presence of low voltage fast waves in the parietal cortex, a mixed theta rhythm (4–7 Hz) in the occipital cortex and relatively high electromyographic activity were used to identify W. Light and deep NREM sleep were determined, but only epochs of established periods of deep NREM sleep were utilized for coherence analysis. Deep NREM sleep was identified by the presence of continuous high amplitude slow (0.5–4 Hz) frontal and occipital waves and sleep spindles (9–15 Hz) combined with a reduced EMG activity. REM sleep was identified by the occurrence of low voltage fast parietal waves, a regular theta rhythm in the occipital cortex, and the absence of EMG activity except for occasional muscular twitches [15].

2.4. Data analysis

Sleep and waking states were determined in epochs of 10 s [15]. In order to obtain power spectral and coherence values between a pair of EEG channels, we used procedures that we have previously employed [6,7]. Artifacts were detected in the raw recording and in the spectrogram (with a 0.5 s resolution); artifacts produced a general increase in power and were usually associated with movements. Twelve independent artifact-free periods of 100 s were selected and examined during each behavioral state (1200 s for each behavioral state per rat).

For each 100 s period, the Magnitude Squared Coherence was determined as follows: $coh_{ab}(f) = [\sum csd_{ab}(f)]^2 / [\sum psd_a(f) \sum psd_b(f)]$, where psd is the power spectral density and a and b are the waves that are analyzed. csd is the cross spectra density, or the Fourier transform of the cross covariance function, which provides a statement of how common activity between two processes is distributed across frequencies. Coherence between two waveforms is a function of frequency and ranges from 0 for totally incoherent waveforms to 1 for maximal coherence. In order for two waveforms to be completely coherent at a particular frequency over a

given time range, the phase shift between the waveforms must be constant and the amplitudes of the waves must have a constant ratio.

We obtained power spectrum and the magnitude squared coherence using the Spike 2 script COHER 1S (Cambridge Electronic Design). By employing this method, we were able to analyze the coherence between two EEG channels that were recorded simultaneously during 100 s periods. This analysis period was divided into 100 time-blocks with a sampling rate of 512 Hz, a bin size of 1024 samples (512 for each channel) and a resolution of 0.5 Hz. Analyses of serial, non-overlapping, 10 s epochs were also used to determine the temporal dynamic of the coherence (Figs. 5 and 6).

We concentrated on examining the coherence of the EEG in the gamma frequency band (30–48 and 52–100 Hz); low and high gamma bands were also analyzed in our previous studies in cats, where they exhibited differences in relation to attentive behaviors [6,7]. Fifty Hz electrical noise was also avoided with this partition. In order to eliminate the possibility that gamma activity and coherence were produced by extra-cerebral potentials, we performed the same procedures and analysis than in our previous studies (see [6,7] for details).

In order to normalize the data and evaluate them by means of parametric statistical tests, we applied the Fisher z′ transform to the gamma coherence values. The z′-coherence of the gamma band for each pair of EEG channels was averaged across behavioral states. z′-Coherence was expressed as the mean ± standard error. The significance of the differences among behavioral states, cortical sites and interactions were evaluated with two-ways ANOVA and Tukey tests. The z′-coherence across behavioral states for the intra or interhemispheric combination of electrodes was also evaluated by one-way ANOVA and Tamhane tests. The gamma power for the different cortices among behavioral states was also evaluated with

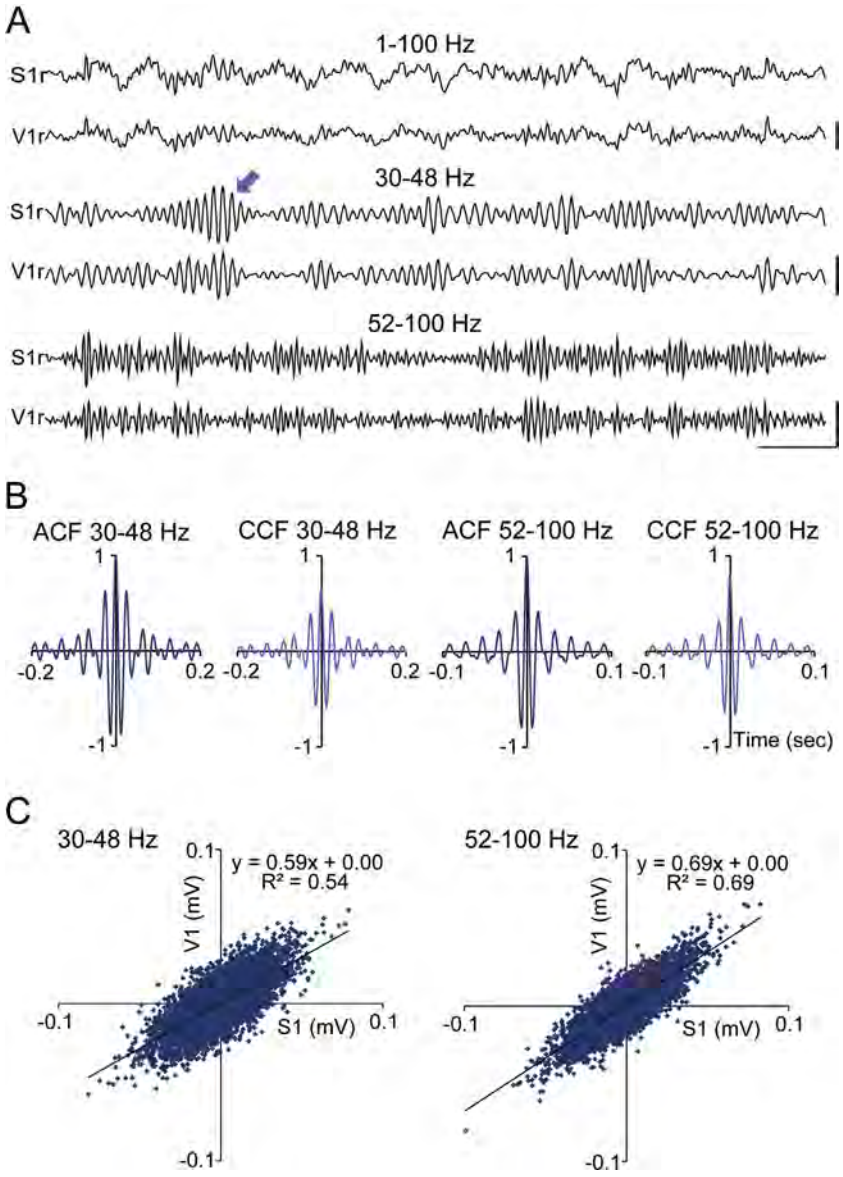

Fig. 2. Gamma oscillations during wakefulness. (A) Simultaneous raw and filtered (35–48 and 52–100 Hz) recordings from the right somatosensory primary (S1r) and right visual primary (V1r) cortices during wakefulness. Gamma oscillations, which are readily observed in the raw recordings, are highlighted after filtering. An arrow signals a "burst" of gamma oscillations. Calibration bars: 200 ms and 200 μV for raw recordings and 100 μV for filtered recordings. (B) Autocorrelation function (ACF) and cross-correlation functions (CCF) from filtered (35–48 Hz and 52–100 Hz) periods of 100 s of simultaneous EEG recordings from S1r and V1r are shown during W. The ACF of both channels are superimposed. (C) Linear regression between the amplitudes of S1r and V1r was performed on representative filtered recordings (30–48 and 52–100 Hz) during 20 s of wakefulness. The determination coefficients and regression line equations are shown.

one-way ANOVA and Tamhane tests. The criterion used to reject the null hypotheses was $p < 0.05$.

Selected recordings were filtered, with a band pass of 30–48 and 52–100 Hz, using Spike 2 digital finite impulse response filters. The amplitude of simultaneously recorded pairs of filtered EEG signals was also analyzed by means of the Pearson correlation. Autocorrelations and cross-correlations functions were also computed.

3. Results

3.1. Raw and filtered (30–48 and 52–100 Hz) EEG recordings during wakefulness and REM sleep

The EEG fluctuates between a desynchronized pattern of activity in the presence of theta rhythm during W and REM sleep and synchronized slow wave activity during NREM sleep. Although EEG activity during W and REM sleep is similar, there are subtle differences. Representative EEG recordings during W and REM sleep are shown in Figs. 2 and 3, respectively. Oscillations of approximately 30–48 Hz can be observed in raw recordings during W (Fig. 2); these electrographic events are not clear during REM sleep (Fig. 3).

Gamma oscillations 30–48 or 52–100 Hz, were unmasked after digital filtering of the recordings. During W, gamma oscillations at 30–48 Hz exhibited some burst of activity with spindle morphology (see example in Fig. 2, arrow); on the other hand, 52–100 Hz oscillations were irregular without a clear pattern. In spite of this, the autocorrelation functions show the presence of an oscillatory pattern of gamma activity (for 30–48 and 52–100 Hz) both during W and REM (Figs. 2 and 3).

Fig. 2 also illustrates a representative example of the coupling of EEG signals recorded from different cortical sites of the same hemisphere during W. Coupling was highlighted when the amplitudes of the signals between pairs of simultaneous EEG recordings were

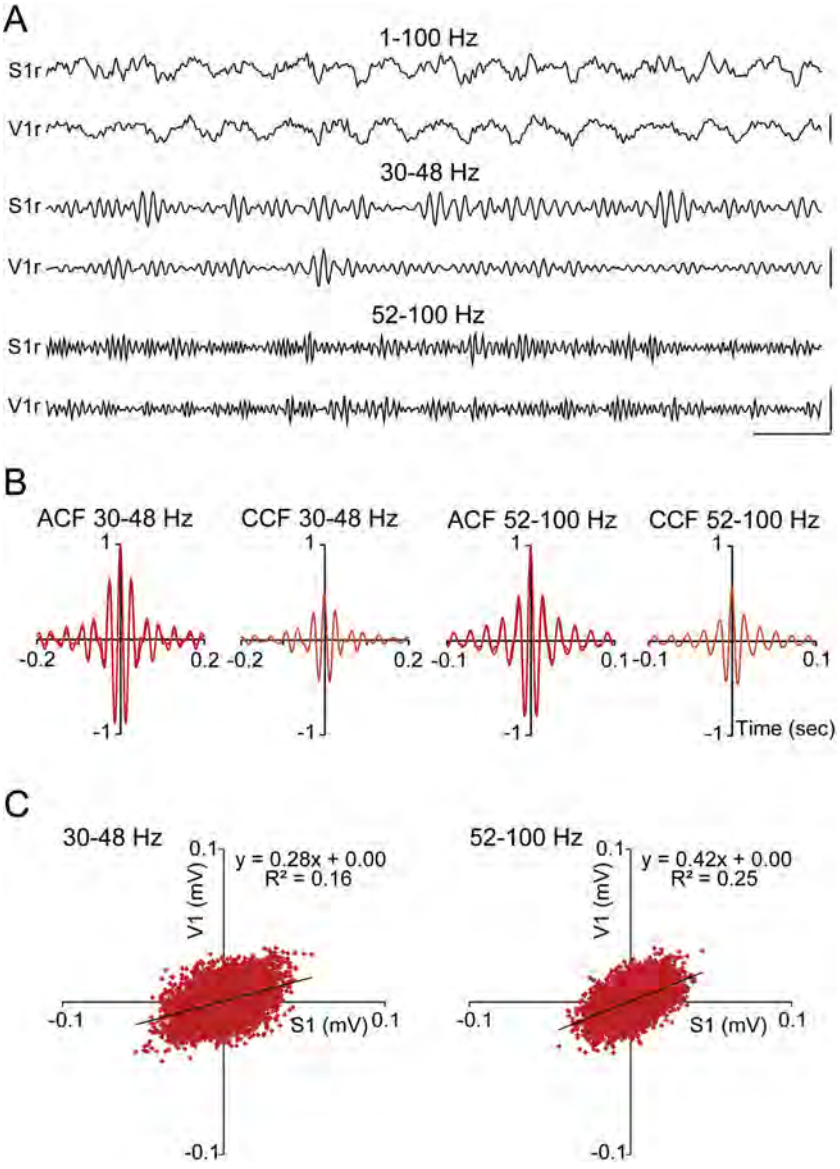

Fig. 3. Gamma oscillations during REM sleep. (A) Simultaneous raw and filtered (35–48 and 52–100 Hz) recordings from the right somatosensory primary (S1r) and right visual primary (V1r) cortices during REM sleep. The amplitude and duration of gamma oscillations decreased compared to wakefulness (see Fig. 2). Calibration bars: 200 ms and 200 μV for raw recordings and 100 μV for filtered recordings. (B) Autocorrelation (ACF) and cross-correlation functions (CCF) from filtered (35–48 Hz and 52–100 Hz) periods of 100 s of simultaneous EEG recordings from S1r and V1r are shown during REM sleep. The ACF of both channels are superimposed. (C) Linear regression between the amplitudes of S1r and V1r were analyzed from representative filtered recordings (30–48 and 52–100 Hz) during 20 s of REM sleep. The determination coefficients and regression line equations are shown.

correlated; the cross-correlation function also shows that both waves are strongly coupled. During REM sleep, the intrahemispheric EEG coupling is reduced, which can be observed in the filtered recordings, the correlation and the cross-correlation histogram exhibited in Fig. 3.

3.2. Coherent 30–48 and 52–100 Hz activity is reduced during REM sleep

In addition to the fact that EEG coupling was minimal during REM sleep when analyzed by filtered recordings and correlation methods, we utilized the magnitude-squared coherence for an in-depth analysis of different pairs of EEG signals that were simultaneously recorded during W and sleep.

As a first step, by means of the two-ways ANOVA we analyzed z′-coherence using behavioral states, and intra- or interhemispheric combination of electrodes (derivates) as factors. The analyses revealed a significant effect of behavioral states (30–48 Hz, $F_{2,423} = 47.28$, $p < 0.0001$; 52–100 Hz, $F_{2,423} = 232.2$, $p < 0.0001$), derivates (30–48 Hz, $F_{2,423} = 335.5$, $p < 0.0001$; 52–100 Hz, $F_{2,423} = 242.4$, $p < 0.0001$) and interactions (30–48 Hz, $F_{4,423} = 8.508$, $p < 0.0001$; 52–100 Hz, $F_{4,423} = 4.497$, $p = 0.001$). Tukey *post hoc* analyses showed that, disregarding the derivates, 30–48 Hz z′-coherence during REM sleep was different than during the other behavioral states ($p < 0.001$). In addition, disregarding behavioral states, 30–48 Hz z′-coherence in the heterotopic interhemispheric combination was different than in the others derivates ($p < 0.001$). All of the combination (behavioral states and derivates) were statistically significant ($p < 0.001$) for 52–100 Hz z′-coherence.

As a second step, we analyzed the z′-coherence in each combination of electrodes across behavioral states using one-way ANOVA. There were significant differences for the intrahemispheric (30–48 Hz, $F_{2,141} = 27.81$, $p < 0.0001$; 52–100 Hz, $F_{2,141} = 94.39$, $p < 0.0001$); the interhemispheric homotopic (30–48 Hz, $F_{2,141} = 8.501$, $p < 0.0001$; 52–100 Hz, $F_{2,141} = 58.95$, $p < 0.0001$) and interhemispheric heterotopic derivates (30–48 Hz, $F_{2,141} = 32.52$, $p < 0.0001$; 52–100 Hz, $F_{2,141} = 95.68$, $p < 0.0001$).

In Fig. 4 is readily observed that, for all the derivates, the minimum values of the z′-coherence for both 30–48 and 52–100 Hz were during REM sleep. For the 30–48 Hz band, in the intrahemispheric derivates, maximum values were present during W. In interhemispheric heterotopic combination, the maximum value of z′-coherence was during NREM sleep. The z′-coherence for 52–100 Hz band was significantly greater during W both for intra and interhemispheric derivates (Fig. 4). The schematic presented in Fig. 4B summarizes the gamma z′-coherence during W and sleep.

For an in-depth analysis of the transitions (t) into and from REM sleep, we analyzed the mean gamma z′-coherence during t (Fig. 5). REM sleep onset was accompanied by a decrease in z′-coherence that was maintained at a low level during this state (Fig. 5A). In contrast, during the transition from REM sleep either to W or NREM sleep, z′-coherence increased (Fig. 5B).

An example of the dynamic evolution of EEG coherence in gamma (30–48 and 52–100 Hz) across behavioral states is shown in Fig. 6 for the intrahemispheric combination of electrodes. While the maximal values of z′-coherence were present during W, the minimal values occurred during REM sleep episodes (Fig. 6).

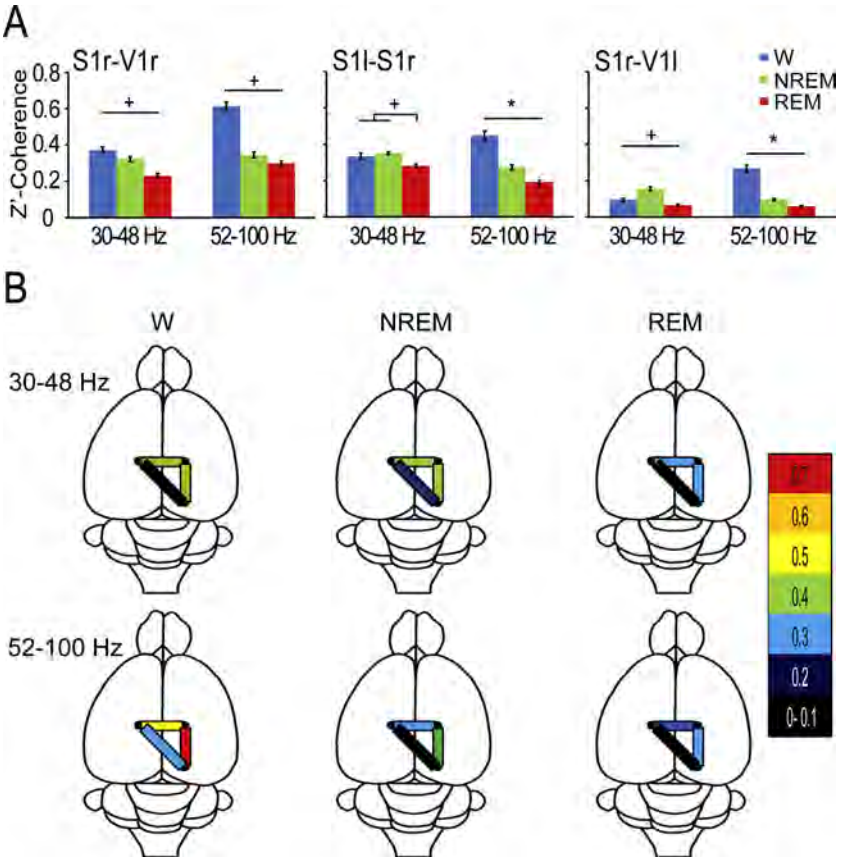

Fig. 4. Gamma band z′-coherence during wakefulness and sleep. (A) Mean z′-coherence (30–48 and 52–100 Hz) of intrahemispheric (G1, S1r–V1r), interhemispheric homotopic (G2, S1l–S1r) and interhemispheric heterotopic (G3, S1r–V1l) combination of electrodes. Data were obtained from 4 rats per group; 12 windows of 100 s per rat for each behavioral state. The values represent the mean ± standard error. Statistical significance: $^{+}P < 0.05$ and $^{*}P < 0.0001$; ANOVA and Tamhane tests. (B) Summary of the gamma band EEG z′-coherence. The lines represent derivates and the color represents the level of z′-coherence. (For interpretation of the references to color in this figure legend, the reader is referred to the web version of this article.)

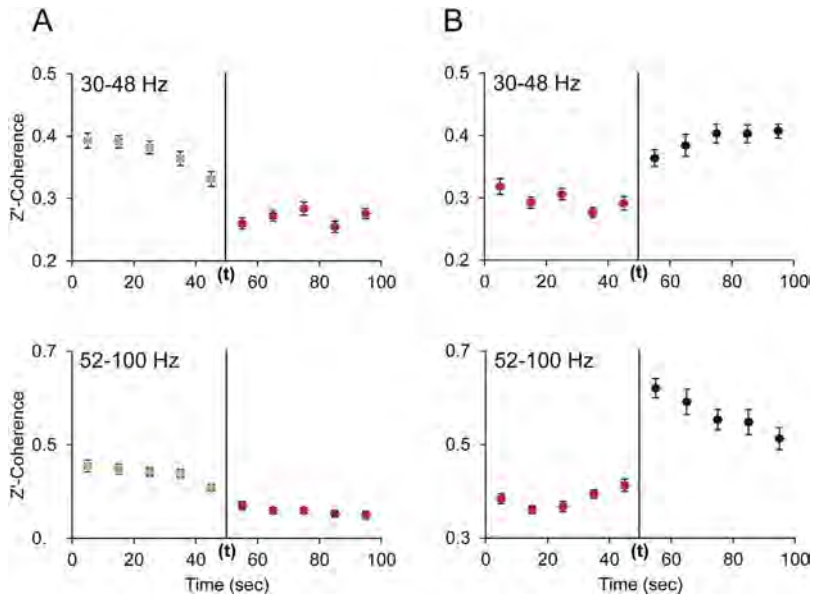

Fig. 5. z′-Coherence during REM sleep transitions. (A) The graphs depict the mean z′-coherence ± standard error (for 30–48 and 52–100 Hz) of 25 transitions of one rat of the G1 group (S1r–V1r, intrahemispheric coherence). (*t*) indicates the onset of REM sleep. (B) Waking from REM sleep. The graphs show the mean z′-coherence ± standard deviation (for 30–48 and 52–100 Hz) of 25 transitions of one rat of the G1 group (S1r–V1r, intrahemispheric coherence). (*t*) indicates the end of the REM sleep episodes. NREM episodes are symbolized in green; REM episodes in red. The states that followed the REM sleep episodes are indicated in black (these epochs were mainly wakefulness but NREM sleep episodes also followed REM sleep). (For interpretation of the references to color in this figure legend, the reader is referred to the web version of this article.)

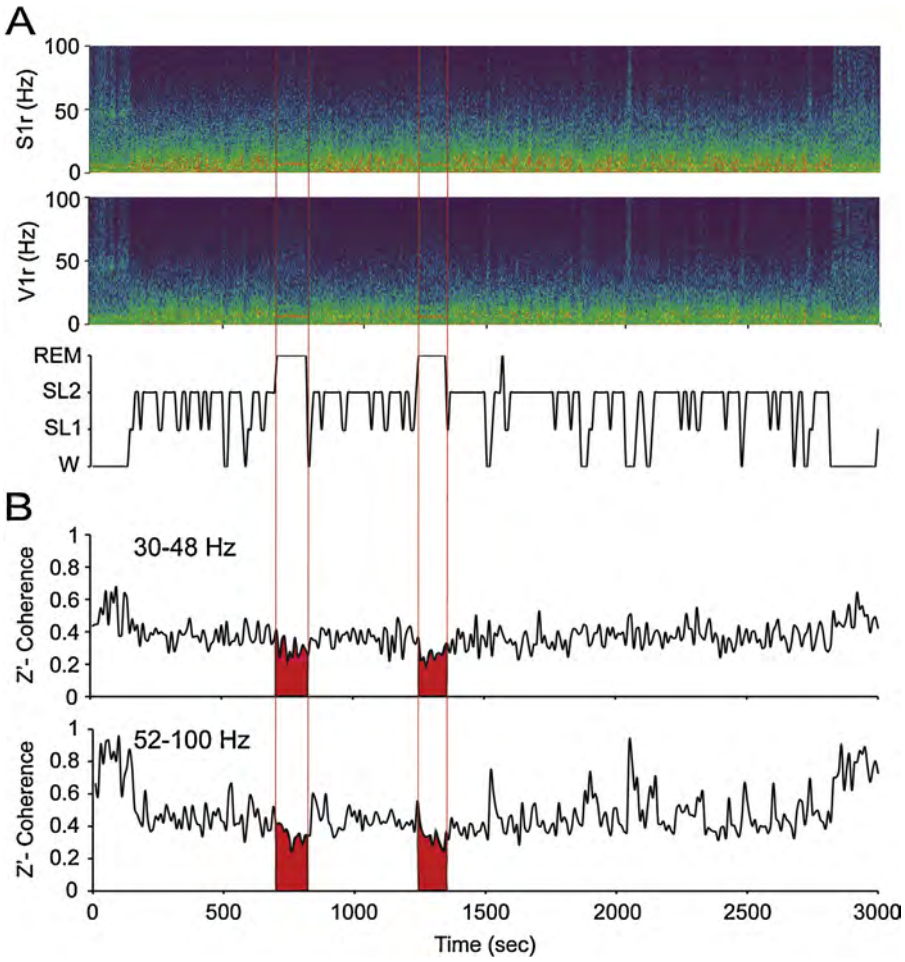

Fig. 6. Dynamic of the gamma coherence during wakefulness and sleep. (A) The spectrogram (0.1–100 Hz) of primary visual (V1r) and primary somatosensory (S1r) cortical recordings and the accompanying hypnogram are shown. During W and REM sleep the theta activity (4–9 Hz) in the spectrograms can be readily observed. Gamma activity is larger during W. During NREM sleep, delta activity (0.5–4 Hz) is more prominent and there are intermittent episodes of sigma activity (9–15 Hz), which correspond to the presence of sleep spindles. (B) The z′-coherence for both gamma bands (30–48 and 52–100 Hz) was analyzed in 10-s epochs. The maximum values of z′-coherence occurred during W; z′-coherence decreased to an intermediate level during NREM sleep and minimum values were present during the periods of REM sleep (segments in red). (For interpretation of the references to color in this figure legend, the reader is referred to the web version of this article.)

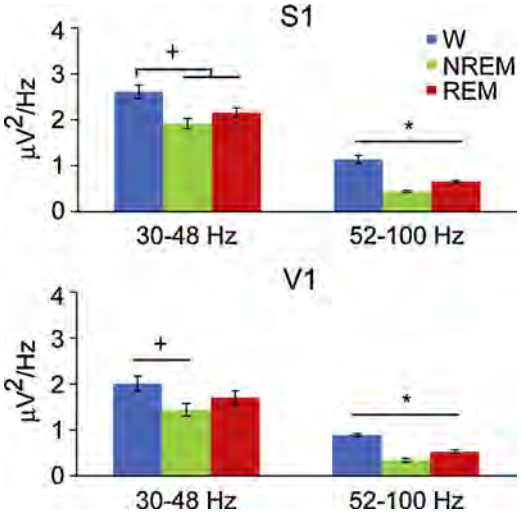

Fig. 7. Gamma power during wakefulness and sleep. Mean gamma band power of the EEG recorded from 3 rats of the intra-hemispheric S1r and V1r cortices of group G1 (see Fig. 1) during wakefulness (W), NREM and REM sleep. The values represent mean ± standard error. Statistical significance: $^{+}P < 0.05$ and $^{*}P < 0.0001$, ANOVA with Tamhane tests.

3.3. Gamma power during wakefulness and sleep

The gamma power was different across behavioral states for S1 (30–48 Hz, $F_{2,105} = 7.941$, $p = 0.001$; 52–100 Hz, $F_{2,105} = 49.37$, $p < 0.0001$) and V1 cortices (30–48 Hz, $F_{2,105} = 6.092$, $p = 0.003$; 52–100 Hz, $F_{2,105} = 45.06$, $p < 0.0001$). Fig. 7 shows that gamma power was significantly greater during W than during REM sleep for 52–100 Hz in S1 and V1 cortices, and for 30–48 Hz in S1 cortex. However, in contrast to z′-coherence values, the minimum power values occurred during NREM sleep.

4. Discussion

In the present study, we demonstrated in rats that the EEG intra-hemispheric and interhemispheric coherence in the gamma (30–48 and 52–100 Hz) frequency band is smaller during REM sleep that during W or NREM sleep. Therefore, these data suggest that during REM sleep, high-frequency functional interaction between different cortical regions is lower compared with other behavioral states.

4.1. Gamma coherence during wakefulness

It is well established that gamma power and gamma coherence increase during W in cats and humans, mainly for intrahemispheric combination of electrodes [4,6,7]. In the cat, gamma band coherence at ≈40 Hz increases during alert W; this fact that can be clearly observed in raw recordings [6,7]. In the present study, the largest gamma power and intrahemispheric coherence was present during W states, but the differences depending on waking conditions were not studied. In this regards, Maloney et al. (1998) showed that the largest values of gamma power occur during periods of active W [22].

4.2. Gamma coherence during REM sleep

In the present report, we demonstrated in rats that gamma intra and interhemispheric coherence reaches a nadir during REM sleep. This result accords with the results of our previous studies in the cat [6,7], where gamma coherence was almost absent during REM sleep in intrahemispheric and interhemispheric derivates. The demonstration that there is a radical reduction in gamma coherence between different cortical regions during REM sleep does not contradict the findings of Steriade el al. (1996), which showed an increase in local coupling (within a column or among closely cortical sites) during activated states [23]. In fact, as shown in Fig. 7, gamma power (as a reflection of local gamma synchronization) during REM sleep was close to W, and larger than during NREM sleep. Therefore, although gamma activity was large during REM sleep, the coupling of gamma oscillations between different cortical areas (reflected by gamma coherence) was minimal.

In humans, an early report showed that during REM sleep magneto-EEG 40-Hz oscillations were similar in distribution, phase and amplitude to those observed during W. In contrast, Perez-Garci et al. (2001) reported that there is a decrease in correlation spectra in 2-s epochs of fast (27–48 Hz) frequencies restricted to intra-hemispheric frontal-perceptual cortical regions during REM sleep. On the contrary, the gamma synchrony between homologous cortical regions of both hemispheres increases during REM sleep in humans [24,25]. Cantero et al. (2004) employed human intracranial EEG recordings for coherence analyses during sleep, which allowed a much finer spatial scale than scalp-recorded signals. They found that local (within neocortical regions) and long-range (between intra-hemispheric neocortical regions) gamma (35–58 Hz) coherence was significantly greater during wakefulness than during sleep. However, no differences in coherence were found between NREM and REM sleep. Furthermore, functional gamma-range coupling between the neocortex and hippocampus was observed during wakefulness, but not during REM sleep. Finally, Voss et al. (2009) demonstrated that gamma coherence decreases during REM sleep compared with wakefulness; during lucid dreaming, coherence values are intermediate between W and REM sleep.

As with other EEG rhythms, gamma oscillations remains remarkable conserved in mammals irrespective of brain size [26]. The decrease in gamma coherence during REM sleep in rats (present report), in cats [6,7] and in humans [24,27,28], indicates that during this behavioral state there is a decrease in the capacity for integration among different cortices within high frequency ranges.

A recent study demonstrated that electrical stimulation of the prefrontal cortex in the lower gamma band (≈40 Hz) during REM sleep influences ongoing brain activity and induces self-reflective awareness (a feature of W) in dreams (*i.e.*, lucid dreams), while other stimulation frequencies were not effective [29]. Thus, the data support the concept that synchronous oscillations of ≈40 Hz are an electrophysiological pattern of activity that is indicative of attentive wakefulness. On the contrary, the reduction of gamma coherence during REM sleep [6,7,24,27,28], may underlie the unique pattern of REM sleep mentation, *i.e.*, dreams [14,30].

5. Conclusions

During REM sleep in the rat, despite an activated EEG, there is an uncoupling of the gamma frequency activities between neocortical sites. Therefore, functional interactions among different cortical areas, which are critical for cognitive functions, are different during W and REM sleep. Since this feature is conserved in other mammals, including humans, we consider that this uncoupling of gamma frequency activity during REM sleep is a defining trait of REM sleep in mammals.

Acknowledgments

We are grateful to Dr. Horacio Igarzabal for his assistance in the experimental procedures. This study was partially supported by the “Programa de Desarrollo de Ciencias Básicas” (PEDECIBA) and the “Agencia Nacional de Investigacion e Innovación” (ANII), Uruguay.

References

[1] Rieder MK, Rahm B, Williams JD, Kaiser J. Human gamma-band activity and behavior. Int J Psychophysiol 2010;79:39–48.
[2] Uhlhaas PJ, Pipa G, Lima B, Melloni L, Neuenschwander S, Nikolic D, et al. Neural synchrony in cortical networks: history, concept and current status. Front Integr Neurosci 2009;3:17.
[3] Uhlhaas PJ, Pipa G, Neuenschwander S, Wibral M, Singer W. A new look at gamma? High- (>60 Hz) gamma-band activity in cortical networks: function, mechanisms and impairment. Prog Biophys Mol Biol 2011;105:14–28.
[4] Llinas R, Ribary U. Coherent 40-Hz oscillation characterizes dream state in humans. Proc Natl Acad Sci U S A 1993;90:2078–81.
[5] Tiitinen H, Sinkkonen J, Reinikainen K, Alho K, Lavikainen J, Naatanen R. Selective attention enhances the auditory 40-Hz transient response in humans. Nature 1993;364:59–60.
[6] Castro S, Falconi A, Chase MH, Torterolo P. Coherent neocortical 40-Hz oscillations are not present during REM sleep. Eur J Neurosci 2013;37:1330–9.
[7] Castro S, Cavelli M, Vollono P, Chase MH, Falconi A, Torterolo P. Interhemispheric coherence of neocortical gamma oscillations during sleep and wakefulness. Neurosci Lett 2014;578:197–202.
[8] Bullock TH, McClune MC, Enright JT. Are the electroencephalograms mainly rhythmic? Assessment of periodicity in wide-band time series. Neuroscience 2003;121:233–52.
[9] Edelman GM, Tononi G. A universe of consciousness. New York: Basic Books; 2000.
[10] Siegel M, Donner TH, Engel AK. Spectral fingerprints of large-scale neuronal interactions. Nat Rev Neurosci 2012;13:121–34.
[11] Llinas R, Ribary U, Contreras D, Pedroarena C. The neuronal basis for consciousness. Philos Trans R Soc Lond B: Biol Sci 1998;353:1841–9.
[12] John ER. The neurophysics of consciousness. Brain Res Brain Res Rev 2002;39:1–28.
[13] Mashour GA. Integrating the science of consciousness and anesthesia. Anesth Analg 2006;103:975–82.
[14] Hobson JA. REM sleep and dreaming: towards a theory of protoconsciousness. Nat Rev Neurosci 2009;10:803–13.
[15] Benedetto L, Rodriguez-Servetti Z, Lagos P, D'Almeida V, Monti JM, Torterolo P. Microinjection of melanin concentrating hormone into the lateral preoptic area promotes non-REM sleep in the rat. Peptides 2013;39C:11–5.
[16] Lagos P, Torterolo P, Jantos H, Chase MH, Monti JM. Effects on sleep of melanin-concentrating hormone microinjections into the dorsal raphe nucleus. Brain Res 2009;1265:103–10.
[17] Bullock TH, Buzsaki G, McClune MC. Coherence of compound field potentials reveals discontinuities in the CA1-subiculum of the hippocampus in freely-moving rats. Neuroscience 1990;38:609–19.
[18] Bullock TH. Signals and signs in the nervous system: the dynamic anatomy of electrical activity is probably information-rich. Proc Natl Acad Sci U S A 1997;94:1–6.
[19] Bullock TH, McClune MC, Achimowicz JZ, Iragui-Madoz VJ, Duckrow RB, Spencer SS. EEG coherence has structure in the millimeter domain: subdural and hippocampal recordings from epileptic patients. Electroencephalogr Clin Neurophysiol 1995;95:161–77.
[20] Cantero JL, Atienza M, Salas RM. Clinical value of EEG coherence as electrophysiological index of cortico-cortical connections during sleep. Rev Neurol 2000;31:442–54.
[21] Nunez PL, Srinivasan R, Westdorp AF, Wijesinghe RS, Tucker DM, Silberstein RB, et al. EEG coherency. I: Statistics, reference electrode, volume conduction, Laplacians, cortical imaging, and interpretation at multiple scales. Electroencephalogr Clin Neurophysiol 1997;103:499–515.
[22] Maloney KJ, Cape EG, Gotman J, Jones BE. High-frequency gamma electroencephalogram activity in association with sleep-wake states and spontaneous behaviors in the rat. Neuroscience 1997;76:541–55.
[23] Steriade M, Amzica F, Contreras D. Synchronization of fast (30–40 Hz) spontaneous cortical rhythms during brain activation. J Neurosci 1996;16:392–417.
[24] Perez-Garci E, del-Rio-Portilla Y, Guevara MA, Arce C, Corsi-Cabrera M. Paradoxical sleep is characterized by uncoupled gamma activity between frontal and perceptual cortical regions. Sleep 2001;24:118–26.
[25] Corsi-Cabrera M, Sifuentes-Ortega R, Rosales-Lagarde A, Rojas-Ramos OA, Del Rio-Portilla Y. Enhanced synchronization of gamma activity between frontal lobes during REM sleep as a function of REM sleep deprivation in man. Exp Brain Res 2014;232:1497–508.
[26] Buzsaki G, Logothetis N, Singer W. Scaling brain size, keeping timing: evolutionary preservation of brain rhythms. Neuron 2013;80:751–64.
[27] Cantero JL, Atienza M, Madsen JR, Stickgold R. Gamma EEG dynamics in neocortex and hippocampus during human wakefulness and sleep. Neuroimage 2004;22:1271–80.
[28] Voss U, Holzmann R, Tuin I, Hobson JA. Lucid dreaming: a state of consciousness with features of both waking and non-lucid dreaming. Sleep 2009;32:1191–200.
[29] Voss U, Holzmann R, Hobson A, Paulus W, Koppehele-Gossel J, Klimke A, et al. Induction of self awareness in dreams through frontal low current stimulation of gamma activity. Nat Neurosci 2014;17:810–2.
[30] Nir Y, Tononi G. Dreaming and the brain: from phenomenology to neurophysiology. Trends Cogn Sci 2010;14:88–100.
[31] Paxinos G, Watson C. The rat brain. New York: Academic Press; 2005.

Algunos estudios preliminares de nuestro grupo también mostraron caídas en coherencia gamma durante el sueño REM en ratones (Cavelli et al., 2017c) y humanos (Castro et al., 2014). Estos resultados nos llevaron a plantear que los cambios dinámicos de la potencia y coherencia gamma durante el ciclo normal de sueño y vigilia se encuentran conservados en la evolución de los mamíferos y, por tanto, pueden servir como índices de diferenciación de los estados comportamentales normales. Con ese objetivo publicamos el **Artículo 2** (Cavelli et al., 2017a).

ARTICULO 2

(Cavelli et al., 2017a)

Translational Brain Rhythmicity

Research Article

Absence of EEG gamma coherence in a local activated cortical state: a conserved trait of REM sleep

Matías Cavelli*, Santiago Castro-Zaballa, Alejandra Mondino, Joaquin Gonzalez, Atilio Falconi and Pablo Torterolo

Laboratory of Sleep Neurobiology, Department of Physiology, School of Medicine, Universidad de la Rep□lica , Montevideo, Uruguay

Abstract

During cognitive processes, there are extensive interactions between various regions of the cerebral cortex. Oscillations in the gamma frequency band (30-100 Hz) of the electroencephalogram are involved in the binding of spatially separated but temporally correlated neural events, which results in a unified perceptual experience.

Like wakefulness, REM sleep is characterized by gamma oscillations in the EEG. Dreams, that are considered a special type of cognitive activity or proto-consciousness, mostly occur during this state.

The power of the gamma band, assessed by the fast Fourier transform, reflects the local degree of synchronization at that frequency. On the other hand, the extent of interactions between different cortical areas at the gamma frequency band can be explored by means of a mathematical function called □coherence□ which reflects the □strength□of functional interactions between cortical areas.

The objective of the present report was to study in the rat the dynamic relationship between gamma power and coherence in the low (30-48 Hz) and high (52-98 Hz) gamma bands during waking and sleep, in occipital, parietal, and frontal neocortical areas, as well as in the olfactory bulb, that is a critical site of gamma rhythm-genesis. In addition, we re-analyzed previous recordings in cats, in order to evaluate the same dynamic relationship as in rats. In both species, the main result was that during REM sleep, gamma power increased, while gamma coherence between distant neocortical areas decreased. The fact that this profile is present in *rodenthia* as well as in *carnivora* suggests that this is a trait that characterize REM sleep in mammals.

Introduction

The brain is a complex, self-organized system with non-linear dynamics, in which distributed and parallel processing coexist with serial operations within highly interconnected networks, but without a single coordinating center [1,2]. This organ integrates fragmentary neural events that occur at different times and locations into a unified perceptual experience. Understanding the mechanisms that are responsible for this integration, "the binding problem", is one of the most important challenges that cognitive neuroscience has to solve [3,4].

One of the binding mechanisms appears to be the synchronization of neuronal activity by phase-locking of self-generated network oscillations [5,6]. The first experimental evidence supporting the potential role of synchrony as a relational code, was described in simultaneously recorded but spatially segregated neurons that engaged in synchronous oscillation when activated by visual stimuli. The frequency of these synchronized oscillations was in the range of 40 Hz [7,8]. This coordinating mechanisms was named "binding-by-synchrony" [2,4]; and this theory assumes that coherence in neuronal activity is critical for information processing [9].

Jasper and Andrews first used the term gamma waves to designate low-amplitude waves at 35-45 Hz in the electroencephalogram (EEG) [10]. These oscillations were later described in the olfactory bulb (OB) of hedgehogs by Adrian [11]. An increase in gamma activity typically appears during states/behaviors that are characterized by the active cognitive processing of external percepts or internally generated thoughts and images [12-16].

Cognitive activities not only occur during wakefulness (W). Dreams, which occur mostly during REM sleep, are considered a special kind of cognitive activity or proto-consciousness [17]. In contrast, during deep non-REM (NREM) sleep, there is an absence, or at least a strong reduction, in oneiric activity [17]. REM sleep dreams are characterized by their vividness, single-mindedness, bizarreness and loss of voluntary control over the plot. Attention is unstable and rigidly focused, facts and reality are not checked, violation of physical laws and bizarreness are passively accepted, contextual congruence is distorted, time is altered and memories become labile [17,18]. Interestingly, some authors have suggested that cognition during REM sleep resembles psychosis [19]. High gamma activity is also present during REM sleep, both in humans and animals [20-23].

Local cortical oscillations in the gamma band can be examined by means of the fast Fourier transform (FFT). The results are expressed in gamma power that reflects the local degree of synchronization of the extracellular potential at that frequency [24]. Local gamma oscillations are higher during REM sleep compared to NREM sleep [21-23,25]. On the other hand, the extent of interactions between different cortices at the gamma frequency band can be explored through a mathematical function called 'coherence', which reflects the 'strength' of functional interactions between cortical areas [26-28]. Gamma coherence between distant areas has been proposed as a neural correlate of

Correspondence to: Dr. Pablo Torterolo, Department of Physiology, Faculty of Medicine, University of the Republic, General Flores 2125, 11800 Montevideo-Uruguay, Tel: (598) 2924 34 14 ext. 3234; E-mail: ptortero@fmed.edu.uy

Key words: *wakefulness, paradoxical sleep, cortex, dreams, synchronization, NREM sleep*

Received: June 29, 2017; **Accepted:** July 28, 2017; **Published:** July 31, 2017

conscious perception and self-awareness [29-33]. In this regard, coherence in the gamma frequency band is lost during anesthesia-induced unconsciousness [34-36], and is severely altered in psychiatric disorders [37,38].

In previous studies, we showed in cats and rats, that gamma coherence is high during W, decreases during NREM sleep and is almost absent during REM sleep [23,39-41]. However, these studies were limited in the extent of the cortical loci studied, as well as in the examination of the dynamic relationship between local and long-range gamma synchronization. Therefore, the aim of the present report was the following: 1. To study in the rat low (30-48 Hz) and high (52-98 Hz) gamma power and coherence during W and sleep in neocortical areas (such as frontal cortices) that were not yet studied. We also aimed to analyze the OB, that is a critical site of gamma rhythm-genesis [11,14,15]. In addition, we evaluated in detail the dynamic relationship between local or short-range synchronization (power) and long-range synchronization (coherence) during W, sleep and transitions into and out REM sleep. 2. To re-analyze previous recordings in cats, in order to evaluate the same dynamic relationships proposed for rats.

Material and methods

Experimental animals

We analyzed data obtained from nine adult Wistar rats and six adult cats. Data from four of these cats were utilized in previous studies [39,41]. The animals were determined to be in good health by veterinarians of the Department of Laboratory Medicine of the School of Medicine, Universidad de la República, Uruguay. All experimental procedures were conducted in accordance with the National Animal Care Law (#18611) and with the "Guide to the care and use of laboratory animals" (8th edition, National Academy Press, Washington D. C., 2010). Furthermore, the Institutional Animal Care Committee approved the experimental procedures. Adequate measures were taken to minimize pain, discomfort or stress of the animals, and efforts were made to use the minimum number of animals necessary to produce reliable data.

Surgical procedures and experimental sessions are summarized below; for details [23,39].

Surgical procedures

Animals were chronically implanted with electrodes to monitor the states of sleep and W. In rats, anesthesia was induced with a mixture of ketamine-xylazine. Cats were pre-medicated with xylazine, atropine and antibiotics, and anesthesia was induced with ketamine and maintained with a gas mixture of isoflourane in oxygen.

The animal's head was positioned in a stereotaxic frame and the skull was exposed. In order to record the EEG, stainless steel screw electrodes (diameter: 1.4 mm cats and 1.0 mm for rats) were placed on the surface (above the dura mater) in different cortices. Figure 1 presents a summary of the positions of the recording electrodes on the surface of the cortex for rats and cats. In the rats, six electrodes were located on the neocortex forming two anterior-posterior consecutive squares centered with respect to the midline and the frontal square centered with respect to Bregma (Figure 1). Each side of the squares has a length of 5 mm. The electrodes were located in primary motor cortex (M1, L: ±2.5 mm, AP: +2.5 mm), primary somato-sensory cortex (S1, L: ±2.5 mm, AP: -2.5 mm), and secondary visual cortex (V2, L: ±2.5 mm, AP: -7.5 mm). The other electrode was located over the right OB (L: +1.25 mm, AP: +7.5 mm). Each cat was implanted with several electrodes throughout the neocortex. However, in this report, we analyzed the signals from the electrodes positioned in the anterior (frontal) and posterior (occipital or parietal) cortices of the same hemisphere.

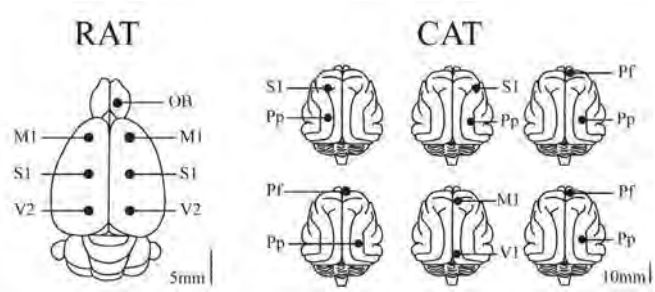

Figure 1. Position of recording electrodes. The figure presents a summary of the positions of the recording sites on the surface of the cerebral cortex of a group of 9 rats sharing the same location of electrodes, and 6 cats with similar but not the same electrode locations as in rats. The electrodes were referred to a common electrode that was located over the cerebellum (rats) or left frontal sinus (cats). OB, olfactory bulb; M1, primary motor cortex; S1, primary somato-sensory cortex; V1, primary visual cortex; V2, secondary visual cortex; Pf, pre-frontal cortex; Pp, posterior parietal cortex.

The electrodes were soldered to a plug and bonded to the skull with acrylic cement. In order to record the electromyogram (EMG), two electrodes were inserted into the neck muscle chronically in the rat, and contact electrodes (with EEG-paste interphase) were acutely positioned on the neck skin of the cat. In the cat, two plastic tubes (which were used to maintain the animal's head fixed without pain or pressure), were also bonded to the skull with acrylic cement.

At the end of the surgical procedures, an analgesic was administered. Incision margins were kept clean and a topical antibiotic was administered on a daily basis. After the animals had recovered from the preceding surgical procedures, they were adapted to the recording environment for a period of at least one week (rats) and two months (cats).

Experimental sessions

Experimental sessions of 4-6 h in duration were conducted during the light period, between 12 AM and 6 PM (rats) and 11 AM to 3 PM (cats) in a temperature-controlled environment (21-24 °C). In rats, the recordings were obtained via a rotating connector in a sound-attenuated chamber which is also a Faraday box; during these sessions (as well as during adaptation sessions), the animals were able to move freely within the confines of the recording chamber (transparent cages (40 x 30 x 20 cm) containing wood shavings) and had free access to water and food. Cats were recorded in a Faraday box in semi-restricted conditions; during experimental sessions' the head of the cat was held in a stereotaxic frame by a head-restraining device, while the body rested in a sleeping bag.

The simultaneous activity of different cortical areas was recorded with monopolar arrangement of electrodes [42]. A common electrode reference montage was employed; it was located in the left frontal sinus of the cats [39], and in the cerebellum of the rats [23]. The EMG was also monitored. Each cat and rat was recorded daily for a period of approximately 30 days and 2 weeks, respectively, in order to obtain a complete data set.

Bioelectric analog signals were amplified with differential AC amplifiers (AM-systems model 1700; 1000 x), filtered (0.1-500 Hz), digitized (1024 Hz, 2^{16} bits) and stored on a PC using the Spike2 software (Cambridge Electronic Design). Data were obtained during W, REM sleep, and NREM sleep.

Data analysis

Sleep and waking states were determined for every 10-seconds epoch for rats and cats. W, light sleep (SL1), deep or slow wave sleep (SL2), NREM sleep (SL1 + SL2) and REM sleep were identified in rats [23,43]. Alert W (AW), quiet W (QW), W (AW+QW), NREM sleep and REM sleep were identified in cats [39]. AW was induced for a period of 300 sec by a sound stimulus, which was introduced approximately 30 minutes after the beginning of the recording. The sound stimulus consisted of clicks (0.1 ms in duration) of 60 to 100 dB SPL in intensity with a variable frequency of presentation (1 to 500 Hz, modified at random by the operator) in order to avoid habituation [39].

We focused on the analysis of low (LG: 30-48 Hz) and high (HG: 52-98 Hz) gamma frequency bands of the EEG; 50 Hz electrical noise was avoided with this partitioning. In rats, we analyzed gamma power in the maximum number of channels and coherence in all the possible cortical combinations. In cats, we focused on a pair of electrodes with similar location in all animals, one in a frontal position and one in a posterior position of the brain. In order to analyze gamma power and gamma coherence between these EEG channels, we used similar procedures as in our previous studies [23,39,41]; however, the analysis in cats and rats were not exactly the same (see below).

CAT

We employed the same methodology that we described in our previous studies [39-41]. Twelve artifact-free periods of 100 seconds were examined during each behavioral state (1200 seconds for each behavioral state, per animal; data were selected from three different recordings).

RAT

The maximum number of non-transitional and artifact-free periods of 30 seconds was selected during each behavioral state to determine the mean power and coherence for each rat. For each animal, we analyzed two complete (6 h) recordings (recordings with the minimal amount of artifacts were selected).

The coherence between two EEG channels that were recorded simultaneously was analyzed in windows of 30 second (rat) or 100 second (cat) windows. For each period, the Magnitude Squared Coherence as well as the power spectrum for each channel, were calculated by means of Spike2 script COHER-HOL 1S (for details about coherence definition see [26,39]). For the coherence analysis, each period was divided into 30 (rat) and 100 (cat) time-blocks with a bin size of 2048 samples, and a resolution of 0.5 Hz. We applied the Fisher z' transform to the gamma coherence values in order to normalize and evaluate them by means of parametric statistical tests. The data was then analyzed through custom-built Python routines.

Analyses of 10-second epochs were also used to determine the temporal dynamic of power and coherence. Hence, low and high gamma power and coherence were normalized, and referred to as normalized power (NP) and normalized z'-coherence (NC). For dynamic analysis (see Results), normalization was undertaken by dividing each value by the maximum value (of either power or coherence) recorded in each analyzed segment. For statistical analysis, the normalization was performed for each animal by dividing each mean value by the maximum-recorded value.

We also analyzed the LG and HG mean global power (MGP) and mean global coherence (MGC) in each rat, by averaging the power measured in all the channels, and the coherence for all combinations of electrodes [36].

In order to determine the relationship between local or short-range synchronization (power) and long-range synchronization (coherence) we applied the following function: ((NP of Ch1 + NP Ch2) / 2)) - (NC between Ch1-Ch2). We named this function Power-Coherence difference (NP-NC). A similar approach was employed for the global power and coherence (MGP – MGC). In previous preliminary analyses, we constructed the function utilizing the ratio between normalized power and coherence with similar results. However, we considered the NP-NC function a more suitable analysis given that the signs of the results differed between states; W (close to zero), NREM sleep (negative values) and REM sleep (positive values).

The data were expressed as mean ± standard deviation of the NP, NC and NP-NC. The significance of the differences across behavioral states was evaluated with one-way ANOVA and Tamhane post hoc tests (for each animal) and repeated measures ANOVA (for comparison between the means of the whole group of cats or rats), along with Tukey post hoc tests. The criterion used to reject the null hypothesis was $p < 0.05$.

Results

Gamma activity in rat

Dynamics of gamma activity in the rat: The gamma dynamic during sleep and W in a representative rat is shown in Figure 2; the spectrograms and hypnograms of Figure 2A, indicate the different states of W and sleep. Low and high gamma NP is shown in Figure 2B. For primary somatosensory (S1) and secondary visual (V2) cortices, both low and high gamma NP was higher during W than during sleep. For the low gamma band in this animal there were not clear changes in the NP between NREM sleep and REM sleep. On the contrary, high gamma NP was minimal in NREM sleep but increased during REM sleep (Figure 2B).

Low and high gamma NC between S1 and V2 were the highest during W and decreased during NREM sleep (Figure 2C). The largest decrement in low and high gamma NC occurred during REM sleep.

In order to analyze the relationship between gamma power (that reflects local or short-range synchronization) and gamma coherence (that reveals long-range or distant synchronization), the NP-NC function was applied (Figure 2C). During W this relationship was close to zero, had negative values during NREM sleep and reverted to positive values during REM sleep. This dynamic profile was similar for both low and high gamma bands.

Cortical extent of LG and HG power and coherence: To study the cortical extent of power and coherence of gamma bands, we analyzed a group of nine rats that shared the same electrode positions. Statistical analyses of gamma power and coherence are shown in Tables 1, 2 and 3; these results are graphically summarized in Figure 3. LG and HG NP showed significant differences across behavioral states in all the cortical regions (Table 1). These results revealed that LG and HG power is high during W than during sleep, both in neocortex and OB. The lowest values were recorded during NREM sleep, while during REM sleep the HG NP increased to an intermediate level in all the cerebral areas recorded. On the other hand, LG showed similar values to those of W in the parietal and frontal areas of the neocortex (Table 1).

For LG, NC displayed significant differences across behavioral states from sixteen of twenty-one possible electrode pair combinations (Table 2). Interestingly, seven combinations displayed a greater coherence during NREM sleep than during W. In contrast, only two

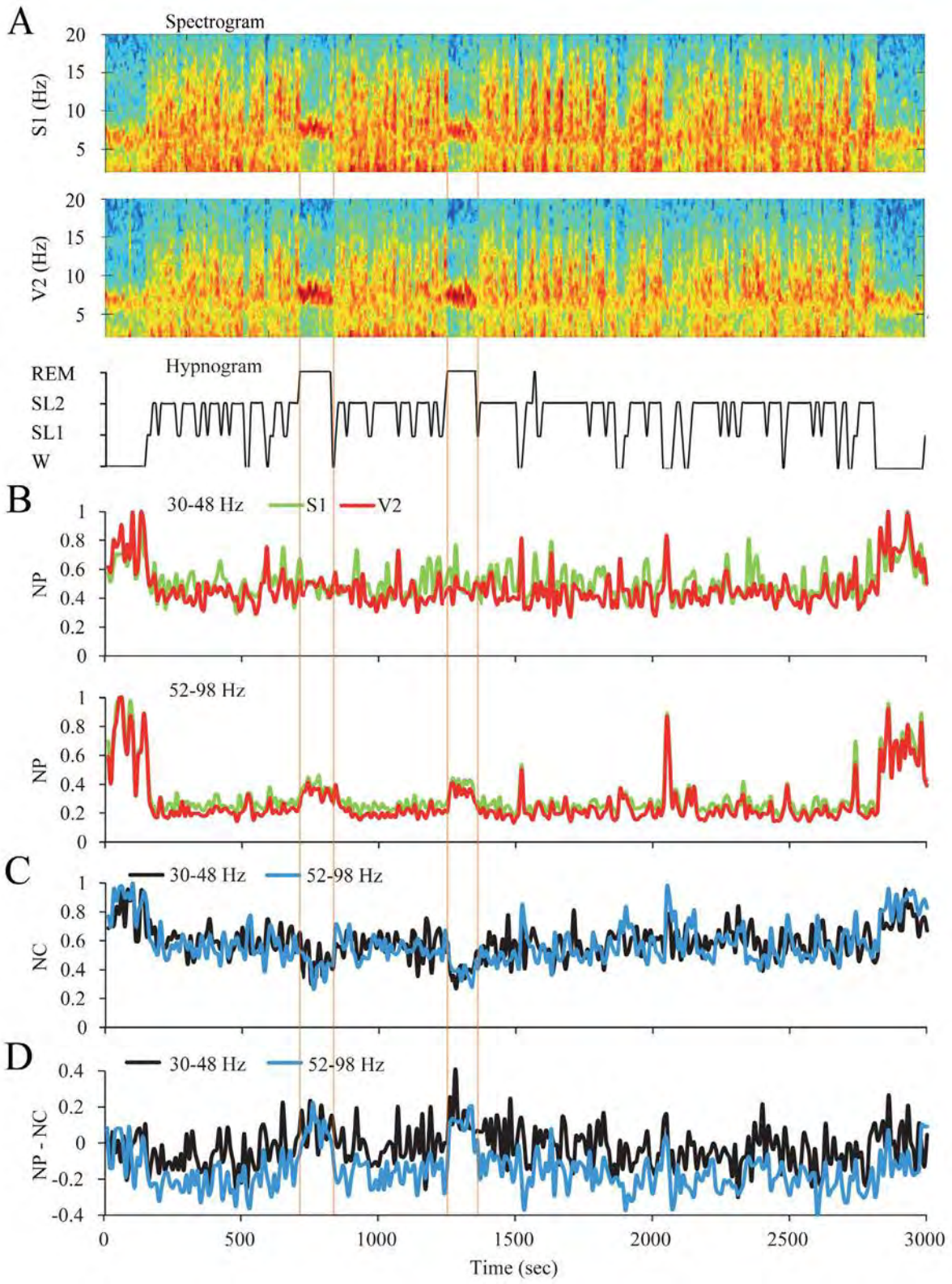

Figure 2. Dynamic of the gamma activity in the rat. A. The spectrograms (1-20 Hz) of secondary visual (V2) and primary somatosensory (S1) cortical recordings and the hypnogram are shown. During W and REM sleep, theta activity (4-9 Hz) in the spectrograms can be readily observed. During NREM sleep, delta activity (0.5-4 Hz) was more prominent and there were intermittent episodes of sigma activity (9-15 Hz), which correspond to the presence of sleep spindles. Color calibration of the spectrogram is not shown. B. Normalized power (NP) of S1 (green) and V1 (red) cortices for low (upper traces) and high (lower traces) gamma bands are shown. C. Normalized z'-coherence (NC) for both gamma bands (30-48 and 52-98 Hz). D. Power-coherence difference function (NP-NC) discriminates between REM sleep with positive values and the rest of states with zero or negative values. All the parameters were analyzed in 10 second epochs. W, wakefulness; SL1, light sleep; SL2, slow wave sleep; REM, REM sleep.

Table 1. Normalized power during sleep and wakefulness in the rat.

		Descriptive Statistics (NP)			Repeated measures ANOVA		Multiple Comparisons-Tukey		
Band	Electrode	W (mean ± SD)	NREM (mean ± SD)	REM (mean ± SD)	F	Sig. (p)	W vs NREM (p)	W vs REM (p)	REM vs NREM (p)
LG	OBr	1.0 ± 0.0	0.48 ± 0.05	0.84 ± 0.10	142.7	**<0.001**	**<0.001**	**< 0.001**	**<0.001**
	M1l	0.89 ± 0.13	0.51 ± 0.11	0.98 ± 0.03	70.9	**<0.001**	**<0.001**	0.122	**<0.001**
	M1r	0.89 ± 0.12	0.52 ± 0.08	0.97 ± 0.04	71.3	**<0.001**	**<0.001**	0.130	**<0.001**
	S1l	0.86 ± 0.15	0.64 ± 0.18	0.95 ± 0.07	13.9	**<0.001**	**0.007**	0.263	**<0.001**
	S1r	0.91 ± 0.15	0.71 ± 0.16	0.96 ± 0.06	12.1	**<0.000**	**0.004**	0.691	**<0.001**
	V2l	1.0 ± 0.0	0.57 ± 0.18	0.81 ± 0.13	38.1	**<0.000**	**<0.000**	**0.003**	**<0.000**
	V2r	0.98 ± 0.03	0.57 ± 0.14	0.78 ± 0.13	36.3	**<0.000**	**<0.000**	**0.001**	**0.001**
HG	OBl	1.0 ± 0.0	0.32 ± 0.10	0.44 ± 0.12	190.1	**<0.001**	**<0.001**	**< 0.001**	**0.001**
	M1r	0.99 ± 0.01	0.33 ± 0.08	0.77 ± 0.16	69.8	**<0.001**	**<0.001**	**0.003**	**<0.001**
	M1l	0.99 ± 0.01	0.36 ± 0.10	0.78 ± 0.12	98.6	**<0.001**	**<0.001**	**< 0.001**	**<0.001**
	S1r	0.99 ± 0.01	0.49 ± 0.10	0.87 ± 0.08	106.3	**<0.001**	**<0.001**	**0.007**	**<0.001**
	S1l	0.99 ± 0.00	0.53 ± 0.09	0.89 ± 0.06	129.1	**<0.001**	**<0.001**	**0.008**	**<0.001**
	V2r	0.99 ± 0.02	0.45 ± 0.15	0.74 ± 0.19	46.8	**<0.001**	**<0.001**	**0.001**	**<0.001**
	V2d	0.99 ± 0.01	0.38 ± 0.17	0.63 ± 0.27	35.4	**<0.001**	**<0.001**	**< 0.001**	**0.011**

The analysis was performed in 9 animals. The degrees of freedom were 2 (between groups) and 16 (within groups). OB, olfactory bulb; M1, primary motor cortex; S1, primary somato-sensory cortex; V2, secondary visual cortex r, right; l, left. W, wakefulness; NREM, non-REM sleep; REM, REM sleep. *, $p < 0.05$.

Table 2. LG normalized coherence during sleep and wakefulness in the rat.

	Descriptive Statistics (NC)			Repeated measures ANOVA		Multiple Comparisons-Tukey		
Electrode pairs	W (mean ± SD)	NREM (mean ± SD)	REM (mean ± SD)	F	Sig. (p)	W vs SWS (p)	W vs REM (p)	REM vs NREM (p)
OBr-M1r	0.91 ± 0.09	0.86 ± 0.12	0.92 ± 0.07	0.9	0.409	0.506	0.994	0.449
OBr-M1l	0.93 ± 0.08	0.86 ± 0.12	0.93 ± 0.07	1.6	0.225	0.285	0.999	0.289
OBr-S1r	0.93 ± 0.07	0.79 ± 0.17	0.82 ± 0.16	2.2	0.135	0.138	0.281	0.898
OBr-S1l	0.93 ± 0.07	0.79 ± 0.15	0.85 ± 0.14	2.4	0.121	0.105	0.401	0.674
OBr-V2r	0.93 ± 0.09	0.90 ± 0.07	0.81 ± 0.16	2.4	0.120	0.870	0.119	0.272
OBr-V2l	0.90 ± 0.09	0.96 ± 0.06	0.83 ± 0.12	4.2	**0.033**	0.370	0.304	**0.025**
M1r-M1l	0.98 ± 0.02	0.95 ± 0.05	0.81 ± 0.09	17.4	**< 0.001**	0.480	**< 0.001**	**0.001**
M1r-S1r	0.98 ± 0.03	0.90 ± 0.05	0.91 ± 0.06	4.4	**0.030**	**0.041**	0.066	0.965
M1r-S1l	0.97 ± 0.04	0.90 ± 0.09	0.80 ± 0.09	11.8	**< 0.001**	0,105	**< 0.001**	**0.042**
M1r-V2r	0.94 ± 0.09	0.94 ± 0.06	0.69 ± 0.12	17.7	**< 0.001**	0,991	**< 0.001**	**< 0.001**
M1r-V2l	0.88 ± 0.08	0.99 ± 0.01	0.68 ± 0.10	31.7	**< 0.001**	**0.031**	**< 0.001**	**< 0.001**
M1l-S1l	0.97 ± 0.03	0.88 ± 0.05	0.92 ± 0.07	4.6	**0.025**	**0.019**	0.275	0.333
M1l-V2l	0.85 ± 0.09	0.99 ± 0.01	0.66 ± 0.11	35.3	**< 0.001**	**< 0.001**	**< 0.001**	**< 0.001**
S1r-M1l	0.98 ± 0.03	0.93 ± 0.06	0.79 ± 0.09	20.4	**< 0.001**	0.296	**< 0.001**	**< 0.001**
S1r-S1l	0.94 ± 0.06	0.97 ± 0.03	0.79 ± 0.10	17.7	**< 0.001**	0.682	**< 0.001**	**< 0.001**
S1r-V2l	0.69 ± 0.13	1.0 ± 0.0	0.59 ± 0.12	77.9	**< 0.001**	**< 0.001**	**0.020**	**< 0.001**
V2r-M1l	0.89 ± 0.13	0.96 ± 0.05	0.73 ± 0.17	8.41	**0.003**	0.544	**0.027**	**0.003**
V2r-S1l	0.77 ± 0.13	1.0 ± 0.0	0.63 ± 0.17	27.1	**< 0.001**	**< 0.001**	**0.041**	**< 0.001**
V2r-V2l	0.61 ± 0.09	1.0 ± 0.0	0.55 ± 0.12	91.4	**< 0.001**	**< 0.001**	0.269	**< 0.001**
S1l-V2l	0.81 ± 0.11	1.0 ± 0.0	0.71 ± 0.06	50.1	**< 0.001**	**< 0.001**	**0.005**	**< 0.001**
S1r-V2r	0.81 ± 0.13	0.98 ± 0.03	0.75 ± 0.15	11.7	**< 0.001**	**0.009**	0.443	**< 0.001**

The analysis was performed in 9 animals. The degrees of freedom were 2 (between groups) and 16 (within groups). OB, olfactory bulb; M1, primary motor cortex; S1, primary somato-sensory cortex; V2, secondary visual cortex r, right; l, left. W, wakefulness; NREM, non-REM sleep; REM, REM sleep. *, $p < 0.05$.

electrode combinations showed the opposite pattern. In adition, NC during W was higher than during REM sleep for eleven combinations while in REM sleep NC was lower than during NREM sleep in fourteen electrode combinations. Interestingly, LG coherence between most of the OB and neocortical combinations were not modified across behavioral states.

For HG, NC also displayed significant differences across behavioral states for nineteen out of twenty-one combinations (Table 3). Coherence was higher during W than during NREM sleep in eighteen combinations, and higher than during REM sleep in nineteen combinations. REM sleep showed lower NC than during NREM sleep in nine combinations of cortical electrodes.

Mean global gamma activity during sleep and wakefulness in the rat: Figure 4A illustrates the MGP, MGC and their difference in nine rats, during the W and sleep. Gamma MGP showed significant differences across behavioral states (LG, $F_{2,16}= 58.1$, $p < 0.001$; HG, $F_{2,16}= 178.1$, $p < 0.001$). Figure 4A reveals that LG MGP did not present significant differences between W and REM sleep. Both during W and REM sleep, LG MGP was higher than during NREM sleep. On the other hand, HG MGP was highest during W, had an intermediate value during REM sleep and reached the minimum value during NREM sleep.

There was a significant difference in MGC across behavioral states (LG, $F_{2,16}= 26.6$, $p < 0.001$; HG, $F_{2,16}= 86.7$, $p < 0.001$). Figure 4B shows that LG MGC did not present significant differences between W and NREM sleep. The lowest values of low and high gamma coherence were present during REM sleep (Figure 4B).

NP-NC was significantly different for low and high gamma bands (LG, $F_{2,16}= 97.1$, $p < 0.001$; HG, $F_{2,16}= 55.3$, $p < 0.001$). During W, the

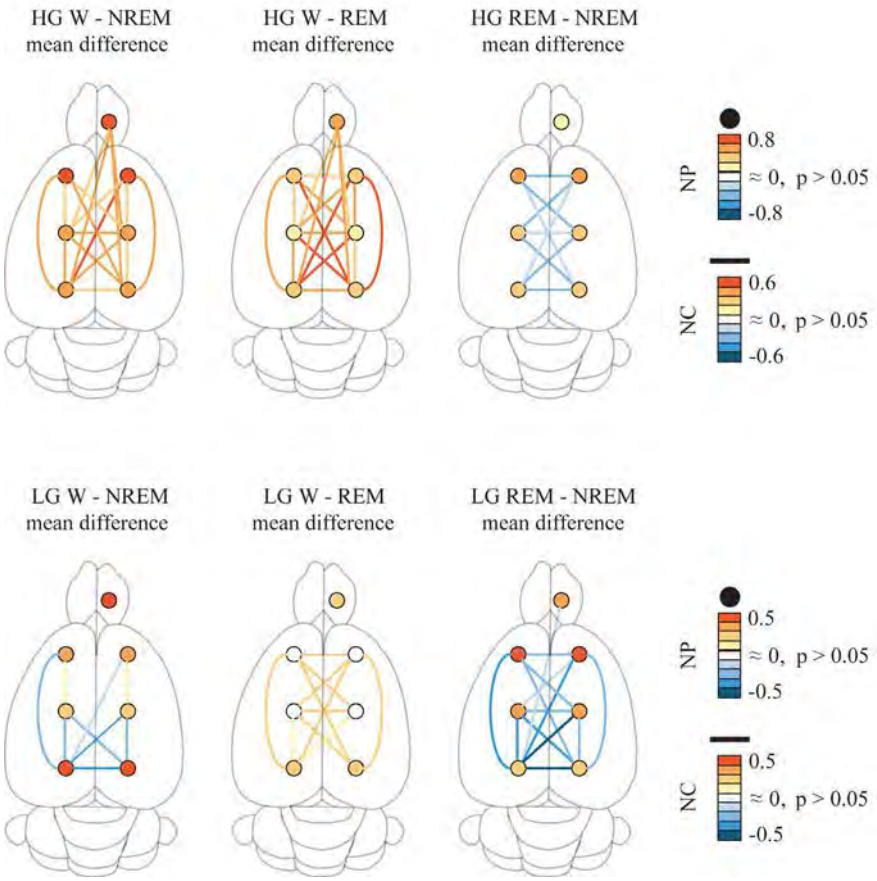

Figure 3. Low (LG) and high gamma (HG) band power and coherence in the rat. Summary of the statistically significant differences between behavioral states of the LG and HG normalized power (NP) and normalized coherence (NC) over the surface of the cerebral cortex. The circles represent the power for the different cortical regions, while the lines represent the coherence for the different combinations of electrodes. The colors represent the mean difference level of NP and NC. Data were obtained from the mean values of all available, non-transitional artifact-free windows per rat for each behavioral state (9 rats). Repeated mesures ANOVA and Tukey paired comparisons tests. OB, olfactory bulb; M1, primary motor cortex; S1, primary somato-sensory cortex; secondary V2, visual cortex.

Table 3. HG normalized coherence during sleep and wakefulness in the rat.

	Descriptive Statistics (NC)			**Repeated measures ANOVA**		**Multiple Comparisons-Tukey**		
Electrode pairs	W (mean ± SD)	NREM (mean ± SD)	REM (mean ± SD)	F	Sig. (p)	W vs SWS (p)	W vs REM (p)	REM vs NREM (p)
OBr-M1r	0.93 ± 0.10	0.76 ± 0.16	0.83 ± 0.16	2.9	0.081	0.0686	0.363	0.580
OBr-M1l	0.93 ± 0.09	0.77 ± 0.12	0.84 ± 0.16	3.5	0.055	0.044	0.325	0.495
OBr-S1r	0.96 ± 0.11	0.64 ± 0.21	0.67 ± 0.22	8.7	**0.002***	**0.004***	**0.008***	0.955
OBr-S1l	0.95 ± 0.13	0.67 ± 0.15	0.72 ± 0.21	6.9	**0.006***	**0.008***	**0.028***	0.806
OBr-V2r	1.0 ± 0.0	0.57 ± 0.19	0.57 ± 0.27	22.1	**< 0.001***	**< 0.001***	**< 0.001***	0.997
OBr-V2l	1.0 ± 0.0	0.60 ± 0.12	0.56 ± 0.18	39.6	**< 0.001***	**< 0.001***	**< 0.001***	0.676
M1r-M1l	0.98 ± 0.03	0.92 ± 0.11	0.74 ± 0.13	12.7	**< 0.001***	0.510	**< 0.001***	**0.005***
M1r-S1r	1.0 ± 0.0	0.72 ± 0.08	0.68 ± 0.08	56.1	**< 0.001***	**< 0.001***	**< 0.001***	0.361
M1r-S1l	0.99 ± 0.01	0.79 ± 0.12	0.63 ± 0.11	38.8	**< 0.001***	**< 0.001***	**< 0.001***	**0.004***
M1r-V2r	0.98 ± 0.05	0.57 ± 0.14	0.52 ± 0.22	26.5	**< 0.001***	**< 0.001***	**< 0.001***	0.805
M1r-V2l	1.0 ± 0.0	0.54 ± 0.12	0.43 ± 0.10	116.5	**< 0.001***	**< 0.001***	**< 0.001***	**0.010***
M1l-S1l	1.0 ± 0.0	0.79 ± 0.08	0.78 ± 0.07	36.4	**< 0.001***	**< 0.001***	**< 0.001***	0.967
M1l-V2l	0.99 ± 0.03	0.59 ± 0.16	0.50 ± 0.13	51.1	**< 0.001***	**< 0.001***	**< 0.001***	0.203
S1r-M1l	1.0 ± 0.0	0.77 ± 0.09	0.56 ± 0.10	89.1	**< 0.001***	**< 0.001***	**< 0.001***	**< 0.001***
S1r-S1l	1.0 ± 0.0	0.68 ± 0.09	0.56 ± 0.04	148.5	**< 0.001***	**< 0.001***	**< 0.001***	**< 0.001***
S1r-V2l	0.98 ± 0.03	0.68 ± 0.17	0.52 ± 0.16	36.6	**< 0.001***	**< 0.001***	**< 0.001***	**0.032***
V2r-M1l	1.0 ± 0.0	0.57 ± 0.15	0.46 ± 0.13	88.4	**< 0.001***	**< 0.001***	**< 0.001***	**0.045***
V2r-S1l	1.0 ± 0.0	0.60 ± 0.16	0.45 ± 0.13	82.3	**< 0.001***	**< 0.001***	**< 0.001***	**0.007***
V2r-V2l	1.0 ± 0.0	0.74 ± 0.16	0.56 ± 0.18	38.4	**< 0.001***	**< 0.001***	**< 0.001***	**0.008***
S1l-V2l	1.0 ± 0.0	0.67 ± 0.12	0.67 ± 0.12	44.9	**< 0.001***	**< 0.001***	**< 0.001***	0.980
S1r-V2r	0.96 ± 0.10	0.76 ± 0.11	0.74 ± 0.13	7.9	**0.004***	**0.013***	**0.006***	0.927

The analysis was performed in 9 animals. The degrees of freedom were 2 (between groups) and 16 (within groups). OB, olfactory bulb; M1, primary motor cortex; S1, primary somato-sensory cortex; V2, secondary visual cortex r, right; l, left. W, wakefulness; NREM, non-REM sleep; REM, REM sleep. *, $p < 0.05$.

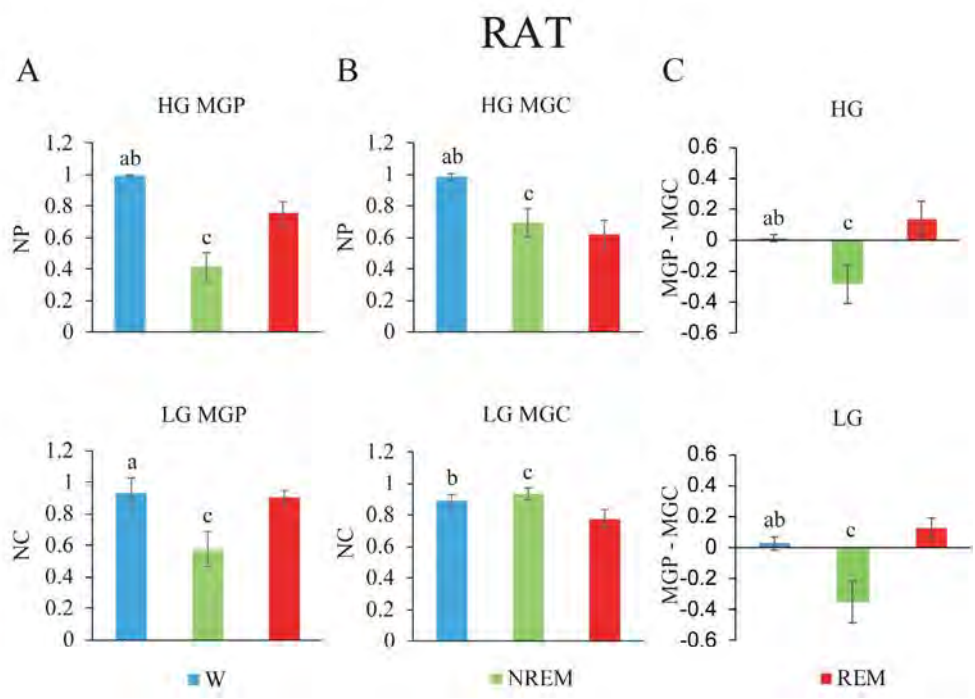

Figure 4. Gamma band mean global power (MGP), mean global coherence (MGC) and their normalized difference during wakefulness and sleep in the rat. A. Low gamma (lower) and high gamma (upper) MGP. B. MGC is depicted. C. Power-coherence difference (NP-NC). The values represent the mean ± standard deviation. Repeated measures ANOVA and Tamhane tests. a, W vs NREM sleep, $p < 0.05$; b, W vs REM sleep, $p < 0.05$; c, NREM sleep vs REM sleep, $p < 0.05$.

value was close to zero, it was negative during NREM sleep and positive during REM sleep (Figure 4C).

Gamma activity in cats

Dynamics of gamma activity in the cat: The dynamic changes in gamma activity in a representative cat are exhibited in Figure 5. The spectrograms and hypnograms of Figure 5A, reflect the different behavioral states of the animal. The NP for the low and high gamma bands was modified along the W-sleep cycle (Figure 5B). Pre-frontal (Pf) and parietal posterior (Pp) NP were highest during AW and decreased progressively during the transition to QW and NREM sleep. During REM sleep, there was a clear increase in the low and high gamma NP in both cortices.

We also analyzed the dynamic changes in gamma NC between Pf and Pp electrodes across behavioral states (Figure 5C). Low and high gamma NC were highest during AW and decreased during QW and NREM sleep to an intermediate value. In contrast to the NP, low and high gamma coherence during REM sleep decreased to its lowest level.

When the NP-NC function was applied (Figure 5D), during AW and QW NP-NC values were close to zero, they decreased to negatives values during NREM sleep, and inverted to positive values during REM sleep.

Gamma activity during sleep and wakefulness in the cat: The analysis in the cat was limited to two cortical areas (anterior and posterior) of the same hemisphere. In cats, the mean NP of the gamma band was different across behavioral states (LG, $F_{2,10}= 132.1$, $p < 0.001$; HG Hz, $F_{2,10}= 36.9$, $p < 0.001$). Figure 6A shows that low and high gamma band power was significantly higher during W than during other states. The minimum level of power was recorded during NREM sleep and reached intermediate values during REM sleep.

These animals showed significant differences in the NC (LG, $F_{2,10}= 46.8$, $p < 0.001$; HG, $F_{2,10}= 56.1$, $p < 0.001$) (Figure 6B). During W, low and high gamma coherence was greater and significantly different compared to the rest of the behavioral states. The lowest values for LG and HG coherence were present during REM sleep.

NP-NC was calculated in the cat. NP-NC was significantly different for the low and high gamma bands across behavioral states (LG Hz, $F_{2,10}= 19.7$, $p < 0.001$; HG, $F_{2,10}= 38.3$, $p < 0.001$) (Figure 6C). During W, NP-NC in LG and HG was nearly zero, while in NREM sleep it presented negative values. Positive values were observed during REM sleep.

Gamma activity during REM sleep transitions: For an in-depth examination of the transitions (t) into and from REM sleep, we analyzed the mean gamma power and mean z'-coherence in 10-second windows in cats (Figure 7) and rats (Figure 8). In both animal models, REM sleep onset was accompanied by a reduction in low and high gamma z'-coherence (Figures 7A and 8A, upper charts). Interestingly, this reduction in gamma coherence tended to precede REM sleep onset by several seconds; we considered EEG activation (desynchronization) as the beginning of REM sleep (time 0). In contrast, at the end of REM sleep episode, z'-coherence increased (Figures 7B and 8B, upper charts).

Low and high gamma power increased during REM sleep onset (Figures 7A and 8A, lower charts). At the end of the REM sleep episodes, on average there was an increase in gamma power (reflecting W) that was followed by a decrease in this parameter (probably driven by NREM sleep) (Figures 7B and 8B, lower charts). A short bout of W (microarousal) followed by NREM sleep, or a sustained period of W, usually followed REM sleep episodes. This phenomenon could determine a more variable low and high gamma power following REM sleep episodes.

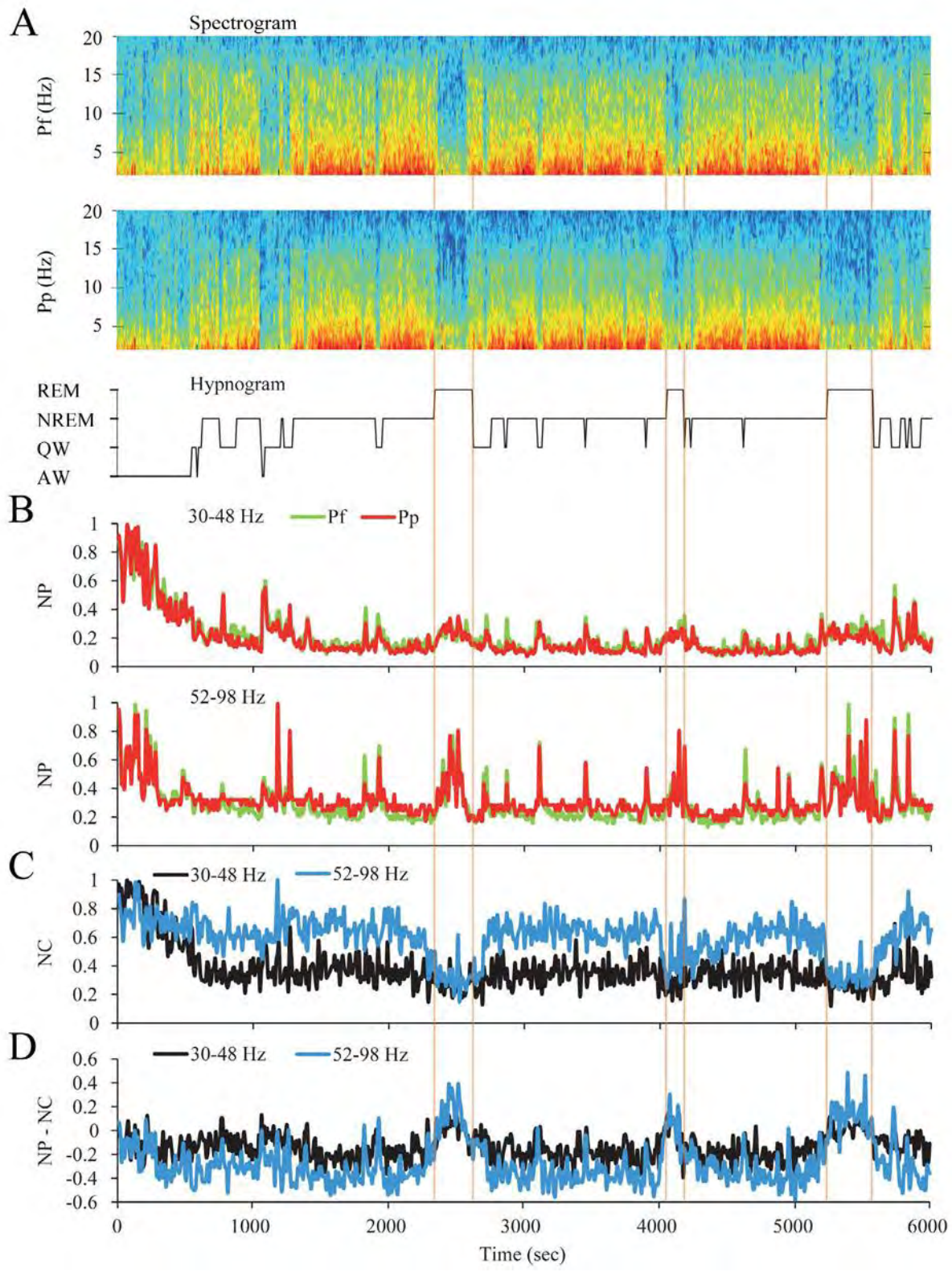

Figure 5. Dynamics of gamma activity in the cat. A. The spectrograms (1-20 Hz) of prefrontal (Pf) and posterior parietal (Pp) cortical recordings and the hypnogram are shown. During W and REM sleep there was weak slow wave activity. During NREM sleep, delta activity (0.5-4 Hz) was more prominent and there were intermittent episodes of sigma activity (9-15 Hz), which correspond to the presence of sleep spindles. Color calibration of the spectrogram is not shown. B. Normalized power (NP) of Pf (green) and Pp (red) cortices for low (upper traces) and high (lower traces) gamma bands are shown. C. Normalized z'-coherence (NC) for both gamma bands (30-48 and 52-98 Hz). D. Power-coherence difference representation (NP-NC) shows near zero values for AW and QW, negative values during NREM sleep and inversion to positives values during REM sleep. All the parameters were analyzed in 10 seconds epochs. AW, alert wakefulness; QW, quiet wakefulness; NREM, NREM sleep; REM, REM sleep.

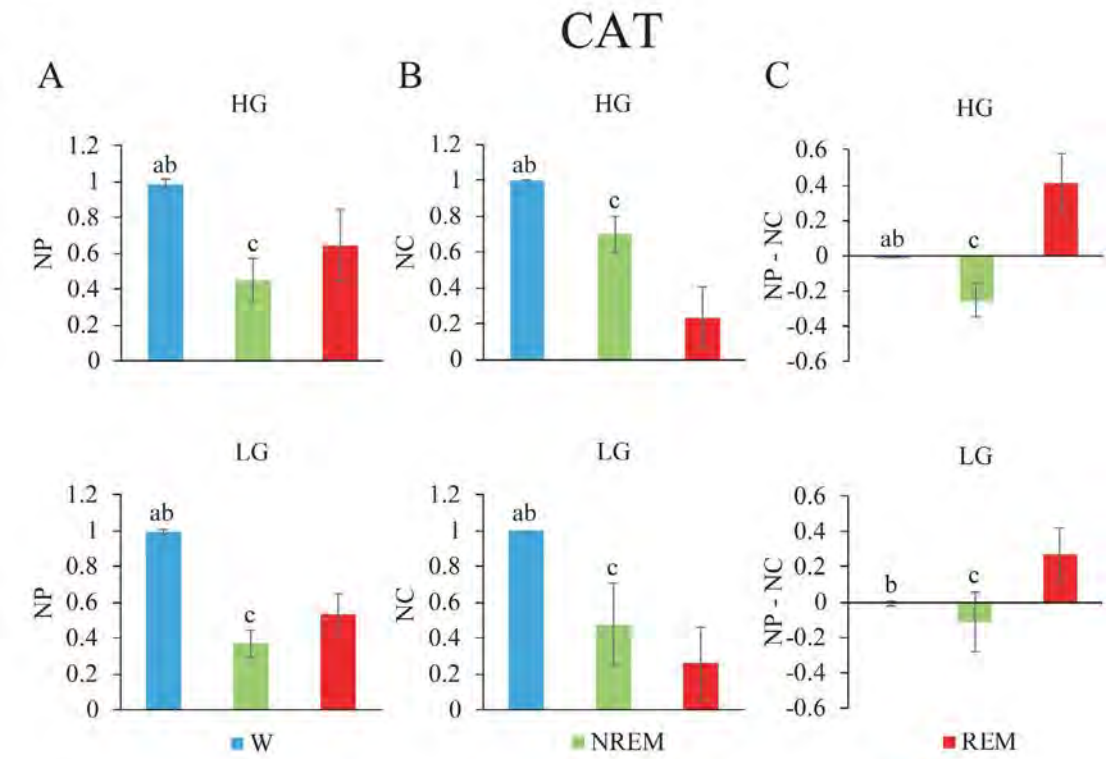

Figure 6. Gamma band normalized power (NP), normalized coherence (NC) and their normalized difference during wakefulness and sleep in the cat. A. Low gamma (lower) and high gamma (upper) mean NP of frontal (f) and posterior (p) electrodes. B. NC between both channels f and p are depicted. C. Power-coherence difference (NP-NC). The values represent the mean ± standard deviation. Repeated measures ANOVA and Tamhane tests. a, W vs NREM sleep, $p < 0.05$; b, W vs REM sleep, $p < 0.05$; c, NREM sleep, vs REM sleep, $p < 0.05$.

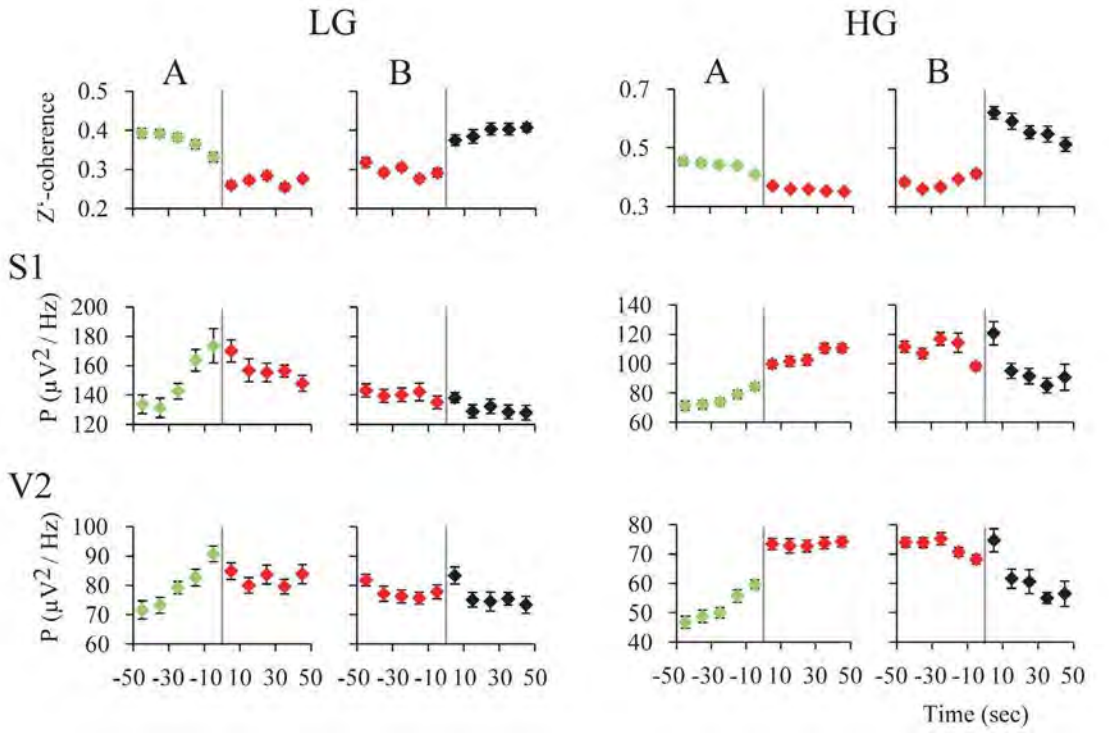

Figure 7. z'-coherence and power during REM sleep transitions in the rat. A. Transition into REM sleep. The graphics depict the mean z'-coherence and power ± standard error for 30-48 and 52-98 Hz, of 30 transitions of one representative rat. Data were taken from recordings of primary somatosensory (S1) and secondary visual (V2) cortices. Change of colors and the vertical line indicate the phase transition. NREM sleep episodes are symbolized in green; REM sleep episodes in red. B. Transition out of REM sleep. The mean z'-coherence and power ± standard error for 30-48 and 52-98 Hz, of 30 transitions of the same rat are shown. Red to black transition indicates the end of the REM sleep episode. The states indicated in black were mainly micro-awakenings but some NREM sleep episodes also followed REM sleep.

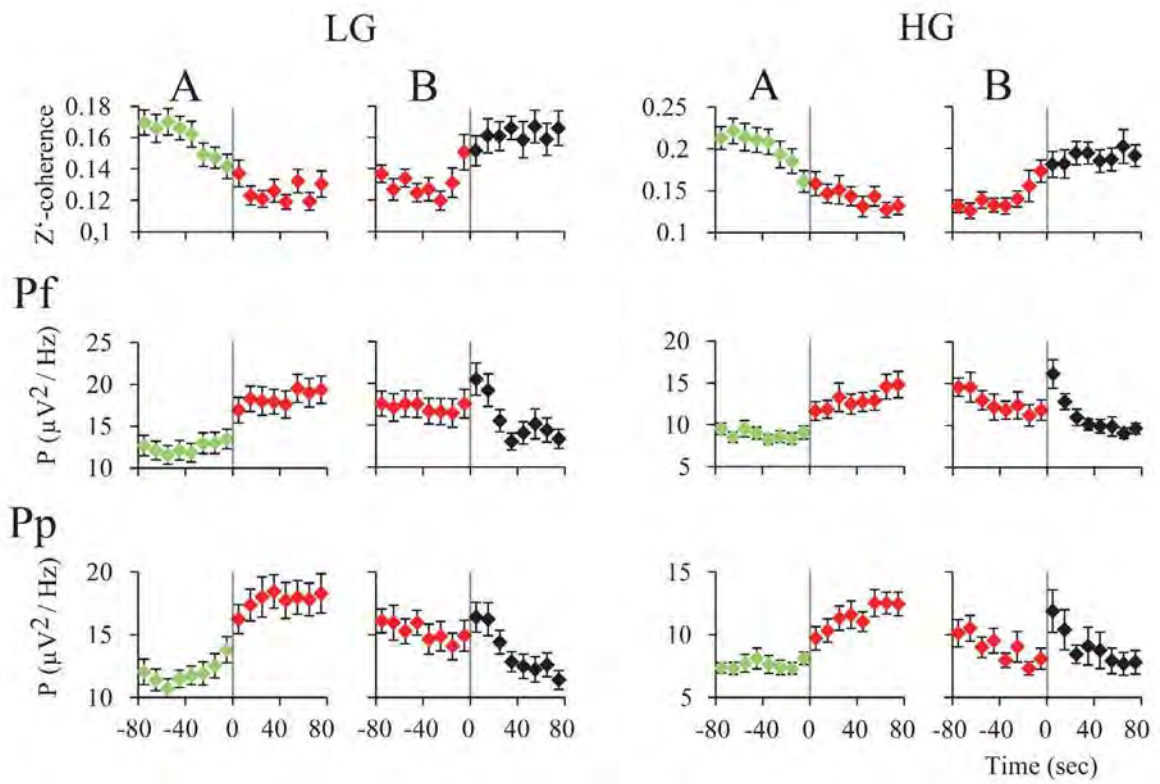

Figure 8. z'-coherence and power during REM sleep transitions in the cat. A. Transition into REM sleep. The graphics represent the mean z'-coherence and power ± standard error for 30-48 and 52-98 Hz, of 30 transitions of one representative cat. Data were taken from recordings of prefrontal (Pf) and posterior parietal (Pp) cortices. Change of colors and the vertical line indicate the phase transition. NREM episodes are symbolized in green; REM sleep episodes in red. B. Transition out of REM sleep. The mean z'-coherence and power ± standard error for 30-48 and 52-98 Hz, of 30 transitions of the same cat are shown. Red to black transition indicates the end of the REM sleep episode. The states indicated in black were mainly micro-awakenings but some NREM sleep episodes also followed REM sleep.

The main relationships during W and sleep between gamma power, reflecting local or short-range synchronization, and gamma coherence, representing distant or large-range coupling, is schematized in Figure 9. High short (local) and long-range (distant) gamma coupling is present during W. In contrast, high local gamma synchronization with long-range gamma uncoupling is present during REM sleep.

Discussion

In the present study, we performed a thorough analysis of gamma power and coherence in rat neocortical areas and OB; and we also performed a more spatially-limited analysis in the cat. The main result of this report is the demonstration in two different animal models (rats and cats), that during REM sleep there was a strong local (short-range) synchronization of the neural population in both gamma (30-48 and 52-98 Hz) frequency bands, while this synchronization was strongly reduced between distant areas. These data suggest that during REM sleep, in spite of a local activated state, high-frequency functional interactions between different cortical regions are lost (or highly diminished).

The relationship between local and distant gamma synchronization was further explored utilizing the gamma NP-NC function as an index (Figures 4 and 6). This index reflects the difference between the normalized power (reflecting local or short-range synchronization) and normalized coherence (distant areas or long-range synchronization); which was close to zero during W, consisted of negative values during NREM sleep, while positive values were found during REM sleep. Therefore, this index of gamma activity was capable of differentiating between W, NREM sleep, and REM sleep both in cats and rats.

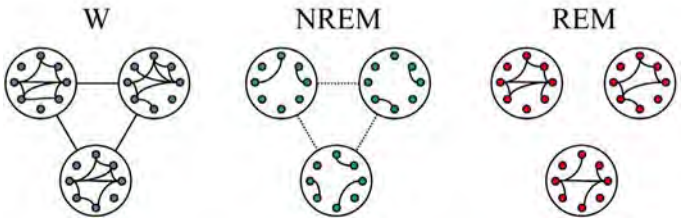

Figure 9. Schematic representation of the short and long-range gamma synchronization during wakefulness (W), NREM sleep and REM sleep. The small circles represent neurons while large circles represent the areas of the cortex where these neurons are located. Colors of neurons represent the behavioral states (blue, W; green, NREM sleep; red, REM sleep) and connecting lines between the circles represent gamma synchronization between distant cortical areas. Short-range (local) and long-range (distant) gamma synchronization occurs during W. During NREM sleep both short and long-range gamma synchronization decrease. During REM sleep, while gamma synchronization is present at local level, distant gamma coupling is absent.

Gamma power and coherence during wakefulness and NREM sleep

It is well established that gamma power and gamma intra-hemispheric coherence is high during W in cats, rats, and humans [21-23,25,39,44]. In the cat, gamma band coherence increases during alert W; a fact that can be clearly observed in raw recordings [39]. Gamma coherence is also high during cataplexy (W with REM sleep atonia) induced by carbachol microinjections into the nucleus pontis oralis (NPO) of the cat [41].

In the present report, we extend previous data in rats [23], showing the cortical extent of gamma power and coherence. As shown in Figure 3, low and high gamma power is higher in W than in NREM sleep and

REM sleep in most of the neocortical areas and OB. The exemption was that low gamma power during W and REM sleep was similar in frontal and parietal cortices (Figure 3).

Coherence for high gamma during W was higher than during NREM sleep and REM sleep across all the combinations of cortical loci. However, low gamma coherence differences between W and NREM sleep varied between different cortices (Figure 4) [23].

Gamma power and coherence during REM sleep

In the present report, we demonstrated in rats and cats that gamma coherence reached a nadir during REM sleep. In the rat, high and low gamma coherence decreased in most combinations of electrodes in comparison to W and NREM sleep (Figure 3). However, the power in this frequency band increased compared to NREM sleep. This power-coherence relationship was also readily observed in the dynamic analysis (Figures 2 and 5), as well as in the transition into and out REM sleep (Figure 7 and 8).

This result is in accordance with the results of our previous analyses in cat [39] and rat [23]. Interestingly, gamma coherence is also lost during REM sleep induced by carbachol microinjections into the NPO of the cat [41].

In preliminary studies in human newborns, cortical gamma coherence was almost absent during REM sleep [45]. The demonstration that there is a reduction in gamma coherence between different cortical regions during REM sleep was also shown in adult humans [20,33,46]. In addition, Voss et al. (2009) demonstrated that gamma coherence during lucid dreaming was intermediate between W and REM sleep [33].

As with other EEG rhythms, gamma oscillations remain remarkably conserved in mammals irrespective of brain size [47]. The decrease in gamma coherence during REM sleep in rats, cats and humans, indicates that during this behavioral state there is a decrease in the capacity for integration across different cortices within this high frequency band, despite high local activity at these frequencies.

A recent study demonstrated that scalp fronto-temporal electrical stimulation in the lower gamma band (≈40 Hz) during REM sleep influences ongoing brain activity and induces self-reflective awareness (a feature of W) in dreams (i.e., lucid dreams), while other stimulation frequencies were not effective [32]. Thus, the data support the concept that synchronous long-range oscillations of ≈40 Hz are an electrophysiological pattern of activity that is indicative of attentive wakefulness. On the contrary, the reduction in gamma coherence during REM sleep together with increased local gamma activity (accompanied by a decrease in low frequency activity), may underlie the unique pattern of REM sleep mentation, i.e., dreams [17,18,48]. During NREM sleep the decrease in local and a small reduction in distant gamma coupling accompanied by an increase in low frequency oscillations (delta waves) and sleep spindles, may be the neurophysiological foundation for the reduction or absence of oneiric activity during deep NREM sleep. Interestingly, Siclari *et al.*, (2017) have demonstrated that reports of dream experience in either REM sleep and NREM sleep were associated with decreases in delta power and increases in gamma power (25-50 Hz) mainly in posterior cortical regions [48].

Gamma power and coherence in the OB during W and sleep

It is well established that local slow field potentials in the OB are associated with breathing, and these oscillations would aid in the exchange of information between olfactory areas and other parts of the brain [49-51]. These respiratory potentials in the OB reflect respiratory rhythms during W and REM sleep, but not during NREM sleep [52], and entrain gamma oscillations in the OB as well as in other areas of the brain [11,14,15,53].

Our data show that in the OB, the maximum gamma power is present during W, decreases during NREM sleep, and increases to intermediate values during REM sleep. LG coherence between OB and most neocortical areas did not differ across behavioral states (Figure 3 and Table 2). However, HG coherence between the OB and medial and posterior areas of neocortex was higher during W than sleep (Figure 3 and Table 3). New studies are needed to shed light in the functional interrelation between the OB and neocortical areas during W and sleep.

Gamma coherence and the waking-promoting systems

Cognitive activity and different EEG rhythms are generated by the activity of cortical and thalamic neurons, which are reciprocally connected [29,54]. Gamma-band rhythmogenesis is also inextricably tied to perisomatic inhibition in the neocortex, wherein the key ingredient is $GABA_A$ receptor-mediated inhibition [12]. However, both neocortical gamma power and coherence during W and sleep are modulated by the activating or waking-promoting systems of the brainstem, hypothalamus and basal forebrain that directly or indirectly project to the thalamus and/or cortex [55,56]. By regulating thalamo-cortical activities, these activating systems produce electrographic and behavioral arousal.

The activating systems decrease their activity during the NREM sleep. However, the activity of the various components of these systems differs markedly during REM sleep. While most monoaminergic systems decrease their firing rate during REM sleep (REM-off neurons), cholinergic neurons increase their discharge during this behavioral state (REM-on neurons), which contributes to the cortical activation [55,56]. Therefore, it is expected that cholinergic REM-on neurons, whose soma are located in the mesopontine and basal forebrain region, may contribute in the promotion of local gamma synchronization (gamma power). In addition, because these cholinergic neurons turn on during REM sleep, they should not be critical to the generation of gamma coherence (distant coupling), which is absent during this state. In fact, systemic muscarinic antagonists do not block gamma coherent activity [57].

Noradrenergic, serotonergic and histaminergic neurons that are active during W [55,56], may be crucial in promoting gamma coherence during this behavioral state. Their lack of activity during REM sleep may be involved in the absence of gamma coherence during this state.

Other neuronal systems, such as hypocretinergic and dopaminergic neurons that are active during W, as well as GABAergic or glutamatergic neurons which are located in the mesopontine reticular formation and basal forebrain, may also contribute to the profile of gamma activity during W and sleep [55,56]. In fact, Kim *et al*., [58], highlighted the role of cortical-projecting GABAergic neurons of the basal forebrain in the generation of gamma oscillations in the EEG [58]. In addition, the authors suggest that cholinergic neurons within this area are not critical for the generation of these oscillations.

It is important to note that firing within the gamma band range is present in different sites of the reticular activating system, including the pedunculo-pontine tegmental nucleus (PPN) [59]. In this area, gamma oscillations are modulated by two independent pathways related to different Ca2+ channel types which suggests different ways

of modulating waking and REM sleep [60,61]. This subcortical gamma activity possibly contribute to "bottom up" neocortical gamma activity during W and REM sleep [62].

Local and distant gamma coupling relationship

The NP-NC index clearly shows that short and long-range gamma synchronization is deeply modified across behavioral states; this fact is illustrated in the model presented in Figure 9. As discussed above, this electrophysiological phenomenon could be related to the cognitive features that characterize W, NREM sleep and REM sleep. Moreover, NREM sleep and REM sleep dream content, and different drugs or processes that affect cognition, must all modify the NP-NC index. We hypothesize that dissociative drugs such as ketamine, or psychiatric conditions such as psychosis, will also increase the index values as in REM sleep. Finally, this NP-NC index, that signals the presence of REM sleep, should be applied to confirm the absence of REM sleep in aquatic mammals, that for its obligate swimming behavior during sleep do not have REM sleep atonia [63-65].

Conclusions

During REM sleep, despite a locally activated EEG, there is uncoupling of gamma frequency oscillations between distant neocortical sites. In spite of regional variations, this gamma activity pattern extends, in rats, from the posterior cortices to the OB. Therefore, although local gamma coupling is similar to W, functional interactions among different cortical area, which are critical for cognitive functions, are radically different during REM sleep. Since this feature is conserved in rats, cats and likely in humans, we consider that this short-range gamma coupling along with gamma long-range uncoupling during REM sleep is a defining trait of REM sleep in mammals.

Acknowledgement

This study was partially supported by a grant of the Comisión Sectorial de Investigación Científica (CSIC) and the "Programa de Desarrollo de Ciencias Básicas, PEDECIBA". S. Castro, A. Mondino and M. Cavelli currently have a postgraduate fellowship from the Agencia Nacional de Investigación en Innovación (ANII) and Comisión de Apoyo a Postgrados (CAP), respectively.

Competing interests

All the authors declare no conflict of interest.

Author contributions

Financial support. P.T., A.F., M.C.

Experimental design. M.C., P.T., S.CZ.

Experimental procedures. M.C., S.CZ., A.M., J.G., P.T.

Analysis of the data. M.C., S.CZ., A.M., J.G.

Discussion and interpretation of the data. M.C., P.T., S.CZ., A.M., J.G., A.F.

Wrote the manuscript. M.C., P.T.

All the authors participated in critical revision the manuscript, added important intellectual content, and approved the definitive version.

References

1. Singer W (2015) Complexity as Substrate for Neuronal Computations. Acad Sci. Pontif. City, Vatican. PP: 1-10.
2. Singer W (2007) Binding by synchrony. *Scholarpedia* 2: 1657.
3. von der Malsburg C, Schneider W (1986) A neural cocktail-party processor. *Biol Cybern* 54: 29-40. [Crossref]
4. von der Malsburg C (1995) Binding in models of perception and brain function. *Curr Opin Neurobiol* 5: 520-526. [Crossref]
5. Singer W (1999) Neuronal Synchrony?: A Versatile Code for the Definition of Relations?? Most of our knowledge about the functional organization. *Neuron* 24: 49-65.
6. Varela F, Lachaux JP, Rodriguez E, Martinerie J (2001) The brainweb: phase synchronization and large-scale integration. *Nat Rev Neurosci* 2: 229-239. [Crossref]
7. Eckhorn R, Bauer R, Jordan W, Brosch M, Kruse W, et al. (1988) Coherent oscillations: a mechanism of feature linking in the visual cortex? Multiple electrode and correlation analyses in the cat. *Biol Cybern* 60: 121-130. [Crossref]
8. Gray CM, König P, Engel AK, Singer W (1989) Oscillatory responses in cat visual cortex exhibit inter-columnar synchronization which reflects global stimulus properties. *Nature* 338: 334-337.
9. Fries P (2005) A mechanism for cognitive dynamics: neuronal communication through neuronal coherence. *Trends Cogn Sci* 9: 474-480. [Crossref]
10. Jasper HH, Andrews HL (1938) Brain potentials and voluntary muscle activity in man. *J Neurophysiol* 1: 87-100.
11. Adrian ED (1942) Olfactory reactions in the brain of the hedgehog. *J Physiol* 100: 459-473. [Crossref]
12. Buzsáki G, Wang XJ (2012) Mechanisms of gamma oscillations. *Annu Rev Neurosci* 35: 203-225. [Crossref]
13. Rieder MK, Rahm B, Williams JD, Kaiser J (2011) Human Î³-band activity and behavior. *Int J Psychophysiol* 79: 39-48. [Crossref]
14. Rojas-Líbano D, Kay LM (2008) Olfactory system gamma oscillations: the physiological dissection of a cognitive neural system. *Cogn Neurodyn* 2: 179-194.
15. Freeman WJ, Schneider W (1982) Changes in spatial patterns of rabbit olfactory EEG with conditioning to odors. *Psychophysiology* 19: 44-56. [Crossref]
16. Uhlhaas PJ, Pipa G, Lima B, Melloni L, Neuenschwander S, et al. (2009) Neural synchrony in cortical networks?: history , concept and current status. *Front Integr Neurosci* 3: 1-19.
17. Hobson JA (2009) REM sleep and dreaming: towards a theory of protoconsciousness. *Nat Rev Neurosci* 10: 803-813. [Crossref]
18. Nir Y, Tononi G (2010) Dreaming and the brain: from phenomenology to neurophysiology. *Trends Cogn Sci* 14: 88-100. [Crossref]
19. Gottesmann C (2006) The dreaming sleep stage: a new neurobiological model of schizophrenia? *Neuroscience* 140: 1105-1115. [Crossref]
20. Cantero JL, Atienza M, Madsen JR, Stickgold R (2004) Gamma EEG dynamics in neocortex and hippocampus during human wakefulness and sleep. *Neuroimage* 22: 1271-1280. [Crossref]
21. Llinás R, Ribary U (1993) Coherent 40-Hz oscillation characterizes dream state in humans. *Proc Natl Acad Sci U S A* 90: 2078-2081. [Crossref]
22. Maloney KJ, Cape EG, Gotman J, Jones BE (1997) High-frequency gamma electroencephalogram activity in association with sleep-wake states and spontaneous behaviors in the rat. *Neuroscience* 76: 541-555.
23. Cavelli M, Castro S, Schwarzkopf N, Chase MH, Falconi A, et al. (2015) Coherent neocortical gamma oscillations decrease during REM sleep in the rat. *Behav Brain Res* 281: 318-325.
24. Buzsáki G, Anastassiou CA, Koch C (2012) The origin of extracellular fields and currents--EEG, ECoG, LFP and spikes. *Nat Rev Neurosci* 13: 407-420. [Crossref]
25. Chrobak JJ, Buzsáki G (1998) Gamma oscillations in the entorhinal cortex of the freely behaving rat. *J Neurosci* 18: 388-398. [Crossref]
26. Bullock TH, McClune MC (1989) Lateral coherence of the electrocorticogram: a new measure of brain synchrony. *Electroencephalogr Clin Neurophysiol* 73: 479-498. [Crossref]
27. Bullock TH, McClune MC, Achimowicz JZ, Iragui-Madoz VJ, Duckrow RB, et al. (1995) Temporal fluctuations in coherence of brain waves. *Proc Natl Acad Sci U S A* 92: 11568-11572. [Crossref]

28. Cantero JL, Atienza M, Salas RM (2000) Valor clínico de la coherencia EEG como índice electrofisiológico de conectividad córtico-cortical durante el sueño. *Rev Neurol* 31: 442-454.

29. Llinás R, Ribary U, Contreras D, Pedroarena C (1998) The neuronal basis for consciousness. *Philos Trans R Soc Lond B Biol Sci* 353: 1841-1849. [Crossref]

30. Hadjipapas A, Hillebrand A, Holliday IE, Singh KD, Barnes GR (2005) Assessing interactions of linear and nonlinear neuronal sources using MEG beamformers: a proof of concept. *Clin Neurophysiol* 116: 1300-1313. [Crossref]

31. Melloni L, Molina C, Pena M, Torres, W. Singer, E. Rodriguez (2007) Synchronization of neural activity across cortical areas correlates with conscious perception. *J Neurosci* 27: 2858-2865.

32. Voss U, Holzmann R, Hobson A, Paulus W, Koppehele-Gossel J, et al. (2014) Induction of self awareness in dreams through frontal low current stimulation of gamma activity. *Nat Neurosci* PP: 1-5.

33. Voss U, Holzmann R, Tuin I, Hobson JA (2009) Lucid dreaming: a state of consciousness with features of both waking and non-lucid dreaming. *Sleep* 32: 1191-1200. [Crossref]

34. John ER (2002) The neurophysics of consciousness. *Brain Res Brain Res Rev* 39: 1-28. [Crossref]

35. Mashour GA (2006) Integrating the science of consciousness and anesthesia. *Anesth Analg* 103: 975-982. [Crossref]

36. Pal D, Silverstein BH, Lee H, Mashour GA (2016) Neural Correlates of Wakefulness, Sleep, and General Anesthesia: An Experimental Study in Rat. *Anesthesiology* 125: 929-942. [Crossref]

37. Uhlhaas PJ, Singer W (2010) Abnormal neural oscillations and synchrony in schizophrenia. *Nat Rev Neurosci* 11: 100-113. [Crossref]

38. Sun Y, Farzan F, Barr MS, Kirihara K, Fitzgerald PB, et al. (2011) Î³ oscillations in schizophrenia: mechanisms and clinical significance. *Brain Res* 1413: 98-114. [Crossref]

39. Castro-Zaballa S, Falconi A, Chase MH, Torterolo P (2013) Coherent neocortical 40-Hz oscillations are not present during REM sleep. *Eur J Neurosci* 37: 1330-1339.

40. Castro-Zaballa S, Cavelli M, Vollono P, Chase MH, Falconi A, et al. (2014) Inter-hemispheric coherence of neocortical gamma oscillations during sleep and wakefulness. *Neurosci Lett* 578: 197-202.

41. Torterolo P, Castro-Zaballa S, Cavelli M, Chase MH, Falconi A (2016) Neocortical 40 Hz oscillations during carbachol-induced rapid eye movement sleep and cataplexy. *Eur J Neurosci* 43: 580-589.

42. Bullock TH, Buzsáki G, McClune MC (1990) Coherence of compound field potentials reveals discontinuities in the CA1-subiculum of the hippocampus in freely-moving rats. *Neuroscience* 38: 609-619.

43. Benedetto L, Rodriguez-Servetti Z, Lagos P, D'Almeida V, Monti JM, et al. (2013) Microinjection of melanin concentrating hormone into the lateral preoptic area promotes non-REM sleep in the rat. *Peptides* 39: 11-15.

44. Steriade M, Amzica F, Contreras D (1996) Synchronization of fast (30-40 Hz) spontaneous cortical rhythms during brain activation. *J Neurosci* 16: 392-417.

45. Castro S, Cavelli M, Torterolo P, Falconi A, Rava M, et al. (2014) Congr Int Neuropediatría Colonia.

46. Pérez-Garci E, del-Río-Portilla Y, Guevara M, Arce C, Corsi-Cabrera M (2001) Paradoxical sleep is characterized by uncoupled gamma activity between frontal and perceptual cortical regions. *Sleep* 24: 118-126.

47. Buzsáki G, Logothetis N, Singer W (2013) Scaling brain size, keeping timing: Evolutionary preservation of brain rhythms. *Neuron* 80: 751-764.

48. Siclari F, Baird B, Perogamvros L, et al. (2017) The neural correlates of dreaming. *Nat Neurosci* 20: 872-878. [Crossref]

49. Rojas-Líbano D, Frederick DE, Egaña JI, Kay LM (2014) The olfactory bulb theta rhythm follows all frequencies of diaphragmatic respiration in the freely behaving rat. *Front Behav Neurosci* 8: 214.

50. Lockmann AL, Laplagne DA, Leão RN, Tort AB (2016) A Respiration-Coupled Rhythm in the Rat Hippocampus Independent of Theta and Slow Oscillations. *J Neurosci* 36: 5338-5352. [Crossref]

51. Nguyen Chi V, Muller C, Wolfenstetter T, Yanovsky Y, Draguhn A, et al. (2016) Hippocampal Respiration-Driven Rhythm Distinct from Theta Oscillations in Awake Mice. *J Neurosci* 36: 162-177.

52. Jessberger J, Zhong W, Brankack J, Draguhn A (2016) Olfactory Bulb Field Potentials and Respiration in Sleep-Wake States of Mice. *Neural Plast* 2016: 1-9.

53. Zhong W, Ciatipis M, Wolfenstetter T, Jessberger J, Müller C, et al. (2017) Selective entrainment of gamma subbands by different slow network oscillations. *Proc Natl Acad Sci U. S. A.*.

54. Llinás R, Ribary U (2001) Consciousness and the brain. The thalamocortical dialogue in health and disease. *Ann N Y Acad Sci* 929: 166-175. [Crossref]

55. Torterolo P, Vanini G (2010) [New concepts in relation to generating and maintaining arousal]. *Rev Neurol* 50: 747-758. [Crossref]

56. Torterolo P, Monti JM, Pandi-Perumal S (2016) Synposis Sleep Med., Apple Academic Press, pp. 1-22.

57. Castro s, Cavelli M, Falconi A, Torterolo P (2016) 23rd Congr Eur Sleep Res Soc Bol, Italy.

58. Kim T, Thankachan S, McKenna JT, McNally JM, Yang C, et al. (2015) Cortically projecting basal forebrain parvalbumin neurons regulate cortical gamma band oscillations. *Proc Natl Acad Sci* 201413625.

59. Garcia-Rill E, Luster B, D'Onofrio S, Mahaffey S, Bisagno V, et al. (2016) Implications of gamma band activity in the pedunculopontine nucleus. *J Neural Transm (Vienna)* 123: 655-665. [Crossref]

60. Luster B1, D'Onofrio S, Urbano F, Garcia-Rill E (2015) High-threshold Ca2+ channels behind gamma band activity in the pedunculopontine nucleus (PPN). *Physiol Rep* 3. [Crossref]

61. Luster br, Urbano FJ, Garcia-rill E (2016) Intracellular mechanisms modulating gamma band activity in the pedunculopontine nucleus (PPN). *Physiol Rep* 4: 1-16.

62. Garcia-Rill E (2017) Bottom-up gamma and stages of waking. *Med Hypotheses* 104: 58-62. [Crossref]

63. Lyamin OI, Kosenko PO, Lapierre JL, Mukhametov LM, Siegel JM (2008) Fur seals display a strong drive for bilateral slow-wave sleep while on land. *J Neurosci* 28: 12614-12621. [Crossref]

64. Lyamin OI, Manger PR, Ridgway SH, Mukhametov LM, Siegel JM (2008) Cetacean sleep: an unusual form of mammalian sleep. *Neurosci Biobehav Rev* 32: 1451-1484. [Crossref]

65. Madan V, Jha SK (2012) Sleep alterations in mammals: did aquatic conditions inhibit rapid eye movement sleep? *Neurosci Bull* 28: 746-758. [Crossref]

Una de las principales diferencias entre la vigilia y el sueño es el tono muscular. El tono muscular es máximo durante la vigilia y cae durante el sueño NREM para luego prácticamente desaparecer durante el sueño REM pudiendo observarse algunas sacudidas esporádicas de los músculos o “twiches” (Chase et al., 1989; Torterolo and Vanini, 2010). Por otra lado, la actividad muscular es el principal artefacto eléctrico que contamina los registros de LFP, ECoG y EEG (Buzsáki and Schomburg, 2015). Para descartar que los artefactos musculares fueran los responsables de los resultados obtenidos hasta el momento, llevamos a cabo una serie de experimentos donde apagamos la actividad muscular durante la vigilia y el sueño REM. La microinyección de carbacol (agonista colinérgico) en el núcleo pontis oralis (NPO) causa que los animales alternen entre estados de cataplexia (CA; vigilia con atonía) y sueño REM inducido por carbacol (REMc; también, con atonía) durante 30 minutos a 2 horas luego de la microinyección. Encontramos que, aunque los animales presentan atonía muscular en ambos estados, la coherencia gamma es máxima durante la cataplejía y prácticamente desaparece durante el REMc. Estos resultados son idénticos a los observados durante la vigilia y el sueño REM natural, y se pueden observar en el **Anexo 2** (Torterolo et al., 2016a)).

En otra serie de trabajos tratamos a las ratas con uretano, un anestésico no tradicional, con el motivo de averiguar qué sucede con la potencia y coherencia gamma durante la anestesia. Encontramos que tanto la potencia como la coherencia caen durante la narcosis (inconsciencia) inducida por esta sustancia (Santana et al., 2017, 2015). Estos resultados son similares a los previamente publicados para anestésicos tradicionales como barbitúricos e isoflurano (John, 2002; Mashour, 2006; Pal et al., 2016).

Por otro lado, y como mencionáramos en la sección **1.3.**, la hipofunción de los receptores NMDA mediante diversos bloqueantes (ketamina o MK-801) a dosis sub-anestésica, es considerado un modelo farmacológico válido para el estudio de las bases neurobiológicas de las enfermedades del espectro psicótico (Javitt & Zukin, 1991; Moghaddam & Jackson, 2003; Rung et al., 2005). Utilizando dosis sub-anestésica de ketamina (modelo farmacológico de psicosis) observamos un estado electrográfico similar al sueño REM con alta potencia y baja coherencia gamma, aunque los animales se encuentren comportamentalmente despiertos. Estos resultados se observan en la **Figura C1.1** y el **Anexo 3** (Castro-Zaballa et al., 2018). Esta caída en las interacciones funcionales entre áreas de la corteza podría estar relacionado con las características cognitivas compartidas entre las ensoñaciones y la psicosis.

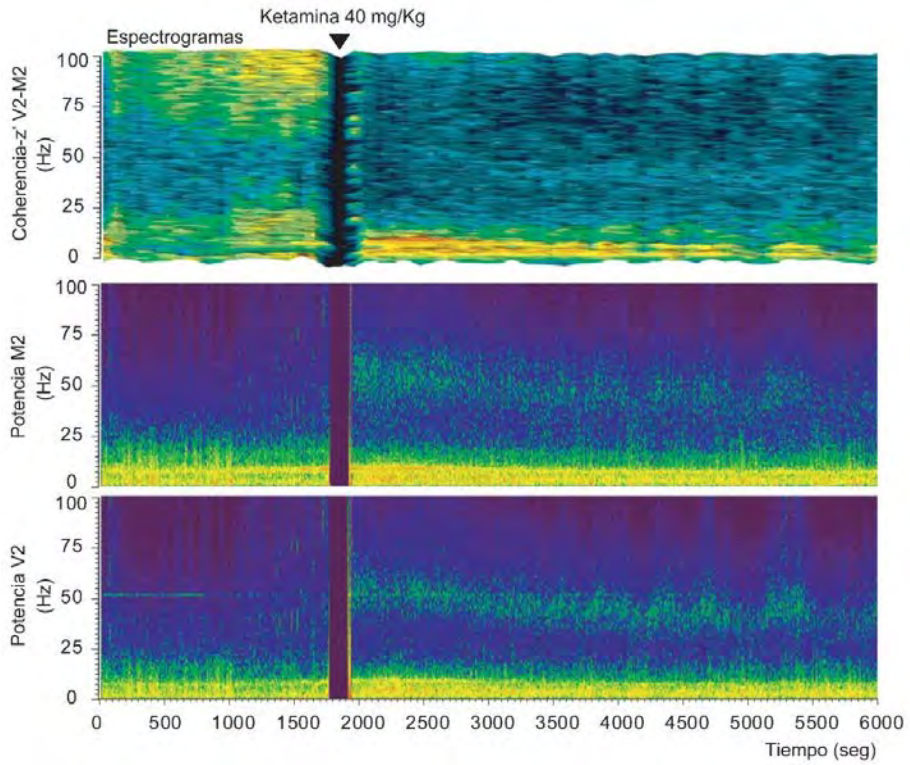

Figura C1.1. Cambios dinámicos de la coherencia y potencia gamma durante la vigilia y los efectos de la aplicación sistémica de ketamina en la rata. Durante la vigilia se inyecta ketamina a dosis sub-anestésicas (15 mg/kg; flecha). Enseguida se observa un pico de potencia gamma en cada espectrograma (0-100 Hz) de cada corteza registrada. Esta actividad se encuentra en el entorno de los 50 Hz, pero se extiende en todo el espectro gamma. Tanto en la vigilia como en los espectrogramas post inyección se puede observar claramente la actividad theta (4-9 Hz) característica de la vigilia activa y del sueño REM (Cavelli, 2015). El registro superior corresponde al espectrograma de coherencia entre las cortezas mostradas en los espectrogramas de potencia (espectrogramas inferiores). Aquí se aprecian picos de coherencia gamma antes de la inyección correspondientes con el ingreso de los investigadores a la sala de registro. Posterior a la inyección se observa una caída marcada de la coherencia gamma en todo su espectro la cual se mantiene durante todo el registro. Por otra parte, la potencia y coherencia theta se mantiene e incluso se incrementa post inyección similar a lo que se observa durante el sueño REM. Corteza visual secundaria (V2) y motora secundaria (M2). La calibración relativa de ambos espectrogramas utiliza los colores tendientes al rojo como mayores valores y menores valores las tendencias al azul y el negro (Tesis de Maestría (Cavelli, 2015)).

Luego de evidenciar que la actividad gamma y específicamente la coherencia gamma es un fenómeno fuertemente vinculado a la vigilia, comenzamos a indagar sobre cuáles serían los sistemas de neuromodulación implicados en la generación y el mantenimiento de la actividad gamma. En este sentido encontramos que el bloqueo la actividad colinérgica (parte importante de los denominados sistemas activadores (Torterolo et al., 2016b; Torterolo and Vanini, 2010)) muscarínica no abole la potencia ni la coherencia gamma, aunque el efecto de esta droga genere ondas lentas y husos de sueño durante

la vigilia, similares a los observados durante el sueño lento normal (Ver **Anexo 4** (Castro-Zaballa et al., 2019).

Por último, en el capítulo "Arousal and normal conscious cognition" del libro "Arousal in Neurological and Psychiatric Disease" discutimos estos trabajos en relación a los procesos neurofisiológicos que son capaces de generan y mantener el estado de conciencia, así como sus alteraciones en varios trastornos psiquiátricos (Ver **Anexo 5** (Torterolo et al., 2019)).

2. Capítulo 2. Acoplamiento entre frecuencias 1

2.1. Actividad de alta frecuencia y su modulación por el ritmo theta durante la vigilia y el sueño REM

En el capítulo anterior mostramos como la actividad gamma (30-100 Hz) es máxima durante la vigilia, decrece durante el sueño NREM y que durante el sueño REM la sincronización local (potencia) crece mientras que la sincronización de largo rango (coherencia) decrece hasta sus valores mínimos (Castro-Zaballa et al., 2014, 2013; Cavelli et al., 2017a, 2015). Durante el análisis de los registros de ratas utilizadas en los trabajos previos (Cavelli et al., 2015) observamos la aparición de un pico de coherencia intra-hemisférica aproximadamente a los ≈130 Hz entre las cortezas somatosensoriales y visuales (Cavelli et al., 2014). Son pocos los estudios que se han encargado de estudiar la actividad oscilatoria por encima de los 100 Hz (Uhlhaas et al., 2011). Sin embargo, recientemente se ha descripto una forma nueva de actividad oscilatoria que se observa en el hipocampo y las cortezas parietales, y cuya oscilación se ubica entre los 110 y los 160 Hz (Sirota et al., 2008; Tort et al., 2008). Algunos autores han nombrado a esta actividad de alta frecuencia "high frequency oscillation" o "HFO" (Caixeta et al., 2013; Scheffer-Teixeira et al., 2012; Tort et al., 2013) mientras que otros autores lo han nombrado como gamma alto, gamma rápido e inclusive gamma 3 (Canolty et al., 2009; Jackson et al., 2011; Pal et al., 2016; Scheffzük et al., 2011; Sirota et al., 2008). Similar a lo que observáramos con la actividad gamma (30-100 Hz), la potencia HFO es máxima durante la vigilia, decrece durante el sueño NREM y aumenta nuevamente durante el sueño REM (Scheffer-Teixeira et al., 2012; Scheffzük et al., 2011). Una de las características más remarcables de las HFO es que su amplitud se encuentra co-modulada por el ritmo theta (5-9 Hz) generado a nivel de la red hipocámpica (Sirota et al., 2008; Tort et al., 2013). Al momento son pocos los trabajos que se han encargado de caracterizar las HFO, y algunas de sus características claves como su distribución espacial y la coherencia inter-cortical durante el ciclo sueño y vigilia son desconocidas.

Con el objetivo de describir en detalle las HFO durante la vigilia y el sueño, realizamos el **Artículo 3** (Cavelli et al., 2017b). En este trabajo identificamos y describimos algunas de las características desconocidas de las HFO durante la vigilia y el sueño. Mostramos que la coherencia HFO es máxima durante la vigilia, que esta cae durante el sueño NREM y que durante el sueño REM la coherencia HFO cae entre las combinaciones inter-hemisféricas, mientras que aumenta en las combinaciones intra-hemisféricas de electrodos principalmente entre las cortezas somatosensoriales y visuales. Por último, mostramos evidencia a favor de que el aumento de coherencia entre algunas de las combinaciones de electrodos se encuentra también efectivamente moduladas por la actividad theta de la red hipocámpica.

ARTICULO 3

(Cavelli et al., 2017b)

EJN European Journal of Neuroscience

FENS Federation of European Neuroscience Societies

European Journal of Neuroscience, pp. 1–10, 2017 doi:10.1111/ejn.13718

Power and coherence of cortical high-frequency oscillations during wakefulness and sleep

Matías Cavelli,[1] Daniel Rojas-Líbano,[2] Natalia Schwarzkopf,[1] Santiago Castro-Zaballa,[1] Joaquín Gonzalez,[1] Alejandra Mondino,[1] Noelia Santana,[1] Luciana Benedetto,[1] Atilio Falconi[1] and Pablo Torterolo[1]

[1]Laboratorio de Neurobiología del Sueño, Departamento de Fisiología, Facultad de Medicina, Universidad de la República, General Flores 2125, 11800 Montevideo, Uruguay

[2]Laboratorio de Neurociencia Cognitiva y Social, Facultad de Psicología, Universidad Diego Portales, Santiago, Chile

Keywords: CFC, gamma, paradoxical sleep, rat, REM, theta

Abstract

Recently, a novel type of fast cortical oscillatory activity that occurs between 110 and 160 Hz (high-frequency oscillations (HFO)) was described. HFO are modulated by the theta rhythm in hippocampus and neocortex during active wakefulness and REM sleep. As theta-HFO coupling increases during REM, a role for HFO in memory consolidation has been proposed. However, global properties such as the cortex-wide topographic distribution and the cortico-cortical coherence remain unknown. In this study, we recorded the electroencephalogram during sleep and wakefulness in the rat and analyzed the spatial extent of the HFO band power and coherence. We confirmed that the HFO amplitude is phase-locked to theta oscillations and is modified by behavioral states. During active wakefulness, HFO power was relatively higher in the neocortex and olfactory bulb compared to sleep. HFO power decreased during non-REM and had an intermediate level during REM sleep. Furthermore, coherence was larger during active wakefulness than non-REM, while REM showed a complex pattern in which coherence increased only in intra and decreased in inter-hemispheric combination of electrodes. This coherence pattern is different from gamma (30–100 Hz) coherence, which is reduced during REM sleep. This data show an important HFO cortico-cortical dialog during active wakefulness even when the level of theta comodulation is lower than in REM. In contrast, during REM, this dialog is highly modulated by theta and restricted to intra-hemispheric medial-posterior cortical regions. Further studies combining behavior, electrophysiology and new analytical tools are needed to plunge deeper into the functional significance of the HFO.

Introduction

The synchronous activity of large population of neocortical neurons generates oscillatory activities in the electroencephalogram (EEG) that vary according to behavior and cognitive functions (Buzsáki *et al.*, 2012). Among the faster oscillations, gamma band activity (30–100 Hz) has been extensively explored (Adrian, 1942; Freeman & Schneider, 1982; Gray *et al.*, 1989; Joliot *et al.*, 1994; Rojas-Líbano & Kay, 2008; Fries, 2009; Buzsáki & Wang, 2012). An increase in gamma activity typically emerges during behaviors characterized by active processing of external percepts or internally generated thoughts and images (Freeman & Schneider, 1982; Tiitinen *et al.*, 1993; Rieder *et al.*, 2011; Uhlhaas *et al.*, 2011). Cognitive activities do not only occur during wakefulness (W). Dreaming, the cognitive counterpart of REM sleep, reveals the existence of another form of cognitive activity or proto-consciousness (Hobson, 2009). Accordingly, gamma power during REM sleep has similar values than W and it is larger compared to deep non-REM (NREM) sleep, where cognitive activity is reduced (Maloney *et al.*, 1997; Chrobak & Buzsáki, 1998; Cavelli *et al.*, 2015).

The coupling of EEG gamma activity between two different cortical areas, as analyzed by spectral coherence, increases during several behaviors and cognitive activities in both animals and humans (Bouyer *et al.*, 1981; Bressler *et al.*, 1993; Härle *et al.*, 2004; Daume *et al.*, 2017). Recently, we showed in cats and rats that long-range gamma coherence is maximum during W, decreases during NREM sleep and reaches its lowest value during REM sleep (Castro-Zaballa *et al.*, 2013, 2014; Cavelli *et al.*, 2015; Torterolo *et al.*, 2016). Also, gamma coherence between distant areas has been proposed as a neural correlate of conscious perception and self-awareness (Llinás *et al.*, 1998; Rodriguez *et al.*, 1999; Melloni *et al.*, 2007; Voss *et al.*, 2009, 2014). In this regard, coherence in the gamma frequency band is lost during anesthesia-induced unconsciousness (John, 2002; Mashour, 2006; Pal *et al.*, 2016) and is severely altered in psychiatric disorders (Uhlhaas & Singer, 2010; Sun *et al.*, 2011).

Correspondence: Dr Pablo Torterolo, as above.
E-mail: ptortero@fmed.edu.uy

Received 19 May 2017, revised 13 September 2017, accepted 13 September 2017

Edited by Gregor Thut

Reviewed by Adriano Tort, Federal University of Rio Grande do Norte, Brazil and Francisco Urbano, University of Buenos Aires, Argentina

The associated peer review process communications can be found in the online version of this article.

Few studies have dealt with EEG oscillations at frequencies higher than 100 Hz (Uhlhaas *et al.*, 2011). Nevertheless, a novel type of fast cortical oscillatory activity occurring between 110 and 160 Hz both in the hippocampus and in the parietal neocortex has been described (Sirota *et al.*, 2008; Tort *et al.*, 2008). Some authors dubbed high-frequency oscillations (HFO) to this activity (Scheffer-Teixeira *et al.*, 2012; Caixeta *et al.*, 2013; Tort *et al.*, 2013), while others called it fast or high gamma (Sirota *et al.*, 2008; Canolty *et al.*, 2009; Jackson *et al.*, 2011; Scheffzük *et al.*, 2011; Pal *et al.*, 2016). Similar to gamma oscillations, HFO are larger during active W and REM sleep (Scheffzük *et al.*, 2011; Scheffer-Teixeira & Tort, 2017) and its amplitude is modulated by theta oscillations both in hippocampus and in parietal neocortex (Sirota *et al.*, 2008; Tort *et al.*, 2013). HFO can co-occur with gamma oscillations nested in the same theta cycle but reach their maximum amplitude at a different theta phase (Scheffzük *et al.*, 2011; Tort *et al.*, 2013). In addition, like gamma activity, HFO have also been related to cognitive functions, such as decision making (Tort *et al.*, 2008). Because of their implication in the neocortex-hippocampal interaction and also due to the mnemonic role of REM sleep (Paller & Voss, 2004), it has been suggested that HFO may specifically be related to memory processing (Tort *et al.*, 2013).

Only a handful of studies have aimed to characterize the HFO, and several key features of these rhythms, such as their spatial patterns and coherence, remain unknown. A crucial step in the assignment of functionality to HFO is to have a larger spatial map of its occurrence across the cortical surface, as well as an assessment of its coherence between cortical regions. Hence, in this report, we studied the HFO spectral power and coherence along several recording sites spanning the entire neocortex and olfactory bulb (OB) of the rat, during W, NREM and REM sleep.

Experimental procedures

Experimental animals

Twenty-one adult male Wistar rats (270–300 g) were used in this study. The animals were obtained from URBE (Unidad de Reactivos Biológicos para Experimentación), of the Department of Laboratory Medicine of the School of Medicine, Universidad de la República, Uruguay. All experimental procedures were conducted in agreement with the National Animal Care Law (#18611) and with the 'Guide to the care and use of laboratory animals' (8th edition, National Academy Press, Washington D. C., 2010). Furthermore, the Institutional Animal Care Committee approved the experimental procedures (File: 071140-001931-12; Registration: CNEA N° 0011/11). Adequate measures were taken to minimize pain, discomfort or stress of the animals, and efforts were made to use the smallest number of animals necessary to obtain reliable data.

Surgical procedures

We employed similar surgical procedures as in our previous studies (Lagos *et al.*, 2009; Benedetto *et al.*, 2013; Cavelli *et al.*, 2015). The animals were chronically implanted with electrodes to monitor the states of sleep and W. Anesthesia was induced with a mixture of ketamine-xylazine (90 mg/kg; 5 mg/kg i.p., respectively). The rat was positioned in a stereotaxic frame, and the skull was exposed. Several craniotomies were made to insert the electrodes. To record the EEG, stainless steel screw electrodes (1 mm diameter) were screwed on the craniotomies to have their tips touching the brain's surface (above the dura mater) in different cortices and the OB. As shown in Fig. 1, four groups of animals (G0–G3) were implanted with different spatial distributions of electrodes on the skull.

G0 group (n = 9). Six electrodes were located on the neocortex forming two anterior–posterior consecutive squares centered with respect to the midline and the frontal square centered with respect to Bregma (Fig. 1). Each side of the squares has a length of 5 mm. The electrodes were located in primary motor cortex (M1, L: ±2.5 mm, AP: +2.5 mm), primary somato-sensory cortex (S1, L: ±2.5 mm, AP: −2.5 mm) and secondary visual cortex (V2, L: ±2.5 mm, AP: −7.5 mm). The other electrode was located over the right OB (L: +1.25 mm, AP: +7.5 mm).

G1, G2 and G3 groups (n = 4 per group). To confirm and extend the results obtained in G0, we analyzed the HFO from recordings that were used in Cavelli *et al.* (2015). G1 group presents intra-hemispheric, while G2 and G3 groups have inter-hemispheric (homotopic and heterotopic, respectively) combinations of electrodes. Note that in G1 and G3, V1 was used instead of V2 (that was used in G0 group).

To record the electromyogram (EMG), two electrodes were inserted into the neck muscle. The electrodes were soldered into a six to 12 pin socket (depending of the number of electrodes) and fixed onto the skull with acrylic cement.

At the end of the surgical procedures, an analgesic (Ketoprofen, 1 mg/Kg s.c.) was administered. Incision margins were kept clean, and a topical antibiotic was applied daily. After the animals recovered from the surgical procedures (minimal recovering time of 4 days), they were adapted to the recording chamber for 1 week.

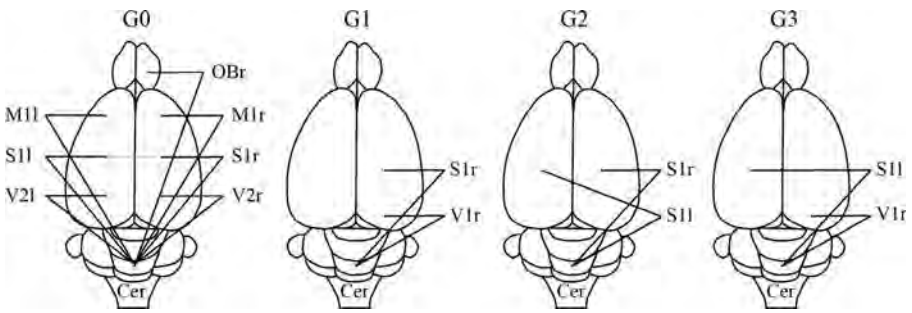

FIG. 1. Position of recording electrodes. The figure presents a summary of the cortical and OB positions of the recording electrodes. The electrodes were referred to a common electrode that was located over the cerebellum (Cer). In this group, the electrodes form two anterior–posterior consecutive squares centered with respect to the midline and with the frontal square centered with respect to Bregma (highlighted in red). OB, olfactory bulb; M1, primary motor cortex; S1, primary somato-sensory cortex; V2, secondary visual cortex; r, right; l, left.

Experimental sessions

All animals were housed individually in transparent cages (40 × 30 × 20 cm) containing wood shavings in a temperature-controlled (21–24 °C) room, with water and food *ad libitum*. Experimental sessions were conducted during the light period, between 12 A.M. and 6 P.M in a sound-attenuated chamber, which was also a Faraday box. The recordings were performed through a rotating connector, to allow the rats to move freely within the recording box.

The simultaneous activity of different cortical areas was recorded using a monopolar configuration with a common reference electrode located in the cerebellum (Bullock *et al.*, 1990; Cavelli *et al.*, 2015) (Fig. 1). The EMG was also monitored. Each rat was recorded daily for approximately 1 week to obtain a complete data set.

Bioelectric analog signals were amplified with a differential AC amplifier (AM-systems model 1700; 1000×), filtered (0.1–500 Hz), digitized (1024 Hz, 2^{16} bits) and stored on a PC using the Spike2 software (Cambridge Electronic Design).

Data analysis

Sleep and waking states were determined for 10-s epochs according to standard criteria (Cavelli *et al.*, 2015). For the analysis of the G0 group of animals, W was divided into active (AW) and quiet (QW) according to the mean level of theta activity averaged from the four posterior electrodes. Epochs that had a theta power above percentile 70 were classified as AW, while the remaining epochs were assigned as QW.

To analyze power spectrum (in each channel) and coherence (between pairs of EEG channels), we used similar procedures as in our previous studies (Castro-Zaballa *et al.*, 2013, 2014; Cavelli *et al.*, 2015; Torterolo *et al.*, 2016); however, the analysis in G0 and G1-G3 groups was not exactly the same (see below).

G0 group. The maximum number of non-transitional and artifact-free periods of 30 s was selected during each behavioral state to determine the mean power and coherence for each rat. For each animal, we analyzed two complete (6 h) recordings (the recordings with the lower number of artifacts were selected).

G1 to G3 groups. We employed exactly the same methodology as in our previous studies (Castro-Zaballa *et al.*, 2013, 2014; Cavelli *et al.*, 2015; Torterolo *et al.*, 2016). Twelve artifact-free periods of 100 s were examined during each behavioral state (1200 s for each behavioral state, per animal; data were selected from three different recordings). For these groups of animals, the 100-s windows of W consisted of a mixture of AW and QW.

The coherence between two EEG channels that were recorded simultaneously was analyzed in 30 s (for G0) or 100 s (for G1- G3) windows. For each period, the magnitude-squared coherence as well as the power spectrum for each channel was calculated by means of Spike2 script COHER-HOL 1S (for details about coherence definition see (Bullock & McClune, 1989; Castro-Zaballa *et al.*, 2013)). For the coherence analysis, each period was divided into 30 (G0) and 100 (G1-G3) time-blocks with a bin size of 2048 samples and a resolution of 0.5 Hz. The data were then analyzed through custom-built Python routines.

We examined the power and coherence of HFO between 105 and 148 Hz, to avoid any possible interference due to 50 Hz electrical noise (power line hum). To normalize the data and use parametric statistical tests, we applied the Fisher z- transform to the coherence values. The power of the HFO for each channel (expressed as the total power (TP) per band; absolute values), and the z'-coherence for each pair of EEG channels, was averaged across behavioral states. The data were expressed as mean ± standard deviation. The significance of the differences among behavioral states was evaluated with one-way ANOVA (for each rat) and repeated measures ANOVA (RMANOVA) (for comparison between the means of the whole group of rats), along with Tamhane and Bonferroni *post hoc* tests, respectively. The criterion used to reject null hypotheses was $P < 0.05$. When the ANOVA test resulted in a significant difference, a measure of effect size (MES) was also reported. The MES was reported as η^2, which was calculated as follows: $\eta^2 = (SS_{effect}/SS_{total})$, where SS_{effect} is the sum of squares between groups, and SS_{total} is the overall sum of squares. Therefore, the range of η^2 goes from 0 to 1 (0 means no effect). This measure estimates the proportion of the total variance of a given variable explained by a treatment (Kline, 2004).

Selected recordings were band-pass filtered to obtain HFO and theta bands using digital finite impulse response filters (FIR). The amplitude relation between simultaneously recorded pairs of filtered HFO epochs was analyzed using regression and correlation analysis. Autocorrelations (ACF) and cross-correlations functions (CCF) were also calculated.

A CCF-map (Fig. 2C) was generated between the theta rhythm (4–9 Hz) and the envelopes of frequencies higher than 20 Hz. To obtain the CCF-map, several band-pass filtered signals were generated from the raw recording. We filtered one in the theta range; for the others band-passed signals, we used 10-Hz bandwidth and 5-Hz steps, covering from 20 up to 190 Hz. The CCF-map was then generated by means of a raster plot of CCFs calculated between theta and the root mean square (RMS) envelopes of each filtered signal.

A RMS coherence map was also constructed to study the coherence of the HFO amplitude in the theta range (Fig. 6A). To construct this map, several pairs of band-pass filtered signals were obtained exactly as before, using a 10-Hz bandwidth and 5-Hz steps, covering from 20 up to 190 Hz. For each pair of filtered signals, the RMS was computed and the coherence calculated. The *X*-axis represents the frequency of coherence below 20 Hz, the *Y*-axis represents the mean frequency of the band-passed signals (the envelope's own frequency) and the Z-axis corresponds to the level of z'-coherence between each pairs of envelopes at a given frequency.

With the purpose of analyzing the modulation of the HFO amplitude by the phase of the theta oscillation, a comodulation map or 'co-modulogram' was performed in Matlab (see Figs 2D and 3A). To build the comodulogram, each pair composed by one slow (phase) and one fast (envelopes) oscillation was assessed by a measure called modulation index (MI); these data were processed in Matlab following previously described procedures (Tort *et al.*, 2010, 2013).

Results

Identification of the HFO: modulation by behavioral states and theta rhythm

As a first step, we confirmed that HFO activity was present in our recordings. As previously described, HFO are modulated by theta rhythm and modified by behavioral states. Figure 2A exhibits the power spectrum profiles of the EEG during W and sleep. This figure shows that there is a larger power between 25 and 250 Hz during W than during sleep states. During REM sleep, the power in S1 and V1 recording sites reveals a peak in the theta band. Also, a small, but clear power peak at the HFO band (arrows) is readily observed, which although lower than waking values, and it was larger than during NREM sleep.

Figure 2B shows raw and filtered recordings during REM sleep of a representative rat. In the raw recordings of S1 and V1 (right

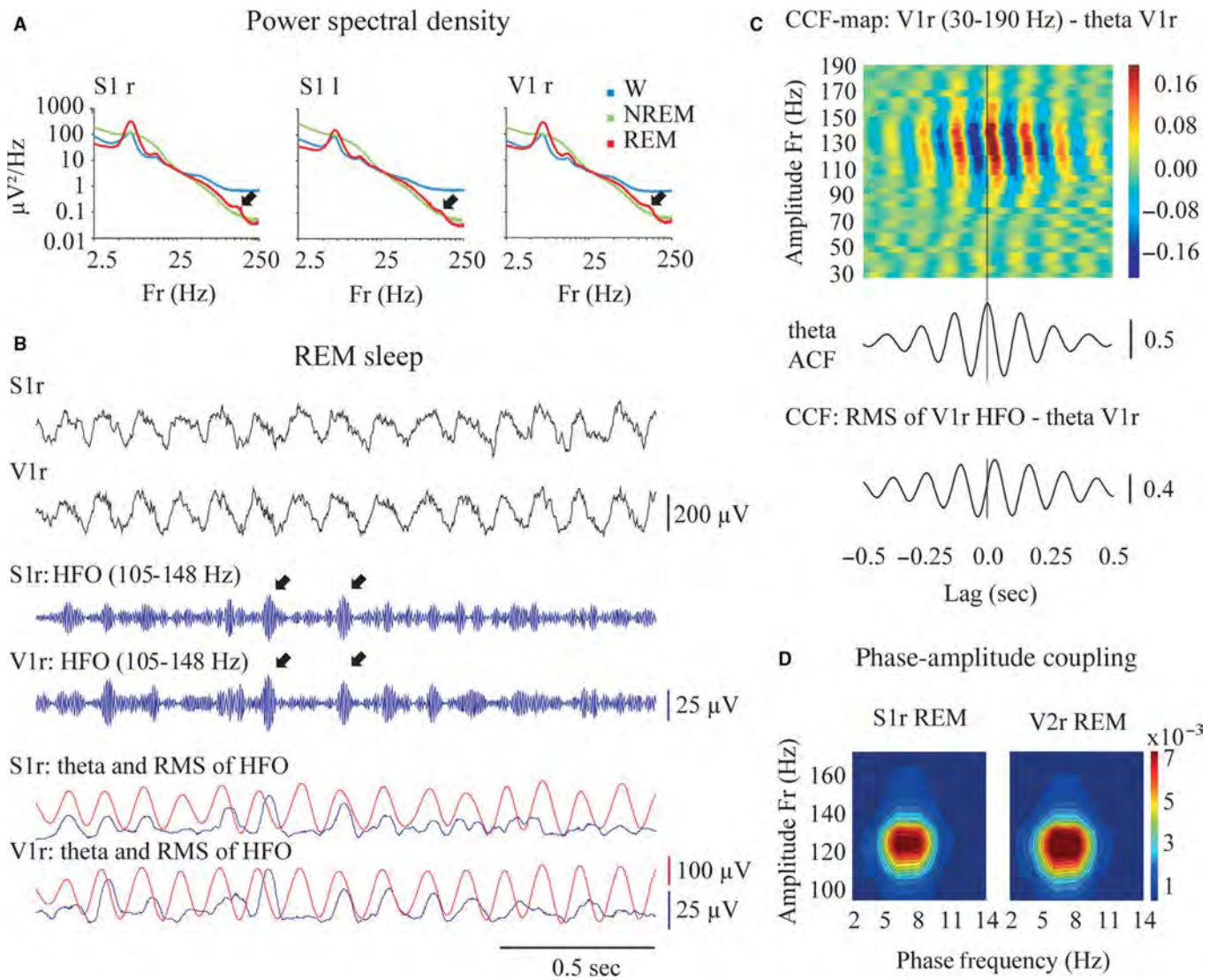

FIG. 2. High-frequency oscillations (HFO) are associated with theta oscillations during REM sleep. (A) S1r, S1l and V1r mean power spectral density during W (blue), NREM (green) and REM sleep (red) is shown. Each trace is the mean of 12 independent 100 s windows per animal (four rats). The arrows point the HFO peaks in the power profile during REM sleep. (B) Simultaneous raw and filtered (105–148 Hz) recordings from the right somato-sensory primary (S1r) and right visual primary (V1r) cortices during REM sleep. HFO were highlighted after filtering. Arrows in the filtered recordings indicate 'bursts' of HFO. The traces in the bottom show that the HFO RMS amplitude envelope (blue traces) seems to follow the theta oscillations (4–12 Hz band-pass filter, red traces). (C) Cross-correlation function (CCF) map of V1 theta and V1 RMS envelop (30–200 Hz, 10-Hz bandwidth and 5-Hz steps), autocorrelation function (ACF) of V1 theta, and CCF of V1 theta and V1 HFO (RMS) envelope are shown. These data were analyzed from 100 s windows during REM sleep. Coupling between HFO RMS and theta are readily observed in both CCF and CCF-map. (D) The comodulation map expressing theta-HFO phase-amplitude coupling (PAC) for S1 and V1 during REM sleep is shown. In the two plots, the modulation maximum reveals correlations between theta and HFO bands.

hemisphere), there is prominent theta activity, while high-frequency activity is present with smaller amplitude. HFO during REM sleep were unmasked after digital filtering of the recordings, and spindle-like 'bursts' of HFO were commonly observed (arrows). The RMS of the HFO amplitude is also shown (blue traces); in this case, the RMS peaks come out predominantly following the theta cycles' maxima (red traces). This strong association between the envelope of the HFO and the theta rhythm during REM sleep can be seen in the CCF and the cross-correlogram map of Fig. 2C. Furthermore, the comodulogram of Fig. 2D shows a high phase-amplitude coupling (PAC) between the amplitude of HFO and the phase of the theta rhythm during REM sleep, both in S1r and in V2r.

In contrast to REM sleep, during W there was not a clear peak in the HFO band power, even when the HFO power level was the highest (Fig. 2A). However, during W, HFO were also modulated by theta rhythm. Figure 3A exhibits by means of PAC that HFO are modulated by theta rhythm during AW (that is accompanied by high theta activity). In fact, AW showed higher modulation than QW, both in S1 and in V2. However, theta modulation during AW remained lower than during REM sleep (Figs 3A and 2D; see calibration bars). Figure 3B shows the z'-coherence between the raw recordings and HFO band envelopes of the same recording. This analysis revealed a clear peak of HFO coherence in the theta range (7–9 Hz) during AW; this modulation is not present during QW, neither in S1 nor in V2 (Fig. 3B).

All these analyses confirmed that the recorded HFO present the same features that have been previously described (Scheffzük *et al.*, 2011; Tort *et al.*, 2013).

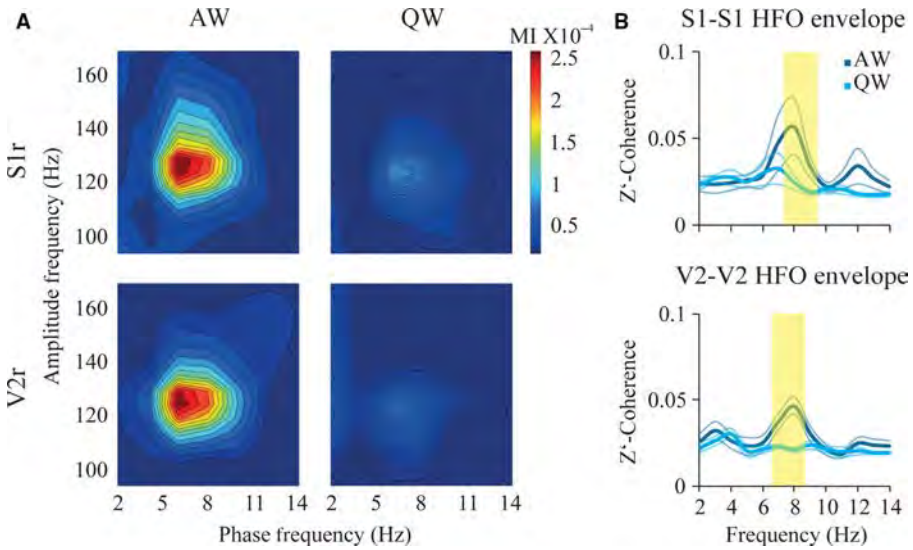

FIG. 3. High-frequency oscillations (HFO) are associated with theta oscillations during AW and not QW. (A) The comodulation map expressing theta-HFO phase-amplitude coupling (PAC) for S1 and V2 during AW (left) and QW (right) is shown. In S1 and V2 plots, the maximum value of modulation index (MI) between theta and HFO bands was observed during AW. (B) The graphics show the z'-coherence between the raw and the HFO envelope of the same record. This analysis reveals a clear peak in the theta range (7–9 Hz) coherence during AW but not during QW for S1 and V2 electrodes. The shaded yellow represents significant differences between AW and QW, paired *t*-test, $P < 0.05$.

Neocortical extent of the HFO power and coherence

To study the neocortical extent of power and coherence of HFO band, we analyzed a group of nine rats with the same electrode position (Fig. 1, G0). Statistical analyses of HFO band power and coherence are shown in Tables 1 and 2, respectively. HFO TP showed significant differences across behavioral states for all the electrodes (Table 1). These results revealed that HFO band power is larger during AW than during sleep, both in neocortex and in OB. The lowest values were recorded during NREM, while during REM sleep, the TP increased to an intermediate level in all the cerebral areas recorded.

Z'-coherence also displayed significant differences across behavioral states for all twenty-one possible electrode pair combinations (Table 2). HFO band coherence was larger during AW than during NREM sleep. During REM sleep, a significant increase in coherence was observed compared with NREM sleep but only for posterior intra-hemispheric combination of electrodes (Table 2, highlighted in a red frame). The rest of the electrodes combinations showed either no change (most of the combinations) or a decrease in coherence compared with NREM; this was the case of six inter-hemispheric combinations of electrodes (Table 2). The schematic presented in Fig. 4 summarizes the statistically significant mean differences of HFO band power and coherence during AW and sleep.

We also analyzed the HFO 'mean global coherence' by averaging the twenty-one electrode combinations (Pal *et al.*, 2016). This estimate of global coherence showed significant differences across behavioral states ($F_{2,24} = 112.3$, $P < 0.001$, $\eta^2 = 0.934$). Global coherence was higher during AW (0.53 ± 0.10), decreased during NREM (0.27 ± 0.07, $P < 0.001$) and reached a minimum during REM sleep (0.23 ± 0.07, $P = 0.032$).

The analyses of HFO band power, as well as intra- and inter-hemispheric coherence, were also performed on twelve animals corresponding to G1, G2 and G3 groups. In these groups, the results were comparable to the G0 group; in spite of that, W was analyzed as whole (AW + QW). The complete analyses for each group of animals and for each rat are shown in Supplementary Information (Fig. S1 and Tables S1 and S2, respectively).

TABLE 1. RMANOVA and Bonferroni tests. The analysis was performed in nine animals. The degrees of freedom were 2 (between groups) and 16 (within groups) for all the cortical regions that were analyzed

	Descriptive statistics (TP μV^2/Hz)			RMANOVA			Multiple comparisons-Bonferroni		
Electrode	AW (mean ± SD)	NREM (mean ± SD)	REM (mean ± SD)	*F*	Sig. (*P*)	Partial Eta Squared (η^2)	AW vs. SWS (*P*)	AW vs. REM (*P*)	REM vs. NREM (*P*)
OBr	124.1 ± 48.3	18.2 ± 9.5	29.6 ± 14.5	58.9	**<0.001**	0.880	**<0.001**	**<0.001**	**0.002**
M1l	71.6 ± 33.1	9.1 ± 1.8	16.5 ± 6.3	30.7	**<0.001**	0.793	**0.001**	**0.002**	**0.023**
M1r	74.5 ± 30.9	9.4 ± 2.6	16.3 ± 6.4	40.5	**<0.001**	0.835	**0.001**	**0.005**	**0.005**
S1l	63.4 ± 24.9	9.7 ± 2.4	23.5 ± 11.3	33.5	**<0.001**	0.808	**<0.001**	**0.004**	**0.010**
S1r	71.1 ± 24.9	17.6 ± 17.4	32.4 ± 19.5	82.9	**<0.001**	0.912	**<0.001**	**<0.001**	**0.001**
V2l	41.3 ± 20.7	10.9 ± 16.5	17.1 ± 19.7	67.7	**<0.001**	0.894	**<0.001**	**<0.001**	**0.015**
V2r	50.3 ± 24.3	12.5 ± 19.5	20.3 ± 23.8	59.5	**<0.001**	0.882	**<0.001**	**<0.001**	**0.024**

OB, olfactory bulb; M1, motor primary cortex; S1, somato-sensory primary cortex; V2, visual secondary cortex; r, right; l, left; AW, active wakefulness; NREM, non-REM sleep; REM, REM sleep, in bold $P < 0.05$.

TABLE 2. RMANOVA and Bonferroni tests. The analysis was performed in nine animals. The degrees of freedom were 2 (between groups) and 16 (within groups) for all the combinations that were analyzed. A significant increase in coherence in the posterior intra-hemispheric combination of electrodes was highlighted in a red frame

	Descriptive statistics (Z'-coherence)			RMANOVA			Multiple comparisons-Bonferroni		
Electrode pairs	AW (mean ± SD)	NREM (mean ± SD)	REM (mean ± SD)	*F*	Sig. (*P*)	Partial Eta Squared (η^2)	AW vs. SWS (*P*)	AW vs. REM (*P*)	REM vs. NREM (*P*)
OBr-M1r	0.66 ± 0.22	0.39 ± 0.25	0.35 ± 0.22	53.8	**<0.001**	0.871	**0.001**	**<0.001**	0.151
OBr-M1l	0.60 ± 0.33	0.33 ± 0.28	0.31 ± 0.27	45.7	**<0.001**	0.851	**0.001**	**<0.001**	0.712
OBr-S1r	0.42 ± 0.17	0.15 ± 0.11	0.11 ± 0.07	54.2	**<0.001**	0.872	**<0.001**	**<0.001**	0.295
OBr-S1l	0.41 ± 0.17	0.15 ± 0.10	0.11 ± 0.01	64.5	**<0.001**	0.890	**<0.001**	**<0.001**	**0.036**
OBr-V2r	0.31 ± 0.13	0.11 ± 0.06	0.09 ± 0.04	25.9	**<0.001**	0.764	**0.002**	**0.002**	0.696
OBr-V2l	0.28 ± 0.11	0.08 ± 0.05	0.06 ± 0.03	46.8	**<0.001**	0.854	**<0.001**	**<0.001**	0.468
M1r-M1l	0.79 ± 0.19	0.42 ± 0.15	0.34 ± 0.17	98.5	**<0.001**	0.925	**<0.001**	**<0.001**	0.145
M1r-S1r	0.80 ± 0.23	0.33 ± 0.12	0.30 ± 0.13	82.1	**<0.001**	0.911	**<0.001**	**<0.001**	0.592
M1r-S1l	0.70 ± 0.23	0.31 ± 0.12	0.19 ± 0.14	75.2	**<0.001**	0.904	**<0.001**	**<0.001**	**0.004**
M1r-V2r	0.51 ± 0.23	0.18 ± 0.10	0.18 ± 0.08	25.6	**<0.001**	0.762	**0.001**	**0.004**	1.000
M1r-V2l	0.45 ± 0.17	0.13 ± 0.07	0.10 ± 0.07	53.1	**<0.001**	0.869	**<0.001**	**<0.001**	0.608
M1l-S1l	0.87 ± 0.13	0.41 ± 0.12	0.38 ± 0.11	201.5	**<0.001**	0.962	**<0.001**	**<0.001**	0.345
M1l-V2l	0.49 ± 0.14	0.14 ± 0.08	0.17 ± 0.09	95.3	**<0.001**	0.923	**<0.001**	**<0.001**	0.179
S1r-M1l	0.59 ± 0.15	0.21 ± 0.07	0.15 ± 0.11	88.9	**<0.001**	0.918	**<0.001**	**<0.001**	0.234
S1r-S1l	0.66 ± 0.31	0.25 ± 0.15	0.11 ± 0.07	39.98	**<0.001**	0.833	**<0.001**	**0.001**	**0.011**
S1r-V2l	0.62 ± 0.28	0.28 ± 0.21	0.16 ± 0.14	51.7	**<0.001**	0.753	**<0.001**	**<0.001**	**0.011**
V2r-M1l	0.41 ± 0.15	0.14 ± 0.05	0.08 ± 0.04	42.2	**<0.001**	0.841	**0.001**	**<0.001**	**0.043**
V2r-S1l	0.40 ± 0.22	0.13 ± 0.06	0.08 ± 0.03	20.3	**<0.001**	0.718	**0.005**	**0.006**	0.071
V2r-V2l	0.49 ± 0.29	0.30 ± 0.22	0.15 ± 0.11	15.8	**<0.001**	0.665	**0.025**	**0.008**	**0.018**
S1l-V2l	0.72 ± 0.21	0.28 ± 0.13	0.44 ± 0.16	50.2	**<0.001**	0.863	**<0.001**	**0.001**	**0.002**
S1r-V2r	0.70 ± 0.35	0.39 ± 0.23	0.53 ± 0.27	17.3	**<0.001**	0.685	**0.003**	**0.034**	**0.031**

OB, olfactory bulb; M1, motor primary cortex; S1, somato-sensory primary cortex; V2, visual secondary cortex; r, right; l, left; W, wakefulness; NREM, non-REM sleep; REM, REM sleep, in bold $P < 0.05$.

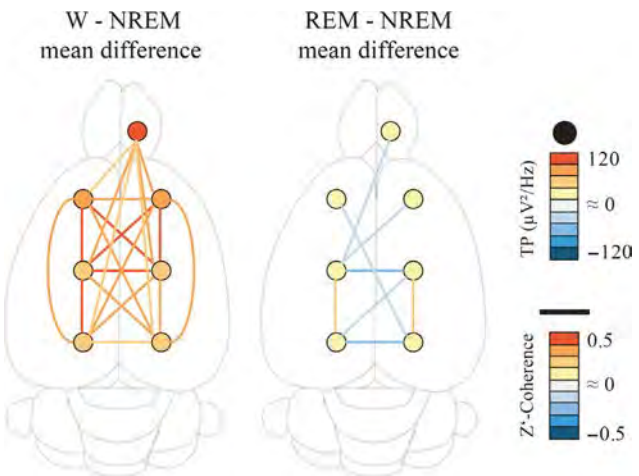

FIG. 4. High-frequency oscillations (HFO) band power and z'-coherence during wakefulness and sleep. Summary of the statistical significance differences between behavioral states of the HFO' total power and z'-coherence over the surface of the cerebral cortex (G0 group, Figure 1). The circles represent the power for the different electrode positions, while the lines represent the coherence for the different combination of electrodes. The colors represent the mean difference level of power and z'- coherence. RMANOVA and Bonferroni paired comparisons tests. Data were obtained from the mean values of all available, non-transitional artifact-free windows per rat for each behavioral state (nine rats). OB, olfactory bulb; M1, motor primary cortex; S1, somato-sensory primary cortex; V2, visual secondary cortex.

Inter-hemispheric differences in HFO coherence during REM sleep

One intriguing result of the analysis was that compared to NREM sleep, HFO coherence during REM increases only in the posterior intra-hemispheric electrode pairs.

Coherence values during REM sleep for three different electrode configurations S1r-V1r (intra-hemispheric), S1r-S1l (inter-hemispheric homotopic) and V1r-S1l (inter-hemispheric heterotopic) are shown in Fig. 5A. This plot highlights that the HFO coherence during REM sleep is relatively large for the intra-hemispheric electrode combinations, but it is absent in the inter-hemispheric configurations. This difference in HFO coupling during REM sleep between intra- and inter-hemispheric configurations is also evident in the filtered recordings (Fig. 5B) and in the cross-correlation and regression/correlation analyses (Fig. 5C and D). In contrast, we consistently observed that during W, the coupling is present for both types of combination of electrodes (Fig 5C and D).

To analyze whether the increase in intra-hemispheric HFO synchronization during REM sleep was associated with HFO bursts that oscillated at the theta frequency, we developed a RMS coherence map (Fig. 6A). This map shows an increase in the HFO RMS coherence at theta frequency, for the intra-hemispheric electrode combinations. Then, the intra- and inter-hemispheric coherence of the HFO RMS was analyzed. This analysis revealed a clear peak in the theta range both for intra- (7.10 ± 0.20 Hz; mean ± SD) and for inter-hemispheric homotopic (7.27 ± 0.26 Hz; mean ± SD) electrode combinations (Fig. 6B). However, HFO RMS theta peak coherence was larger for intra- (0.87 ± 0.07; mean ± SD) than for inter-hemispheric (0.55 ± 0.07; mean ± SD) combination of electrodes (*t*-test; $P < 0.001$). Hence, during REM sleep, the HFO burst envelopes oscillated at theta frequency and were more coupled within hemispheres than between hemispheres.

Discussion

In the present study, we analyzed the neocortical distribution of the HFO band (105–148 Hz), as well as its intra- and inter-hemispheric

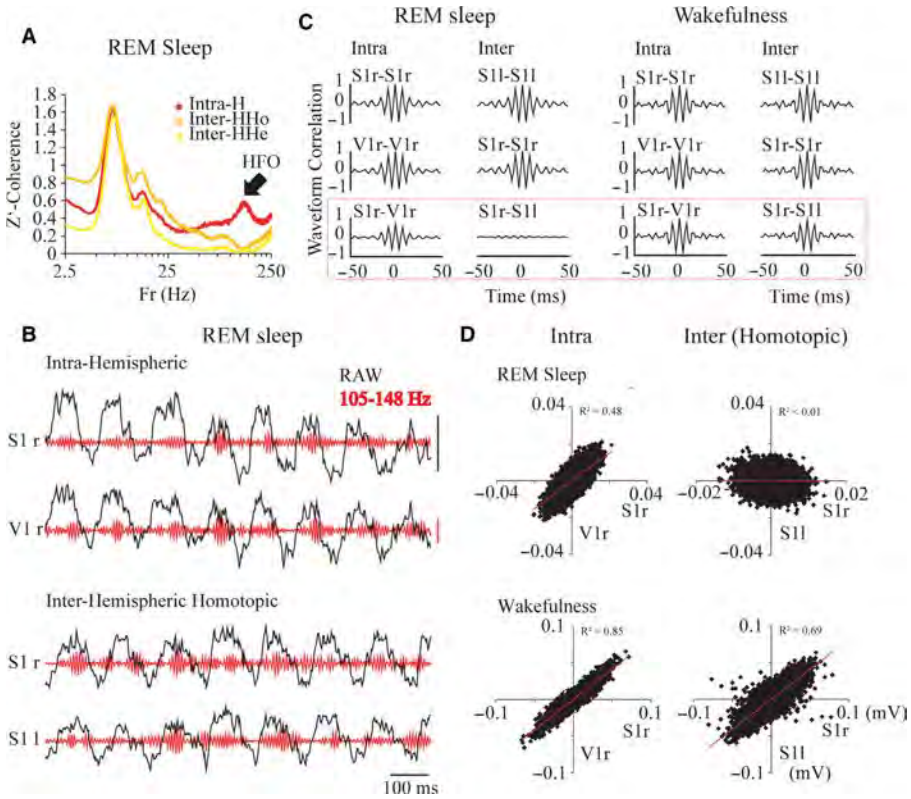

FIG. 5. High-frequency oscillations (HFO) intra- and inter-hemispheric coupling during REM sleep. (A) Mean coherence profiles during REM sleep. Traces from intra-hemispheric (red), inter-hemispheric homotopic (orange) and heterotopic (yellow) configuration of electrodes are shown. A peak of coherence in the HFO band is observed in the intra-hemispheric configuration (arrow), while in the inter-hemispheric combinations, the HFO coherence expressed its lowest values. (B) Simultaneous raw and filtered (105–148 Hz, red traces) recordings from the right somato-sensory primary (S1r) and right visual primary (V1r) cortices (top traces) and from the right somato-sensory primary (S1r) and left somato-sensory primary cortex (S1l) (bottom traces) during REM sleep. HFO, which are readily observed in the raw recordings, were highlighted after filtering. Synchrony in the HFO 'bursts' is more pronounced in the intra-hemispheric combination of electrodes. (C) Autocorrelation functions (ACF; two superior traces) and cross-correlation functions (CCF; inferior traces, framed in red) from filtered (105–148 Hz) periods of 100 s of simultaneous EEG recordings from somato-sensory and visual cortices are shown during W and REM sleep. (D) Linear regressions between the amplitudes of S1r-V1r and S1r-S1l were performed on representative filtered recordings (105–148 Hz) during 50 s of wakefulness and REM sleep. The determination coefficients are also shown. S1, somato-sensory primary cortex; V1, visual primary cortex; r, right; l, left.

(homotopic and heterotopic) cortico-cortical coherence, during W and sleep. We showed that the HFO band power, as well as the intra- and inter-hemispheric HFO band coherence, was greater during W than during sleep throughout the neocortex and OB. Similar results were obtained when W, or just AW, was analyzed. We also found an increase in the HFO band coherence during REM sleep, but only for the intra-hemispheric combination of electrodes located in the medial and posterior neocortical regions. Furthermore, we presented evidences that support the hypothesis that these levels of intra-hemispheric coherence are related to the burst of activity that is effectively modulated by theta waves generated by the hippocampal networks.

HFO characterization

We verified the presence of HFO activity in our recordings through filtering, correlation analysis and an estimate of cross-frequency coupling. Furthermore, we found HFO-theta coupling during AW and REM sleep in neocortical areas, consistent with previously published data (Scheffzük *et al.*, 2011).

We also confirmed a precise comodulation of HFO amplitude and theta activity. In fact, we observed that HFO envelope maxima appeared predominantly after the maximum of the theta wave (Fig. 2B and C), consistent with previous reports (Sirota *et al.*, 2008; Scheffzük *et al.*, 2011). This selective comodulation of HFO and theta activity, both during AW and REM sleep, makes it difficult to postulate another source than the brain contributing to this theta-coupled HFO. However, we cannot totally discard that muscle activity may contribute to part of the raw signal during AW and contributed to the high HFO power, even when the coherence of each channel with the EMG was negligible (data not shown). In other words, during W, although the theta-modulated HFO signal exists, part of the HFO band might include either an intracranial HFO not modulated by theta or an extracranial source. Hence, new studies would be important to develop new analytical tools to figure out how much of the HFO power and coherence levels are effectively modulated by the theta rhythm of the hippocampal network.

In contrast to W, during REM sleep, there is muscle atonia and is during this state where the maximum modulation between theta and HFO is expressed ((Scheffzük *et al.*, 2011) and present study); these facts practically discard the possibility that this signal has an extracranial source. Finally, it is worth to note that the HFO coherence decreases with electrode distance, as expected for signals of cortical origin (Bullock *et al.*, 1990) (Fig. S2).

HFO power and coherence during wakefulness and REM sleep

In all the neocortical areas explored as well as in the OB, the largest HFO band power was recorded during W. Compared to W, HFO

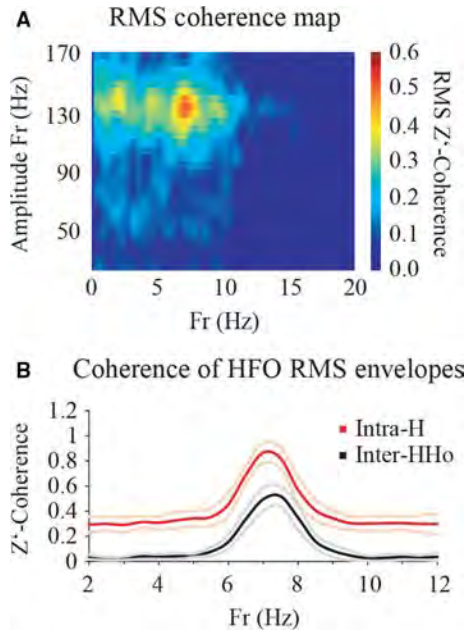

FIG. 6. Spectral z'-coherence of HFO root mean square (RMS) envelopes. (A) The plot shows the RMS coherence map between the envelopes of V1r and S1r (30–180 Hz, 10-Hz bandwidth and 5-Hz steps). This map shows an increase in envelopes coherence in the HFO band at theta frequency. (B) The graphic shows the mean ± standard deviation of the z'-coherence RMS amplitude envelopes of the filtered HFO for the intra- and inter-hemispheric combination of electrodes. The HFO RMS envelopes coherence shows only one peak in the theta range. The envelope coherence is greater for the intra-hemispheric (red trace) compared to the inter-hemispheric (black trace) combination of electrodes ($P < 0.001$). H, hemispheric; HHo, hemispheric homotopic.

power decreased during NREM and increased to intermediate values during REM sleep. This result agrees with Scheffzük *et al.* (2011), who showed that, in the parietal cortex, the HFO band power was more prominent during W compared to REM sleep.

We also showed that intra- and inter-hemispheric coherence was larger during W compared to sleep. While HFO band coherence decreases during NREM sleep, an interesting pattern emerged during REM sleep; there were major differences between intra- and inter-hemispheric HFO band coherence. Intra-hemispheric HFO band coherence values during REM sleep were intermediate between NREM and W. This fact was observed only for the medial and posterior electrode combinations. In contrast, HFO band coherence during REM sleep dropped in the inter-hemispheric (both homotopic and heterotopic) combinations of electrodes. In other words, cortical coupling in the HFO band during REM sleep occurs predominantly between posterior-medial cortical sites of the same hemisphere. Accordingly, the coherence of the HFO envelopes (which oscillate at theta frequencies) for the intra-hemispheric combination of electrodes was significantly higher than the one of the inter-hemispheric combination (Fig. 6B), even when theta coherence values were high and similar for the posterior intra- and inter-hemispheric combinations (Fig. 5A).

The present results suggest that the cortico-cortical dialog within the HFO band during REM sleep is high for each hemisphere but low or absent across them. These data also suggest that during REM sleep, sensory cortices (medial to posterior) are the main active participants of this cortico-cortical dialog at high frequency, while more motor-executive (anterior) cortices are not. In accordance, a recent work demonstrated an absence of theta-HFO coupling in the anterior lateral prefrontal cortex (Zhang *et al.*, 2016). Further studies are needed to identify the functional consequences of this phenomenon, and if subcortical areas such as the thalamus, whose neurons present high-frequency discharge bursts (Llinas & Steriade, 2006), are involved in the development of this cortico-cortical coherence.

HFO and gamma oscillations

In the parietal cortex, both HFO and gamma (30–100 Hz) are associated with theta oscillations (Tort *et al.*, 2008; Scheffer-Teixeira *et al.*, 2012) but in a different phase of the theta cycle (Scheffzük *et al.*, 2011). In contrast, in the lateral prefrontal cortex, only gamma activity (but not HFO) emerges during active W and REM sleep associated with theta (Zhang *et al.*, 2016). Hence, both gamma and HFO are related to the theta generated in the hippocampal network (Sirota *et al.*, 2008; Tort *et al.*, 2013).

In recent studies, we found both in rats and in cats that the long-range neocortical synchronization in the gamma frequency band (30–100 Hz), coherence is almost absent during REM sleep (Castro-Zaballa *et al.*, 2013, 2014; Cavelli *et al.*, 2015), even when gamma power is similar to W (Maloney *et al.*, 1997; Chrobak & Buzsáki, 1998; Cavelli *et al.*, 2015). Although HFO and gamma band coherence during REM sleep were almost absent in the inter-hemispheric electrode combinations (both for homotopic and for heterotopic cortices), HFO but not gamma band coherence increase in the posterior-medial combination of intra-hemispheric electrodes during this behavioral state. This pattern of activity differentiates HFO from gamma oscillations.

Recently, Pal *et al.* (2016) confirmed the loss of gamma band coherence during REM in rats. In addition, they showed a decrease in the HFO band (the authors dubbed HFO as high gamma), 'mean global coherence' during NREM and even more during REM sleep. The 'mean global coherence' was obtained by averaging the coherence for individual channel pairs for each animal. When we calculated the average of the twenty-one electrode combinations, the result was identical to Pal *et al*. (2016). Nevertheless, the 'mean global coherence' masks subtle changes that are generated in specific combinations of electrodes such as the case of the posterior intra-hemispheric combination of electrodes (Fig. 3).

HFO and cognition

The role of HFO in cognition is an unexplored area. During REM sleep, where dreams occur, high HFO coherence coexists with low gamma coherence, in posterior-medial intra-hemispheric cortices. We hypothesize that this may have cognitive implications. In this regard, due to the similarities between the neurobiology of REM sleep dreams with the neurobiology of the psychosis, REM sleep is considered a natural model of psychosis (Gottesmann, 2006; Gottesmann & Gottesman, 2007; Hobson & Voss, 2011). In fact, HFO is prominent in a pharmacological model of psychosis, such as the induced by Ketamine or MK-801 (both NMDA-receptor glutamatergic antagonists) (Caixeta *et al.*, 2013; Hunt & Kasicki, 2013; Cordon *et al.*, 2015).

Interestingly, HFO have been also recorded during epileptic seizures (Bragin *et al.*, 1999; Jirsch *et al.*, 2006; Zijlmans *et al.*, 2012). More studies are needed to understand the functional relationships between physiological HFO and HFO recorded in pathological conditions such as psychosis and seizures.

Conclusions

In the present study, we described the cortical spatial extent of HFO power and intra- and inter-hemispheric coherence across behavioral states in the rat. We identified and described previously unknown features of neocortical HFO during W and sleep. While there is a high-frequency cortico-cortical dialog throughout the cortex during W in the HFO band, this dialog is restricted during REM sleep to the intra-hemispheric medial-posterior (sensory/perceptual) cortical regions. We presented evidences that support the hypothesis that these levels of intra-hemispheric coherence during REM sleep are related to the burst of activity that is effectively modulated by theta. Further studies are needed to directly address the functional significance of the HFO.

Supporting Information

Additional supporting information can be found in the online version of this article:

Fig. S1. HFO band mean total power (TP) and coherence during wakefulness and sleep in each rat of the G1, G2 and G3 groups.
Fig. S2. HFO coherence as a function of the electrode distance.
Table S1. HFO Total Power during sleep and wakefulness in each rat of the G1, G2 and G3 groups.
Table S2. HFO z'-coherence during sleep and wakefulness in each rat of the G1, G2 and G3 groups.

Acknowledgements

This study was partially supported by the 'Programa de Desarrollo de Ciencias Básicas, PEDECIBA' and 'Comision Sectorial de Investigacion Cientifica', CSIC. S. CZ. and A. M. currently have a postgraduate fellowship from the 'Agencia Nacional de Investigación en Innovación (ANII)', while M. C. has a fellowship from 'Comisión de Apoyo a Postgrados (CAP)' D.RL. acknowledges funding from Proyecto Fondecyt 3120185.

Abbreviations

ACF, autocorrelation function; ANOVA, ANalysis Of VAriance; AP, antero-posterior; CCF, cross-correlation function; CFC, cross-frequency coupling; EEG, electroencephalogram; EMG, electromyogram; FIR, finite impulse response; HFO, high-frequency oscillations; i.p., intraperitoneal; L, lateral; M1, primary motor cortex; MES, measure of effect size; MI, modulation index; NREM, non-REM sleep; OB, olfactory bulb; PAC, phase-amplitude coupling; REM, rapid eyes movement; RMANOVA, repeated measures ANOVA; RMS, root mean square; s.c., subcutaneous; S1, primary somato-sensory cortex; SD, standard deviation; SS, sum of square; TP, total power; V1, primary visual cortex; V2, secondary visual cortex; W, wakefulness.

Conflict of interest

All the authors declare no conflict of interest.

Authors contributions

P.T., A.F., and M.C. financially supported. M.C., P.T., and S.CZ. did experimental design. M.C., and N.Schwarzkopf involved in experimental procedures. M.C., D.RL., J.G., A.M., and N.Santana analyzed the data. M.C., P.T., D.RL., S.CZ., J.G., A.F., and L.B. discussed and interpreted the data. M.C., and P.T. wrote the manuscript. All the authors participated in critical revision of the manuscript, added important intellectual content and approved the definitive version.

Data accessibility

For access to data contact Dr. Pablo Torterolo (ptortero@fmed.edu.uy).

References

Adrian, E.D. (1942) Olfactory reactions in the brain of the hedgehog. *J. Physiol.*, **100**, 459–473.
Benedetto, L., Rodriguez-Servetti, Z., Lagos, P., D'Almeida, V., Monti, J.M. & Torterolo, P. (2013) Microinjection of melanin concentrating hormone into the lateral preoptic area promotes non-REM sleep in the rat. *Peptides*, **39**, 11–15.
Bouyer, J.J., Montaron, M.F. & Rougeul, A. (1981) Fast fronto-parietal rhythms during combined focused attentive behaviour and immobility in cat: cortical and thalamic localizations. *Electroen. Clin. Neuro.*, **51**, 244–252.
Bragin, A., Engel, J., Wilson, C.L., Fried, I. & Buzsáki, G. (1999) High-frequency oscillations in human brain. *Hippocampus*, **9**, 137–142.
Bressler, S.L., Coppola, R. & Nakamura, R. (1993) Episodic multiregional cortical coherence at multiple frequencies during visual task performance. *Nature*, **366**, 153–156.
Bullock, T.H. & McClune, M.C. (1989) Lateral coherence of the electrocorticogram : a new measure of brain synchrony. *Electroen. Clin. Neuro*, **73**, 479–498.
Bullock, T.H., Buzsáki, G. & McClune, M.C. (1990) Coherence of compound field potentials reveals discontinuities in the CA1-subiculum of the hippocampus in freely-moving rats. *Neuroscience*, **38**, 609–619.
Buzsáki, G. & Wang, X.-J. (2012) Mechanisms of gamma oscillations. *Annu. Rev. Neurosci.*, **35**, 203–225.
Buzsáki, G., Anastassiou, C.A. & Koch, C. (2012) The origin of extracellular fields and currents — EEG, ECoG, LFP and spikes. *Nat. Rev. Neurosci.*, **13**, 407–420.
Caixeta, F.V., Cornélio, A.M., Scheffer-Teixeira, R., Ribeiro, S. & Tort, A.B.L. (2013) Ketamine alters oscillatory coupling in the hippocampus. *Sci. Rep.*, **3**, 2348.
Canolty, R.T., Edwards, E., Dalal, S.S., Soltani, M., Nagarajan, S.S., Berger, M.S., Barbaro, N.M., Knight, R.T. *et al.* (2009) High gamma power is phase-locked to theta oscillations in human neocortex. *Science*, **313**, 1626–1628.
Castro-Zaballa, S., Falconi, A., Chase, M.H. & Torterolo, P. (2013) Coherent neocortical 40-Hz oscillations are not present during REM sleep. *Eur. J. Neurosci.*, **37**, 1330–1339.
Castro-Zaballa, S., Cavelli, M., Vollono, P., Chase, M.H., Falconi, A. & Torterolo, P. (2014) Inter-hemispheric coherence of neocortical gamma oscillations during sleep and wakefulness. *Neurosci. Lett.*, **578**, 197–202.
Cavelli, M., Castro, S., Schwarzkopf, N., Chase, M.H., Falconi, A. & Torterolo, P. (2015) Coherent neocortical gamma oscillations decrease during REM sleep in the rat. *Behav. Brain Res.*, **281**, 318–325.
Chrobak, J.J. & Buzsáki, G. (1998) Gamma oscillations in the entorhinal cortex of the freely behaving rat. *J. Neurosci.*, **18**, 388–398.
Cordon, I., Nicolás, M.J., Arrieta, S., Lopetegui, E., López-Azcárate, J., Alegre, M., Artieda, J. & Valencia, M. (2015) Coupling in the cortico-basal ganglia circuit is aberrant in the ketamine model of schizophrenia. *Eur. Neuropsychopharm.*, **25**, 1375–1387.
Daume, J., Gruber, T., Engel, A.K. & Friese, U. (2017) Phase-amplitude coupling and long-range phase synchronization reveal frontotemporal interactions during visual working memory. *J. Neurosci.*, **37**, 313–322.
Freeman, W.J. & Schneider, W. (1982) Changes in spatial patterns of rabbit olfactory EEG with conditioning to odors. *Psychophysiology*, **19**, 44–56.
Fries, P. (2009) Neuronal gamma-band synchronization as a fundamental process in cortical computation. *Annu. Rev. Neurosci.*, **32**, 209–224.
Gottesmann, C. (2006) The dreaming sleep stage: a new neurobiological model of schizophrenia? *Neuroscience*, **140**, 1105–1115.
Gottesmann, C. & Gottesman, I. (2007) The neurobiological characteristics of rapid eye movement (REM) sleep are candidate endophenotypes of depression, schizophrenia, mental retardation and dementia. *Prog. Neurobiol.*, **81**, 237–250.
Gray, C.M., König, P., Engel, A.K. & Singer, W. (1989) Oscillatory responses in cat visual cortex exhibit inter-columnar synchronization which reflects global stimulus properties. *Nature*, **338**, 334–337.
Härle, M., Rockstroh, B.S., Keil, A., Wienbruch, C. & Elbert, T.R. (2004) Mapping the brain's orchestration during speech comprehension: task-specific facilitation of regional synchrony in neural networks. *BMC Neurosci.*, **5**, 40.

Hobson, J.A. (2009) REM sleep and dreaming: towards a theory of protoconsciousness. *Nat. Rev. Neurosci.*, **10**, 803–813.
Hobson, A. & Voss, U. (2011) A mind to go out of: reflections on primary and secondary consciousness. *Conscious. Cogn.*, **20**, 993–997.
Hunt, M.J. & Kasicki, S. (2013) A systematic review of the effects of NMDA receptor antagonists on oscillatory activity recorded in vivo. *J. Psychopharmacol.*, **27**, 972–986.
Jackson, J., Goutagny, R. & Williams, S. (2011) Fast and slow γ rhythms are intrinsically and independently generated in the subiculum. *J. Neurosci.*, **31**, 12104–12117.
Jirsch, J.D., Urrestarazu, E., LeVan, P., Olivier, A., Dubeau, F. & Gotman, J. (2006) High-frequency oscillations during human focal seizures. *Brain*, **129**, 1593–1608.
John, E.R. (2002) The neurophysics of consciousness. *Brain Res. Rev.*, **39**, 1–28.
Joliot, M., Ribary, U. & Llinás, R. (1994) Human oscillatory brain activity near 40 Hz coexists with cognitive temporal binding. *Proc. Natl. Acad. Sci. USA*, **91**, 11748–11751.
Kline, R.B. 2004. *Beyond Significance Testing: Reforming Data Analysis Methods in Behavioral Research*. American Psychological Association, Washington, DC.
Lagos, P., Torterolo, P., Jantos, H., Chase, M.H. & Monti, J.M. (2009) Effects on sleep of melanin-concentrating hormone (MCH) microinjections into the dorsal raphe nucleus. *Brain Res.*, **1265**, 103–110.
Llinas, R.R. & Steriade, M. (2006) Bursting of thalamic neurons and states of vigilance. *J. Neurophysiol.*, **95**, 3297–3308.
Llinás, R., Ribary, U., Contreras, D. & Pedroarena, C. (1998) The neuronal basis for consciousness. *Philos. T. Roy. Soc. B.*, **353**, 1841–1849.
Maloney, K.J., Cape, E.G., Gotman, J. & Jones, B.E. (1997) High-frequency gamma electroencephalogram activity in association with sleep-wake states and spontaneous behaviors in the rat. *Neuroscience*, **76**, 541–555.
Mashour, G.A. (2006) Integrating the science of consciousness and anesthesia. *Anest. Analg.*, **103**, 975–982.
Melloni, L., Molina, C., Pena, M., Torres, D., Singer, W. & Rodriguez, E. (2007) Synchronization of neural activity across cortical areas correlates with conscious perception. *J. Neurosci.*, **27**, 2858–2865.
Pal, D., Silverstein, B.H., Lee, H. & Mashour, G.A. (2016) Neural correlates of wakefulness, sleep, and general anesthesia. *Anesthesiology*, **125**, 929–942.
Paller, K.A. & Voss, J.L. (2004) Memory reactivation and consolidation during sleep. *Learn. Memory*, **11**, 664–670.
Rieder, M.K., Rahm, B., Williams, J.D. & Kaiser, J. (2011) Human γ-band activity and behavior. *Int. J. Psychophysiol.*, **79**, 39–48.
Rodriguez, E., George, N., Lachaux, J.P., Martinerie, J., Renault, B. & Varela, F.J. (1999) Perception's shadow: long-distance synchronization of human brain activity. *Nature*, **397**, 430–433.
Rojas-Líbano, D. & Kay, L.M. (2008) Olfactory system gamma oscillations: the physiological dissection of a cognitive neural system. *Cogn. Neurodynamics*, **2**, 179–194.
Scheffer-Teixeira, R. & Tort, A.B.L. (2017) Unveiling fast field oscillations through comodulation. *eNeuro*, **4**, https://doi.org/10.1523/ENEURO.0079-17.2017. [Epub ahead of print].
Scheffer-Teixeira, R., Belchior, H., Caixeta, F.V., Souza, B.C., Ribeiro, S. & Tort, A.B.L. (2012) Theta phase modulates multiple layer-specific oscillations in the CA1 region. *Cereb. Cortex*, **22**, 2404–2414.
Scheffzük, C., Kukushka, V.I., Vyssotski, A.L., Draguhn, A., Tort, A.B.L. & Brankačk, J. (2011) Selective coupling between theta phase and neocortical fast gamma oscillations during REM-sleep in mice. *PLoS One*, **6**, e28489.
Sirota, A., Montgomery, S., Fujisawa, S., Isomura, Y., Zugaro, M. & Buzsáki, G. (2008) Entrainment of neocortical neurons and gamma oscillations by the hippocampal theta rhythm. *Neuron*, **60**, 683–697.
Sun, Y., Farzan, F., Barr, M.S., Kirihara, K., Fitzgerald, P.B., Light, G.A. & Daskalakis, Z.J. (2011) Gamma oscillations in schizophrenia: mechanisms and clinical significance. *Brain Res.*, **1413**, 98–114.
Tiitinen, H., Sinkkonen, J., Reinikainen, K., Alho, K., Lavikainen, J. & Näätänen, R. (1993) Selective attention enhances the auditory 40-Hz transient response in humans. *Nature*, **364**, 59–60.
Tort, A.B.L., Kramer, M.A., Thorn, C., Gibson, D.J., Kubota, Y., Graybiel, A.M. & Kopell, N.J. (2008) Dynamic cross-frequency couplings of local field potential oscillations in rat striatum and hippocampus during performance of a T-maze task. *P. Natl. Acad. Sci. USA*, **105**, 20517–20522.
Tort, A.B.L., Komorowski, R., Eichenbaum, H. & Kopell, N. (2010) Measuring phase-amplitude coupling between neuronal oscillations of different frequencies. *J. Neurophysiol.*, **104**, 1195–1210.
Tort, A.B.L., Scheffer-Teixeira, R., Souza, B.C., Draguhn, A. & Brankačk, J. (2013) Theta-associated high-frequency oscillations (110-160 Hz) in the hippocampus and neocortex. *Prog. Neurobiol.*, **100**, 1–14.
Torterolo, P., Castro-Zaballa, S., Cavelli, M., Chase, M.H. & Falconi, A. (2016) Neocortical 40 Hz oscillations during carbachol-induced rapid eye movement sleep and cataplexy. *Eur. J. Neurosci.*, **43**, 580–589.
Uhlhaas, P.J. & Singer, W. (2010) Abnormal neural oscillations and synchrony in schizophrenia. *Nat. Rev. Neurosci.*, **11**, 100–113.
Uhlhaas, P.J., Pipa, G., Neuenschwander, S., Wibral, M. & Singer, W. (2011) A new look at gamma? High- (>60 Hz) γ-band activity in cortical networks: function, mechanisms and impairment. *Prog. Biophys. Mol. Bio.*, **105**, 14–28.
Voss, U., Holzmann, R., Tuin, I. & Hobson, J.A. (2009) Lucid dreaming: a state of consciousness with features of both waking and non-lucid dreaming. *Sleep*, **32**, 1191–1200.
Voss, U., Holzmann, R., Hobson, A., Paulus, W., Koppehele-Gossel, J., Klimke, A. & Nitsche, M.A. (2014) Induction of self awareness in dreams through frontal low current stimulation of gamma activity. *Nat. Neurosci.*, **17**, 1–5.
Zhang, X., Zhong, W., Brankačk, J., Weyer, S.W., Müller, U.C., Tort, A.B.L. & Draguhn, A. (2016) Impaired theta-gamma coupling in APP-deficient mice. *Sci. Rep.*, **6**, 21948.
Zijlmans, M., Jiruska, P., Zelmann, R., Leijten, F.S.S., Jefferys, J.G.R. & Gotman, J. (2012) High-frequency oscillations as a new biomarker in epilepsy. *Ann. Neurol.*, **71**, 169–178.

3. Capítulo 3. Acoplamiento entre frecuencias 2

3.1. Modulación respiratoria de la actividad gamma neocortical

En el capítulo anterior vimos como la actividad de alta frecuencia neocortical podía ser modulada por la actividad oscilatoria de baja frecuencia en un fenómeno que se denomina “acoplamiento entre frecuencias” o “cross frequecy coupling” (CFC) (Tort et al., 2010). Particularmente observamos como la fase de la onda theta (5-9 Hz) correspondiente a la actividad oscilatoria de la red hipocampica era capaz de modular la actividad HFO (110-160 Hz) a nivel neocortical (**Artículo 3** (Cavelli et al., 2017b). También observamos indirectamente que una onda lenta como theta puede ser capaz de modular no solo la amplitud de una onda rápida, sino la coherencia inter-cortical de alta frecuencia (Cavelli et al., 2017b). De los trabajos analizados hasta el momento se evidencia la existencia de diferentes sub-bandas de actividad gamma y/o HFO las cuales pueden tener diferente frecuencia, ser moduladas por diferentes ondas lentas o inclusive, estar moduladas por diferentes fases de una misma onda lenta (Sirota et al., 2008; Tort et al., 2013; Zhong et al., 2017). Estos resultados dejan en evidencia que cuando uno se refiere a una banda de frecuencia, por ejemplo, gamma, uno se puede estar refiriendo a una suma de actividades o sub-bandas de actividad con distinta co-modulación y distribuciones anatomo-funcionales.

Si nos remontamos a las primera evidencias experimentales del fenómeno de “acoplamiento entre frecuencias”, nos topamos con los trabajos pioneros de Adrian en la década del cuarenta (Adrian, 1942). Adrian observó como la actividad lenta generada por el pasaje de aire por las fosas nasales era capaz de acoplar a las oscilaciones gamma en el bulbo olfatorio del erizo (Adrian, 1942). Estos resultados luego se extenderían a otros animales como el gato y el conejo (Adrian, 1950). En tiempos presentes, está bien documentado que el pasaje de aire por el epitelio olfatorio es capaz de acoplar fielmente tanto la actividad lenta (Ver **Figura C3.1** y (Grosmaitre et al., 2007; Iwata et al., 2017)) como la actividad gamma a nivel del bulbo olfatorio (Ver **Figura C3.2** y (Manabe and Mori, 2013; Rojas-Líbano et al., 2014). Los trabajos de Fontanini (Fontanini and Bower, 2006, 2005) mostraron la existencia de cierto grado de internalización de potenciales respiratorios del bulbo olfatorio, los cuales podían ser registrados en los potenciales de membrana y el LFP de la corteza olfatoria.

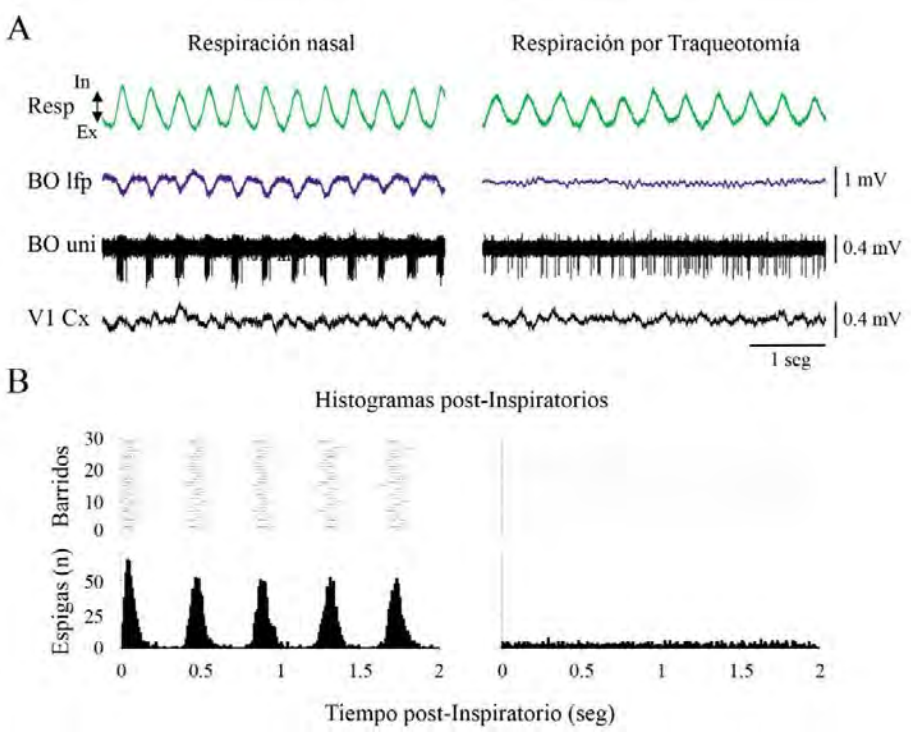

Figura C3.1 Los potenciales respiratorios y la actividad neuronal rítmica del bulbo olfatorio (BO) necesitan del pasaje de aire por las fosas nasales (rata). A. en verde se observan los esfuerzos respiratorios (movimientos torácicos), por debajo y en azul el LFP registrado a nivel del BO y por debajo (en negro) el registro extracelular de una neurona del BO y el ECoG de la corteza visual primaria (V1), respectivamente. A la izquierda se observan los registros durante la respiración nasal normal del animal mientras que a la derecha se registran los mismos canales durante la respiración traqueal. B. Histogramas post inspiratorios de las neuronas registradas a nivel del BO antes (izquierda) y después de realizada la traqueotomía (derecha). Se observa como la actividad rítmica neuronal y de campo depende del pasaje rítmico de aire por las fosas nasales (Cavelli *et al.,* resultados no publicados).

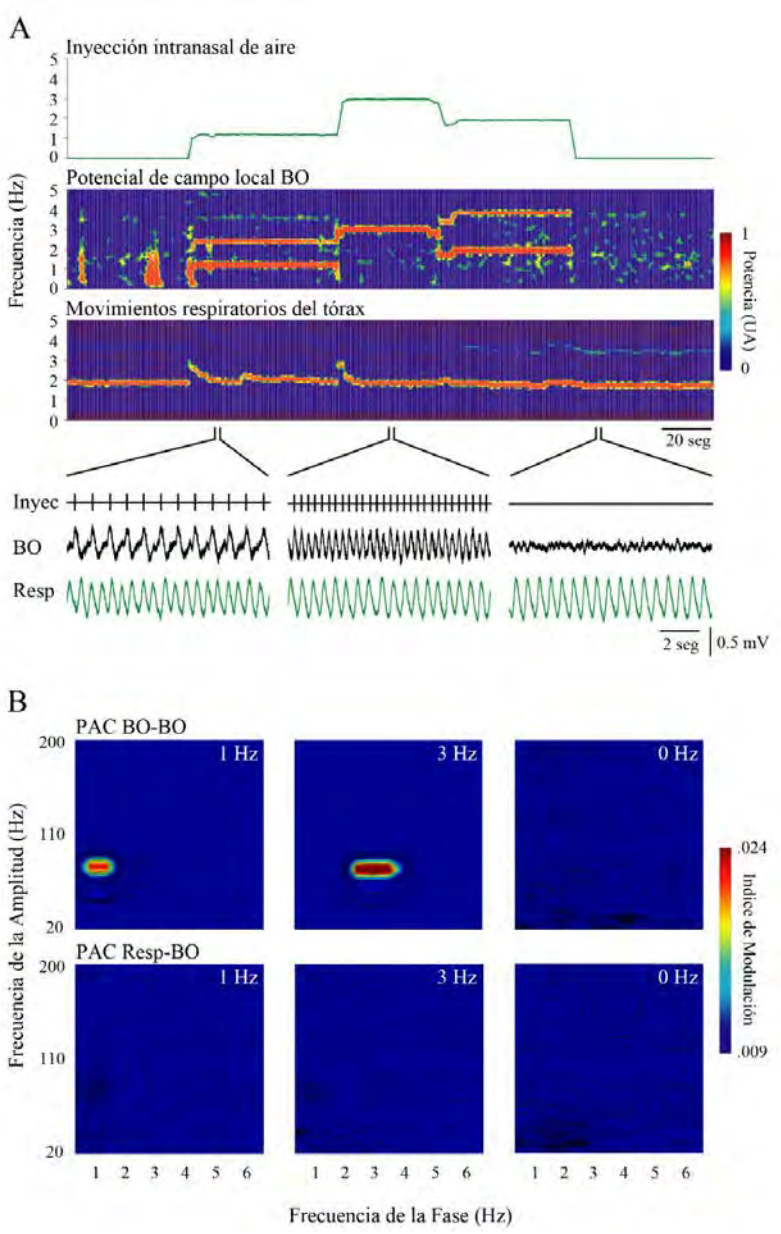

Figura C3.2 El pasaje de aire por las fosas nasales es suficiente para acoplar los potenciales lentos y la actividad gamma a nivel del BO. En esta imagen se muestran los registros electrográficos obtenidos durante la inyección de aire por las fosas nasales en una rata traqueotomizada. A. Arriba se observa la frecuencia de inyección de pulsos de aire (200 ms; 20 PSI/pulso). Por debajo los espectrogramas de potencias correspondientes al LFP del BO y del registro de esfuerzos respiratorios (movimiento torácico), respectivamente. Por debajo se observan ampliaciones de tres momentos distintos del registro. Durante la inyección de aire a 1, 3 y 0 Hz. B. Comodulogramas de acoplamiento entre frecuencias fase-amplitud. Por encima se observa la modulación fase-amplitud (PAC) entre los potenciales lentos registrados en el BO y la actividad de alta frecuencia también registrada en el BO. Por debajo se muestran comodulogramas correspondientes a la fase de la onda respiratoria y la amplitud de las oscilaciones registradas a nivel del BO. Se puede observar un aumento de la modulación gamma solo cuando se inyecta el aire en las fosas nasales y se toma como referencia la fase de la actividad bulbar (arriba, 1 y 3 Hz), no así si se toma como referencia la fase de la respiración (Cavelli *et al.,* resultados no publicados; por detalles sobre construcción de espectrogramas y comodulogramas de fase-amplitud ver **Articulo 2** (Cavelli et al., 2017b)).

Recientemente, se ha observado que la respiración nasal también es capaz de acoplar actividad lenta de áreas del cerebro que no están directamente relacionadas con el olfato, como lo son la corteza somatosensorial (Ito et al., 2014), la circunvolución dentada del hipocampo (Lockmann et al., 2016; Nguyen Chi et al., 2016; Yanovsky et al., 2014), la córtex prefrontal medial (Pf) y orbitofrontal (Biskamp et al., 2017; Zhong et al., 2017), así como en la corteza visual primaria y motora (Rojas-Líbano et al., 2018) de ratas y ratones. Otros estudios han demostrado que estos potenciales respiratorios corticales también se producen en varias regiones del cerebro humano (Herrero et al., 2018; Zelano et al., 2016). En todas estas áreas también se ha registrado modulación respiratoria de la actividad gamma (Biskamp et al., 2017; Ito et al., 2014; Lockmann et al., 2016; Nguyen Chi et al., 2016; Tort et al., 2018; Yanovsky et al., 2014; Zelano et al., 2016). Este "acoplamiento entre frecuencias (CFC)" entre la respiración y la actividad gamma se ha hipotetizado que podría desempeñar un papel en la integración de la actividad de redes neurales distribuidas (Tort et al., 2018; Zhong et al., 2017). En este sentido, nos preguntamos si sería posible que el concepto de "acoplamiento por sincronía" entre áreas alejadas del encéfalo en la banda gamma de frecuencias (**Capítulo 1**), y los fenómenos de "acoplamiento entre frecuencias" (**Capítulo 2**), podrían ser parte de un único fenómeno donde la coherencia gamma inter-cortical también se encuentre modulada por una onda de lenta como los potenciales respiratorios.

Con el objetivo de contestar esta pregunta publicamos el **Artículo 4** (Cavelli et al., 2018). Los resultados de este trabajo muestran que, durante la vigilia hay una clara interacción entre la respiración nasal y la actividad neocortical del gato. Se observan potenciales respiratorios neocorticales, así como acoplamientos con la actividad gamma en cada una de las áreas registradas. Observamos que esta internalización moduladora de la actividad neocortical desaparece durante el sueño. Además, mostramos que la respiración nasal es capaz de modular la coherencia gamma inter-cortical acoplando áreas del cerebro que no se han relacionado previamente ni con el olfato ni con la respiración.

ARTICULO 4

(Cavelli et al., 2018)

Nasal respiration entrains neocortical long-range gamma coherence during wakefulness

Matías Cavelli[1], Santiago Castro-Zaballa[1], Joaquín González[1], Daniel Rojas-Líbano[2], Nicolás Rubido[3], Noelia Velásquez[1], and Pablo Torterolo[1,*]

[1]Universidad de la República, Departamento de Fisiología de Facultad de Medicina, Laboratorio de Neurobiología del Sueño, Montevideo, General Flores 2125, 11800, Uruguay
[2]Universidad Diego Portales, Facultad de Psicología, Laboratorio de Neurociencia Cognitiva y Social, Santiago, Vergara 275, Chile
[3]Universidad de la República, Instituto de Física de Facultad de Ciencias, Montevideo, Iguá 4225, 11400, Uruguay
[*]ptortero@fmed.edu.uy

ABSTRACT

Recent studies have shown that slow cortical potentials in archi-, paleo- and neocortex, can phase-lock with nasal respiration. In some of these areas, gamma activity ($\gamma: 30-100 Hz$) is also coupled to the animal's respiration. It has been hypothesized that these functional relationships play a role in coordinating distributed neural activity. In a similar way, inter-cortical interactions at γ frequency have been also associated as a binding mechanism by which the brain generates temporary opportunities necessary for implementing cognitive functions. The aim of the present study was to explore if nasal respiration entrains inter-cortical communications at γ frequency, both during wakefulness (W) and sleep. Six adult cats chronically prepared for electrographic recordings were employed in this study. Our results show that during W, slow cortical respiratory potentials are present in the olfactory bulb and several areas of the neocortex. We also found that these areas exhibit cross-frequency coupling between respiratory phase and γ oscillations amplitude. Importantly, we demonstrate for the first time, that respiratory phase modulates the inter-cortical γ coherence between neocortical electrode pairs. On the contrary, slow respiratory oscillation and γ cortical oscillatory entrainments disappear during NREM and REM sleep. These results suggest that a single unified phenomenon involves cross-frequency coupling and long-range γ coherence across the neocortex. This fact could be related to the temporal binding process necessary for cognitive functions during W.

Introduction

The brain is a complex system, in which parallel processing coexist with serial operations within highly interconnected networks, but without a single coordinating center. This organ integrates neural events that occur at different times and locations into a unified perceptual experience. Understanding the mechanisms responsible for this integration, is a crucial challenge for cognitive neuroscience[1–3].

Neural synchronization at gamma frequency band ($\gamma: 30-100 Hz$) is considered a binding mechanism utilized by the brain to generate transient opportunities for communication and integration of the distributed neural activity necessary for cognitive functions[1–7].For example, cortical γ power increases during active behavioral states as well as during the performance of cognitive tasks[2,5,8–11]. Besides, γ synchronization between distant areas of the brain (γ coherence) also increases during several cognitive functions in both animals and humans[2,5,9,12–14]. γ coherence has been considered as a neural correlate of conscious perception[5,13–15]; it decreases during sleep[2,9] and is absent during narcosis (unconsciousness) induced by general anesthetics[16,17]. Recently, it was shown that slow oscillations such as theta rhythm of the hippocampal networks[18,19], cortical potentials caused by the rhythmic movement of the eyes[20,21], and respiration[18,22,23], modulate γ activity.

Adrian[24] report was the first description of nasal respiration driving neural oscillations in the olfactory bulb (OB)[11]. In the nasal epithelium, inhaled air activates olfactory sensory neurons (OSNs), which can detect both odor and mechanical stimuli[25,26]. The air flowing through the nostrils can also synchronize the neuronal activity and local field potentials (LFPs) in olfactory piriform cortex[27]. Recently, it has been observed that breathing also couples with the slow activity of brain areas that are not related to olfaction. Ito et al.[22] showed that spikes and delta (1-4 Hz) oscillations from the somatosensory cortex (S1), phase-lock with respiration in awake mice. This cortical respiratory potential (CRP) is lost after bulbectomy. CRPs were also observed in the dentate gyrus[28–30], medial prefrontal (Pf), and orbitofrontal cortex[18,31–34], as well as in the primary visual (V1) and motor (M1) cortex[35] of rats and mice. Other studies have showed that CRP also occurs in several regions of the human brain[36,37]. Respiratory modulation of local γ activity was also observed in most of the above-mentioned areas[10,11,18,22,23,29,31,35]. This "Cross Frequency Coupling" (CFC)[38] has been also hypothesized to play a role in integrating distributed network activity[18,23].

Utilizing the cat as an animal model, the aim of the present study was to seek if slow regional oscillatory activity phase-locks to respiration, and couples with the γ activity in cortical areas during wakefulness (W) and sleep. In addition, we studied if nasal respiration modulates inter-cortical long-range γ

coherence. Our results show that during W there is a clear an interaction between nasal respiration and cat's cortical γ activity (CRP and CFC). In addition, we show for the first time, that breathing modulates inter-cortical long-range γ coherence, notably entangling areas that have not been previously related neither to olfaction nor to breathing. Both CRP and γ modulation disappeared during both, non-REM (NREM) and rapid-eye-movement (REM) sleep.

Results

Cortical respiratory potentials are present during wakefulness but not during sleep

Electrocorticogram recordings (ECoG) from several areas of the neocortex and OB were obtained during the sleep-wake cycle of six cats (see Figure S1 for electrode location). We also simultaneously monitored the nuchal electromyogram (EMG) and the respiratory activity through a thermistor in the nostrils and a micro-effort sensor in the chest. Recordings were performed in a head-restricted condition with the body resting in a sleeping bag[9,39,40] (see Methods for details).

First, we determined the presence of CRP in the ECoG, and its dependence on the animal's behavioral state. Figure 1A shows the polysomnographic recording of a representative animal (C1) during W, NREM and REM sleep. During W, we observed that slow respiratory waves were accompanied by high amplitude oscillations of similar frequency in the OB. Similar potentials of lower amplitude were also present in the neocortex (Fig. 1A, top left). We detected similar CPR in the ECoG for all animals during W. During NREM sleep, although we observed the characteristic slow waves and sleep spindles, these oscillations do not seem associated with the respiratory cycle (Fig. 1A, middle traces). During REM sleep, CPRs were not observed in any of the recorded areas (Fig. 1A, right traces). We also found in all the animals that respiration and cortical activity were spectrally coherent during W, but not during NREM and REM sleep (Fig. 1B). We then calculated the respiratory rate through spectral analysis of the respiratory signal. As expected, the respiratory frequency was dependent of the behavioral state[39] (repeated measurements ANOVA (rmANOVA) and Bonferroni post-hoc tests; $F_{(1.144,5.721)} = 8.158$, $p = 0.028$). During NREM sleep, respiration rate was lower in comparison to W and REM sleep (Fig. 1C). Thereafter, we computed the average coherence levels for each animal, at the frequency that corresponds to the peak of the respiratory wave's power spectrum[23]. Figure 1D shows that coherence values between respiratory oscillations and ECoG are large during W and decrease during sleep (rmANOVA; $F_{(1.094,5.469)} = 66.56$; $p = 0.0003$). Next, we sought to determine whether these CRPs were related to the passage of air through the nostrils. As shown in Figure 1E, the coherence between respiration and ECoG that is observed during nasal respiration in W, is absent during mouth breathing (two-tailed t-tests, $p < 0.05$). Circular distribution analysis of the phase differences between the OB and the neocortical electrodes exhibits phase differences other than 0° or 180° (Fig. S2), suggesting that CRPs were not a result of volume conduction from the OB[34].

Respiration entrains cortical γ activity during wakefulness

Sleep and W transitions are displayed in Figure 2A; CRPs are clearly associated with W but are absent during sleep. Spectrograms of Figure 2B and filtered recordings shown in Figure S3, exhibit that bursts of coupled γ band ($30-50\,Hz$) activity are also related with W and associated with breathing.

In order to quantify the cross-frequency coupling ($CFC_{(Resp\text{-}\gamma)}$) between respiration and γ oscillations, we constructed cross-correlation function maps (CCFmap)[19] between respiratory signal and ECoGs amplitude envelopes in the 10 to $100\,Hz$ frequency band. Figure 3 shows the CCFmap of five neocortical areas and OB of a representative animal during W, NREM and REM sleep, as well as the auto-correlation function (ACF) of the respiratory wave. We observed a clear cross-correlation between respiration and γ activity for all the recorded areas during W. On the other hand, during sleep (NREM and REM) the $CFC_{(Resp\text{-}\gamma)}$ levels are negligible. In the ACF (bottom panels in Fig. 3), zero lag corresponds to the end of expiration and beginning of inspiration. Note that γ-respiration correlation increases mainly during the expiratory phase of the cycle. Also, the end of inspiration is accompanied by higher γ frequencies that become progressively lower as expiration develops (see W panels in Fig. 3). We found similar behavioral state dependent changes in $CFC_{(Resp\text{-}\gamma)}$ for each recorded animal (see Fig. S4). This analysis also revealed some variability among the animals regarding the frequency limits of the γ burst; in some animals the frequency range of the bursts goes up to $60\,Hz$ (Fig. S4).

In addition, we analyzed the relationships between the phase (in degrees) of the respiratory wave and the amplitude (envelopes) of γ activity (phase amplitude coupling or PAC), using the modulation index (MI) designed by Tort et al[38]. The phase-amplitude MI quantifies the deviation of the empirical phase-amplitude distribution from a uniform distribution. Figure 4A shows the average $MI_{(Resp\text{-}\gamma)}$ values of all the recorded areas for each animal (n=6) during W and sleep. This analysis revealed that the highest $MI_{(Resp\text{-}\gamma)}$ values were observed during W (Fig. 4A; rmANOVA; $F_{(1.011,5.057)} = 14.45$; $p = 0.0123$). Furthermore, we evaluated how the $MI_{(Resp\text{-}\gamma)}$ values varied depending on the type of breathing, buccal or nasal. Figure 4B shows the MI value for all areas of a representative animal recorded during buccal and nasal breathing during W. $MI_{(Resp\text{-}\gamma)}$ was significantly higher during nasal breathing.

Respiratory cortical entrainment is also present during cataplexy (wakefulness without muscle tone)

Muscle tone is one of the main differences between W and sleep[2,9,39,40] and is typically the main artefactual signal recorded in the EEG, ECoG and LFPs during W[8]. In order to rule out the possibility that muscle activity was affecting

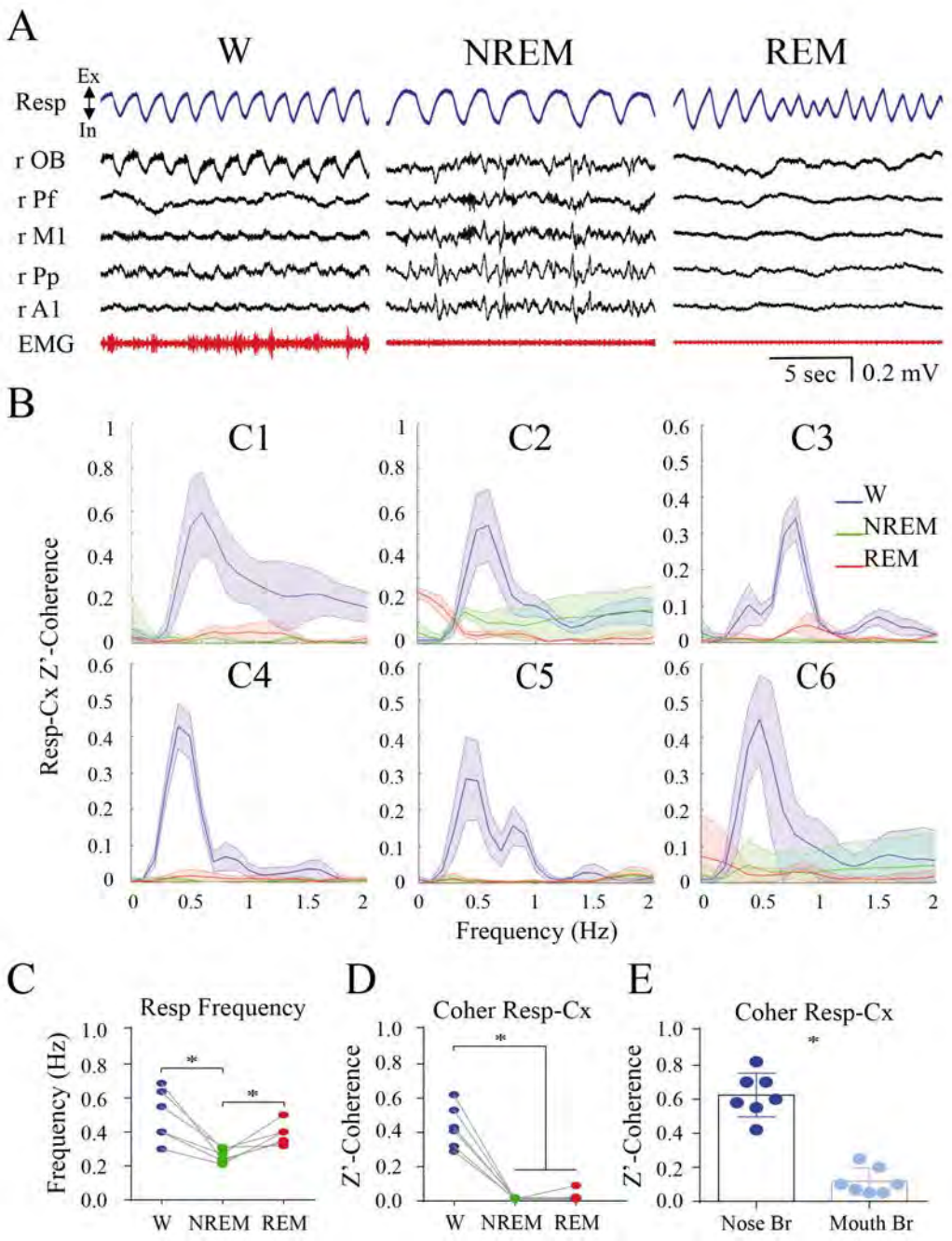

Figure 1. Cortical respiratory potential (CRP) in the cat's cortex during wakefulness (W) and sleep . A. CRPs in cortical areas of a representative cat (C1) during wakefulness (W), NREM and REM sleep. Breathing is recorded by a thermistor in the nostrils (Resp, blue) simultaneously with the ECoG (black) and the electromyogram (EMG, red). B. Z'-Coherence between the respiratory waves and ECoG signals during sleep and W. The analyses were performed in each animal (C1 to C6). Each trace is the average of all the recorded channels. Shaded areas correspond to the standard deviation. C. Respiratory frequency during W and sleep stages, which was extracted from the peak of the respiratory signal's power spectrum. D. Z'-Coherence values between the respiratory wave and the ECoG (measured at the peak of the respiratory frequency) during W, NREM, and REM sleep. E. The same analysis as in D, is displayed during mouth and nose breathing for a representative animal. *, $p < 0.05$. Br, breathing; Cx, cortex; Ex, exhalation; In, inhalation; OB, olfactory bulb; Pf, prefrontal cortex; M1, primary motor cortex; Pp, posterior parietal cortex; A1, primary auditory cortex; r, right hemisphere.

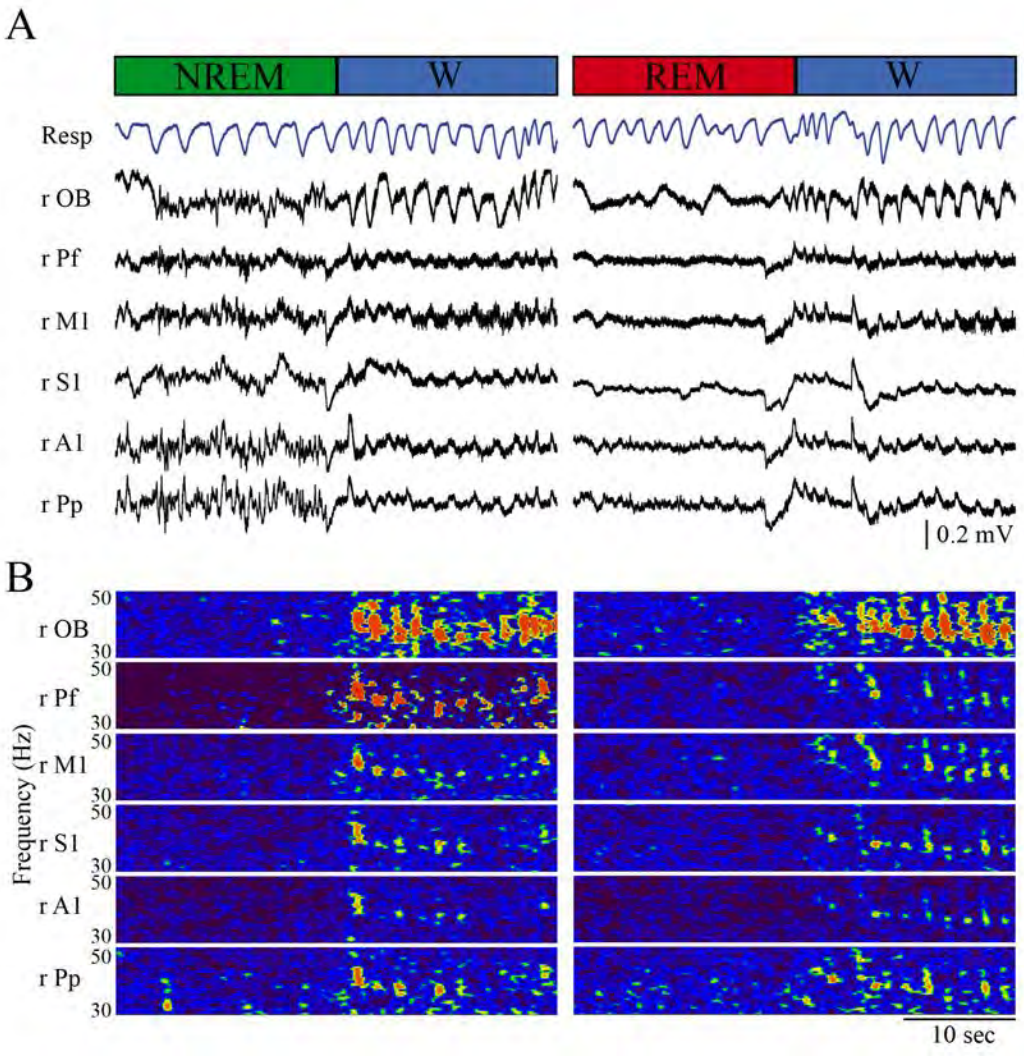

Figure 2. Cortical respiratory potential (CRP) during sleep/wakefulness transitions. A. Polysomnographic recordings during the transition from NREM sleep to wakefulness (W, left), and from REM sleep to W (right). Breathing was recorded with a thermistor placed in the nostrils (Resp, blue) simultaneously with the ECoGs (black). The ECoGs are from C1 animal. B. Spectrograms $30-50\,Hz$ of the recordings showed in A. They were constructed using a 1 second sliding window ($0.5\,Hz$ resolution). OB, olfactory bulb; Pf, prefrontal cortex; M1, primary motor cortex; S1, primary somatosensory cortex A1, primary auditory cortex; Pp, posterior parietal cortex

the results, we carried out experiments in four animals where we turned off the muscular activity. The nucleus pontis oralis (NPO) is considered to exert executive control over the initiation and maintenance of REM sleep. In the cat, a single microinjection of carbachol (a cholinergic agonist) into the NPO can produce either REM sleep (REM sleep induced by carbachol, REMc) or a waking state with muscle atonia, i.e. cataplexy (cataplexy induced by carbachol, CA) for 30 minutes to 2 hours[39,40]. In both states, upon carbachol microinjections, we found that although the animals exhibited muscle atonia (CA and REMc), only during CA we observed CRP (Fig. 5A and B) and $CFC_{(Resp\text{-}\gamma)}$ (Fig. 5C and D).

Respiration entrains neocortical long-range γ coherence

In order to investigate if respiratory rhythms facilitate intercortical communication through high frequency channels, we studied the co-modulation between the respiratory waves and the cortico-cortical γ synchronization using different metrics. Figure 6A shows a polysomnographic raw recording of a representative animal during W. The same recordings but filtered for the γ band ($30-60\,Hz$; blue traces) and with the corresponding amplitudes superimposed (RMS envelopes; red traces) are exhibited in Figure 6B. It is readily observed that γ amplitude relationships between different cortex, seems to

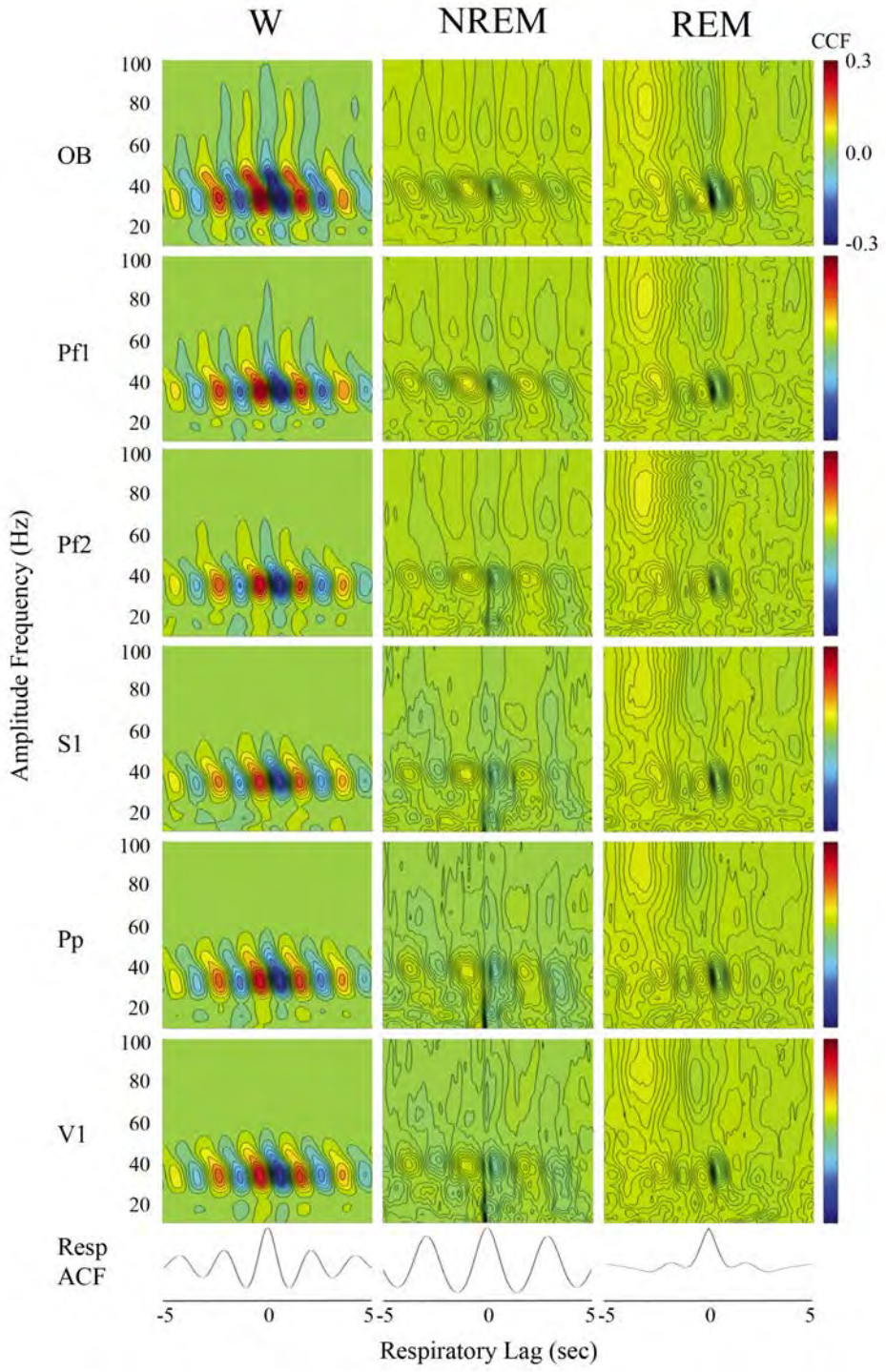

Figure 3. Cross-frequency coupling between cortical activity and respiration during wakefulness (W) and sleep. Color-coded panels show the cross-correlation function (CCF) between the respiratory wave and the amplitude envelope of the ECoG signals between 10 and 100 Hz (i.e., 10 Hz bandwidth with 5 Hz steps) during W, NREM and REM sleep, of a representative animal (C2). The respiratory wave auto-correlation function (ACF) is also shown (bottom). Olfactory bulb (OB), anterior prefrontal cortex (Pf1), posterior prefrontal cortex (Pf2), primary somatosensory cortex (S1), posterior parietal cortex (Pp) and primary visual cortex (V1) of the right hemisphere.

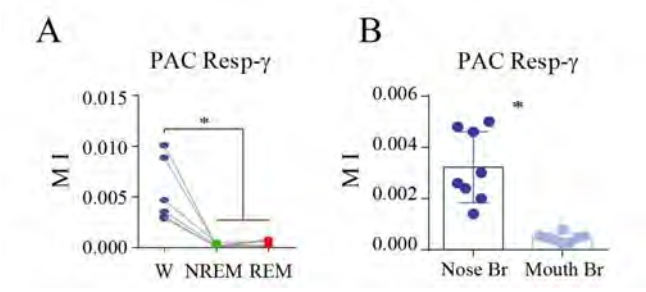

Figure 4. Phase amplitude coupling (PAC) between respiration and γ cortical activity $PAC_{(Resp\text{-}\gamma)}$ during wakefulness (W), NREM and REM sleep. A. PAC between the respiratory waveform and the amplitude (envelope) of the γ activity for 6 cats, quantified by the modulation index (MI)[38]. Each MI value represents the average over all cortical areas recorded for each of the 6 animals. B. MI between respiratory phase and γ amplitude during mouth or nose breathing of a representative animal (C1). The values correspond to the mean standard deviation of the seven cortical areas recorded. *, $p < 0.05$.

be in phase with the respiratory wave (Fig. 6, S3 and S5). In order to quantify this phase relationship, we analyzed the coherence of all pairs of cortices recorded as a function of the respiratory phase. Figure. 7A shows the differences in coherence among behavioral states for all the animals and electrodes pairs. During W, respiratory phase modulates the γ coherence and this phenomenon is absent during sleep. We obtained similar results when we analyzed the normalized phase locking value (PLV; Fig. S6). Also, in Figure 7B we computed the coherence between the coefficient of determination (R^2) for all pairs of filtered ECoG recordings (γ: $30-60\,Hz$) and the respiratory signal. We note from Figure 7B1 that large coherence at the respiratory frequency is only observed during W, where R^2 values are modulated by the respiratory phase (Fig. 7B2). Moreover, we determined which pairs of electrodes the inter-cortical γ synchronization is modulated by respiration. Figure 7C shows that γ coherence between all neocortical recording pairs was phase-locked with the respiratory signal. However, when coherence was analyzed between neocortical areas and OB, there was not a clear phase preference (Fig. 7C). In fact, while γ coherence is mostly present between neocortical pair of electrodes (Fig. 7D), OB-neocortical pairs do not exhibit this phenomenon, despite each of the recorded areas shows $CFC_{(Resp\text{-}\gamma)}$ (see Figs. 2B, 3, and S3).

Discussion

Our findings provide evidence about the ability of nasal respiration to entrain neural oscillatory activity in several regions of the cat's brain. We found that nasal respiration is involved in the generation of the slow CRP and $CFC_{(Resp\text{-}\gamma)}$ in all recorded areas, in a behavioral state-dependent fashion. Furthermore, we demonstrated that the phase of the respiratory cycle modulates inter-cortical γ coherence during W. This fact could suggest that cross-frequency modulation between respiration and cortical γ rhythms on one side, and long-range inter-cortical γ coherence on the other, could be components of a single phenomenon.

Cortical respiratory potentials

The existence of CRP in the OB is a well-known phenomenon[10,11,24,25]. It has been shown that the slow activity of the OB faithfully follows respiration in freely behaving rats[11]. Moreover, respiratory slow potentials can be recorded in olfactory and non-olfactory cortical areas[18,22,27,29,30,33,35]. In the present work, we demonstrated the presence of CRPs in the neocortex of the cat.

Cross frequency coupling between respiration and γ activity

CFC has been reported in electrophysiological signals, such as membrane potential, LFPs, ECoG and EEG[38]. A well-known CFC example occurs between the phase of the hippocampal theta rhythm ($5-10\,Hz$) and the γ amplitude in the hippocampus and neocortex[18,19,38]. As mentioned in the Introduction, the respiratory rhythm modulates γ activity in several areas of rodent and humans brain[10,11,18,22,23,29,31,33,35,36]. Interestingly, recent studies in humans showed that the change from nasal to mouth breathing decreases CFC between theta and γ in the temporal lobe and alter limbic-based behavior[36]. In the present study, we demonstrate the existence of CFC between the phase of the respiratory wave and the amplitude of γ oscillation in the cat neocortex. It is important to note that the average frequency and limits of the γ burst differ between species[23,36,37], varies according to the animal's alertness level[35], and to the recording site[33]. In addition, we show that this coupling remains intact during the carbachol-induced cataplexy, which strongly suggest that the muscular tone is not involved in this phenomenon. Karalis Sirota have recently shown in mice, the coexistence of respiratory re-afferent signal and the apparently corollary discharge in limbic's areas[33]. However, at the neocortical level this modulation of brain waves depends on air passage through the nostrils (present work), and on an intact OB[22]. For this reason, it is probably a breathing reafferent signal that modulates multiples neocortical areas[22,35]. It interesting to remember that breathing, through central autonomic integration, is also capable of regulating cardiac activity[39]. The bottom panel in Figure S3 (Tachogram; red traces) shows how respiratory sinus arrhythmia is also coupled to CRP and $CFC_{(Resp\text{-}\gamma)}$ during W. In fact, the first time we were aware of this cortical respiratory coupling was indirectly through the analysis of cat's heart rate variability[39]. These observations are indicative of a generalized role of respiration in the coordination of bodily rhythms[33]. The existence of CRP and $CFC_{(Resp\text{-}\gamma)}$ in Rodentia, Primate and our results in Carnivora, suggests a preserved mammal trait. Given the evolutionary importance of smell

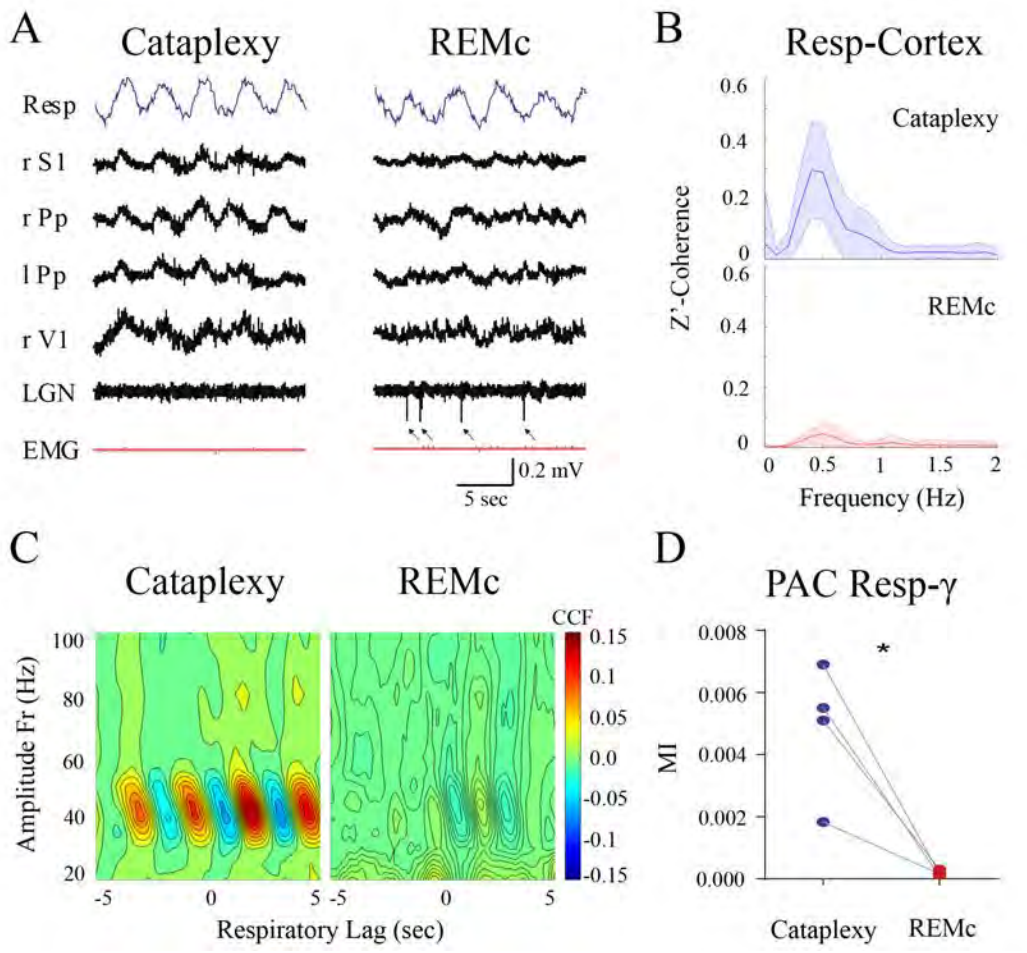

Figure 5. CRP and $CFC_{(Resp\text{-}\gamma)}$ were independent of the muscular tone. A. Simultaneous polysomnographic recordings during cataplexy (CA) and REM sleep induced by carbachol (REMc). Breathing was recorded with a micro-effort piezo crystal infant sensor (Resp, blue) in simultaneous with the ECoG from the primary sensory cortex (S1), left and right posterior parietal cortex (Pp l and Pp r) and primary visual cortex (V1). Lateral geniculate nucleus (LGN) electrogram and EMG (red) are also shown. Muscle tone absence is observed in both states, but only during REM-Carb PGO waves were present in the LGN (arrows). B. Z'-coherence between the respiratory wave and ECoG signals during CA and REMc. Each graph represents the mean ± standard deviation of all the cortical areas, and all the animals (n = 4; C3-C6). C. Mean CCF maps during CA and REMc. Mean cross-correlation function (CCF) between the respiratory waves and the amplitude envelope of the ECoG signals (between 10 to 100Hz; 10Hz bandwidth and 5Hz steps) during CA, and REMc. The CCF map for each condition corresponds to the mean of all the CCF maps of every area and animal. D. $PAC_{(Resp\text{-}\gamma)}$ during CA and REMc. Each value represents the mean MI value for all areas of each animal. The statistical significance between CA and REMc was evaluated with the two-tailed paired t-test (*, $p < 0.05$).

and the dense OB connectivity, it is highly probable to find similar phenomena in other non-mammalian vertebrates.

Are $CFC_{(Resp\text{-}\gamma)}$ and inter-cortical γ coherence part of the same phenomenon?

Olfaction is considered an "active sensing" function, where the animals produce motor actions (breathing) specifically tuned to obtain useful sensory information about their environment[35,41–43]. Other examples are whisking and sniffing in rodents, electrolocation in fishes, echolocation in bats and odontocetes cetaceans as well as fingers and eye movements in primates[11,44,45]. In particular, visual exploration in primates is related to eye movement, specifically saccades and micro-saccades[46,47] which are highly rhythmic[20,21]. In visual areas there are low frequency oscillations phase-locked to the rhythmic saccadic movements which exhibit a clear CFC with the γ band activity[20,21]. Something similar happens in the cortex with whisker movement in rats[35,43] and also with nasal respiration[18,22,29,30,35]. Furthermore, slow waves coupled to saccadic movement are capable of modulating inter-cortical

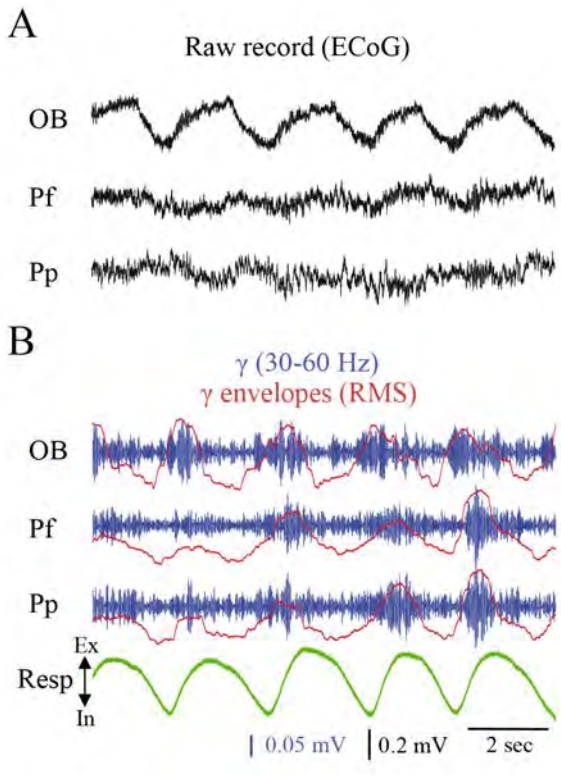

Figure 6. Respiratory modulation of inter-cortical γ synchronization. Panel A shows raw ECoG recordings from different cortical areas during wakefulness (W). The respective γ-band filtered ECoG signals (blue traces) with their root-mean-square (RMS) envelopes (red), in simultaneous with the respiratory signal (Resp, green) are shown in panel B.

spikes and LFP γ coherence in visual areas[21]. Recently, we showed that during REM sleep, hippocampal theta activity modulates the coherence of intra-hemispheric high frequency oscillations ($110-160\,Hz$) in medial and posterior cortices of the rat[19]. In addition, the present work demonstrates, for the first time, that long-range γ coherence occurs modulated by the respiratory phase, suggesting a unified phenomenon. This "respiratory binding effect" is observed at the neocortical level; however, γ coherence between OB and neocortical regions is not modulated by the respiratory activity. Recent works propose that respiratory rhythms facilitated inter-regional communication via $CFC_{(Resp\text{-}\gamma)}$ [18,23]. Other lines of research propose that phase synchrony between areas of the brain, especially at γ frequencies, constitutes a dynamical mechanism for the control of cross-regional information flow[3,48,49]. The findings of this work can potentially bring together these two theoretical frameworks in a global neocortical processing scheme; i.e., high frequency interregional binding is modulated by physiological rhythms such as respiration.

Cortical respiratory entrainment is not present during sleep

A remarkable result in our work is that neocortical respiratory entrainment is absent during sleep. Specifically, we demonstrated that CRP, $CFC_{(Resp\text{-}\gamma)}$ and inter-cortical γ coherence are absent during NREM and REM sleep. Hence, breathing appears unable to entrain oscillatory activity in the OB as well as in the neocortex during sleep. Recently, Zhong et al.[18]showed that during REM sleep no CRP or $CFC_{(Resp\text{-}\gamma)}$ is observed in any neocortical areas of the rat. Nevertheless, during NREM sleep power-spectrum peaks coincide in frequency between respiration and limbic or pre-limbic areas[18,33]. On the other hand, they also observed CFC between slow cortical oscillations and γ activity ($CFC_{(Slow\text{-}\gamma)}$)) in the OB and pre-limbic areas. However, two matching frequency peaks do not necessarily imply two coherent time-series at that frequency. It is also important to note that during NREM sleep there are slow cortical waves in the same frequency range as breathing (delta, $0.5-4\,Hz$). In this sense, this delta activity may generate the $CFC_{(Slow\text{-}\gamma)}$ observed in the OB and pre-limbic areas. In this regard, Manabe Mori[10] showed that during REM and NREM sleep breathing was unable to entrain γ activity in the OB[10]. At last, it was recently shown that breathing can modulate the dynamics of limbic areas, such as hipocampal ripples, and cortical UP and DOWN states, both involved in the offline processes of memory consolidation during sleep[33]. Cognitive activity and different electrographic rhythms are generated by the activity of cortical and subcortical neurons, which are reciprocally connected. These networks are modulated by the activating or waking-promoting systems of the brainstem, hypothalamus and basal forebrain that directly or indirectly project to the thalamus and/or cortex[2,50]. By regulating thalamocortical activities, these activating systems produce electrographic and behavioral arousal. The activating systems decrease their activity during the NREM sleep. However, while most monoaminergic systems decrease their activity during REM sleep (REM-off neurons), cholinergic neurons increase their discharge during this behavioral state (REM-on neurons), which contributes to cortical activation[2,50]. In addition, because these cholinergic neurons are active during REM sleep, they should not be critical to the generation of CRP and $CFC_{(Resp\text{-}\gamma)}$ which is absent during this state. In fact, systemic muscarinic antagonists do not block CRP and $CFC_{(Resp\text{-}\gamma)}$ in the dorsal hippocampus[28] or coherent gamma activity in the cat's neocortex[51]. More efforts must be made to unravel what neurotransmitters are involved in the gaiting, generation and maintenance of this cortical respiratory entrainment.

Conclusions

The results obtained in rodents, humans and the present results in felines strongly suggest that CRP and $CFC_{(Resp\text{-}\gamma)}$ is a conserved phenomenon in mammals. Extending previous findings to the cat, we confirmed the dependency on behavioral state of the cortical-respiratory coupling. We also demonstrated for the first time, that nasal respiration can modulate inter-cortical

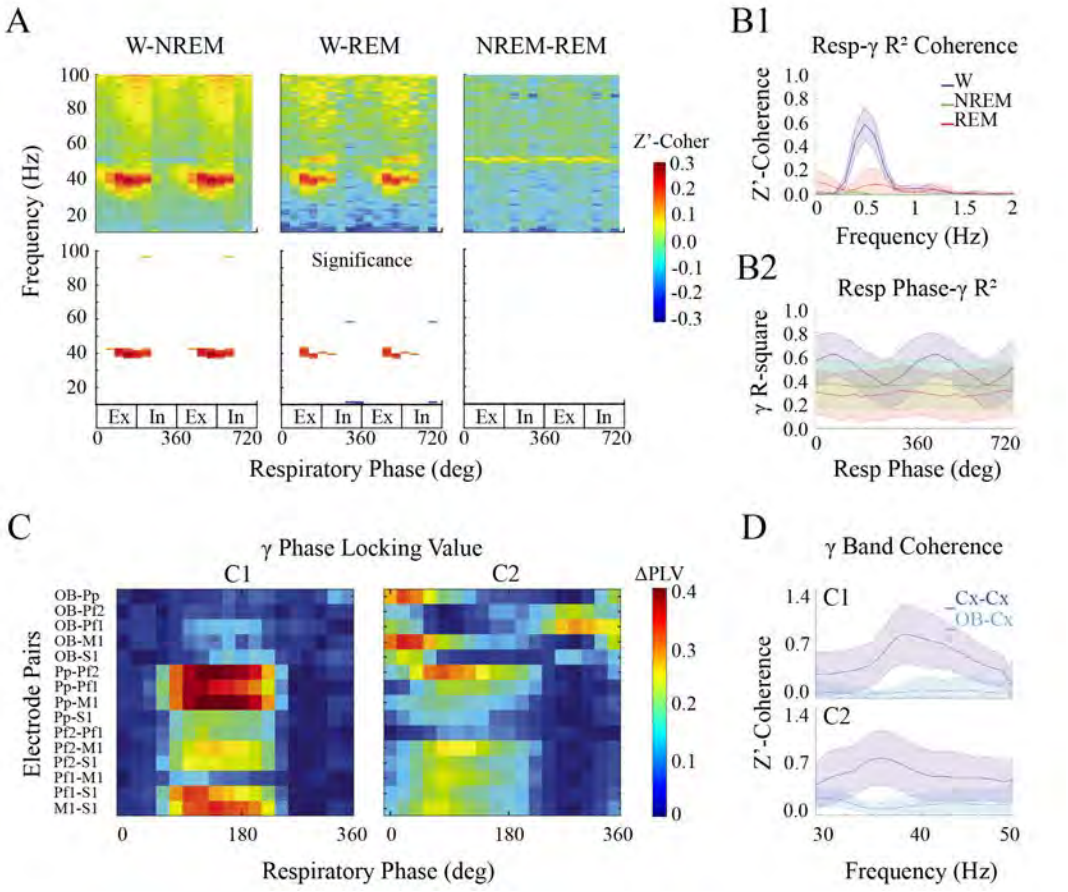

Figure 7. Respiratory modulation of inter-cortical γ coherence. A. Inter-cortical Z'-coherence as a function of respiratory phase and frequency. The ECoG's coherence was computed for each respiratory-phase bin (40 degrees, 9 bins) with a frequency resolution of $0.5\,Hz$. Each color map at the top is the difference between two behavioral states averaged over all animals and ECoG recording pairs; W-NREM, W-REM, and NREM-REM sleep. The maps at the bottom of the panel show only the statistically-significant values with a $p < 0.0001$. B. Respiratory modulation of γ linear correlation. B1 shows the coherence between all the cortical γ R^2 waves and the respiratory waveform for all animals, electrode pairs, and behavioral states. Each pair of ECoG recordings was band-pas filtered $(30-60\,Hz)$, and the square root of the linear correlation was calculated with a moving window of 0.088 seconds (4 γ cycles) with $\simeq 99\,\%$ of superposition. B2 displays R^2 as a function of the respiratory phase. After the respiratory phase bin extraction, the average R^2 was calculated for each respiratory-phase bin and behavioral state. C. Average phase-locking values (PLV) for all pairs of γ-band filtered $(30-60\,Hz)$ ECoG signals as a function of the respiratory phase. Specifically, the average PLV is the mean value over each phase bin interval for the animals C1 (left) and C2 (right), which we set to 18-degree interval per bin. Moreover, the color maps represent only the PLV values that are effectively modulated by respiration, i.e., we find PLV by subtracting from the average the minimum PLV value found throughout the respiratory cycle. Panel D shows the inter-cortical γ z'-coherence between the neocortical pair (Cx-Cx) and between the OB and the neocortex pair (OB-Cx) for the animals in panel D. In, inhalation; Ex, exhalation.

coherence at γ frequency, especially between remote neocortical areas. This evidence suggests that the respiratory rhythm could facilitate inter-regional communication[18,23]. Previously described γ synchrony between areas of the brain as a dynamical mechanism for the control of cross-regional information flow or "communication through coherence"[3,48,49], could be part of a larger phenomenon which includes respiratory modulations. The strong modulation of the electrocortical activity by the respiratory rhythms could be the foundation of the effect of breathing on critical functions such as memory, cognition, affection and stress responses[33,36,37,52].

Acknowledgements

This study was partially supported by the "Programa de Desarrollo de Ciencias Basicas -PEDECIBA", Comisión Sectorial de Investigación Científica - CSIC", and "Agencia Nacional de Investigación e Innovación - ANII". S. CZ. and N. V. re-

ceived a postgraduate scholarship from the ANII, while M. C. received a fellowship from "Comisión de Apoyo a Postgrados - CAP". D.RL. acknowledges funding from "Proyecto Fondecyt 3120185".

Author contributions statement

Financial support: P.T.. Experimental design: M.C., S.CZ., and P.T.. Experimental procedures: M.C., S.CZ., N.V., and P.T.. Analysis of the data: M.C., J.G., D.RL., and N.R.. Discussion and interpretation of the data: M.C., P.T., J.G., D.RL., N.R., S.CZ., and N.V.. Wrote the manuscript: M.C. and P.T.. All the authors participated in critical revision the manuscript, added important intellectual content, and approved the final version.

Data Availability

For access to data and custom computer code contact Dr. Pablo Torterolo (ptortero@fmed.edu.uy) or Matías Cavelli (mcavelli@fmed.edu.uy).

Abbreviations

Abbreviations γ, gamma; ACF, autocorrelation function; ANOVA, ANalysis Of VAriance; CA, cataplexy; CCF, cross-correlation function; CFC, cross-frequency coupling; CRP, cortical respiratory potential; EEG, electroencephalogram; ECoG, electrocorticogram; EMG, electromyogram; i.p., intraperitoneal; L, left; LGN, lateral geniculate nucleus; LFP, local field potential; M1, primary motor cortex; MI, modulation index; NPO, nucleus pontis oralis; NREM, non-REM sleep; REMc, REM carbachol; OB, olfactory bulb; OSN, olfactory sensory neurons; PAC, phase-amplitude coupling; Pf, prefrontal cortex; PGO, ponto geniculo occipital; PLV, phase locking value; REM, rapid eyes movement; rmANOVA, repeated measures ANOVA; RMS, root mean square; s.c., subcutaneous; S1, primary somato-sensory cortex; SD, standard deviation; V1, primary visual cortex; V2, secondary visual cortex; W, wakefulness.

References

1. Singer, W. Neuronal Synchrony : A Versatile Code for the Definition of Relations ? Most of our knowledge about the functional organization. *Neuron* **24**, 49–65, DOI: https://doi.org/10.1016/S0896-6273(00)80821-1 (1999).
2. Cavelli, M. *et al.* Translational Brain Rhythmicity Absence of EEG gamma coherence in a local activated cortical state: a conserved trait of REM sleep. *Transl Brain Rhythm.* **2**, 1–13, DOI: 10.15761/TBR.1000115 (2017).
3. Fries, P. Neuronal Gamma-Band Synchronization as a Fundamental Process in Cortical Computation. *Annu. Rev. Neurosci.* **32**, 209–224, DOI: 10.1146/annurev.neuro.051508.135603 (2009).
4. Gray, C. M., König, P., Engel, A. K. & Singer, W. Oscillatory responses in cat visual cortex exhibit inter-columnar synchronization which reflects global stimulus properties. *Nature* **338**, 334–7, DOI: 10.1038/338334a0 (1989).
5. Varela, F., Lachaux, J. P., Rodriguez, E. & Martinerie, J. The brainweb: phase synchronization and large-scale integration. *Nat. reviews. Neurosci.* **2**, 229–239, DOI: 10.1038/35067550 (2001).
6. Engel, A. K., Fries, P. & Singer, W. Dynamic predictions: Oscillations and synchrony in top–down processing. *Nat. Rev. Neurosci.* **2**, 704–716, DOI: 10.1038/35094565 (2001).
7. Buzsáki, G. & Draguhn, A. Neuronal oscillations in cortical networks. *Sci. (New York, N.Y.)* **304**, 1926–9, DOI: 10.1126/science.1099745 (2004).
8. Buzsáki, G. & Schomburg, E. W. What does gamma coherence tell us about inter-regional neural communication? *Nat. Neurosci.* **18**, 484–489, DOI: 10.1038/nn.3952 (2015).
9. Castro-Zaballa, S., Falconi, A., Chase, M. H. & Torterolo, P. Coherent neocortical 40-Hz oscillations are not present during REM sleep. *The Eur. journal neuroscience* **37**, 1330–9, DOI: 10.1111/ejn.12143 (2013).
10. Manabe, H. & Mori, K. Sniff rhythm-paced fast and slow gamma-oscillations in the olfactory bulb: relation to tufted and mitral cells and behavioral states. *J. Neurophysiol.* **110**, 1593–1599, DOI: 10.1152/jn.00379.2013 (2013).
11. Rojas-Líbano, D., Frederick, D. E., Egaña, J. I. & Kay, L. M. The olfactory bulb theta rhythm follows all frequencies of diaphragmatic respiration in the freely behaving rat. *Front. behavioral neuroscience* **8**, 214, DOI: 10.3389/fnbeh.2014.00214 (2014).
12. Bressler, S. L., Coppola, R. & Nakamura, R. Episodic multiregional cortical coherence at multiple frequencies during visual task performance. *Nature* **366**, 153–6, DOI: 10.1038/366153a0 (1993).
13. Rodriguez, E. *et al.* Perception's shadow: long-distance synchronization of human brain activity. *Nature* **397**, 430–3, DOI: 10.1038/17120 (1999).
14. Melloni, L. *et al.* Synchronization of neural activity across cortical areas correlates with conscious perception. *The J. neuroscience* **27**, 2858–65, DOI: 10.1523/JNEUROSCI.4623-06.2007 (2007).
15. Joliot, M., Ribary, U. & Llinás, R. Human oscillatory brain activity near 40 Hz coexists with cognitive temporal binding. *Proc. Natl. Acad. Sci. United States Am.* **91**, 11748–51, DOI: https://doi.org/10.1073/pnas.91.24.11748 (1994).
16. John, E. R. The neurophysics of consciousness. *Brain Res. Rev.* **39**, 1–28, DOI: https://doi.org/10.1016/S0165-0173(02)00142-X (2002).

17. Mashour, G. a. Integrating the science of consciousness and anesthesia. *Anesth. analgesia* **103**, 975–82, DOI: 10.1213/01.ane.0000232442.69757.4a (2006).

18. Zhong, W. *et al.* Selective entrainment of gamma subbands by different slow network oscillations. *Proc. Natl. Acad. Sci. United States Am.* **114**, 4519–4524, DOI: 10.1073/pnas.1617249114 (2017).

19. Cavelli, M. *et al.* Power and coherence of cortical high-frequency oscillations during wakefulness and sleep. *Eur. J. Neurosci.* 1–10, DOI: 10.1111/ejn.13718 (2017).

20. Ito, J., Maldonado, P. & Grün, S. Cross-frequency interaction of the eye-movement related LFP signals in V1 of freely viewing monkeys. *Front. Syst. Neurosci.* **7**, 1, DOI: 10.3389/fnsys.2013.00001 (2013).

21. Lowet, E. *et al.* Microsaccade-rhythmic modulation of neural synchronization and coding within and across cortical areas V1 and V2. *PLOS Biol.* **16**, e2004132, DOI: 10.1371/journal.pbio.2004132 (2018).

22. Ito, J. *et al.* Whisker barrel cortex delta oscillations and gamma power in the awake mouse are linked to respiration. *Nat. communications* **5**, 3572, DOI: 10.1038/ncomms4572 (2014).

23. Tort, A. B., Brankačk, J. & Draguhn, A. Respiration-Entrained Brain Rhythms Are Global but Often Overlooked. *Trends Neurosci.* **41**, 186–197, DOI: 10.1016/j.tins.2018.01.007 (2018).

24. Adrian, E. D. Olfactory reactions in the brain of the hedgehog. *The J. physiology* **100**, 459–73, DOI: https://doi.org/10.1113/jphysiol.1942.sp003955 (1942).

25. Iwata, R., Kiyonari, H. & Imai, T. Mechanosensory-Based Phase Coding of Odor Identity in the Olfactory Bulb. *Neuron* **96**, 1139–1152.e7, DOI: 10.1016/j.neuron.2017.11.008 (2017).

26. Grosmaitre, X., Santarelli, L. C., Tan, J., Luo, M. & Ma, M. Dual functions of mammalian olfactory sensory neurons as odor detectors and mechanical sensors. *Nat. Neurosci.* **10**, 348–354, DOI: 10.1038/nn1856 (2007).

27. Fontanini, A., Spano, P. & Bower, J. M. Ketamine-xylazine-induced slow (< 1.5 Hz) oscillations in the rat piriform (olfactory) cortex are functionally correlated with respiration. *The J. neuroscience : official journal Soc. for Neurosci.* **23**, 7993–8001, DOI: https://doi.org/10.1523/JNEUROSCI.23-22-07993.2003 (2003).

28. Yanovsky, Y., Ciatipis, M., Draguhn, A., Tort, A. B. L. & Branka k, J. Slow Oscillations in the Mouse Hippocampus Entrained by Nasal Respiration. *J. Neurosci.* **34**, 5949–5964, DOI: 10.1523/JNEUROSCI.5287-13.2014 (2014).

29. Nguyen Chi, V. *et al.* Hippocampal Respiration-Driven Rhythm Distinct from Theta Oscillations in Awake Mice. *J. Neurosci.* **36**, 162–177, DOI: 10.1523/JNEUROSCI.2848-15.2016 (2016).

30. Lockmann, A. L. V., Laplagne, D. A., Leão, R. N. & Tort, A. B. L. A Respiration-Coupled Rhythm in the Rat Hippocampus Independent of Theta and Slow Oscillations. *The J. neuroscience : official journal Soc. for Neurosci.* **36**, 5338–52, DOI: 10.1523/JNEUROSCI.3452-15.2016 (2016).

31. Biskamp, J., Bartos, M. & Sauer, J.-F. Organization of prefrontal network activity by respiration-related oscillations. *Sci. reports* **7**, 45508, DOI: 10.1038/srep45508 (2017).

32. Kőszeghy, Á., Lasztóczi, B., Forro, T. & Klausberger, T. Spike-Timing of Orbitofrontal Neurons Is Synchronized With Breathing. *Front. Cell. Neurosci.* **12**, 105, DOI: 10.3389/fncel.2018.00105 (2018).

33. Karalis, N. & Sirota, A. Breathing coordinates limbic network dynamics underlying memory consolidation. *bioRxiv* 392530, DOI: 10.1101/392530 (2018).

34. Moberly, A. H. *et al.* Olfactory inputs modulate respiration-related rhythmic activity in the prefrontal cortex and freezing behavior. *Nat. Commun.* **9**, DOI: 10.1038/s41467-018-03988-1 (2018).

35. Rojas-Líbano, D., Wimmer del Solar, J., Aguilar-Rivera, M., Montefusco-Siegmund, R. & Maldonado, P. E. Local cortical activity of distant brain areas can phase-lock to the olfactory bulb's respiratory rhythm in the freely behaving rat. *J. Neurophysiol.* **120**, 960–972, DOI: 10.1152/jn.00088.2018 (2018).

36. Zelano, C. *et al.* Nasal Respiration Entrains Human Limbic Oscillations and Modulates Cognitive Function. *The J. neuroscience : official journal Soc. for Neurosci.* **36**, 12448–12467, DOI: 10.1523/JNEUROSCI.2586-16.2016 (2016).

37. Herrero, J. L., Khuvis, S., Yeagle, E., Cerf, M. & Mehta, A. D. Breathing above the brain stem: volitional control and attentional modulation in humans. *J. Neurophysiol.* **119**, 145–159, DOI: 10.1152/jn.00551.2017 (2018).

38. Tort, A. B. L., Komorowski, R., Eichenbaum, H. & Kopell, N. Measuring Phase-Amplitude Coupling Between Neuronal Oscillations of Different Frequencies. *J. Neurophysiol.* **104**, 1195–1210, DOI: 10.1152/jn.00106.2010 (2010).

39. Torterolo, P. *et al.* Heart rate variability during carbachol-induced REM sleep and cataplexy. *Behav. Brain Res.* **291**, 72–79, DOI: 10.1016/j.bbr.2015.05.015 (2015).

40. Torterolo, P., Castro-Zaballa, S., Cavelli, M., Chase, M. H. & Falconi, A. Neocortical 40 Hz oscillations during carbachol-induced rapid eye movement sleep and cataplexy. *The Eur. journal neuroscience* **43**, 580–9, DOI: 10.1111/ejn.13151 (2016).

41. Najemnik, J. & Geisler, W. S. Optimal eye movement strategies in visual search. *Nature* **434**, 387–391, DOI: 10.1038/nature03390 (2005).

42. Verhagen, J. V., Wesson, D. W., Netoff, T. I., White, J. A. & Wachowiak, M. Sniffing controls an adaptive filter of sensory input to the olfactory bulb. *Nat. neuroscience* **10**, 631–9, DOI: 10.1038/nn1892 (2007).

43. Curtis, J. C. & Kleinfeld, D. Phase-to-rate transformations encode touch in cortical neurons of a scanning sensorimotor system. *Nat. neuroscience* **12**, 492–501, DOI: 10.1038/nn.2283 (2009).

44. Schroeder, C. E., Wilson, D. A., Radman, T., Scharfman, H. & Lakatos, P. Dynamics of Active Sensing and perceptual selection. *Curr. Opin. Neurobiol.* **20**, 172–176, DOI: 10.1016/j.conb.2010.02.010 (2010).

45. Hofmann, V. *et al.* Sensory flow shaped by active sensing: sensorimotor strategies in electric fish. *The J. experimental biology* **216**, 2487–500, DOI: 10.1242/jeb.082420 (2013).

46. Otero-Millan, J., Troncoso, X. G., Macknik, S. L., Serrano-Pedraza, I. & Martinez-Conde, S. Saccades and microsaccades during visual fixation, exploration, and search: Foundations for a common saccadic generator. *J. Vis.* **8**, 21–21, DOI: 10.1167/8.14.21 (2008).

47. Kagan, I. & Hafed, Z. Active Vision: Microsaccades Direct the Eye to Where It Matters Most. *Curr. Biol.* **23**, R712–R714, DOI: 10.1016/j.cub.2013.07.038 (2013).

48. Womelsdorf, T. *et al.* Modulation of neuronal interactions through neuronal synchronization. *Sci. (New York, N.Y.)* **316**, 1609–1612, DOI: 10.1126/science.1139597 (2007).

49. Fries, P. Rhythms for Cognition: Communication through Coherence. *Neuron* **88**, 220–235, DOI: 10.1016/j.neuron.2015.09.034 (2015).

50. Torterolo, P., Monti, J. M. & Pandi-Perumal, S. Neuroanatomy and Neuropharmacology of Sleep and Wakefulness. In *Synposis of Sleep Medicine*, 1, 1–22 (Apple Academic Press, 2016).

51. Castro-Zaballa, S. *et al.* EEG dissociation induced by muscarinic receptor antagonists: Coherent 40Hz oscillations in a background of slow waves and spindles. *Behav. Brain Res.* **359**, 28–37, DOI: 10.1016/j.bbr.2018.10.016 (2019).

52. Ma, X. *et al.* The Effect of Diaphragmatic Breathing on Attention, Negative Affect and Stress in Healthy Adults. *Front. Psychol.* **8**, 874, DOI: 10.3389/fpsyg.2017.00874 (2017).

53. Lachaux, J. P., Rodriguez, E., Martinerie, J. & Varela, F. J. Measuring phase synchrony in brain signals. *Hum. brain mapping* **8**, 194–208, DOI: 10.1002/(SICI)1097-0193(1999)8:4<194::AID-HBM4>3.0.CO;2-C (1999).

Methods

Experimental animals

Six adult cats were used in this study. Part of these animals were also utilized in previous studies[40]. The animals were obtained from and determined to be in good health by the Institutional Animal Care Facility. All experimental procedures were conducted in accordance with the *Guide for the Care and Use of Laboratory Animals (8th edition, National Academy Press, Washington DC, 2011)*, and were approved by the Institutional Animal Care Commission ($N°C: 070153-000089-17$). Adequate measures were taken to minimize pain, discomfort or stress. In addition, all efforts were made to use the minimum number of animals necessary to produce reliable scientific data.

Surgical procedures

The animals were chronically implanted with electrodes to monitor the states of sleep and W[2,9,39,40]. Prior to being anesthetized, each cat was premedicated with xylazine ($2.2 mg/kg$, i.m.), atropine ($0.04 mg/kg$, i.m.) and antibiotics (Tribrissen®, $30 mg/kg$, i.m.). Anesthesia, which was initially induced with ketamine ($15 mg/kg$, i.m.), was maintained with a gas mixture of isoflourane in oxygen ($1-3\%$). The head was positioned in a stereotaxic frame and the skull was exposed. Stainless steel screw electrodes ($1 mm$ diameter) were placed on the surface (above the dura matter) of different cortical areas (Fig. S1). In addition, bipolar electrodes were implanted in both lateral geniculate nuclei (LGN) to monitor ponto-geniculo-occipital (PGO) waves, and in the orbital portion of the frontal bone to record the electro-oculogram (EOG). The electrodes were connected to a Winchester plug, which together with two plastic tubes were bonded to the skull with acrylic cement, to maintain the animals in a stereotaxic head-fixed position without pain or pressure. In four animals, a craniotomy was drilled in the skull overlying the cerebellar cortex, filled with bone-wax and was subsequently used to provide access to the pons for carbachol administration[39,40]. After the animals had recovered from the preceding surgical procedures, they were adapted to the recording environment for a period of at least two weeks[9,39,40].

Experimental sessions

Sessions of 4 hours were conducted between 11 A.M. and 3 P.M in a temperature-controlled environment ($21-23°C$). During these sessions (as well as during the adaptation), the animals' head was held in a stereotaxic position by four steel bars that were placed into the chronically implanted plastic tubes, while the body rested in a sleeping bag[9,39,40]. The ECoG activity was recorded with a monopolar (referential) configuration, utilizing a common reference electrode located in the left frontal sinus[9,39,40]. Control experiments were made using other references electrodes[9]. Bipolar electromyogram (EMG) of the nuchal muscles was also monitored. The electrocardiogram, by electrodes acutely placed on the skin over the pre-cordial region, and respiratory activity by means of

a micro-effort piezo crystal infant sensor and a thermistor located in the nostril were also recorded. In selected experiments we also recorded the electrogram of the LGN and the EOG. Each cat was recorded daily for approximately 30 days to obtain complete data sets. Bioelectric signals were amplified ($\times 1000$), filtered ($0.1-500\,Hz$), sampled ($2048\,Hz$, 2^{16} bits) and stored in a PC using the Spike 2 software (CED). Data were obtained during spontaneously occurring W, NREM, REM sleep, and during the induction of REM carbachol (REMc) or cataplexy (CA)[39,40].

Carbachol microinjection into the NPO

In order to induce REMc or CA, carbachol ($0.8\,\mu g$ in $0.2\,\mu L$ of saline) was microinjected unilaterally for a period of one minute into the NPO with a Hamilton syringe[39,40]. Carbachol microinjections were performed either during NREM sleep or W. Two successful carbachol microinjections (in these experiments REMc and CA episodes were generated) were carried out for each animal (cats C3 to C6 in Fig. S1). The animals' eyes were examined throughout the recording sessions to determine if they were closed or open, and if the pupils were mydriatic or miotic. We also monitored the degree of relaxation of the nictitating membrane and whether the animals were able to track visual or auditory stimuli[39,40]. During CA, the ECoG resembles W, PGO waves in the LGN were not observed, the eyes were open with moderate pupillary dilatation and auditory and visual stimuli were tracked as during natural W. In contrast, during REMc, the ECoG and PGO waves in the LGN did not differ from naturally-occurring REM sleep (Fig. 5A; arrowheads). Additionally, the eyes were closed, and the nictitating membrane was relaxed[39,40]. REMc and CA share the same muscle atonia (Fig. 5A, EMG).

Data analysis

Sleep and W were quantified in 10 second epochs applying standard classification criteria[9,40]. Then, the maximum number of non-transitional and artifact-free periods of $30\,s$ was selected for analysis during each behavioral state[2,19]. For each animal, we analyzed up to four complete recording to guarantee a minimum 500 seconds length for each cat and behavioral state (REM sleep is the limiting factor since it is a small percentage of the total recording time). This data was imported and analyzed offline using built-in and custom-written MATLAB codes (Mathworks). All data was previously filtered (low-pas $100\,Hz$) and down sample at $256\,Hz$ to decrease the computational load of subsequent analyzes.

Power Spectrum was calculated by means of Welch's periodogram (built-in MATLAB *pwelch* function). Coherence spectra (Figs. 1B and 5B) of electrode pairs were computed using magnitude-squared coherence (built-in MATLAB *mscohere* function) and Fisher z' transform was applied (z'-coherence). Both power and coherence spectra calculations were carried out in all the data segments using 10 seconds Hamming windows and a frequency resolution of $0.1\,Hz$.

CCF-map (Figs. 3 and S3) was generated between respiration and the envelopes of frequencies between $20-100\,Hz$ (custom-written MATLAB code). To obtain the CCF-map, several band-pass filtered signals were generated from the raw recordings (built-in MATLAB *eegfilt* function). We used $10\,Hz$ bandwidth and $5\,Hz$ steps, covering from 15 up to $105\,Hz$. The CCF-map was then generated by means of a raster plot of CCFs (built-in MATLAB *xcross* function) calculated between respiration and the envelopes (built-in MATLAB *hilbert* function) of each filtered signal.

Phase amplitude coupling(PAC) and modulation index(MI) (Figs. 4 and Figs. 5D) were calculated used the framework previously described by Tort et al[38]. First, the phase of the respiratory wave was extracted (built-in MATLAB *hilbert* function). Second, the γ band was band pass filtered ($30-60\,Hz$) and envelopes were generated (*eegfilt* and *hilbert*, respectively). Phase-amplitude plots were computed using 20° phase bins of the respiratory signal. The mean amplitude in each phase bin was normalized by the sum across bins, so that the amplitude values in each plot summed to 1. MI was calculated by the equation:

$$MI = \frac{H_{max} - H_{pac}}{H_{max}}, \tag{1}$$

;where H_{max} is the maximum entropy (Shannon entropy) value that can be obtained from the phase-amplitude relations (uniform distribution) and H_{pac} is the entropy of the phase-amplitude relations for the original signal[38]. $MI \to 1$ means maximum PAC while $MI \to 0$ means absence of PAC.

γ Coherence in function of the respiratory phase (Figs. 7A) was calculated (custom-written MATLAB code) using the phase of the respiratory signal and the coherence between pairs of the ECoG signals. After the respiratory phase extraction (*hilbert*) the pair of ECoG recordings was divided into nine parts (40° each) taking as reference the respiratory wave. Then the coherence of each bin phase was computed using magnitude-squared coherence (*mscohere*). Then, the spectral coherence was plotted as a function of the respiratory phase as a heat map.

Phase looking value (PLV) as a function of the respiratory phase (Figs. 7C and S6) were calculated (custom-written MATLAB code) using the bin phase of the respiratory signal and the phase coherence (PLV) between each pair of the ECoG signals. After the respiratory phase bin extraction (*hilbert*) each pair of ECoG records was band-pass filtered ($10\,Hz$ bandwidth and $5\,Hz$ steps, covering from 15 up to $105\,Hz$; or $30-60\,Hz$) and phase extracted (*eegfilt* and *hilbert*, respectively). Then, the ECoG phase difference was computed and the mean phase difference in the complex plane of each respiratory phase bin (20°) was calculated (PLV)[53]. PLV$\to 1$ means that phase difference is constant through all the respiratory bin and PLV$\to 0$ means that phase difference changes randomly through respiratory bins.

R^2 in function of the respiratory phase (Figs. 7B) was calculated (custom-written MATLAB code) using phase bin of the respiratory signal and the square root of the linear correlation between a pair of electrodes. After the respiratory phase

bin extraction (*hilbert*) each pair of ECoG recordings was band-pas filtered ($30-60\,Hz$; *eegfilt*) and then square root of the linear correlation (R^2; built-in MATLAB *corr* function) was calculated with a moving window of 0.088 seconds (4 γ cycles) with $\simeq 99\,\%$ of superposition. Then, the mean of R^2 was calculated for each respiratory phase bin (Figs. 7B2). We also calculated the coherence between the γ R^2 wave and the respiratory waveform (Figs. 7B1).

Statistics. Group data are expressed as mean $\pm$ standard deviation. Most of the statistical analyses were assessed by paired two-tailed t-test (see Results and Figures' legends). The significance of the differences among behavioral states was evaluated with repeated measures ANOVA (rmANOVA) along with Bonferroni post hoc tests. When sphericity criteria was not accomplished (tested by Mauchly's test), the Greenhouse-Geisser correction was applied. The criterion used to reject null hypotheses was $p < 0.05$. For Figure. 7A and S6, a paired two-tailed t-test was performed with a Bonferroni correction for multiple comparisons. With this correction, $p < 0.0001$ was considered statistically significant.

Competing interests

The authors declare no competing financial interests.

Supplementary Material

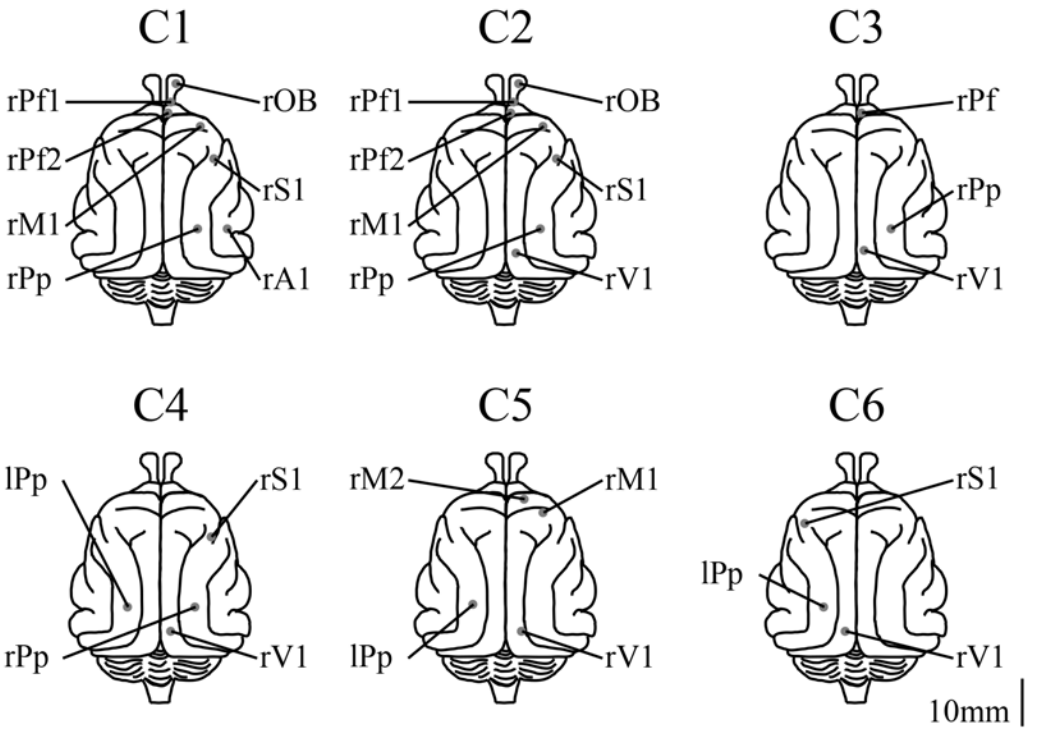

Figure S1. Electrode locations on the cerebral cortex surface of 6 cats (C1 to C6). Electrical activity was band-pass filtered between 0.1 up to 500 Hz, recorded at a 2048 Hz sampling rate and referenced to a common electrode located over the left frontal sinus. The acronyms in the panels are as follows: OB, olfactory bulb; M1, primary motor cortex; M2, secondary motor cortex; S1, primary somato-sensory cortex; V1 primary visual cortex; V2, secondary visual cortex; A1, primary auditory cortex; Pf, prefrontal cortex; Pf1, rostral prefrontal cortex; Pf2, dorso-lateral prefrontal cortex; Pp, posterior parietal cortex; r, right; l, left.

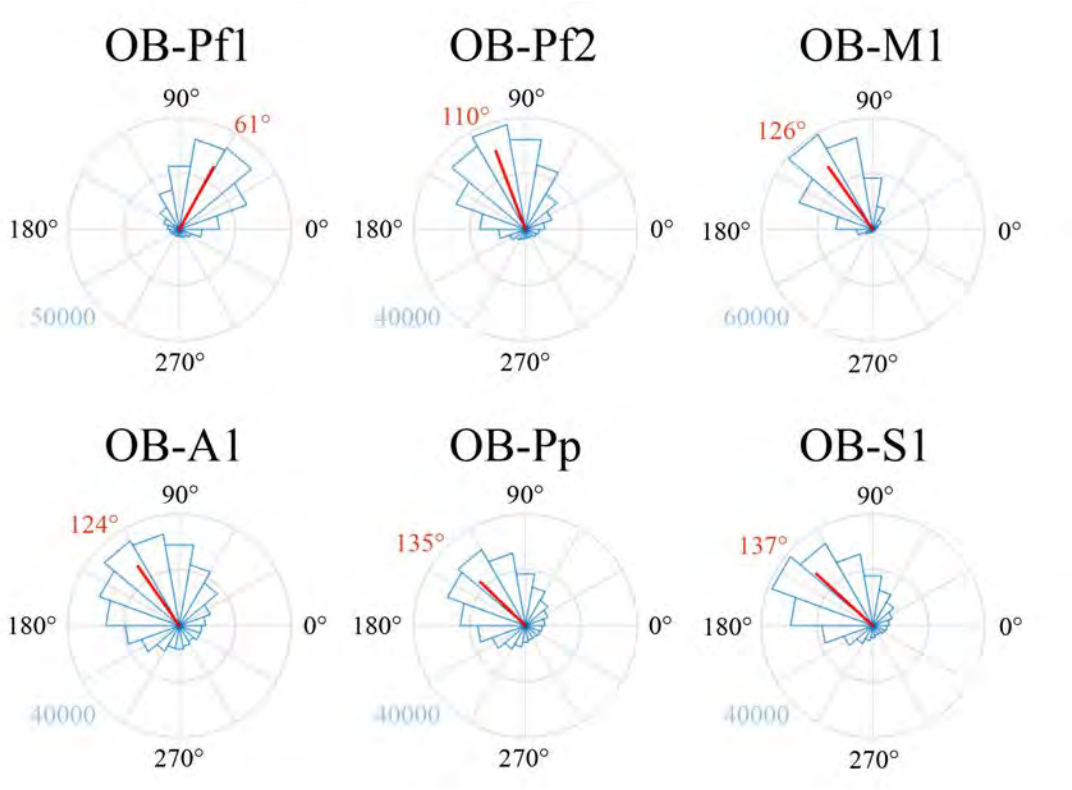

Figure S2. Polar histogram of the CRP phase differences. Each graph shows the circular distribution of phase differences between the olfactory bulb (OB) and the neocortical electrode locations. Each ECoG signal was band pass filtered (0.1 - 4 Hz), the phase extracted (*hilbert* function) and the phase difference was calculated. The mean direction of the distribution is represented in a red line. Pf1, rostral prefrontal cortex; Pf2, dorsolateral prefrontal cortex; M1, primary motor cortex; A1, primary auditory cortex; Pp, posterior parietal; S1, primary somato-sensory cortex.

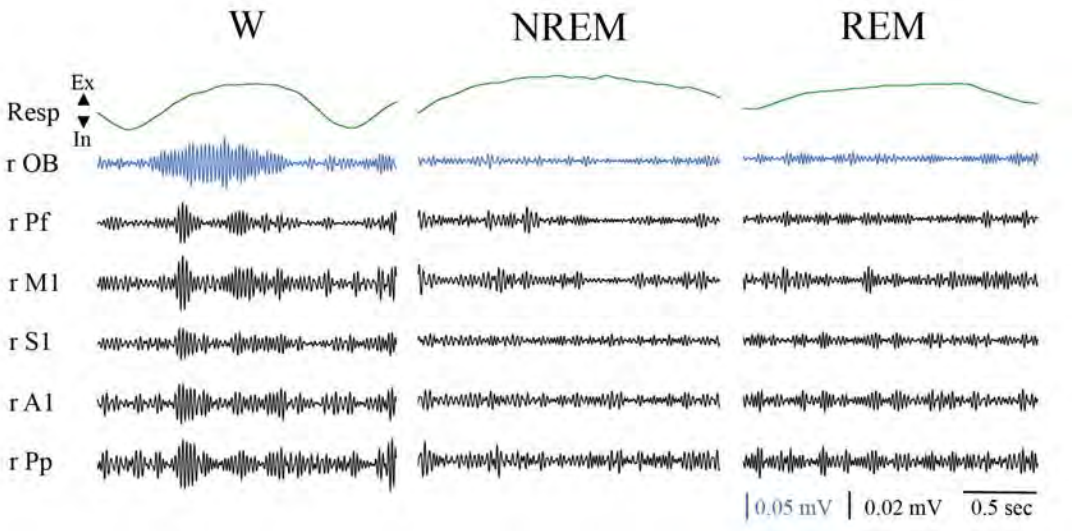

Figure S3. Simultaneous band pass (30 - 60 Hz) filtered recordings during wakefulness (W), NREM and REM sleep (C2). Breathing was recorded through a thermistor in the nostrils (green) in simultaneous with the neocortical (black) and OB ECoG (blue). The recordings are from the Olfactory bulb (OB), prefrontal cortex (Pf), primary motor cortex (M1), posterior parietal cortex (Pp), primary somato-sensory cortex (S1) and primary auditory cortex (A1) from the right hemisphere (r).

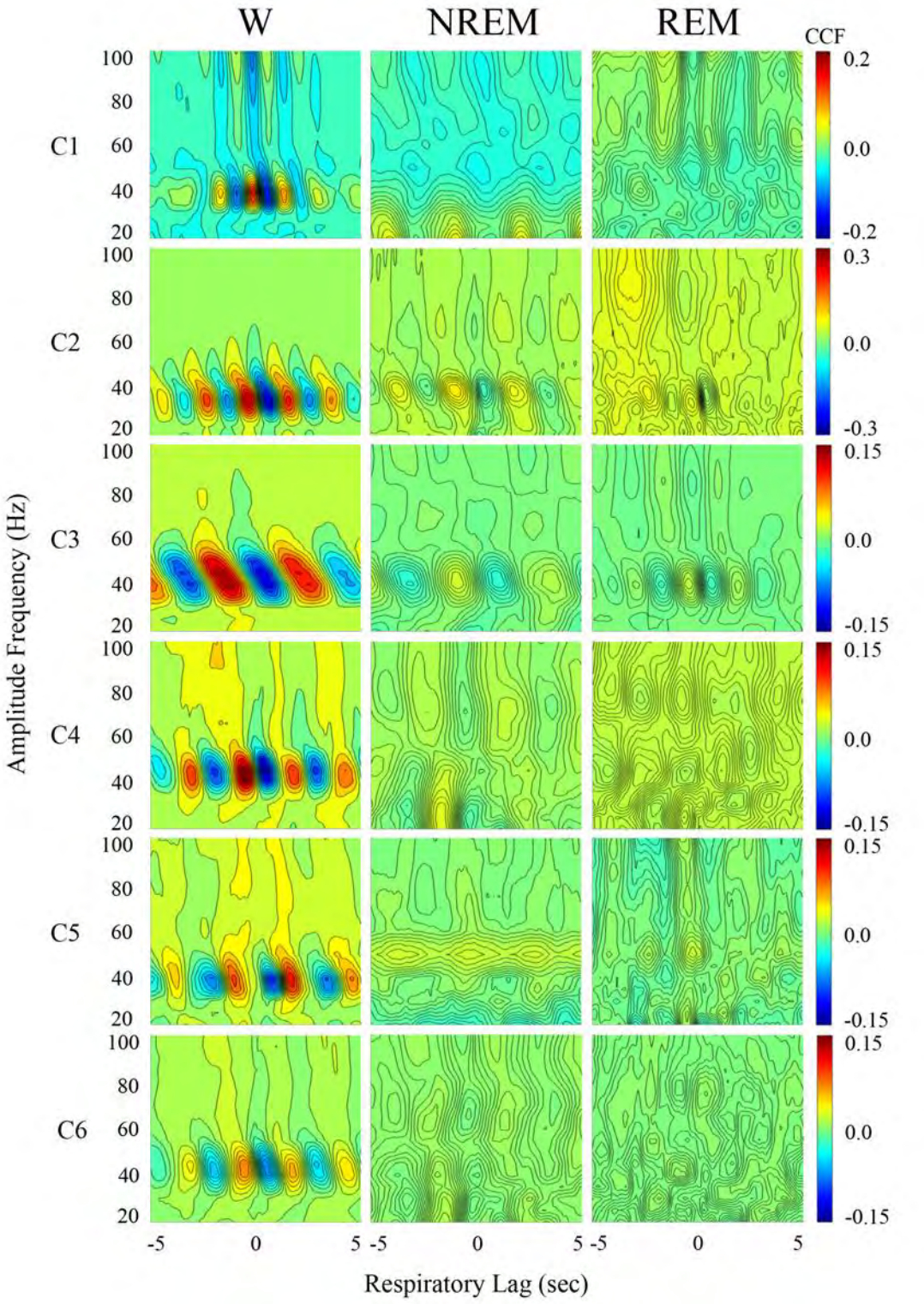

Figure S4. Mean CCF maps during wakefulness (W) and sleep. Mean cross-correlation function (CCF) between respiratory waves (produced by the airflow though the nostrils) and the amplitude envelope of the ECoG signals. The CCF have been done between 10 and 100 Hz (10 Hz bandwidth and 5 Hz steps) during W, NREM, and REM sleep. The CCF maps correspond to the mean of the CCF maps from all the recorded areas of each animal (C1 to C6).

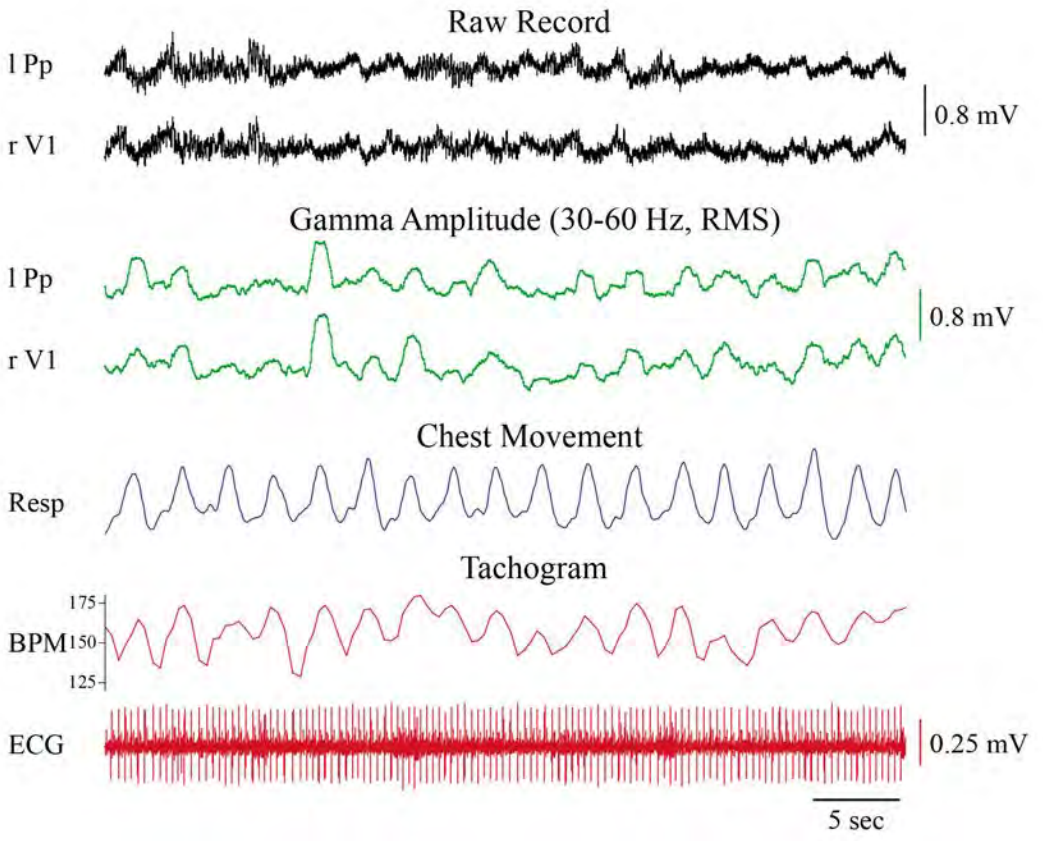

Figure S5. Neocortical cardio-respiratory entrainment. In black, the CRP in a cat's cortex during wakefulness. In green, the γ envelopes of the same ECoG raw recordings. Breathing is recorded using a micro-effort piezo-crystal infant sensor (blue). In the lower part (in red) the ECG and its tachogram are shown. The respiratory sinus arrhythmia is readily observed in the tachogram.

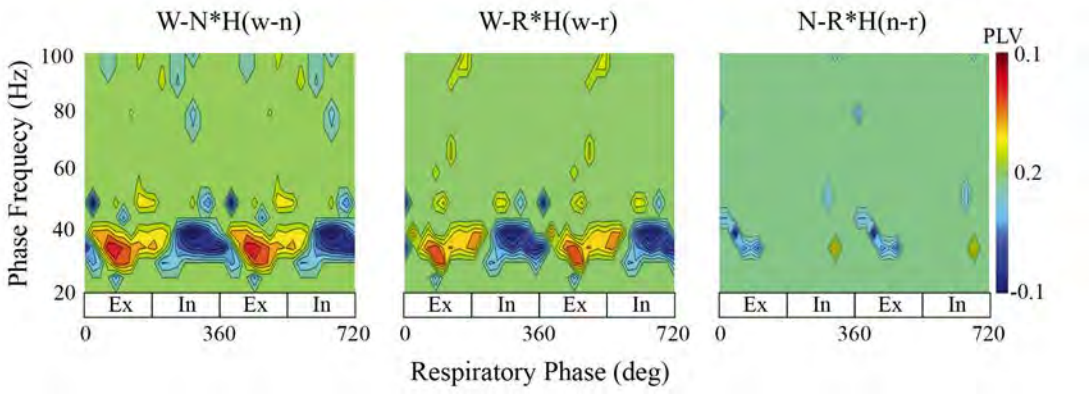

Figure S6. Respiratory modulation of inter-cortical γ synchronization. A. Inter-cortical phase locking values (PLV) as a function of the respiratory phase. The respiratory phase was binned 18 times and each pair of ECoG records was band-pass filtered ($10\,Hz$ bandwidth and $5\,Hz$ steps, covering from 15 up to $105\,Hz$) and the phase was extracted. Then, the ECoG phase difference was computed and the mean phase difference in the complex plane of each respiratory phase bin (20°) was calculated. The PLV was calculated between 20 to $100\,Hz$. Each graph represents the mean difference of the normalized PLV between wakefulness (W and w) and NREM sleep (N and n) on the left; wakefulness (W and w) and REM sleep (R and r) in the middle; and NREM and REM sleep on the right, of all the ECoG recordings pairs of one animal (C2). The mean PLV difference was then multiplied by 0 if $p > 0.0001$ or 1 if $p < 0.0001$ (t-test). H is the matrix of 0 and 1 referents of the statistical significance. Ex, exhalation; In, inhalation.

4. Capítulo 4. Rol del sistema dopaminérgico en la generación, mantenimiento y modulación de la actividad gamma cortical

4.1. Actividad gamma en un modelo animal de enfermedad de Parkinson

Hasta este momento hemos observado que las oscilaciones de alta frecuencia del cerebro (actividad gamma) se presentan como un fenómeno característico de la vigilia y que su disminución durante el sueño deja a entrever el rol de los sistemas activadores en el mantenimiento de estos patrones oscilatorios (**Capítulo 1**). Por otra parte, el bloqueo colinérgico muscarínico no altera la actividad gamma durante la vigilia (**Anexo 4**) lo cual sugiere que los sistemas monoaminérgicos (dopaminérgicos, noradrenérgicos, etc.,) podrían ser las responsables de generar y modular la actividad gamma cortical (Cavelli et al., 2017a; Torterolo et al., 2016b). En los capítulos precedentes observamos como la actividad gamma podía ser modulada por otros ritmos lentos como los potenciales respiratorios (**Capítulo 2 y 3**). En este sentido, mostramos como la respiración nasal es capaz de acoplar a la coherencia gamma inter-cortical durante la vigilia acoplando áreas del cerebro que no presentan relación directa ni con la respiración ni con el olfato.

La enfermedad de Parkinson (EP) es la segunda enfermedad neurodegenerativa más prevalente a nivel mundial (Hirsch et al., 2016; Lang and Lozano, 1998; Pringsheim et al., 2014). En esta enfermedad el deterioro olfativo es la primera alteración que se observa, inclusive antes de la detección de los síntomas motores característicos (Braak et al., 2003; Doty, 2012). La hiposmia se detecta en más del 90% de los pacientes con EP (Knudsen et al., 2015). Esta enfermedad se caracteriza por la degeneración de las neuronas dopaminérgicas de la Sustancia Nigra pars compacta (SNpc). La lesión de la SNpc con Rotenona o 6 hidroxidopamina (6-OHDA) es utilizada como modelo animal de la EP (Costa et al., 2001; Mouhape et al., 2019; Urbanavicius et al., 2007). Dichos modelos presentan un claro trastorno motor, deterioro de la capacidad olfativa de los animales (Aurich et al., 2017; Höglinger et al., 2015; Rodrigues et al., 2014) y claras alteraciones anatomo-funcionales a nivel del bulbo (Huisman et al., 2004; Mundiñano et al., 2011; Rodrigues et al., 2014). Por este motivo pensamos que la caída en la actividad dopaminérgica podría estar relacionada a una pérdida de las funciones motoras y de la capacidad para internalizar la información olfativa al resto del cerebro.

Con respecto a esta idea fue que realizamos el **Artículo 5** (Cavelli et al. 2019). Aquí mostramos como la lesión unilateral dopaminérgica de la SNpc con 6-OHDA es capaz de disminuir la potencia y coherencia gamma de la corteza motora y el bulbo olfatorio durante la vigilia. Por otra parte, observamos que la lesión dopaminérgica genera importantes alteraciones en el acople respiratorio de la actividad gamma cortical.

Artículo 5.

(Cavelli et al. 2019)

Electrocortical high frequency activity and respiratory entrainment in 6-hydroxydopamine model of Parkinson's disease

Matías Cavelli[1], Giselle Prunell[2], Gustavo Costa[2], Noelia Velásquez[1], Joaquín Gonzalez[1], Santiago Castro-Zaballa[1], Marcelo M. S. Lima[3] and Pablo Torterolo[1*]

(1) Laboratorio de Neurobiología del Sueño, Departamento de Fisiología, Facultad de Medicina, Universidad de la República, Avenida General Flores 2125, CP. 11800, Montevideo - Uruguay.
(2) Departamento de Neuroquímica, Instituto de Investigaciones Biológicas Clemente Estable, Ministerio de Educación y Cultura, Avenida Italia 3318, CP. 11600, Montevideo - Uruguay.
(3) Laboratório de Neurofisiologia. Departamento de Fisiologia, Universidade Federal do Paraná, Avenida Coronel Francisco H. dos Santos 100, CP. 19031, Paraná - Brazil.

*** Please address correspondence to:**
Dr. Pablo Torterolo, (ptortero@fmed.edu.uy)

Abstract

Parkinson's disease is characterized by motor symptoms (akinesia, rigidity, etc.), which are associated with the degeneration of the dopaminergic neurons of the midbrain. In addition, olfactory impairment that usually develops before the detection of motor deficits, is detected in 90% of Parkinsonian patients.

Recent studies in mammals, have shown that slow cortical potentials phase-lock with nasal respiration. In several cortical areas, gamma synchronization of the electrographic activity is also coupled to respiration, suggesting than nasal respiratory entrainment could have a role in the processing of olfactory information.

In the present study, we evaluate the role of midbrain dopaminergic neurons, in the modulation of the electrocorticogram activity and its respiratory entrainment during wakefulness and sleep. For this purpose, we performed a unilateral lesion of dopaminergic neurons of the substantia nigra pars compacta of the rat, with 6-hydroxydopamine.

An increase in beta (20-35 Hz) together with a decrease in gamma power (60-95 Hz) in the motor cortex ipsilateral to the lesion was observed during wakefulness. These results correlated with the degree of motor alterations and dopamine measured at the striatum. Moreover, we found a decline in gamma coherence between the ipsilateral olfactory bulb and motor cortex. Also, at the olfactory bulb we noticed an increase in respiratory-gamma cross-frequency coupling after the lesion, while at the motor cortex, a decrease in respiratory potential entrainment of gamma activity was observed. Interestingly, we did not observe any significant modification either during Non-REM or REM sleep.

These waking dysrhythmias may play a role both in the anosmia and motor deficits present in Parkinson disease.

Keywords: dopamine, substantia nigra, gamma, EEG, sleep

1. Introduction

Parkinson's disease (PD) is the second most prevalent neurodegenerative disease worldwide (Hirsch et al., 2016; Lang and Lozano, 1998; Pringsheim et al., 2014), characterized by motor symptoms (akinesia, tremor, rigidity, etc.), which are associated with the degeneration of the dopaminergic (DA) neurons of the substantia nigra pars compacta (SNpc) (Dauer and Przedborski, 2003). In addition, olfactory impairment is detected in up to 90% of PD patients and usually develops before the detection of motor symptoms (Braak et al., 2003; Doty, 2012a, 2012b; Knudsen et al., 2015). SNpc lesion with rotenone or 6-hydroxydopamine (6-OHDA) leads to the death of local DA neurons and reproduces these symptoms (Aurich et al., 2017; Costa et al., 2001; Höglinger et al., 2015; Ilkiw and Lima, 2019; Mouhape et al., 2019; Rodrigues et al., 2014; Urbanavicius et al., 2007; Valle-Leija and Drucker-Colín, 2014; Zhang et al., 2019). Hence, SNpc-lesioned animals are utilized as model of PD.

Neural synchronization at gamma frequency band (30-100 Hz) is considered a binding mechanism utilized by the brain to generate transient opportunities for communication and integration of the distributed neural activity

necessary for cognitive functions (Buzsáki and Draguhn, 2004; Engel et al., 2001; Fries, 2009; Gray et al., 1989; Salinas and Sejnowski, 2001; Singer, 1999; Varela et al., 2001). Gamma power of the electroencephalogram (EEG) increases during active behavioral states as well as during the performance of cognitive tasks (Buzsáki and Schomburg, 2015; Castro-Zaballa et al., 2013; Cavelli et al., 2017a; Maloney et al., 1997; Manabe and Mori, 2013; Rojas-Líbano et al., 2014; Varela et al., 2001). Besides, gamma synchronization between distant areas of the brain (gamma coherence) also increases during several cognitive functions in both animals and humans (Bressler et al., 1993; Castro-Zaballa et al., 2013; Cavelli et al., 2017a, 2015; Rodriguez et al., 1999; Varela et al., 2001). The coherence of the gamma band between different cortical areas has been considered a neural correlate of consciousness (Joliot et al., 1994; Llinás and Ribary, 2001; Varela et al., 2001), and plays a critical role in perception (Melloni et al., 2007; Rodriguez et al., 1999). In fact, the electrocortical gamma coherence is absent during narcosis (unconsciousness) induced by general anesthetics (John, 2002; Mashour, 2006; Pal et al., 2016).

Adrian originally described the process currently coined as "cross-frequency coupling" (CFC), where nasal respiration drives gamma oscillations in the olfactory bulb (OB) (Adrian, 1942). Recent studies in humans', cats and rodents, have shown that slow cortical potentials in archi-, paleo- and neocortex phase-lock with nasal respiration, and in some of these areas gamma activity is also coupled to the animal's respiration (Biskamp et al., 2017; Cavelli et al., 2018; Ito et al., 2014; Lockmann et al., 2016; Manabe and Mori, 2013; Nguyen Chi et al., 2016; Rojas-Líbano et al., 2014, 2018; Tort et al., 2018; Yanovsky et al., 2014; Zhong et al., 2017). Recently, we showed that nasal respiration

entrains inter-cortical gamma synchronization, suggesting a role in the integrative process of cognition (Cavelli et al., 2018).

During sleep there is a progressive decrease in gamma synchronization (Castro-Zaballa et al., 2014, 2013; Cavelli et al., 2017a, 2015; Voss et al., 2009), as well as its respiratory coupling (Cavelli et al., 2018). This fact strongly suggests that one or more of the neuroregulatory systems (activating systems) that promote wakefulness (W), may have a role in the generation and modulation of gamma activity (Torterolo et al., 2016; Torterolo and Vanini, 2010). Whereas the blockade of the muscarinic cholinergic receptor does not modify gamma activity (Castro-Zaballa et al., 2019), it is likely that monoamines (dopamine, noradrenaline, serotonin, and histamine) may be involved in the regulation of these oscillations (Castro-Zaballa et al., 2019; Cavelli et al., 2017a; Torterolo et al., 2016). In this sense, treatment with DA agonists increases gamma synchronization in the basal ganglia-thalamo-cortical circuit (Brown et al., 2001; Cassidy et al., 2002; Williams, 2002).

The aim of the present study was to evaluate the role of the DA neurons of the SNpc in the generation and modulation of gamma activity, both during W and sleep. In order to do that, we studied the neocortex and OB electrocorticogram (ECoG) of the rat in the 6-OHDA model of PD.

2. Materials and Methods

2.1. Experimental animals

Six adult Wistar rats were used in this study (280-320 g). The animals were obtained from and determined to be in good health by the Institutional

Animal Care Facility. All experimental procedures were conducted in accordance with the *Guide for the Care and Use of Laboratory Animals* (8th edition, National Academy Press, Washington DC, 2011), and were approved by the Institutional Animal Care Commission (Exp. Nº 070153-000952-15). Adequate measures were taken to minimize pain, discomfort or stress. In addition, all efforts were made to use the minimum number of animals necessary to produce reliable scientific data.

2.2. Surgical procedures

We employed similar surgical procedures as in our previous studies (Cavelli et al., 2017b, 2017a, 2015). The animals were chronically implanted with electrodes to monitor the states of sleep and W. Anesthesia was induced with a mixture of ketamine-xylazine (100 mg/kg; 5 mg/kg i.p, respectively). The rat was positioned in a stereotaxic frame and the skull was exposed. In order to record the ECoG, stainless steel screw electrodes (1 mm diameter) were placed on the surface (above the dura mater) at the OB (lateral 1.5 mm, anterior 8 mm; distances were measured from Bregma, according to Paxinos and Watson, 1982 atlas, whiskers primary motor area (M1: lateral 1.5 mm, anterior 2 mm) and whisker primary somatosensory (“barrel”) cortex (S1: lateral 5 mm, posterior 2.7 mm), of both hemispheres. All cortical records were referenced to a common electrode located above the cerebellum (midline, posterior 13 mm). With the purpose of recording the electromyogram (EMG), two electrodes were inserted into the neck muscle. The electrodes were connected to a plug and bonded to the skull with acrylic cement.

For microinjections of 6-OHDA a stainless-steel guide cannula was implanted unilaterally (right) above the SNpc (right 2.2 mm, posterior 5 mm, height 7.5 mm).

At the end of the surgical procedures, an analgesic (ketoprofen, 1 mg/Kg s.c.) was administered. Incision margins were kept clean and a topical antibiotic was administered on a daily basis. After the animals had recovered from the preceding surgical procedures, they were adapted to the recording environment for a period of at least one week.

2.3. Experimental sessions

Experimental sessions of 10 h duration was conducted between 1 and 21 p.m (light off at 6 p.m) in a temperature-controlled (21–24 °C) room. The rats were recorded in a sound-attenuated chamber, which is also a Faraday box, and had free access to water and food. The recordings were performed through a rotating connector, to allow the animals to move freely within the recording box.

The simultaneous activity of different cortical areas was recorded using a monopolar configuration; this monopolar montage is critical for posterior analysis of coherence (Bullock, 1997; Bullock et al., 1995; Cantero et al., 2000; Nunez et al., 1997). The EMG was also monitored. Each rat was recorded daily during two consecutive days to obtain basal records. Then, the animals were anaesthetized (Ketamine 90 mg/kg) and unilateral injected with 6-OHDA (10 µg in 2 µl dissolved in artificial cerebrospinal fluid containing 0.2 % ascorbic acid; 0.2 µL/min) in the SNpc using a Hamilton microinjection syringe through the previously implanted guide cannula. Following the drug administration, the

needle was left in place for 5 min. After stabilizing the lesion with 6-OHDA (two weeks), two other consecutive recordings were made.

Bioelectric signals were amplified (1000 x), filtered (0.1-500 Hz), digitalized (1024 Hz, 16 bits) and stored in a PC using the Spike 2 software (Cambridge Electronic Design). Data were obtained during W, non-REM (NREM) and REM sleep (Cavelli et al., 2017b, 2017a, 2015).

2.4. Behavior evaluation: rotational behavior

The day after de last electrographic recording, motor asymmetry induced by the SNpc unilateral lesion was evaluated. Briefly, the animals were stimulated with amphetamine (5 mg / kg i.p.). Thirty minutes later, the number of 360º turns to the left and right were recorded during 15 minutes with a rotometer (Ungerstedt and Arbuthnott, 1970).

2.5. Evaluation of monoamine levels by HPLC

Following behavioral studies, the animals were sacrificed by decapitation and the left and right corpus striatum (CS, the main projection nucleus of the DA neurons of the SNpc) were dissected out. In order to evaluate the extent of the 6-OHDA lesion on the SNpc, the levels of DA and its main metabolites 3,4-dihydroxyphenylacetic acid (DOPAC) and homovanilic acid (HVA) were determined in the CS by “high performance liquid chromatography” (HPLC) with electrochemical detection (Costa et al., 2001). Briefly, the samples were sonicated in 0,1 mol/L perchloric acid, centrifuged for 15 min (15000g, 4°C) and the supernatants were injected into an HPLC system (PM. 80; Bioanalytical Systems, West Lafayette, IN, USA) equipped with a C-18 column (5 µm

particles, 220 mm x 4,6 mm; Bioanalytical Systems) and electrochemical detector (LC-4C-, Bioanalytical Systems) with oxidation potential at +0,65V (glassy working carbon electrode vs. an Ag/AgCl reference electrode). The mobile phase was composed of citric acid (0,15 mol/L), sodium octyl sulpahte (0,6 mmol/L), 4% acetonitrile and 1,6% tetrahydrofuran at pH 3.0. The flow rate was set at 1,2 mL/min. The results were expressed either as absolute values (ng/gr) or the results obtained from the side of the lesion were normalized to the levels determined on the contralateral side and expressed as a percentage (% R/L). Serotonin (5-HT) and its metabolite, 5-hydroxyindolacetic acid (5-HIAA), were also evaluated as control of the specificity of the 6-OHDA lesion on DA cells (Abin-Carriquiry et al., 2002; Costa et al., 2001; Urbanavicius et al., 2007).

2.6. Data analysis

Sleep and W were quantified in 10 second epochs applying standard classification criteria (Benedetto et al., 2017; Cavelli et al., 2015; González et al., 2018; Mondino et al., 2019). Then, 1000 s of non-transitional and artifact-free periods of 5 s was selected for analysis during each behavioral state and record (Cavelli et al., 2017b). These data were imported and analyzed offline using built-in and custom-written MATLAB codes (Mathworks).

Power Spectrum was calculated by means of Multi-taper time-frequency spectrum (Chronux, MATLAB *mtspecgramc* function) using 10 s time windows (non-overlap), time band-windows product of 2.5 and 4 tapers. In each animal and recording, the average power of all the 10 seconds' time windows was calculated. Power was expressed as a relative power, where each value was divided by the total power of all the analyzed spectrum.

Coherence spectra of the ECoGs of a pair of cortical areas were computed by means of Multi-taper time-frequency coherence (Choronux, MATLAB *cohgramc* function) using 10 s time windows (non-overlap), time band-windows product of 5 and 8 tapers. Then the Fisher z' transform was applied (z'-coherence). For each animal, the average coherence in all the 10 seconds time windows was calculated for each ECoG pair. Power and coherence of the ECoG were also analyzed for each of the following frequency bands: delta (1 - 4 Hz); theta (5 – 9 Hz); sigma (10 – 15 Hz); beta (20 – 35 Hz); low gamma (35 – 60 Hz) and high gamma (60-95 Hz). In order to avoid 50 Hz electrical noise, frequencies between 49 and 51 Hz were excluded from the frequency analysis and replaced in figures by the average result at 48 and 52 Hz.

CFC, phase amplitude coupling (PAC) and modulation index (MI) were calculated by means of the framework previously described by Tort *et al.* (Tort et al., 2010). First, in order to extract the slow phases, several band-pass filtered signals were generated from the raw recordings (Eeglab, MATLAB *eegfilt* function). We used 2 Hz bandwidth and 0.5 Hz steps, covering from 0 up to 10 Hz., and the phase of each slow wave was extracted (MATLAB *hilbert* function). Second, several band-pass filtered signals (*eegfilt*) were again generated using 10 Hz bandwidth and 5 Hz steps, covering from 5 up to 195 Hz., and envelopes (amplitudes) were generated (*eegfilt* and *Hilbert,* respectively). For each pair of phase and amplitude envelop, phase-amplitude plots were computed using 20° phase bins of the phase signal. The mean amplitude in each phase bin was normalized by the sum across bins, so that amplitude values in each plot summed to 1. To build the comodulograms, each

pair phase-amplitude, was assessed by a measure called modulation index (*MI*) (Tort et al., 2010).

MI was calculated by the equation:

$$MI = \frac{Hmax - Hpac}{Hmax}$$

; where *Hmax* is the maximum entropy (Shannon entropy) value that can be obtained from the phase-amplitude relations (uniform distribution) and *Hpac* is the entropy of the phase-amplitude relations for the original signal (Tort et al., 2010). *MI* = 1 means maximum PAC while *MI* = 0 means absence of PAC.

Statistics. Group data are expressed as mean ± standard deviation. For electrographic results, all the statistical analyses were assessed by paired two-tailed t-test between basal and 6-OHDA treatment. For power and coherence, the frequency band was compared before and after the lesion, and if there is a significant difference, an analysis per individual frequency was performed (see Results and Figures' legends). Then, when a statistical result was obtained, the linear regression (Pearson) was evaluated between rotational behavior or DA levels and the differences (∆) in the bands spectral results. The criterion used to reject null hypotheses was $p<0.05$.

3. Results

3.1. Rotational behavior and neurochemical analysis

Each of the treated animals showed a motor lateralization ipsilateral to the lesion site. On average, the turns to the right were 108.5 ± 48.6, whereas the turns to the left were 0 **(Table 1**).

Table 1 and **2** show the tissue levels of DA, serotonin (5-HT) and their metabolites in the CS, respectively.

Table 1. Motor lateralization and levels of DA and its metabolites

	Turns		DA		DOPAC		HVA	
Rats	right	left	right (ng/gr)	left (ng/gr)	right (ng/gr)	left (ng/gr)	right (ng/gr)	left (ng/gr)
1	171	0	106	10,330	44	1,363	200	987
2	36	0	4,987	9,082	761	1,195	502	1,028
3	110	0	106	8,143	31	1,358	93	682
4	54	0	4,425	10,570	1135	3,500	842	1,564
5	145	0	714	11,686	51	1,546	232	1,191
6	135	0	79	10,200	33	1,457	154	708
mean	108.5	0	1,736.1	10,001.8	342.5	1,736.5	337.1	1,026.6
SD	48.5	0	2,319.6	1,233.4	483.7	871.8	284.6	327.9
p	< 0.0001		0.0007		0.0026		0.0002	

Table 2. Levels of 5-HT and its metabolite 5-HIAA

	5-HT		5-HIAA	
Rats	right (ng/gr)	left (ng/gr)	right (ng/gr)	left (ng/gr)
1	652	516	580	413
2	528	460	410	440
3	435	501	483	446
4	442	352	492	417
5	488	625	542	463
6	485	465	539	472
mean	505	486.5	507.6	441.8
SD	79.6	88.9	59.6	23.7
p	0.677		0.092	

The levels of DA and its metabolites were decreased on the side of the lesion (right) compared to the contralateral side (two-tailed paired t-test; **Table 1**). On the other hand, the levels of 5-HT and its metabolites did not show differences between both hemispheres (**Table 2**). We found that the rotation to the right correlates with the decrease in DA and its metabolites (turns right vs. DA % R/L, $r = -0.922$, $p = 0.008$; turns right vs. DOPAC % R/L, $r = -0.887$, $p = 0.018$; turns right vs. HVA % R/L, $r = -0.856$, $p = 0.029$).

3.2. Power spectral analysis

Figure 1 shows a diagram of the electrode location on the cerebral cortex of the rat (A), and the ECoGs of the right hemisphere before and after treatment with 6-OHDA during W (B)**.**

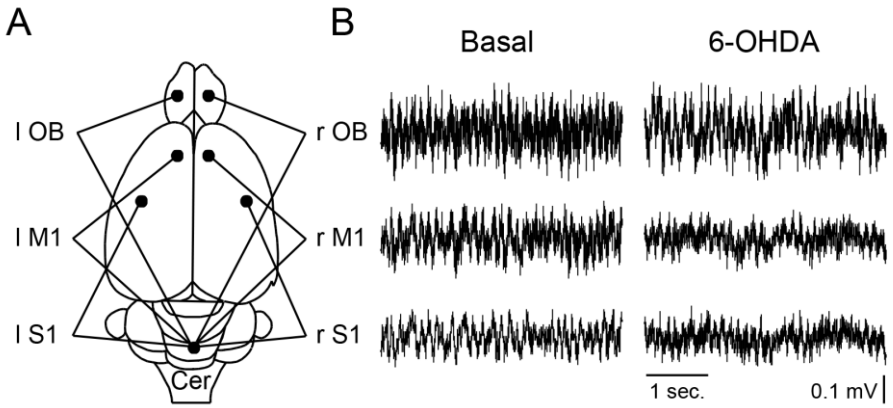

Figure 1. A. The Figure presents a summary of the cortical positions of the recording electrodes. The electrodes were referred to a common electrode that was located over the cerebellum (Cer). B. Simultaneous ECoG raw recordings from the right hemisphere during wakefulness. Records were taken before and after the 6-OHDA lesion. OB, olfactory bulb; M1, whisker primary motor cortex; S1, whisker primary somatosensory ("barrel") cortex; r, right; l, left.

Figure S1 shows the mean and SD of the spectral power of each electrode recorded during W before and after the injury with 6-OHDA. **Figure 2A** highlights the cortical regions where significant differences were found; in the whiskers motor cortex (M1) on the side of the lesion there was an increase in beta (20-35 Hz) together with a decrease in high gamma activity (60-95 Hz). No changes were observed on the contralateral side. These changes in beta and gamma power are better represented with the interhemispheric differences (**Figure 2B**). The increase in beta and the decrease in gamma band, were correlated with the rotational behavior, as well as with the percentage of DA on the side of the lesion (**Figure 2C**).

No spectral changes were observed during NREM sleep (**Figure S2**). During REM sleep although there was a peak in the beta power in the right M1

cortex following the lesion **(Figure S3)**, this increment did not reach significance.

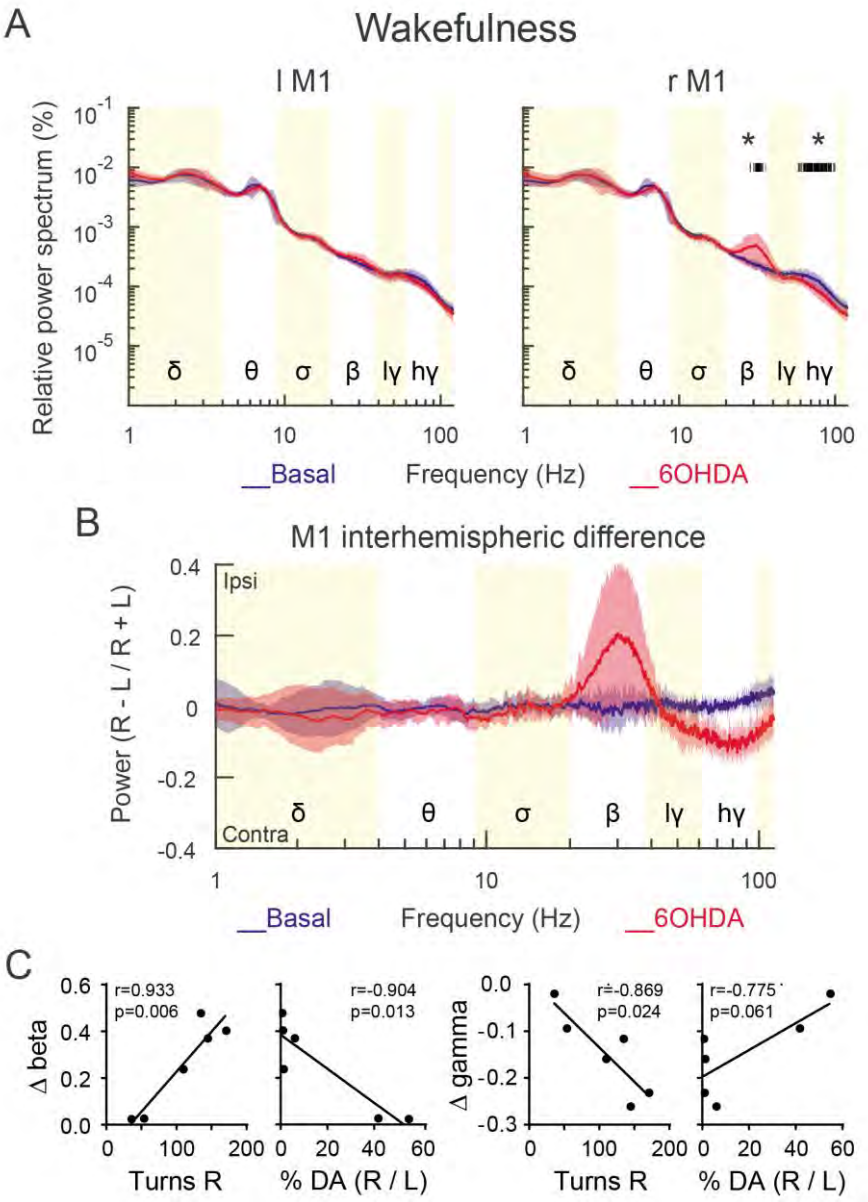

Figure 2. Power spectrum before and after the treatment with 6-OHDA. A. Each graph shows the mean ± SD of the motor cortex relative spectral power before and after treatment with 6-OHDA during wakefulness. Shaded areas correspond to the standard deviation. The yellow and white background correspond to the limits of the bands. The black dotted lines above the spectra correspond to the frequencies that showed statistically significant differences (two-tailed paired t-test, $p < 0.05$). The statistics for the individual frequencies were performed only if the whole band showed a significant difference (statistical differences of the whole band is indicated by an asterisk). B. Interhemispheric difference of the M1 cortex. C. linear correlation between right M1 total power per band (beta and gamma) and % DA (R/L) and motor behavior.

Δ = (post lesion – pre lesion) / (post lesion + pre lesion). r, Pearson correlation coefficient; R, right; L, left; contra, contralateral; ipsi, ipsilateral; M1, whisker primary motor cortex.

3.3. Inter-cortical spectral coherence after 6-OHDA treatment

Figure S4-S6 shows the mean and SD of the fifteen intercortical combination of z'-coherence during W, NREM and REM sleep respectively, before and after DA lesion. Significant differences were observed in some combinations only during W and are displayed in **Figure 3**. The lesion decreased the coherence in the high gamma band between both whisker motor cortices (M1) and the right OB (**Figure 3**; two-tails paired t-test, p = 0.034 and p = 0.044; right and left respectively). In this case, we did not find any correlation between the changes in gamma coherence and motor asymmetry or the DA levels in the CS. Moreover, we found a decrease in delta (1 – 4 Hz) and theta (5 – 9 Hz) coherence between the motor cortex of both hemispheres (**Figure 3**).

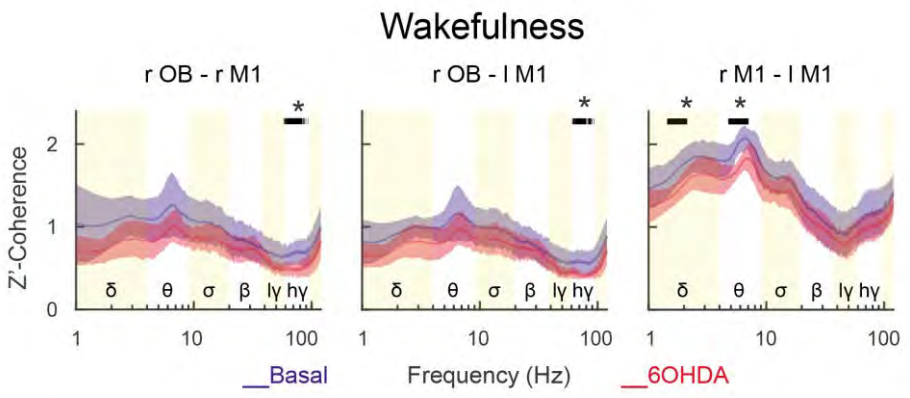

Figure 3. Spectral coherence before and after the treatment with 6-OHDA. Each graph shows the mean ± SD of the z'-coherence before and after treatment with 6-OHDA during wakefulness. Shaded areas correspond to the standard deviation. The yellow and white background correspond to the limits of the bands. The black lines above the spectra correspond to the frequencies that showed statistically significant differences (two-tailed paired t-test, $p < 0.05$). The statistics for the individual frequencies were performed only if the whole band showed a significant difference (statistical differences of the whole band is indicated by an asterisk). OB, olfactory bulb; M1, whisker primary motor cortex; r, right; l, left.

3.4. Respiratory entrainment of gamma activity after 6-OHDA lesion

It is well-known that in the OB the slow respiratory potential (RP) faithfully follows the respiratory rate (between 2 and 10 Hz; (Rojas-Líbano et al., 2014)). **Figure 4** (Basal) shows that this RP is strongly comodulated with gamma activity (as previously shown (Biskamp et al., 2017; Rojas-Líbano et al., 2018, 2014; Tort et al., 2018; Zhong et al., 2017)).

In order to evaluate if DA neurons regulate the RP comodulation with gamma activity, we analyzed the PAC before and after the SNpc lesion. Comodulograms of all electrodes recorded before and after treatment with 6-OHDA are shown in **Figure 4**. A clear "cross frequency coupling" between the phase of the RP and gamma amplitude ($PAC_{(RP\text{-}gamma)}$) was appreciated at the OBs and whiskers motor areas (**Figure 4**). After 6-OHDA treatment, a significant increase in $PAC_{(RP\text{-}gamma)}$ was observed at both OBs (**Figure 4**, top right). However, the levels of RP entrainment of gamma activity decreased in both M1 cortex. It is interesting to note that these changes are bilateral and have no correlation with motor asymmetry or CS DA levels.

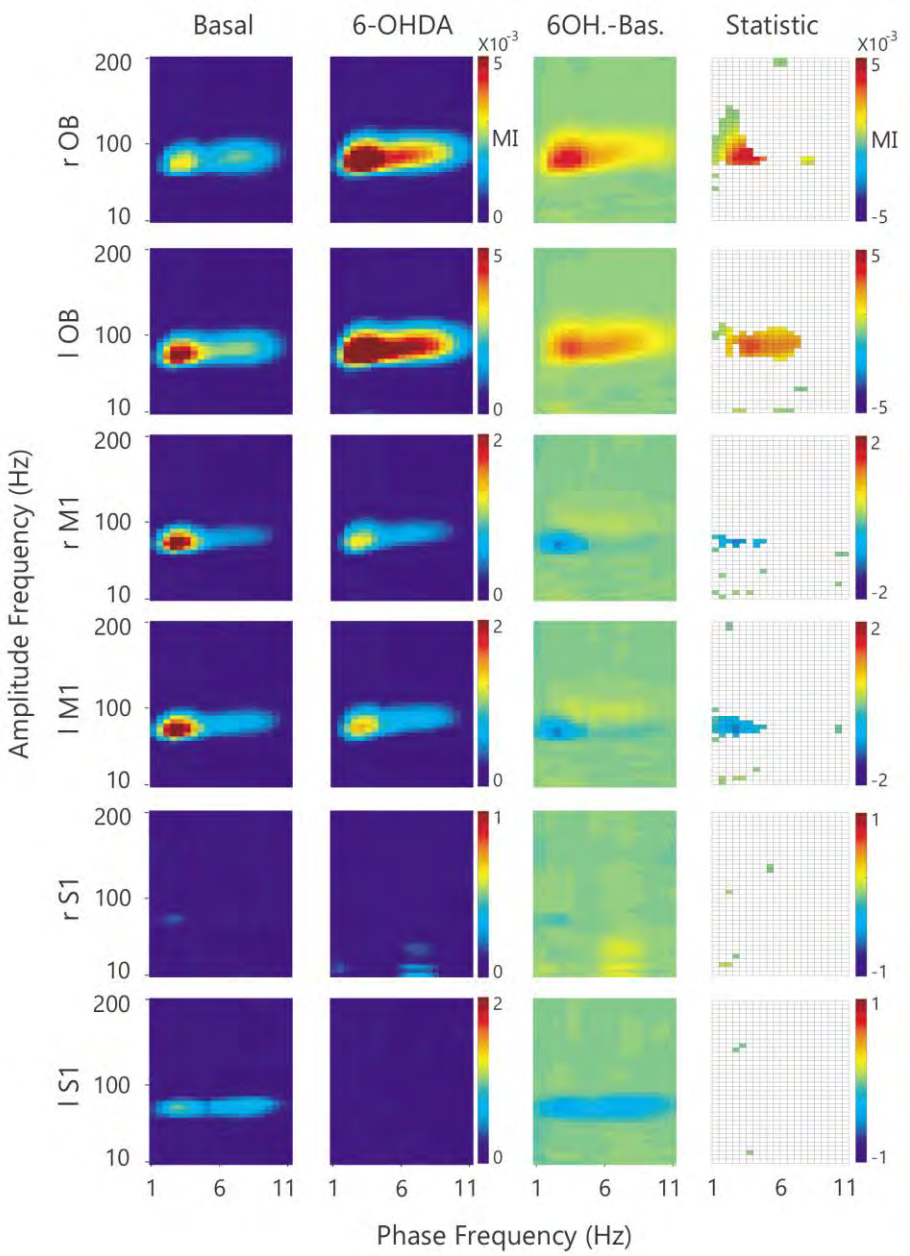

Figure 4. Comodulograms before and after the treatment with 6-OHDA. Comodulograms of phase amplitude coupling (PAC) between the phase and the amplitudes of ECoGs during W quantified by the modulation index (MI) (Tort et al., 2010). Each MI value represents the average over 6 animals (first two columns from the left). On the right, the differences between before and after the injury and their statistically significant differences are shown (two-tailed paired t-test, $p < 0.05$). OB, olfactory bulb; M1, whisker primary motor cortex; S1, whisker primary somatosensory ("barrel") cortex; r, right; l, left.

4. Discussion

In the present study, the damage of the DA neurons in the SNpc with 6-OHDA generated a decrease in the DA levels measured at the CS (**Table 1**). This decrease (mean ≈ 80 %) was accompanied by a marked motor lateralization that correlated with DA differences between hemispheres. In contrast, the levels of 5-HT and its metabolites showed no interhemispheric differences or correlation with motor lateralization (**Table 2**). These results suggest that our approach was adequate to evaluate the ECoG synchronization in an animal model of PD.

4.1. Increase in beta power in motors areas after treatment with 6-OHDA

Beta power increased in the motor area only on the side of the lesion (**Figure 2**). This increment correlates positively with the degree of injury measured by the levels of DA in the CS or the rotation behavior induced by amphetamines. Increases in beta activity and synchronization (15–30 Hz) in the cortico-basal ganglia-thalamo-cortical circuit associated with DA depletion have been observed in untreated patients with PD (Bouthour et al., 2019; Brown et al., 2001; DeLong and Wichmann, 2010; Hammond et al., 2007; Levy et al., 2002; Obeso and Lanciego, 2011; Weinberger et al., 2006). In this patients, beta rhythms are diminished by treatments such as DA replacement therapy (Beudel et al., 2017; Weinberger et al., 2006; West et al., 2016) and deep brain stimulation at high frequencies (> 60 Hz; (Bouthour et al., 2019; Eusebio et al., 2011; Whitmer et al., 2012)) in a way that correlates with the degree of motor improvement (akinesia and rigidity). In this sense, beta amplitude in the subthalamic nucleus positively correlates with the severity of bradykinesia and rigidity symptoms (Bouthour et al., 2019; Lofredi et al., 2018; Neumann et al., 2016). This has strengthened the argument that the pathological beta rhythms are directly related to the motor impairment seen in PD patients (Brittain and Brown, 2014).

Sharrot *et al.* demonstrated that 6-OHDA lesions of midbrain DA neurons are associated with significant increases in the power and coherence of beta oscillatory activity present in local field potentials recorded from frontal cortex (motor areas) and sub-thalamic nucleus (STN) of awake rats, as compared with

the healthy animal (Sharott et al., 2005). In that work, the administration of the DA receptor agonist apomorphine to lesioned animals suppressed beta hyperactivity (Sharott et al., 2005). Thus, the pattern of synchronization between population activity in the basal ganglia and cortex in the 6-OHDA-lesioned rodent model of PD (present report and (Sharott et al., 2005; West et al., 2018)) closely parallels what have been described in humans (Bouthour et al., 2019; Marsden et al., 2001; Williams et al., 2003).

4.2. Decrease in gamma power in the whisker motor cortex after treatment with 6-OHDA

We also found a decrease in gamma power (60-95 Hz) in the ipsilateral M1 cortex. This gamma changes correlates negatively with the degree of injury measured by the levels of DA in the CS, and with the rotation behavior induced by amphetamines.

In Sharrot *et al.* work (Sharott et al., 2005), no fall in gamma activity was detected; however, the administration of the DA receptor agonist apomorphine to 6-OHDA-lesioned rats led to a suppression of beta-frequency oscillations with an increase in the synchronized oscillatory population activity at higher frequencies (> 35 Hz or gamma). Our results are in line with studies in Parkinsonian humans showing an increase in gamma activity after DA medication (Brown et al., 2001; Williams, 2002), particularly when movements are performed following treatment (Bouthour et al., 2019; Brown, 2003; Cassidy et al., 2002; Lofredi et al., 2018). Furthermore, gamma activity in the motor system has been hypothesized to be prokinetic (Brown, 2003; Fries et al., 2005). In fact, spectral power from the subthalamic nucleus (STN) at 40–90 Hz have been demonstrated to be negatively correlated with bradykinetic symptoms (Sharott et al., 2014). It is important to note that beta and gamma frequency bands are inversely affected by movement and DA levels at dorsal striatum (present result and (Brown, 2003; Fries et al., 2005)). Therefore, the balance between these modes of oscillation are probably determined by the effects of basal ganglia-thalamus projections toward the motor areas of the cortex (Brown, 2003). Hence, beta oscillations at the motor cortex may hinder

movements, while gamma oscillations restore the dynamic activity of the cortical set related to the motor task (Brown, 2003; Cassidy et al., 2002; Lofredi et al., 2018).

4.3. Gamma coherence between the OB and the whisker motor cortex falls after the 6-OHDA injection

When we analyzed the intercortical coherence before and after the 6-OHDA lesion, we found a reduction in gamma coherence (60-95 Hz) between the right OB and the whisker M1 of both hemispheres (**Figure 3**). In contrast to the gamma power decrease in M1, this effect in gamma coherence does not correlate with the rotational behavior or the striatum DA levels. We also found an interhemispheric fall of the delta and theta coherence at M1 level.

As mentioned above, the gamma activity recorded at the OB level is coupled to the RP (Adrian, 1950; Buonviso et al., 2003; Manabe and Mori, 2013; Rojas-Líbano et al., 2014), which depends on the passage of air through the olfactory epithelium (Grosmaitre et al., 2007; Iwata et al., 2017), and in rodents has a frequency within the delta and theta bands (Rojas-Líbano et al., 2014). The RP can also be recorded in non-olfactory cortical areas (Biskamp et al., 2017; Cavelli et al., 2018; Ito et al., 2014; Lockmann et al., 2016; Nguyen Chi et al., 2016; Rojas-Líbano et al., 2018; Tort et al., 2018; Yanovsky et al., 2014; Zhong et al., 2017). The RP and the comodulation with gamma can be observed at the level of the whisker motor area (**Figure 4** and (Ito et al., 2014; Rojas-Líbano et al., 2018)). In this area, the RP can synchronize with the movement of the whiskers during the active exploration of the environment, in a kind of olfactory-orofacial sensorimotor synchronization (Ito et al., 2014; Moore et al., 2013; Rojas-Líbano et al., 2018). Olfaction is considered an “active sensing” function, where the animals produce motor actions (breathing) specifically tuned to obtain useful sensory information about their environment (Curtis and Kleinfeld, 2009; Najemnik and Geisler, 2005; Rojas-Líbano et al., 2018; Verhagen et al., 2007). Other examples are electrolocation in fishes, echolocation in bats and odontocetes cetaceans, fingers and eye movements in primates as well as whisking and sniffing in rodents, (Hofmann et al., 2013; Rojas-Líbano et al., 2018; Schroeder et al., 2010). In the present study, the loss

of gamma coupling between the OB and the whisker M1 cortex following SNpc lesion, strongly suggest that breathing lost its effectiveness in the gamma bursts modulation.

There are direct nigral DA axons towards the OB; interestingly, all the DA neurons that innervate the OB appear to branch into the striatum (Höglinger et al., 2015). This would imply a synchronous DA modulation between these structures and could explain the fall of gamma synchronization (coherence) between the OB and the whisker M1 cortex after 6-OHDA injury (**Figure 3**). This lack of synchronization may determine a decrease in the capacity of synchronize the olfactory-orofacial exploration (Ito et al., 2014; Kleinfeld et al., 2016; Moore et al., 2013; Rojas-Líbano et al., 2018). New experiments are needed to confirm this hypothesis.

4.4. Phase amplitude coupling between RP and gamma activity in the 6-OHDA model of PD

As mentioned above, at the OB the slow RP faithfully follows the respiratory rate during W (between 2 and 10 Hz; (Rojas-Líbano et al., 2014)) and was strongly comodulated with gamma activity (**Figure 4** basal (Biskamp et al., 2017; Rojas-Líbano et al., 2018, 2014; Tort et al., 2018; Zhong et al., 2017). Unilateral SNpc lesion increased the $PAC_{(RP\text{-}gamma)}$ at the OB level (**Figure 4**) but surprisingly, this effect was bilateral.

Anosmia or behavioral alterations associated with olfaction have been described in several animal models of PD (Aurich et al., 2017; Fleming et al., 2008; Höglinger et al., 2015; Ilkiw and Lima, 2019; Ilkiw et al., 2019; Rodrigues et al., 2014; Valle-Leija and Drucker-Colín, 2014; Zhang et al., 2019), together with anatomical and functional alterations of the OB (Fleming et al., 2008; Höglinger et al., 2015; Rodrigues et al., 2014; Zhang et al., 2019). In the early and partial SNpc lesion, Zhang et al. shows that anosmia can appear without the characteristic motor alterations (Zhang et al., 2019) raising the possibility that the olfactory dysfunction present during the early stages of PD is directly linked to the loss of a sub-population SNpc neurons (≈ 3% of SNpc DA neurons) that directly contact the central part of the OB (Höglinger et al., 2015).

However, there are other possible explanations, such as the increase in periglomerular DA interneurons of OB, changes in neurogenesis balances at this level or changes at others levels of the olfactory system (Aurich et al., 2017; Höglinger et al., 2015, 2004; Ilkiw et al., 2019; Rodrigues et al., 2014; Xiong and Wesson, 2016; Zhang et al., 2019).

Recently, Zhang *et al.* (Zhang et al., 2019) publish the first study where neural activity is recorded at the OB level after a partial 6-OHDA injury in the SNpc. In this study, seven days after injection of 6-OHDA, motor ability was unchanged but olfactory-driven behaviors were significantly impaired. They also observed an increase in total power and odor-evoked calcium responses in the mitral cells in the OB of awake mice. The authors suggest that the olfactory deficits caused by depletion of the SNpc DA neurons are likely due to abnormal hyperactivity of the mitral cells in the OB (Zhang et al., 2019). Consistent with this result, we showed an increase in PAC between the phase of the respiratory potentials and the gamma amplitude of the OB after treatment with 6-OHDA, suggesting an increase in the respiratory entrainment of the gamma activity at OB level (**Figure 4**). More efforts must be made in order to clarify the changes that the SNpc injury generates over the phase coding related to olfactory perception at the OB (Iwata et al., 2017).

Following SNpc lesions, Zhang et al. have shown some hyperactivity at the OB (Zhang et al., 2019), while the present work demonstrate and increase in RP-gamma coupling at this level (**Figure 4**). Nevertheless, at the level of whisker motor cortex the coupling between the RP and the gamma amplitude decreased bilaterally (**Figure 4**). Then, internalization of the nasal respiratory activity and/or its comodulation with gamma activity decreases mainly at the motor cortex. This decrease in $PAC_{(RP\text{-}gamma)}$ at the motor cortex may disturb olfactory-orofacial coordination (Curtis and Kleinfeld, 2009; Ito et al., 2014; Moore et al., 2013; Rojas-Líbano et al., 2018).

It is thought-provoking why a unilateral SNpc lesion affects OB and M1 $PAC_{(RP\text{-}gamma)}$ bilaterally. New experiments are needed to understand this finding.

5. Conclusions

In concordance with previous results in patients and animal models of PD, in this work we showed that unilateral degeneration of DA neurons in the SNpc, results in reciprocal changes between beta and gamma activity in the ipsilateral motor cortex. Furthermore, we found a decrease in the synchronous oscillatory activity between populations of the OB and the motor cortex in the gamma band. In adition, we observed an increase in the coupling between the RP and the gamma activity in the OB together with a decrease in the respiratory entrainment of the gamma activity at the level of the motor cortices. It is important to note, that during sleep no clear alterations were observed, either in the synchronization or in the modulation of cortical gamma activity. These waking dysrhythmias may play a role both in the anosmia and motor alteration present PD patients.

6. Acknowledgements

This study was partially supported by the “Programa de Desarrollo de Ciencias Basicas - PEDECIBA”, “Comision Sectorial de Investigacion Cientifica – CSIC”, Modalidad 1 - 2015 - Iniciación a la Investigación (ID: 245), and “Agencia Nacional de Investigación en Innovación, - ANII”. S. CZ. and N. V. received a postgraduate scholarship from the ANII, while M. C. received a fellowship from “Comisión de Apoyo a Postgrados - CAP”. M.M.S.L. is the recipient of the Conselho Nacional de Desenvolvimento Científico e Tecnológico - CNPq fellowship, Research Grants 431279/2016-0, 305986/2016-3.

7. Conflict of interest

All the authors declare no conflict of interest.

8. Authors Contributions

Financial support: P.T., G.P., M.C.. Experimental design: M.C., P.T., G.P.. Experimental procedures: M.C., N.V., G.P., G.C.. Analysis of the data: M.C., J.G.. Discussion and interpretation of the data: M.C., P.T., G.P., G.C., N.V.. J.G., S.C.., M.M.S.L.. Wrote the manuscript: M.C.. All the authors participated in critical revision the manuscript, added important intellectual content, and approved the final version.

9. Data Availability

For access to data and custom computer code contact Dr. Pablo Torterolo (ptortero@fmed.edu.uy) or Matías Cavelli (mcavelli@fmed.edu.uy).

10. Bibliography

Abin-Carriquiry, J.A., McGregor-Armas, R., Costa, G., Urbanavicius, J., Dajas, F., 2002. Presynaptic Involvement in the Nicotine Prevention of the Dopamine Loss Provoked by 6-OHDA Administration in the Substantia Nigra. Neurotox. Res. doi:10.1080/10298420290015863

Adrian, E.D., 1950. The electrical activity of the mammalian olfactory bulb.

Electroencephalogr. Clin. Neurophysiol. 2, 377–388. doi:10.1016/0013-4694(50)90075-7

Adrian, E.D., 1942. Olfactory reactions in the brain of the hedgehog. J. Physiol. 100, 459–73. doi:https://doi.org/10.1113/jphysiol.1942.sp003955

Aurich, M.F., Rodrigues, L.S., Targa, A.D.S., Noseda, A.C.D., Cunha, F.D.W., Lima, M.M.S., 2017. Olfactory impairment is related to REM sleep deprivation in rotenone model of Parkinson's disease. Sleep Sci. 10, 47–54. doi:10.5935/1984-0063.20170008

Benedetto, L., Rivas, M., Cavelli, M., Peña, F., Monti, J., Ferreira, A., Torterolo, P., 2017. Microinjection of the dopamine D2-receptor antagonist Raclopride into the medial preoptic area reduces REM sleep in lactating rats. Neurosci. Lett. 659, 104–109. doi:10.1016/j.neulet.2017.08.077

Beudel, M., Oswal, A., Jha, A., Foltynie, T., Zrinzo, L., Hariz, M., Limousin, P., Litvak, V., 2017. Oscillatory Beta Power Correlates With Akinesia-Rigidity in the Parkinsonian Subthalamic Nucleus. Mov. Disord. 32, 174–175. doi:10.1002/mds.26860

Biskamp, J., Bartos, M., Sauer, J.-F., 2017. Organization of prefrontal network activity by respiration-related oscillations. Sci. Rep. 7, 45508. doi:10.1038/srep45508

Bouthour, W., Mégevand, P., Donoghue, J., Lüscher, C., 2019. Biomarkers for closed-loop deep brain stimulation in Parkinson disease and beyond. Nat. Rev. Neurol. doi:10.1038/s41582-019-0166-4

Braak, H., Rub, U., Gai, W.P., Del Tredici, K., 2003. Idiopathic Parkinson's disease: possible routes by which vulnerable neuronal types may be subject to neuroinvasion by an unknown pathogen. J. Neural Transm. 110, 517–536. doi:10.1007/s00702-002-0808-2

Bressler, S.L., Coppola, R., Nakamura, R., 1993. Episodic multiregional cortical coherence at multiple frequencies during visual task performance. Nature 366, 153–6. doi:10.1038/366153a0

Brittain, J.S., Brown, P., 2014. Oscillations and the basal ganglia: Motor control

and beyond. Neuroimage 85, 637–647. doi:10.1016/j.neuroimage.2013.05.084

Brown, P., 2003. Oscillatory nature of human basal ganglia activity: Relationship to the pathophysiology of parkinson's disease. Mov. Disord. 18, 357–363. doi:10.1002/mds.10358

Brown, P., Oliviero, A., Mazzone, P., Insola, A., Tonali, P., Di Lazzaro, V., 2001. Dopamine dependency of oscillations between subthalamic nucleus and pallidum in Parkinson's disease. J. Neurosci. 21, 1033–8. doi:https://doi.org/10.1523/JNEUROSCI.21-03-01033.2001

Bullock, T.H., 1997. Signals and signs in the nervous system : The dynamic anatomy of electrical activity is probably information-rich 94, 14–19. doi:10.1073/pnas.94.1.1

Bullock, T.H., McClune, M.C., Achimowicz, J.Z., Iragui-Madoz, V.J., Duckrow, R.B., Spencer, S.S., 1995. Temporal fluctuations in coherence of brain waves. Proc. Natl. Acad. Sci. U. S. A. 92, 11568–72. doi:10.1073/pnas.92.25.11568

Buonviso, N., Amat, C., Litaudon, P., Roux, S., Royet, J.P., Farget, V., Sicard, G., 2003. Rhythm sequence through the olfactory bulb layers during the time window of a respiratory cycle. Eur. J. Neurosci. 17, 1811–1819. doi:10.1046/j.1460-9568.2003.02619.x

Buzsáki, G., Draguhn, A., 2004. Neuronal oscillations in cortical networks. Science 304, 1926–9. doi:10.1126/science.1099745

Buzsáki, G., Schomburg, E.W., 2015. What does gamma coherence tell us about inter-regional neural communication? Nat. Neurosci. 18, 484–489. doi:10.1038/nn.3952

Cantero, J.L., Atienza, M., Salas, R.M., 2000. Valor clínico de la coherencia EEG como índice electrofisiológico de conectividad córtico-cortical durante el sueño 31, 442–454. doi:https://doi.org/10.33588/rn.3105.99472

Cassidy, M., Mazzone, P., Oliviero, A., Insola, A., Tonali, P., Lazzaro, V. Di, Brown, P., 2002. Movement-related changes in synchronization in the

human basal ganglia 125, 1235–1246. doi:10.1093/brain/awf135

Castro-Zaballa, S., Cavelli, M., González, J., Monti, J., Falconi, A., Torterolo, P., 2019. EEG dissociation induced by muscarinic receptor antagonists: Coherent 40 Hz oscillations in a background of slow waves and spindles. Behav. Brain Res. 359, 28–37. doi:10.1016/j.bbr.2018.10.016

Castro-Zaballa, S., Cavelli, M., Vollono, P., Chase, M.H., Falconi, A., Torterolo, P., 2014. Inter-hemispheric coherence of neocortical gamma oscillations during sleep and wakefulness. Neurosci. Lett. 578, 197–202. doi:10.1016/j.neulet.2014.06.044

Castro-Zaballa, S., Falconi, A., Chase, M.H., Torterolo, P., 2013. Coherent neocortical 40-Hz oscillations are not present during REM sleep. Eur. J. Neurosci. 37, 1330–9. doi:10.1111/ejn.12143

Cavelli, M., Castro-Zaballa, S., Gonzalez, J., Rojas-Líbano, D., Rubido, N., Velásquez, N., Torterolo, P., 2018. Nasal respiration entrains neocortical long-range gamma coherence during wakefulness. bioRxiv 430579. doi:10.1101/430579

Cavelli, M., Castro-Zaballa, S., Mondino, A., Gonzalez, J., Falconi, A., Torterolo, P., 2017a. Absence of EEG gamma coherence in a local activated cortical state: a conserved trait of REM sleep. Transl Brain Rhythm. 2, 1–13. doi:10.15761/TBR.1000115

Cavelli, M., Castro, S., Schwarzkopf, N., Chase, M.H., Falconi, A., Torterolo, P., 2015. Coherent neocortical gamma oscillations decrease during REM sleep in the rat. Behav. Brain Res. 281, 318–25. doi:10.1016/j.bbr.2014.12.050

Cavelli, M., Rojas-Líbano, D., Schwarzkopf, N., Castro-Zaballa, S., Gonzalez, J., Mondino, A., Santana, N., Benedetto, L., Falconi, A., Torterolo, P., 2017b. Power and coherence of cortical high-frequency oscillations during wakefulness and sleep. Eur. J. Neurosci. 48, 2728–2737. doi:10.1111/ejn.13718

Costa, G., Abin-Carriquiry, J. a., Dajas, F., 2001. Nicotine prevents striatal dopamine loss produced by 6-hydroxydopamine lesion in the substantia nigra. Brain Res. 888, 336–342. doi:10.1016/S0006-8993(00)03087-0

Curtis, J.C., Kleinfeld, D., 2009. Phase-to-rate transformations encode touch in cortical neurons of a scanning sensorimotor system. Nat. Neurosci. 12, 492–501. doi:10.1038/nn.2283

Dauer, W., Przedborski, S., 2003. Parkinson's Disease: Models and mechanisms. Neuron 39, 889–909. doi:https://doi.org/10.1016/S0896-6273(03)00568-3

DeLong, M., Wichmann, T., 2010. Changing views of basal ganglia circuits and circuit disorders. Clin. EEG Neurosci. 41, 61–67. doi:10.1177/155005941004100204

Doty, R.L., 2012a. Olfactory dysfunction in Parkinson disease. Nat. Rev. Neurol. 8, 329–39. doi:10.1038/nrneurol.2012.80

Doty, R.L., 2012b. Olfaction in Parkinson's disease and related disorders. Neurobiol. Dis. 46, 527–52. doi:10.1016/j.nbd.2011.10.026

Engel, A.K., Fries, P., Singer, W., 2001. Dynamic predictions: Oscillations and synchrony in top–down processing. Nat. Rev. Neurosci. 2, 704–716. doi:10.1038/35094565

Eusebio, A., Thevathasan, W., Doyle Gaynor, L., Pogosyan, A., Bye, E., Foltynie, T., Zrinzo, L., Ashkan, K., Aziz, T., Brown, P., 2011. Deep brain stimulation can suppress pathological synchronisation in parkinsonian patients. J. Neurol. Neurosurg. Psychiatry 82, 569–573. doi:10.1136/jnnp.2010.217489

Fleming, S.M., Tetreault, N.A., Mulligan, C.K., Hutson, C.B., Masliah, E., Chesselet, M.F., 2008. Olfactory deficits in mice overexpressing human wildtype α-synuclein. Eur. J. Neurosci. 28, 247–256. doi:10.1111/j.1460-9568.2008.06346.x

Fries, P., 2009. Neuronal Gamma-Band Synchronization as a Fundamental Process in Cortical Computation. Annu. Rev. Neurosci. 32, 209–224. doi:10.1146/annurev.neuro.051508.135603

Fries, P., Schoffelen, J.M., Oostenveld, R., 2005. Neuronal coherence as a mechanism of effective corticospinal interaction. Science (80-.). 308, 111–

3. doi:10.1126/science.1107027

González, J., Prieto, J.P., Rodríguez, P., Cavelli, M., Benedetto, L., Mondino, A., Pazos, M., Seoane, G., Carrera, I., Scorza, C., Torterolo, P., 2018. Ibogaine Acute Administration in Rats Promotes Wakefulness, Long-Lasting REM Sleep Suppression, and a Distinctive Motor Profile. Front. Pharmacol. 9, 374. doi:10.3389/fphar.2018.00374

Gray, C.M., König, P., Engel, A.K., Singer, W., 1989. Oscillatory responses in cat visual cortex exhibit inter-columnar synchronization which reflects global stimulus properties. Nature 338, 334–7. doi:10.1038/338334a0

Grosmaitre, X., Santarelli, L.C., Tan, J., Luo, M., Ma, M., 2007. Dual functions of mammalian olfactory sensory neurons as odor detectors and mechanical sensors. Nat. Neurosci. 10, 348–354. doi:10.1038/nn1856

Hammond, C., Bergman, H., Brown, P., 2007. Pathological synchronization in Parkinson's disease: networks, models and treatments. Trends Neurosci. 30, 357–364. doi:10.1016/j.tins.2007.05.004

Hirsch, L., Jette, N., Frolkis, A., Steeves, T., Pringsheim, T., 2016. The Incidence of Parkinson's Disease: A Systematic Review and Meta-Analysis. Neuroepidemiology 46, 292–300. doi:10.1159/000445751

Hofmann, V., Sanguinetti-Scheck, J.I., Künzel, S., Geurten, B., Gómez-Sena, L., Engelmann, J., 2013. Sensory flow shaped by active sensing: sensorimotor strategies in electric fish. J. Exp. Biol. 216, 2487–500. doi:10.1242/jeb.082420

Höglinger, G.U., Alvarez-Fischer, D., Arias-Carrión, O., Djufri, M., Windolph, A., Keber, U., Borta, A., Ries, V., Schwarting, R.K.W., Scheller, D., Oertel, W.H., 2015. A new dopaminergic nigro-olfactory projection. Acta Neuropathol. 130, 333–348. doi:10.1007/s00401-015-1451-y

Höglinger, G.U., Rizk, P., Muriel, M.P., Duyckaerts, C., Oertel, W.H., Caille, I., Hirsch, E.C., 2004. Dopamine depletion impairs precursor cell proliferation in Parkinson disease. Nat. Neurosci. 7, 726–735. doi:10.1038/nn1265

Ilkiw, J., Lima, M.S., 2019. Perspectives for the association between olfactory

disturbances and depression in Parkinson's disease. Neural Regen. Res. 14, 591. doi:10.4103/1673-5374.247461

Ilkiw, J.L., Kmita, L.C., Targa, A.D.S., Noseda, A.C.D., Rodrigues, L.S., Dorieux, F.W.C., Fagotti, J., dos Santos, P., Lima, M.M.S., 2019. Dopaminergic Lesion in the Olfactory Bulb Restores Olfaction and Induces Depressive-Like Behaviors in a 6-OHDA Model of Parkinson's Disease. Mol. Neurobiol. 56, 1082–1095. doi:10.1007/s12035-018-1134-5

Ito, J., Roy, S., Liu, Y., Cao, Y., Fletcher, M., Lu, L., Boughter, J.D., Grün, S., Heck, D.H., 2014. Whisker barrel cortex delta oscillations and gamma power in the awake mouse are linked to respiration. Nat. Commun. 5, 3572. doi:10.1038/ncomms4572

Iwata, R., Kiyonari, H., Imai, T., 2017. Mechanosensory-Based Phase Coding of Odor Identity in the Olfactory Bulb. Neuron 96, 1139-1152.e7. doi:10.1016/j.neuron.2017.11.008

John, E.R., 2002. The neurophysics of consciousness. Brain Res. Rev. 39, 1–28. doi:https://doi.org/10.1016/S0165-0173(02)00142-X

Joliot, M., Ribary, U., Llinás, R., 1994. Human oscillatory brain activity near 40 Hz coexists with cognitive temporal binding. Proc. Natl. Acad. Sci. U. S. A. 91, 11748–51. doi:https://doi.org/10.1073/pnas.91.24.11748

Kleinfeld, D., Deschênes, M., Ulanovsky, N., 2016. Whisking, Sniffing, and the Hippocampal θ-Rhythm: A Tale of Two Oscillators. PLoS Biol. 14, e1002385. doi:10.1371/journal.pbio.1002385

Knudsen, K., Flensborg Damholdt, M., Mouridsen, K., Borghammer, P., 2015. Olfactory function in Parkinson's Disease - effects of training. Acta Neurol. Scand. 132, 395–400. doi:10.1111/ane.12406

Lang, A.E., Lozano, A.M., 1998. Parkinson's Disease. N. Engl. J. Med. 339, 1044–1053. doi:10.1056/NEJM199810083391506

Levy, R., Ashby, P., Hutchison, W.D., Lang, A.E., Lozano, A.M., Dostrovsky, J.O., 2002. Dependence of subthalamic nucleus oscillations on movement and dopamine in Parkinson's disease. Brain 125, 1196–209.

doi:10.1093/brain/awf128

Llinás, R., Ribary, U., 2001. Consciousness and the brain. The thalamocortical dialogue in health and disease. Ann. N. Y. Acad. Sci. 929, 166–175. doi:10.1111/j.1749-6632.2001.tb05715.x

Lockmann, A.L. V., Laplagne, D.A., Leão, R.N., Tort, A.B.L., 2016. A Respiration-Coupled Rhythm in the Rat Hippocampus Independent of Theta and Slow Oscillations. J. Neurosci. 36, 5338–5352. doi:10.1523/JNEUROSCI.3452-15.2016

Lofredi, R., Neumann, W.-J., Bock, A., Horn, A., Huebl, J., Siegert, S., Schneider, G.-H., Krauss, J.K., Kühn, A.A., 2018. Dopamine-dependent scaling of subthalamic gamma bursts with movement velocity in patients with Parkinson's disease. Elife 7, 1–22. doi:10.7554/elife.31895

Maloney, K.J., Cape, E.G., Gotman, J., Jones, B.E., 1997. High-frequency gamma electroencephalogram activity in association with sleep-wake states and spontaneous behaviors in the rat. Neuroscience 76, 541–55. doi:https://doi.org/10.1016/S0306-4522(96)00298-9

Manabe, H., Mori, K., 2013. Sniff rhythm-paced fast and slow gamma-oscillations in the olfactory bulb: relation to tufted and mitral cells and behavioral states. J. Neurophysiol. 110, 1593–1599. doi:10.1152/jn.00379.2013

Marsden, J.F., Ashby, P., Pollak, P., Brown, P., 2001. Subthalamic nucleus, sensorimotor cortex and muscle interrelationships in Parkinson's disease. Brain 124, 378–388. doi:10.1093/brain/124.2.378

Mashour, G. a, 2006. Integrating the science of consciousness and anesthesia. Anesth. Analg. 103, 975–82. doi:10.1213/01.ane.0000232442.69757.4a

Melloni, L., Molina, C., Pena, M., Torres, D., Singer, W., Rodriguez, E., 2007. Synchronization of neural activity across cortical areas correlates with conscious perception. J. Neurosci. 27, 2858–65. doi:10.1523/JNEUROSCI.4623-06.2007

Mondino, A., Cavelli, M., González, J., Santana, N., Castro-Zaballa, S.,

Mechozo, B., Bracesco, N., Fernandez, S., Garcia-Carnelli, C., Castro, M.J., Umpierrez, E., Murillo-Rodriguez, E., Torterolo, P., Falconi, A., 2019. Acute effect of vaporized Cannabis on sleep and electrocortical activity. Pharmacol. Biochem. Behav. 179, 113–123. doi:10.1016/j.pbb.2019.02.012

Moore, J.D., Deschênes, M., Furuta, T., Huber, D., Smear, M.C., Demers, M., Kleinfeld, D., 2013. Hierarchy of orofacial rhythms revealed through whisking and breathing. Nature 497, 205–210. doi:10.1038/nature12076

Mouhape, C., Costa, G., Ferreira, M., Abin-Carriquiry, J.A., Dajas, F., Prunell, G., 2019. Nicotine-Induced Neuroprotection in Rotenone In Vivo and In Vitro Models of Parkinson's Disease: Evidences for the Involvement of the Labile Iron Pool Level as the Underlying Mechanism. Neurotox. Res. 35, 71–82. doi:10.1007/s12640-018-9931-1

Najemnik, J., Geisler, W.S., 2005. Optimal eye movement strategies in visual search. Nature 434, 387–391. doi:10.1038/nature03390

Neumann, W.J., Degen, K., Schneider, G.H., Brücke, C., Huebl, J., Brown, P., Kühn, A.A., 2016. Subthalamic synchronized oscillatory activity correlates with motor impairment in patients with Parkinson's disease. Mov. Disord. 31, 1748–1751. doi:10.1002/mds.26759

Nguyen Chi, V., Muller, C., Wolfenstetter, T., Yanovsky, Y., Draguhn, A., Tort, A.B.L., Branka k, J., 2016. Hippocampal Respiration-Driven Rhythm Distinct from Theta Oscillations in Awake Mice. J. Neurosci. 36, 162–177. doi:10.1523/JNEUROSCI.2848-15.2016

Nunez, P.L., Srinivasan, R., Westdorp, A.F., Wijesinghe, R.S., Tucker, D.M., Silberstein, R.B., Cadusch, P.J., 1997. EEG coherency. I: Statistics, reference electrode, volume conduction, Laplacians, cortical imaging, and interpretation at multiple scales. Electroencephalogr. Clin. Neurophysiol. 103, 499–515.

Obeso, J. a, Lanciego, J.L., 2011. Past, present, and future of the pathophysiological model of the Basal Ganglia. Front. Neuroanat. 5, 39. doi:10.3389/fnana.2011.00039

Pal, D., Silverstein, B.H., Lee, H., Mashour, G.A., 2016. Neural Correlates of

Wakefulness, Sleep, and General Anesthesia. Anesthesiology 125, 929–942. doi:10.1097/ALN.0000000000001342

Paxinos, G., Watson, C., 1982. The Rat Brain in Stereotaxic Coordinates.

Pringsheim, T., Jette, N., Frolkis, A., Steeves, T.D.L., 2014. The prevalence of Parkinson's disease: a systematic review and meta-analysis. Mov. Disord. 29, 1583–90. doi:10.1002/mds.25945

Rodrigues, L.S., Targa, A.D.S., Noseda, A.C.D., Aurich, M.F., Da Cunha, C., Lima, M.M.S., 2014. Olfactory impairment in the rotenone model of Parkinsonâ€™s disease is associated with bulbar dopaminergic D2 activity after REM sleep deprivation. Front. Cell. Neurosci. 8, 383. doi:10.3389/fncel.2014.00383

Rodriguez, E., George, N., Lachaux, J.P., Martinerie, J., Renault, B., Varela, F.J., 1999. Perception's shadow: long-distance synchronization of human brain activity. Nature 397, 430–3. doi:10.1038/17120

Rojas-Líbano, D., Frederick, D.E., Egaña, J.I., Kay, L.M., 2014. The olfactory bulb theta rhythm follows all frequencies of diaphragmatic respiration in the freely behaving rat. Front. Behav. Neurosci. 8, 214. doi:10.3389/fnbeh.2014.00214

Rojas-Líbano, D., Wimmer del Solar, J., Aguilar-Rivera, M., Montefusco-Siegmund, R., Maldonado, P.E., 2018. Local cortical activity of distant brain areas can phase-lock to the olfactory bulb's respiratory rhythm in the freely behaving rat. J. Neurophysiol. 120, 960–972. doi:10.1152/jn.00088.2018

Salinas, E., Sejnowski, T.J., 2001. Correlated neuronal activity and the flow of neural information. Nat. Rev. Neurosci. 2, 539–550. doi:10.1038/35086012

Schroeder, C.E., Wilson, D.A., Radman, T., Scharfman, H., Lakatos, P., 2010. Dynamics of Active Sensing and perceptual selection. Curr. Opin. Neurobiol. 20, 172–176. doi:10.1016/j.conb.2010.02.010

Sharott, A., Gulberti, A., Zittel, S., Tudor Jones, A.A., Fickel, U., Munchau, A., Koppen, J.A., Gerloff, C., Westphal, M., Buhmann, C., Hamel, W., Engel, A.K., Moll, C.K.E., 2014. Activity Parameters of Subthalamic Nucleus

Neurons Selectively Predict Motor Symptom Severity in Parkinson's Disease. J. Neurosci. 34, 6273–6285. doi:10.1523/jneurosci.1803-13.2014

Sharott, A., Magill, P.J., Harnack, D., Kupsch, A., Meissner, W., Brown, P., 2005. Dopamine depletion increases the power and coherence of β-oscillations in the cerebral cortex and subthalamic nucleus of the awake rat. Eur. J. Neurosci. 21, 1413–1422. doi:10.1111/j.1460-9568.2005.03973.x

Singer, W., 1999. Neuronal Synchrony : A Versatile Code for the Definition of Relations ? Most of our knowledge about the functional organization. Neuron 24, 49–65. doi:https://doi.org/10.1016/S0896-6273(00)80821-1

Tort, A.B.L., Brankačk, J., Draguhn, A., 2018. Respiration-Entrained Brain Rhythms Are Global but Often Overlooked. Trends Neurosci. 41, 186–197. doi:10.1016/j.tins.2018.01.007

Tort, A.B.L., Komorowski, R., Eichenbaum, H., Kopell, N., 2010. Measuring Phase-Amplitude Coupling Between Neuronal Oscillations of Different Frequencies. J. Neurophysiol. 104, 1195–1210. doi:10.1152/jn.00106.2010

Torterolo, P., Monti, J.M., Pandi-Perumal, S., 2016. Neuroanatomy and Neuropharmacology of Sleep and Wakefulness, in: Synposis of Sleep Medicine. Apple Academic Press, pp. 1–22.

Torterolo, P., Vanini, G., 2010. [New concepts in relation to generating and maintaining arousal]. Rev. Neurol. 50, 747–58. doi:https://doi.org/10.33588/rn.5012.2009681

Ungerstedt, U., Arbuthnott, G.W., 1970. Quantitative recording of rotational behavior in rats after 6-hydroxy-dopamine lesions of the nigrostriatal dopamine system. Brain Res. 24, 485–493. doi:10.1016/0006-8993(70)90187-3

Urbanavicius, J., Ferreira, M., Costa, G., Abin-Carriquiry, J. a., Wonnacott, S., Dajas, F., 2007. Nicotine induces tyrosine hydroxylase plasticity in the neurodegenerating striatum. J. Neurochem. 102, 723–730. doi:10.1111/j.1471-4159.2007.04560.x

Valle-Leija, P., Drucker-Colín, R., 2014. Unilateral olfactory deficit in a hemiparkinson's disease mouse model. Neuroreport 25, 948–953. doi:10.1097/WNR.0000000000000218

Varela, F., Lachaux, J.P., Rodriguez, E., Martinerie, J., 2001. The brainweb: phase synchronization and large-scale integration. Nat. Rev. Neurosci. 2, 229–239. doi:10.1038/35067550

Verhagen, J. V, Wesson, D.W., Netoff, T.I., White, J.A., Wachowiak, M., 2007. Sniffing controls an adaptive filter of sensory input to the olfactory bulb. Nat. Neurosci. 10, 631–9. doi:10.1038/nn1892

Voss, U., Holzmann, R., Tuin, I., Hobson, J.A., 2009. Lucid dreaming: a state of consciousness with features of both waking and non-lucid dreaming. Sleep 32, 1191–200. doi:10.1093/sleep/32.9.1191

Weinberger, M., Mahant, N., Hutchison, W.D., Lozano, A.M., Moro, E., Hodaie, M., Lang, A.E., Dostrovsky, J.O., 2006. Beta Oscillatory Activity in the Subthalamic Nucleus and Its Relation to Dopaminergic Response in Parkinson's Disease. J. Neurophysiol. 96, 3248–3256. doi:10.1152/jn.00697.2006

West, T., Farmer, S., Berthouze, L., Jha, A., Beudel, M., Foltynie, T., Limousin, P., Zrinzo, L., Brown, P., Litvak, V., 2016. The Parkinsonian Subthalamic Network: Measures of Power, Linear, and Non-linear Synchronization and their Relationship to L-DOPA Treatment and OFF State Motor Severity. Front. Hum. Neurosci. 10. doi:10.3389/fnhum.2016.00517

West, T.O., Berthouze, L., Halliday, D.M., Litvak, V., Sharott, A., Magill, P.J., Farmer, S.F., 2018. Propagation of Beta/Gamma Rhythms in the Cortico-Basal Ganglia Circuits of the Parkinsonian Rat. J. Neurophysiol. 1608–1628. doi:10.1152/jn.00629.2017

Whitmer, D., de Solages, C., Hill, B., Yu, H., Henderson, J.M., Bronte-Stewart, H., 2012. High frequency deep brain stimulation attenuates subthalamic and cortical rhythms in Parkinson's disease. Front. Hum. Neurosci. 6, 1–18. doi:10.3389/fnhum.2012.00155

Williams, D., 2002. Dopamine-dependent changes in the functional connectivity

between basal ganglia and cerebral cortex in humans. Brain 125, 1558–1569. doi:10.1093/brain/awf156

Williams, D., Kühn, A., Kupsch, A., Tijssen, M., Van Bruggen, G., Speelman, H., Hotton, G., Yarrow, K., Brown, P., 2003. Behavioural cues are associated with modulations of synchronous oscillations in the human subthalamic nucleus. Brain 126, 1975–1985. doi:10.1093/brain/awg194

Xiong, A., Wesson, D.W., 2016. Illustrated review of the ventral striatum's olfactory tubercle. Chem. Senses 41, 549–555. doi:10.1093/chemse/bjw069

Yanovsky, Y., Ciatipis, M., Draguhn, A., Tort, A.B.L., Branka k, J., 2014. Slow Oscillations in the Mouse Hippocampus Entrained by Nasal Respiration. J. Neurosci. 34, 5949–5964. doi:10.1523/JNEUROSCI.5287-13.2014

Zhang, W., Sun, C., Shao, Y., Zhou, Z., Hou, Y., Li, A., 2019. Partial depletion of dopaminergic neurons in the substantia nigra impairs olfaction and alters neural activity in the olfactory bulb. Sci. Rep. 9, 1–13. doi:10.1038/s41598-018-36538-2

Zhong, W., Ciatipis, M., Wolfenstetter, T., Jessberger, J., Müller, C., Ponsel, S., Yanovsky, Y., Brankačk, J., Tort, A.B.L., Draguhn, A., 2017. Selective entrainment of gamma subbands by different slow network oscillations. Proc. Natl. Acad. Sci. U. S. A. 114, 4519–4524. doi:10.1073/pnas.1617249114

Figure 1

Click here to download high resolution image

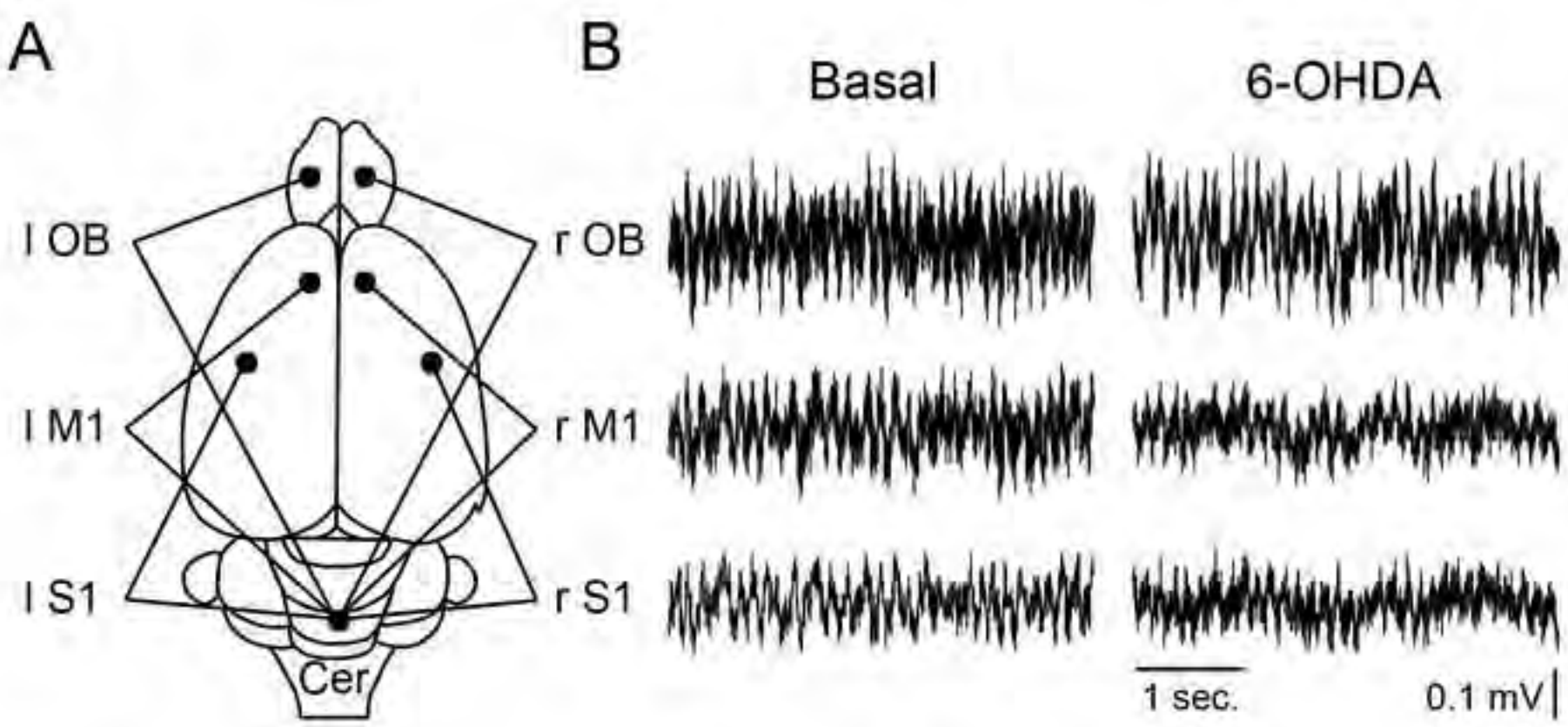

Figure 2

Click here to download high resolution image

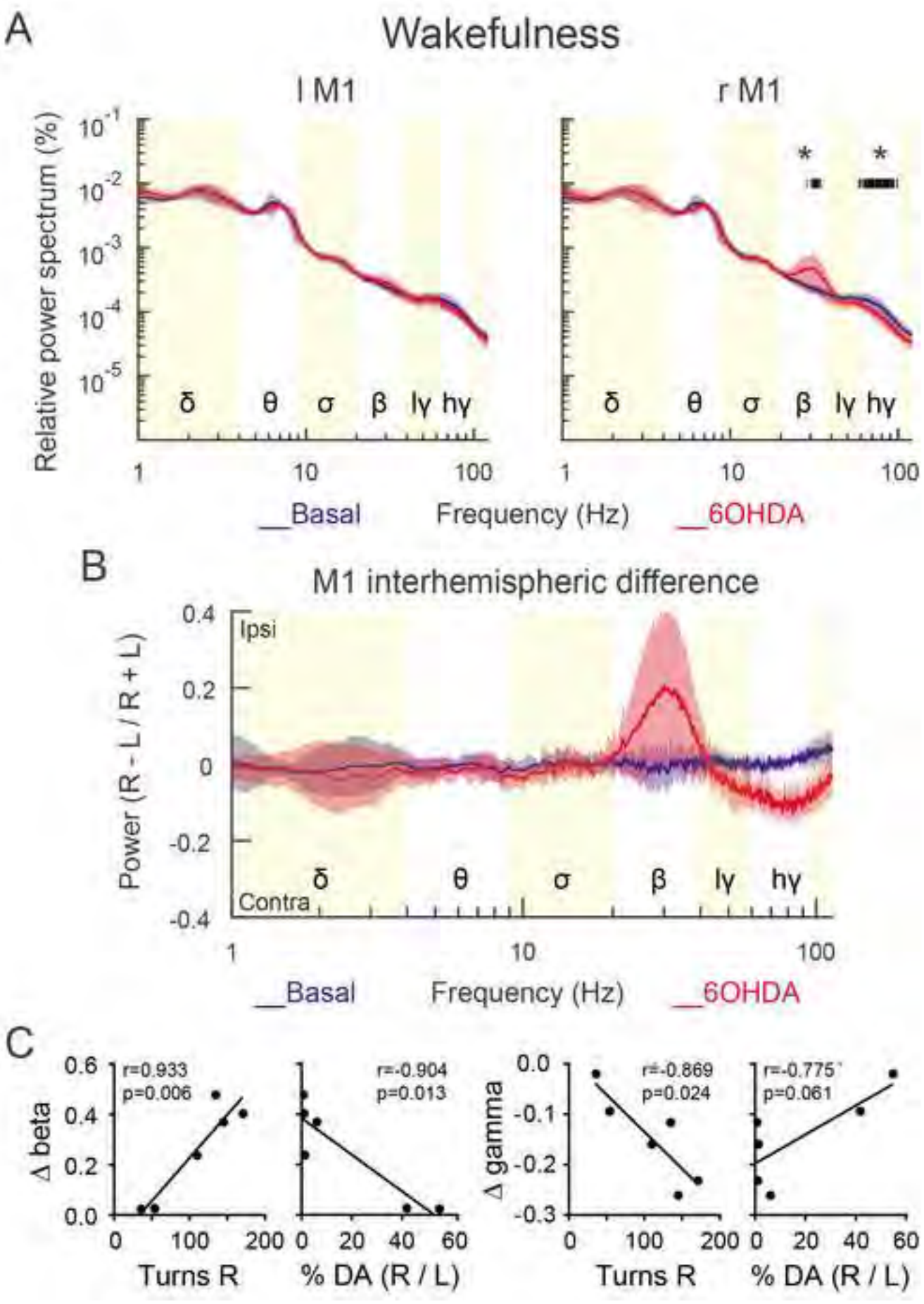

Figure 3

Click here to download high resolution image

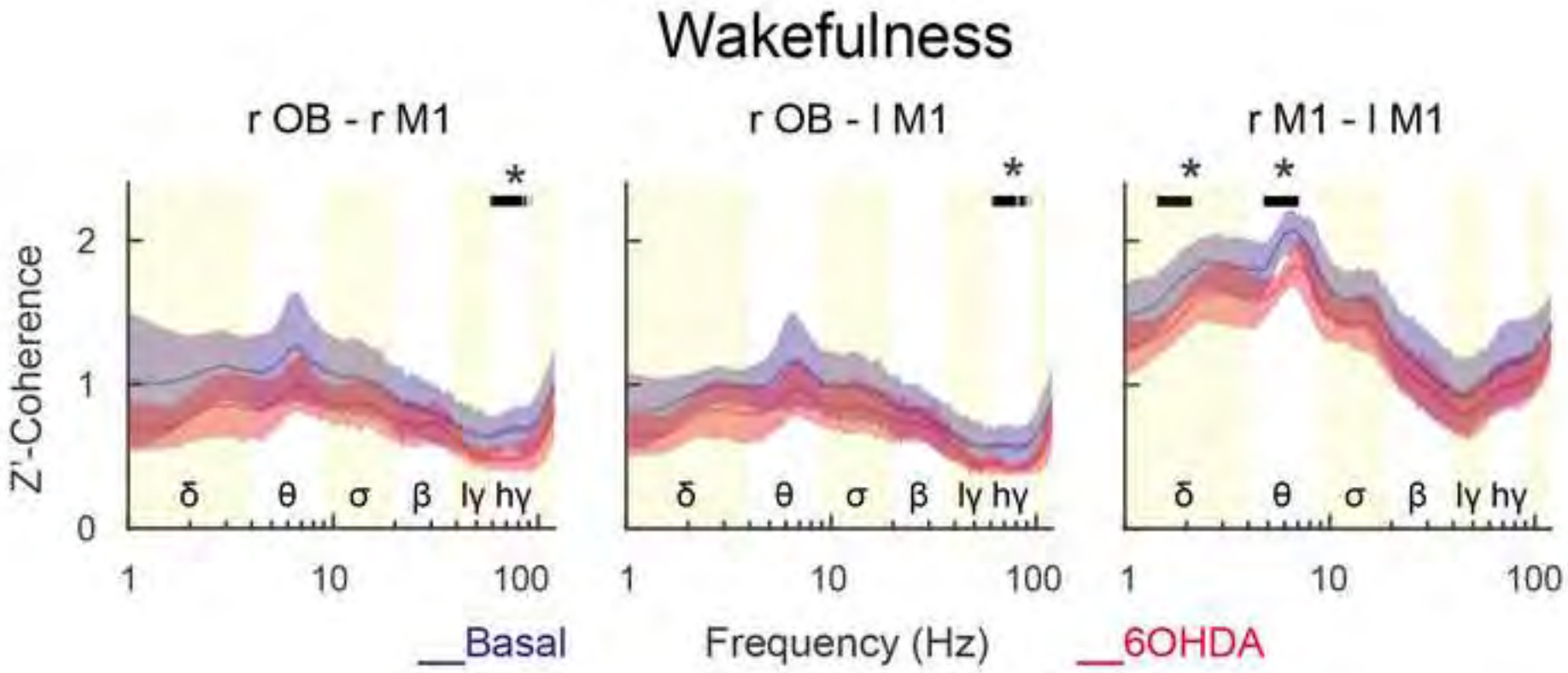

Figure 4

Click here to download high resolution image

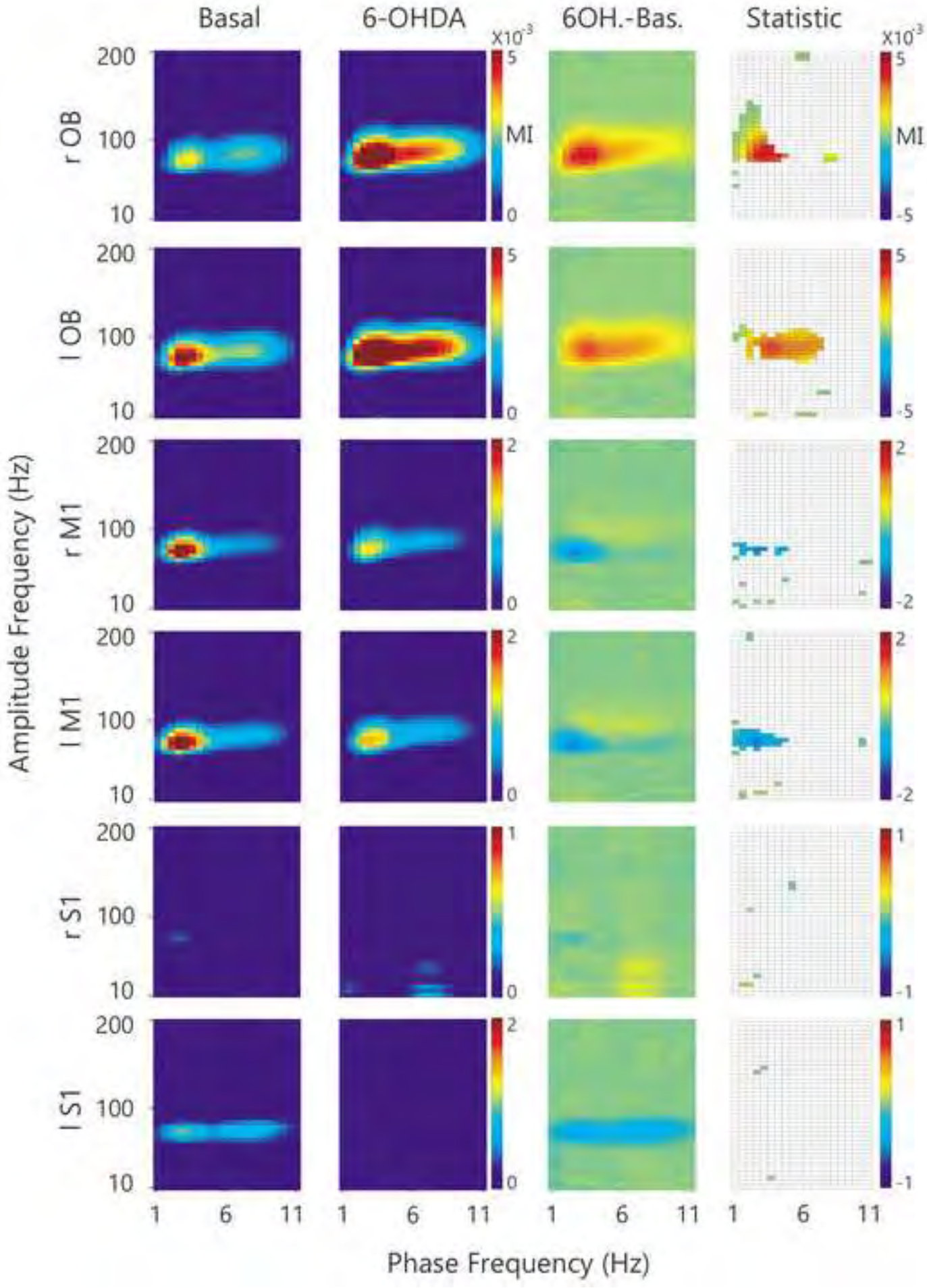

Tables

Table 1. Motor lateralization and levels of DA and its metabolites

	Turns		DA		DOPAC		HVA	
Rats	right	left	right (ng/gr)	left (ng/gr)	right (ng/gr)	left (ng/gr)	right (ng/gr)	left (ng/gr)
1	171	0	106	10,330	44	1,363	200	987
2	36	0	4,987	9,082	761	1,195	502	1,028
3	110	0	106	8,143	31	1,358	93	682
4	54	0	4,425	10,570	1135	3,500	842	1,564
5	145	0	714	11,686	51	1,546	232	1,191
6	135	0	79	10,200	33	1,457	154	708
mean	108.5	0	1,736.1	10,001.8	342.5	1,736.5	337.1	1,026.6
SD	48.5	0	2,319.6	1,233.4	483.7	871.8	284.6	327.9
p	< 0.0001		0.0007		0.0026		0.0002	

Table 2. Levels of 5-HT and its metabolite 5-HIAA

	5-HT		5-HIAA	
Rats	right (ng/gr)	left (ng/gr)	right (ng/gr)	left (ng/gr)
1	652	516	580	413
2	528	460	410	440
3	435	501	483	446
4	442	352	492	417
5	488	625	542	463
6	485	465	539	472
mean	505	486.5	507.6	441.8
SD	79.6	88.9	59.6	23.7
p	0.677		0.092	

Electronic Supplementary Material (online publication only)

Click here to download Electronic Supplementary Material (online publication only): Supplementary Material Cavelli el al.docx

5. Conclusiones Generales

La bibliografía referente a la temática, así como los resultados obtenidos en esta Tesis dejan en evidencia que durante la vigilia grandes poblaciones neuronales tiendes a coordinar su actividad eléctrica a alta frecuencia. Esta sincronización neuronal genera la sumatoria de los potenciales extracelulares que se registran en el ECoG (actividad gamma > 30 Hz). Dicha sincronía se puede observar en cada área registrada, así como entre áreas distantes del cerebro. Esta tiende a variar durante los diferentes estados comportamentales, así como durante las diferentes funciones cognitivas. Cuando nos dormimos, esta sincronía tiende a disminuir a medida que nuestro sueño se hace más profundo. Durante el sueño lento las poblaciones neuronales tienden a acoplarse en regímenes de sincronización mucho más lentos. Cuando entramos a la etapa de sueño REM nuestro cerebro vuelve a activarse generando patrones electrográficos similares a la vigilia. En esta etapa, donde ocurren preferentemente las ensoñaciones, la actividad gamma registrada en cada área cortical aumenta a valores similares a los de la vigilia; sin embargo, la capacidad de acople entre áreas alejadas del cerebro disminuye. Durante la psicosis como durante la actividad onírica del sueño REM existe una clara incapacidad de entender que las experiencias que estamos experimentando no son reales o, mejor dicho, no son experiencias que se formen a partir de la interpretación e integración de la información intero y exteroceptiva (por lo menos de la forma que ocurre durante la vigilia). Interesantemente, tanto en el sueño REM, la psicosis y los modelos animales de hipofunción aguda de los receptores NMDA, existe una pérdida de la capacidad de acoplar la actividad gamma entre áreas distantes del cerebro.

Recientemente el desarrollo de herramientas analíticas de acoplamiento entre frecuencia ha comenzado a revelar que la actividad de alta frecuencia se encuentra ampliamente regulada por diversos ritmos de nuestro cuerpo, que pueden expresarse a nivel cerebral como potenciales electrográficos lentos. Algunos ejemplos son los movimientos rítmicos de los ojos o los potenciales respiratorios dependientes del pasaje del aire por las fosas nasales. Como hemos mostrado, este acoplamiento entre frecuencias es capaz de acoplar la sincronía entre áreas alejadas del cerebro durante la vigilia, lo que sugiere que estos fenómenos podrían ser parte de procesos de unificación de la información sensorial distribuida. Por otra parte, estos potenciales lentos y la co-modulación con la actividad de alta frecuencia, deja en evidencia que lo que normalmente llamamos actividad gamma o actividad de alta frecuencia podría ser el resultado de la sumatoria de la actividad de múltiples sub-bandas de actividad. Cada una de estas, estaría acoplada a una fase partícula de un ritmo característico, o inclusive cada sub-banda podría acoplarse en distintas fases de una misma onda lenta. Se destaca que cuando nos dormimos, estos

patrones de acople entre frecuencias desaparecen, o se alteran dramáticamente.

La pérdida de actividad gamma y su acople durante el sueño sugiere que estas capacidades de sincronización y modulación inter-cortical dependen en cierta medida de los sistemas de neuro-modulación que generan, mantienen y regulan la vigilia. Las manipulaciones experimentales de los sistemas activadores o sus alteraciones durante diversas patologías han demostrado cursar con múltiples alteraciones en la capacidad de generar, modular y mantener la actividad gamma cortical. Por esto pensamos que varias alteraciones cognitivas que se observan en diversos trastornos psiquiátricos o neurológicos (por ejemplo, psicosis o Parkinson), podrían tener como base la imposibilidad de sincronizar y acoplar normalmente la actividad gamma cerebral durante la vigilia.

5. Bibliografía

Adrian, E.D., 1950. The electrical activity of the mammalian olfactory bulb. Electroencephalogr. Clin. Neurophysiol. 2, 377–388. doi:10.1016/0013-4694(50)90075-7

Adrian, E.D., 1942. Olfactory reactions in the brain of the hedgehog. J. Physiol. 100, 459–73. doi:https://doi.org/10.1113/jphysiol.1942.sp003955

Aurich, M.F., Rodrigues, L.S., Targa, A.D.S., Noseda, A.C.D., Cunha, F.D.W., Lima, M.M.S., 2017. Olfactory impairment is related to REM sleep deprivation in rotenone model of Parkinson's disease. Sleep Sci. 10, 47–54. doi:10.5935/1984-0063.20170008

Benson, K.L., Zarcone, V.P., 1985. Testing the REM sleep phasic event intrusion hypothesis of schizophrenia. Psychiatry Res. 15, 163–73.

Biskamp, J., Bartos, M., Sauer, J.-F., 2017. Organization of prefrontal network activity by respiration-related oscillations. Sci. Rep. 7, 45508. doi:10.1038/srep45508

Bouyer, J.J., Montaron, M.F., Rougeul, A., 1981. Fast fronto-parietal rhythms during combined focused attentive behaviour and immobility in cat: cortical and thalamic localizations. Electroencephalogr. Clin. Neurophysiol. 51, 244–52.

Braak, H., Rub, U., Gai, W.P., Del Tredici, K., 2003. Idiopathic Parkinson's disease: possible routes by which vulnerable neuronal types may be subject to neuroinvasion by an unknown pathogen. J. Neural Transm. 110, 517–536. doi:10.1007/s00702-002-0808-2

Braun, A.R., Balkin, T.J., Wesenten, N.J., Carson, R.E., Varga, M., Baldwin, P., Selbie, S., Belenky, G., Herscovitch, P., 1997. Regional cerebral blood flow throughout the sleep-wake cycle. An H2(15)O PET study. Brain 120 Pt 7, 1173–97.

Bressler, S.L., Coppola, R., Nakamura, R., 1993. Episodic multiregional cortical coherence at multiple frequencies during visual task performance. Nature 366, 153–6. doi:10.1038/366153a0

Buhl, D.L., Harris, K.D., Hormuzdi, S.G., Monyer, H., Buzsáki, G., 2003. Selective impairment of hippocampal gamma oscillations in connexin-36 knock-out mouse in vivo. J. Neurosci. 23, 1013–1018.

Bullock, T.H., Mcclune, M.C., Enright, J.T., 2003. Are the electroencephalograms mainly rhythmic? Assessment of periodicity in wide-band time series. Neuroscience 121, 233–52.

Buzsáki, G., 2006. Rhythms of the Brain. Oxford University Press, Inc., Oxford New York.

Buzsáki, G., Schomburg, E.W., 2015. What does gamma coherence tell us about inter-regional neural communication? Nat. Neurosci. 18, 484–489. doi:10.1038/nn.3952

Buzsáki, G., Wang, X.-J., 2012. Mechanisms of Gamma Oscillations. Annu. Rev. Neurosci. 35, 203–225.

Caixeta, F. V., Cornélio, A.M., Scheffer-Teixeira, R., Ribeiro, S., Tort, A.B.L., 2013. Ketamine alters oscillatory coupling in the hippocampus. Sci. Rep. 3, 2348. doi:10.1038/srep02348

Canolty, R.T., Edwards, E., Dalal, S.S., Soltani, M., Nagarajan, S.S., Berger, M.S., Barbaro, N.M., Knight, R.T., Kirsch, H.E., Berger, M.S., Barbaro, N.M., Knight, R.T., 2009. High Gamma Power is Phase-Locked to Theta Oscillations in Human Neocortex. Science 313, 1626–1628. doi:10.1126/science.1128115.High

Castro-Zaballa, S., Cavelli, M., González, J., Monti, J., Falconi, A., Torterolo, P., 2019. EEG dissociation induced by muscarinic receptor antagonists: Coherent 40 Hz oscillations in a background of slow waves and spindles. Behav. Brain Res. 359, 28–37. doi:10.1016/j.bbr.2018.10.016

Castro-Zaballa, S., Cavelli, M., Vollono, P., Chase, M.H., Falconi, A., Torterolo, P., 2014. Inter-hemispheric coherence of neocortical gamma oscillations during sleep and wakefulness. Neurosci. Lett. 578, 197–202. doi:10.1016/j.neulet.2014.06.044

Castro-Zaballa, S., Cavelli, M.L., Gonzalez, J., Nardi, A.E., Machado, S., Scorza, C., Torterolo, P., 2018. EEG 40 Hz Coherence Decreases in REM Sleep and Ketamine Model of Psychosis. Front. psychiatry 9, 766. doi:10.3389/fpsyt.2018.00766

Castro-Zaballa, S., Falconi, A., Chase, M.H., Torterolo, P., 2013. Coherent neocortical 40-Hz oscillations are not present during REM sleep. Eur. J. Neurosci. 37, 1330–9. doi:10.1111/ejn.12143

Castro, S., Cavelli, M., Torterolo, P., Falconi, A., Rava, M., Criado, A., Chiappella, L., Scavone, C., Ardanaz, J.L., Gonzalez, G., 2014. Análisis cuantitativo de la actividad eléctrica cortical en recién nacidos: estudio de la coherencia del EEG para la banda gamma de frecuencias, in: Congreso Internacional de Neuropediatría. Colonia.

Cavelli, M., 2015. Potencia y coherencia de la banda gamma (30-100 Hz) de frecuencias del EEG durante el ciclo sueño y vigilia. Pedeciba, master's thesis. FCien, Montevideo.

Cavelli, M., Castro-Zaballa, S., Gonzalez, J., Rojas-Líbano, D., Rubido, N., Velásquez, N., Torterolo, P., 2018. Nasal respiration entrains neocortical long-range gamma coherence during wakefulness. bioRxiv 430579. doi:10.1101/430579

Cavelli, M., Castro-Zaballa, S., Mondino, A., Gonzalez, J., Falconi, A., Torterolo, P., 2017a. Absence of EEG gamma coherence in a local activated cortical state: a conserved trait of REM sleep. Transl Brain Rhythm. 2, 1–13. doi:10.15761/TBR.1000115

Cavelli, M., Castro, S., Schwarzkopf, N., Chase, M.H., Falconi, A., Torterolo, P., 2015. Coherent neocortical gamma oscillations decrease during REM sleep in the rat. Behav. Brain Res. 281, 318–25. doi:10.1016/j.bbr.2014.12.050

Cavelli, M., Falconi, A., Igarzabal, H., Schwarzkopf, N., Torterolo, P., 2014. XV Jornadas de la SUB, 2014, in: SUB (Ed.), Máximo Desacoplamiento de La Actividad Gamma (30-100 Hz) Del EEG Durante El Sueño REM. Un Rasgo Conservado Del Sueño REM En Los Mamíferos. SUB, Piriapolis.

Cavelli, M., Prunell, G., Costa, G., Velásquez, N., Gonzalez, J., Castro-Zaballa, S., Lima, M.M.S., Torterolo, P., 2019. Electrocortical high frequency activity and respiratory entrainment in 6-hydroxydopamine model of Parkinson's disease. Brain Res. in Review.

Cavelli, M., Rojas-Líbano, D., Schwarzkopf, N., Castro-Zaballa, S., Gonzalez, J., Mondino, A., Santana, N., Benedetto, L., Falconi, A., Torterolo, P., 2017b. Power and coherence of cortical high-frequency oscillations during wakefulness and sleep. Eur. J. Neurosci. 48, 2728–2737. doi:10.1111/ejn.13718

Cavelli, M., Zoccoli, G., Silvani, A., Castro-Zaballa, S., Gonzalez, J., Mondino, A., Santana, N., Falconi, A., Torterolo, P., 2017c. Acoplamiento local y desacoplamiento de largo rango caracterizan a la actividad gamma (30-100 Hz) cortical durante el sueño REM, in: XVI Jornadas de La Sociedad de Neurociencias Del Uruguay Congreso Nacional de Biociencias 2017. Montevideo.

Chase, M.H., Soja, P.J., Morales, F.R., 1989. Evidence that glycine mediates

the postsynaptic potentials that inhibit lumbar motoneurons during the atonia of active sleep. J. Neurosci. 9, 743–51.

Corsi-Cabrera, M., Miró, E., del-Río-Portilla, Y., Pérez-Garci, E., Villanueva, Y., Guevara, M.A., 2003. Rapid eye movement sleep dreaming is characterized by uncoupled EEG activity between frontal and perceptual cortical regions. Brain Cogn. 51, 337–45.

Costa, G., Abin-Carriquiry, J. a., Dajas, F., 2001. Nicotine prevents striatal dopamine loss produced by 6-hydroxydopamine lesion in the substantia nigra. Brain Res. 888, 336–342. doi:10.1016/S0006-8993(00)03087-0

Doty, R.L., 2012. Olfactory dysfunction in Parkinson disease. Nat. Rev. Neurol. 8, 329–39. doi:10.1038/nrneurol.2012.80

Edelman, G.M., Tononi, G., 2000. A universe of consciousness., Basic Book. ed. New York.

Fontanini, A., Bower, J.M., 2006. Slow-waves in the olfactory system: an olfactory perspective on cortical rhythms. Trends Neurosci. 29, 429–437.

Fontanini, A., Bower, J.M., 2005. Variable coupling between olfactory system activity and respiration in ketamine/xylazine anesthetized rats. J. Neurophysiol. 93, 3573–3581. doi:10.1152/jn.01320.2004

Fries, P., 2015. Rhythms for Cognition: Communication through Coherence. Neuron 88, 220–235. doi:10.1016/j.neuron.2015.09.034

Fries, P., 2005. A mechanism for cognitive dynamics: neuronal communication through neuronal coherence. Trends Cogn. Sci. 9, 474–480. doi:10.1016/j.tics.2005.08.011

Garcia-rill, E., 2017. Bottom-up gamma and stages of waking. Med. Hypotheses 104, 58–62. doi:10.1016/j.mehy.2017.05.023

Garcia-Rill, E., Kezunovic, N., D'Onofrio, S., Luster, B., Hyde, J., Bisagno, V., Urbano, F.J., 2014. Gamma band activity in the RAS-intracellular mechanisms. Exp. brain Res. 232, 1509–22. doi:10.1007/s00221-013-3794-8

Gottesmann, C., 2006. The dreaming sleep stage: a new neurobiological model of schizophrenia? Neuroscience 140, 1105–15.

Gottesmann, C., Gottesman, I., 2007. The neurobiological characteristics of rapid eye movement (REM) sleep are candidate endophenotypes of depression, schizophrenia, mental retardation and dementia. Prog. Neurobiol. 81, 237–50.

Gray, C.M., König, P., Engel, A.K., Singer, W., 1989. Gray_Nature_1989.pdf. Nature.

Gray, C.M., Singer, W., 1989. Stimulus-specific neuronal oscillations in

orientation columns of cat visual cortex. Proc. Natl. Acad. Sci. U. S. A. 86, 1698–1702.

Grosmaitre, X., Santarelli, L.C., Tan, J., Luo, M., Ma, M., 2007. Dual functions of mammalian olfactory sensory neurons as odor detectors and mechanical sensors. Nat. Neurosci. 10, 348–354. doi:10.1038/nn1856

Grossberg, S., 1976. Adaptive pattern classification and universal recoding: II. Feedback, expectation, olfaction, illusions. Biol. Cybern. 23, 187–202.

Härle, M., Rockstroh, B.S., Keil, A., Wienbruch, C., Elbert, T.R., 2004. Mapping the brain's orchestration during speech comprehension: task-specific facilitation of regional synchrony in neural networks. BMC Neurosci. 5, 40.

Herrero, J.L., Khuvis, S., Yeagle, E., Cerf, M., Mehta, A.D., 2018. Breathing above the brain stem: volitional control and attentional modulation in humans. J. Neurophysiol. 119, 145–159. doi:10.1152/jn.00551.2017

Hirsch, L., Jette, N., Frolkis, A., Steeves, T., Pringsheim, T., 2016. The Incidence of Parkinson's Disease: A Systematic Review and Meta-Analysis. Neuroepidemiology 46, 292–300. doi:10.1159/000445751

Hobson, J.A., 2009. REM sleep and dreaming: towards a theory of protoconsciousness. Nat. Rev. Neurosci. 10, 803–813.

Hobson, J.A., 1997. Dreaming as delirium: a mental status analysis of our nightly madness. Semin. Neurol. 17, 121–8. doi:10.1055/s-2008-1040921

Höglinger, G.U., Alvarez-Fischer, D., Arias-Carrión, O., Djufri, M., Windolph, A., Keber, U., Borta, A., Ries, V., Schwarting, R.K.W., Scheller, D., Oertel, W.H., 2015. A new dopaminergic nigro-olfactory projection. Acta Neuropathol. 130, 333–348. doi:10.1007/s00401-015-1451-y

Huisman, E., Uylings, H.B.M., Hoogland, P. V, 2004. A 100% increase of dopaminergic cells in the olfactory bulb may explain hyposmia in Parkinson's disease. Mov. Disord. 19, 687–92. doi:10.1002/mds.10713

Ito, J., Roy, S., Liu, Y., Cao, Y., Fletcher, M., Lu, L., Boughter, J.D., Grün, S., Heck, D.H., 2014. Whisker barrel cortex delta oscillations and gamma power in the awake mouse are linked to respiration. Nat. Commun. 5, 3572. doi:10.1038/ncomms4572

Iwata, R., Kiyonari, H., Imai, T., 2017. Mechanosensory-Based Phase Coding of Odor Identity in the Olfactory Bulb. Neuron 96, 1139-1152.e7. doi:10.1016/j.neuron.2017.11.008

Jackson, J., Goutagny, R., Williams, S., 2011. Fast and slow γ rhythms are intrinsically and independently generated in the subiculum. J. Neurosci. 31, 12104–17. doi:10.1523/JNEUROSCI.1370-11.2011

Jasper, H.H., Andrews, H.L., 1938. Brain potentials and voluntary muscle activity in man. J Neurophysiol 1, 87–100.

Javitt, D.C., Zukin, S.R., 1991. Recent advances in the phencyclidine model of schizophrenia. Am. J. Psychiatry 148, 1301–8.

John, E.R., 2002. The neurophysics of consciousness. Brain Res. Rev. 39, 1–28. doi:https://doi.org/10.1016/S0165-0173(02)00142-X

Joliot, M., Ribary, U., Llinás, R., 1994. Human oscillatory brain activity near 40 Hz coexists with cognitive temporal binding. Proc. Natl. Acad. Sci. U. S. A. 91, 11748–51. doi:https://doi.org/10.1073/pnas.91.24.11748

Knudsen, K., Flensborg Damholdt, M., Mouridsen, K., Borghammer, P., 2015. Olfactory function in Parkinson's Disease - effects of training. Acta Neurol. Scand. 132, 395–400. doi:10.1111/ane.12406

Lang, A.E., Lozano, A.M., 1998. Parkinson's Disease. N. Engl. J. Med. 339, 1044–1053. doi:10.1056/NEJM199810083391506

Lazarewicz, M.T., Ehrlichman, R.S., Maxwell, C.R., Gandal, M.J., Finkel, L.H., Siegel, S.J., 2010. Ketamine modulates theta and gamma oscillations. J. Cogn. Neurosci. 22, 1452–1464.

Llinás, R., Ribary, U., 2006. Consciousness and the Brain. Ann. N. Y. Acad. Sci. 929, 166–175.

Llinás, R., Ribary, U., 1993. Coherent 40-Hz oscillation characterizes dream state in humans. Proc. Natl. Acad. Sci. U. S. A. 90, 2078–81.

Llinás, R., Ribary, U., Contreras, D., Pedroarena, C., 1998. The neuronal basis for consciousness. Philos. Trans. R. Soc. Lond. B. Biol. Sci. 353, 1841–1849. doi:10.1098/rstb.1998.0336

Lockmann, A.L. V., Laplagne, D.A., Leão, R.N., Tort, A.B.L., 2016. A Respiration-Coupled Rhythm in the Rat Hippocampus Independent of Theta and Slow Oscillations. J. Neurosci. 36, 5338–5352. doi:10.1523/JNEUROSCI.3452-15.2016

Luster, B.R., Urbano, F.J., Garcia-rill, E., Garcia-rill, E., 2016. Intracellular mechanisms modulating gamma band activity in the pedunculopontine nucleus (PPN) 4, 1–16. doi:10.14814/phy2.12787

Maloney, K.J., Cape, E.G., Gotman, J., Jones, B.E., 1997. High-frequency gamma electroencephalogram activity in association with sleep-wake states and spontaneous behaviors in the rat. Neuroscience 76, 541–55. doi:https://doi.org/10.1016/S0306-4522(96)00298-9

Manabe, H., Mori, K., 2013. Sniff rhythm-paced fast and slow gamma-oscillations in the olfactory bulb: relation to tufted and mitral cells and behavioral states. J. Neurophysiol. 110, 1593–1599. doi:10.1152/jn.00379.2013

Mashour, G. a, 2006. Integrating the science of consciousness and anesthesia. Anesth. Analg. 103, 975–82. doi:10.1213/01.ane.0000232442.69757.4a

Melloni, L., Molina, C., Pena, M., Torres, D., Singer, W., Rodriguez, E., 2007. Synchronization of neural activity across cortical areas correlates with conscious perception. J. Neurosci. 27, 2858–65. doi:10.1523/JNEUROSCI.4623-06.2007

Milner, P.M., 1974. A model for visual shape recognition. Psychol. Rev. 81, 521–35.

Moghaddam, B., Jackson, M.E., 2003. Glutamatergic animal models of schizophrenia. Ann. N. Y. Acad. Sci. 1003, 131–7.

Mouhape, C., Costa, G., Ferreira, M., Abin-Carriquiry, J.A., Dajas, F., Prunell, G., 2019. Nicotine-Induced Neuroprotection in Rotenone In Vivo and In Vitro Models of Parkinson's Disease: Evidences for the Involvement of the Labile Iron Pool Level as the Underlying Mechanism. Neurotox. Res. 35, 71–82. doi:10.1007/s12640-018-9931-1

Mundiñano, I.-C., Caballero, M.-C., Ordóñez, C., Hernandez, M., DiCaudo, C., Marcilla, I., Erro, M.-E., Tuñon, M.-T., Luquin, M.-R., 2011. Increased dopaminergic cells and protein aggregates in the olfactory bulb of patients with neurodegenerative disorders. Acta Neuropathol. 122, 61–74. doi:10.1007/s00401-011-0830-2

Nguyen Chi, V., Muller, C., Wolfenstetter, T., Yanovsky, Y., Draguhn, A., Tort, A.B.L., Branka k, J., 2016. Hippocampal Respiration-Driven Rhythm Distinct from Theta Oscillations in Awake Mice. J. Neurosci. 36, 162–177. doi:10.1523/JNEUROSCI.2848-15.2016

Nir, Y., Tononi, G., 2010. Dreaming and the brain: from phenomenology to neurophysiology. Trends Cogn. Sci. 14, 88–100.

Pal, D., Hambrecht-Wiedbusch, V.S., Silverstein, B.H., Mashour, G.A., 2015. Electroencephalographic coherence and cortical acetylcholine during ketamine-induced unconsciousness. Br. J. Anaesth. aev095-.

Pal, D., Silverstein, B.H., Lee, H., Mashour, G.A., 2016. Neural Correlates of Wakefulness, Sleep, and General Anesthesia. Anesthesiology 125, 929–942. doi:10.1097/ALN.0000000000001342

Pringsheim, T., Jette, N., Frolkis, A., Steeves, T.D.L., 2014. The prevalence of Parkinson's disease: a systematic review and meta-analysis. Mov. Disord. 29, 1583–90. doi:10.1002/mds.25945

Rechtschaffen, A., 1978. The single-mindedness and isolation of dreams. Sleep 1, 97–109.

Rieder, M.K., Rahm, B., Williams, J.D., Kaiser, J., 2011. Human γ-band activity and behavior. Int. J. Psychophysiol. 79, 39–48.

Rodrigues, L.S., Targa, A.D.S., Noseda, A.C.D., Aurich, M.F., Da Cunha, C., Lima, M.M.S., 2014. Olfactory impairment in the rotenone model of Parkinsonâ€™s disease is associated with bulbar dopaminergic D2 activity

after REM sleep deprivation. Front. Cell. Neurosci. 8, 383. doi:10.3389/fncel.2014.00383

Rodriguez, E., George, N., Lachaux, J.P., Martinerie, J., Renault, B., Varela, F.J., 1999. Perception's shadow: long-distance synchronization of human brain activity. Nature 397, 430–3. doi:10.1038/17120

Rojas-Líbano, D., Frederick, D.E., Egaña, J.I., Kay, L.M., 2014. The olfactory bulb theta rhythm follows all frequencies of diaphragmatic respiration in the freely behaving rat. Front. Behav. Neurosci. 8, 214. doi:10.3389/fnbeh.2014.00214

Rojas-Líbano, D., Kay, L.M., 2008. Olfactory system gamma oscillations: the physiological dissection of a cognitive neural system. Cogn. Neurodyn. 2, 179–94.

Rojas-Líbano, D., Wimmer del Solar, J., Aguilar-Rivera, M., Montefusco-Siegmund, R., Maldonado, P.E., 2018. Local cortical activity of distant brain areas can phase-lock to the olfactory bulb's respiratory rhythm in the freely behaving rat. J. Neurophysiol. 120, 960–972. doi:10.1152/jn.00088.2018

Rung, J.P., Carlsson, A., Rydén Markinhuhta, K., Carlsson, M.L., 2005. (+)-MK-801 induced social withdrawal in rats; a model for negative symptoms of schizophrenia. Prog. Neuropsychopharmacol. Biol. Psychiatry 29, 827–32.

Santana, N., Cavelli, M., Castro-Zaballa, S., Falconi, A., Torterolo, P., 2015. El anestésico uretano suprime la coherencia de la banda gamma (30-100 Hz) del EEG, in: SNU 2015. Montevideo.

Santana, N., Cavelli, M., Castro-Zaballa, S., Torterolo, P., 2017. EFECTO DEL ANESTÉSICO URETANO SOBRE LA ACTIVIDAD DE LA BANDA GAMMA (30-100 Hz) DE FRECUENCIA DEL ELECTROENCEFALOGRAMA, in: XVI Jornadas de La Sociedad de Neurociencias Del Uruguay Congreso Nacional de Biociencias 2017. Montevideo.

Scarone, S., Manzone, M.L., Gambini, O., Kantzas, I., Limosani, I., D'Agostino, A., Hobson, J.A., 2008. The dream as a model for psychosis: an experimental approach using bizarreness as a cognitive marker. Schizophr. Bull. 34, 515–22.

Scheffer-Teixeira, R., Belchior, H., Caixeta, F. V., Souza, B.C., Ribeiro, S., Tort, A.B.L., 2012. Theta Phase Modulates Multiple Layer-Specific Oscillations in the CA1 Region. Cereb. Cortex 22, 2404–2414. doi:10.1093/cercor/bhr319

Scheffzük, C., Kukushka, V.I., Vyssotski, A.L., Draguhn, A., Tort, A.B.L., Brankačk, J., 2011. Selective coupling between theta phase and neocortical fast gamma oscillations during REM-sleep in mice. PLoS One 6, e28489.

Singer, W., 2015. Complexity as Substrate for Neuronal Computations. Acad. Sci. Pontif. City, Vatican 1–10.

Singer, W., 2007. Binding by synchrony. Scholarpedia 2, 1657. doi:10.4249/scholarpedia.1657

Singer, W., 2004. Synchrony, oscillations, and relational codes, in: Chalupa, L. M., Werner, J.S. (Ed.), The Visual Neurosciences. The MIT Press, Cambridge, Massachusetts, pp. 1665–1681.

Singer, W., 1999. Neuronal Synchrony: A Versatile Code Review for the Definition of Relations? temporal relations requires the joint evaluation of re-sponses from more than one neuron, only experiments that permit simultaneous measurements of responses. Neuron 24, 49–65. doi:10.1016/S0896-6273(00)80821-1

Sirota, A., Montgomery, S., Fujisawa, S., Isomura, Y., Zugaro, M., Buzsáki, G., 2008. Entrainment of Neocortical Neurons and Gamma Oscillations by the Hippocampal Theta Rhythm. Neuron 60, 683–697.

Steriade, M., Amzica, F., Contreras, D., 1996. Synchronization of fast (30-40 Hz) spontaneous cortical rhythms during brain activation. J. Neurosci. 16, 392–417.

Tiitinen, H., Sinkkonen, J., Reinikainen, K., Alho, K., Lavikainen, J., Näätänen, R., 1993. Selective attention enhances the auditory 40-Hz transient response in humans. Nature 364, 59–60.

Tort, A.B.L., Brankačk, J., Draguhn, A., 2018. Respiration-Entrained Brain Rhythms Are Global but Often Overlooked. Trends Neurosci. 41, 186–197. doi:10.1016/j.tins.2018.01.007

Tort, A.B.L., Komorowski, R., Eichenbaum, H., Kopell, N., 2010. Measuring Phase-Amplitude Coupling Between Neuronal Oscillations of Different Frequencies. J. Neurophysiol. 104, 1195–1210. doi:10.1152/jn.00106.2010

Tort, A.B.L., Kramer, M. a, Thorn, C., Gibson, D.J., Kubota, Y., Graybiel, A.M., Kopell, N.J., 2008. Dynamic cross-frequency couplings of local field potential oscillations in rat striatum and hippocampus during performance of a T-maze task. Proc. Natl. Acad. Sci. U. S. A. 105, 20517–20522. doi:10.1073/pnas.0810524105

Tort, A.B.L., Scheffer-Teixeira, R., Souza, B.C., Draguhn, A., Brankačk, J., 2013. Theta-associated high-frequency oscillations (110-160Hz) in the hippocampus and neocortex. Prog. Neurobiol. 100, 1–14.

Torterolo, P., Castro-Zaballa, S., Cavelli, M., Chase, M.H., Falconi, A., 2016a. Neocortical 40 Hz oscillations during carbachol-induced rapid eye movement sleep and cataplexy. Eur. J. Neurosci. 43, 580–9. doi:10.1111/ejn.13151

Torterolo, P., Castro-zaballa, S., Cavelli, M., Gonzalez, J., 2019. Arousal and normal conscious cognition, in: Arousal in Neurological and Psychiatric Disease. pp. 1–24.

Torterolo, P., Monti, J.M., Pandi-Perumal, S., 2016b. Neuroanatomy and Neuropharmacology of Sleep and Wakefulness, in: Synposis of Sleep Medicine. Apple Academic Press, pp. 1–22.

Torterolo, P., Vanini, G., 2010. [New concepts in relation to generating and maintaining arousal]. Rev. Neurol. 50, 747–58. doi:https://doi.org/10.33588/rn.5012.2009681

Uhlhaas, P.J., Linden, D.E.J., Singer, W., Haenschel, C., Lindner, M., Maurer, K., Rodriguez, E., 2006. Dysfunctional long-range coordination of neural activity during Gestalt perception in schizophrenia. J. Neurosci. 26, 8168–75.

Uhlhaas, P.J., Pipa, G., Lima, B., Melloni, L., Neuenschwander, S., Nikolic, D., Lin, S., 2009. Neural synchrony in cortical networks : history , concept and current status. Front Integr Neurosci 3, 1–19.

Uhlhaas, P.J., Pipa, G., Neuenschwander, S., Wibral, M., Singer, W., 2011. A new look at gamma? High- (>60 Hz) ??-band activity in cortical networks: Function, mechanisms and impairment. Prog. Biophys. Mol. Biol. 105, 14–28.

Uhlhaas, P.J., Singer, W., 2010. Abnormal neural oscillations and synchrony in schizophrenia. Nat. Rev. Neurosci. 11, 100–13.

Uhlhaas, P.J., Singer, W., 2006. Neural synchrony in brain disorders: relevance for cognitive dysfunctions and pathophysiology. Neuron 52, 155–68.

Urbanavicius, J., Ferreira, M., Costa, G., Abin-Carriquiry, J. a., Wonnacott, S., Dajas, F., 2007. Nicotine induces tyrosine hydroxylase plasticity in the neurodegenerating striatum. J. Neurochem. 102, 723–730. doi:10.1111/j.1471-4159.2007.04560.x

Varela, F., Lachaux, J.P., Rodriguez, E., Martinerie, J., 2001. The brainweb: phase synchronization and large-scale integration. Nat. Rev. Neurosci. 2, 229–239. doi:10.1038/35067550

Von der Malsburg, C., 1995. Binding in models of perception and brain function. Curr. Opin. Neurobiol. 5, 520–526.

Von der Malsburg, C., Schneider, W., 1986. A neural cocktail-party processor. Biol. Cybern. 54, 29–40.

Wang, X., 2010. Neurophysiological and Computational Principles of Cortical Rhythms in Cognition 1195–1268.

Womelsdorf, T., Schoffelen, J.-M., Oostenveld, R., Singer, W., Desimone, R., Engel, A.K., Fries, P., 2007. Modulation of neuronal interactions through neuronal synchronization. Science 316, 1609–1612. doi:10.1126/science.1139597

Yanovsky, Y., Ciatipis, M., Draguhn, A., Tort, A.B.L., Branka k, J., 2014. Slow

Oscillations in the Mouse Hippocampus Entrained by Nasal Respiration. J. Neurosci. 34, 5949–5964. doi:10.1523/JNEUROSCI.5287-13.2014

Zelano, C., Jiang, H., Zhou, G., Arora, N., Schuele, S., Rosenow, J., Gottfried, J.A., 2016. Nasal Respiration Entrains Human Limbic Oscillations and Modulates Cognitive Function. J. Neurosci. 36, 12448–12467. doi:10.1523/JNEUROSCI.2586-16.2016

Zhong, W., Ciatipis, M., Wolfenstetter, T., Jessberger, J., Müller, C., Ponsel, S., Yanovsky, Y., Brankačk, J., Tort, A.B.L., Draguhn, A., 2017. Selective entrainment of gamma subbands by different slow network oscillations. Proc. Natl. Acad. Sci. U. S. A. 114, 4519–4524. doi:10.1073/pnas.1617249114

7. Anexos

Anexo 1

(Castro-Zaballa et al., 2014)

Neuroscience Letters 578 (2014) 197–202

Contents lists available at ScienceDirect

Neuroscience Letters

journal homepage: www.elsevier.com/locate/neulet

Inter-hemispheric coherence of neocortical gamma oscillations during sleep and wakefulness

Santiago Castro[a], Matias Cavelli[a], Patricia Vollono[a], Michael H. Chase[b,c], Atilio Falconi[a], Pablo Torterolo[a,*]

[a] Laboratorio de Neurobiología del Sueño, Departamento de Fisiología, Facultad de Medicina, Universidad de la República, Montevideo, Uruguay
[b] WebSciences International, Los Angeles, CA, USA
[c] UCLA School of Medicine, Los Angeles, CA, USA

HIGHLIGHTS

- The electroencephalogram of adult cats was recorded during sleep and wakefulness.
- The inter-hemispheric coherence of the EEG gamma frequency band was analyzed.
- The coherence was larger in alert wakefulness and almost absent during REM sleep.

ARTICLE INFO

Article history:
Received 17 March 2014
Received in revised form 18 May 2014
Accepted 20 June 2014
Available online 30 June 2014

Keywords:
Cortex
Consciousness
EEG
Synchronization
REM

ABSTRACT

Oscillations in the gamma frequency band (mainly ≈40 Hz) of the electroencephalogram (EEG) have been involved in the binding of spatially separated but temporally correlated neural events that result in a unified perceptual experience. The extent of these interactions can be examined by means of a mathematical algorithm called "coherence", which reflects the "strength" of functional interactions between cortical areas. As a continuation of a previous study of our group, the present study was conducted to analyze the inter-hemispheric coherence of the EEG gamma frequency band in the cat during alert wakefulness (AW), quiet wakefulness (QW), non-REM (NREM) sleep and REM sleep. Cats were implanted with electrodes in the frontal, parietal and occipital cortices to monitor EEG activity. The degree of coherence in the low (30–45 Hz) and high (60–100 Hz) gamma frequency bands from pairs of EEG recordings was analyzed. A large increase in coherence between all inter-hemispheric cortical regions in the low gamma bands during AW was present compared to the other behavioral states. Furthermore, both low and high gamma coherence between inter-hemispheric heterotopic cortices (different cortical areas of both hemispheres) decreased during REM sleep; this is a pattern that we previously reported between the cortical areas of the same hemisphere (intrahemispheric coherence). In the high gamma band, coherence during REM sleep also decreased compared to the other behavioral states. In contrast, between most of the inter-hemispheric homotopic cortical areas (equivalent or mirror areas of both hemispheres), low gamma coherence was similar during NREM compared to REM sleep. We conclude that in spite of subtle differences between homotopic and heterotopic inter-hemispheric cortices, functional interactions at high frequency decrease during REM sleep.

1. Introduction

Inter-hemispheric communication is achieved by information that is carried by the corpus callosum, anterior commisure and subcortical pathways [1]. Classical split-brain research wherein the corpus callosum is severed has demonstrated that inter-hemispheric communication subserves a large range of behaviors and cognitive functions [16]. For example, recent experiments have pointed out that transient coherent inter-hemispheric coordination underlies functions such as lexical processing [13].

Electroencephalographic (EEG) oscillations in the gamma frequency band (mainly ≈40 Hz) are involved in the integration or binding of spatially separated but temporally correlated neural events. An increase in gamma power typically appears during states/behaviors that are characterized by active cognitive

* Corresponding author at: Facultad de Medicina, Universidad de la República, General Flores 2125, 11800 Montevideo, Uruguay. Tel.: +598 2924 34 14x3234.
E-mail address: ptortero@fmed.edu.uy (P. Torterolo).

http://dx.doi.org/10.1016/j.neulet.2014.06.044
0304-3940/

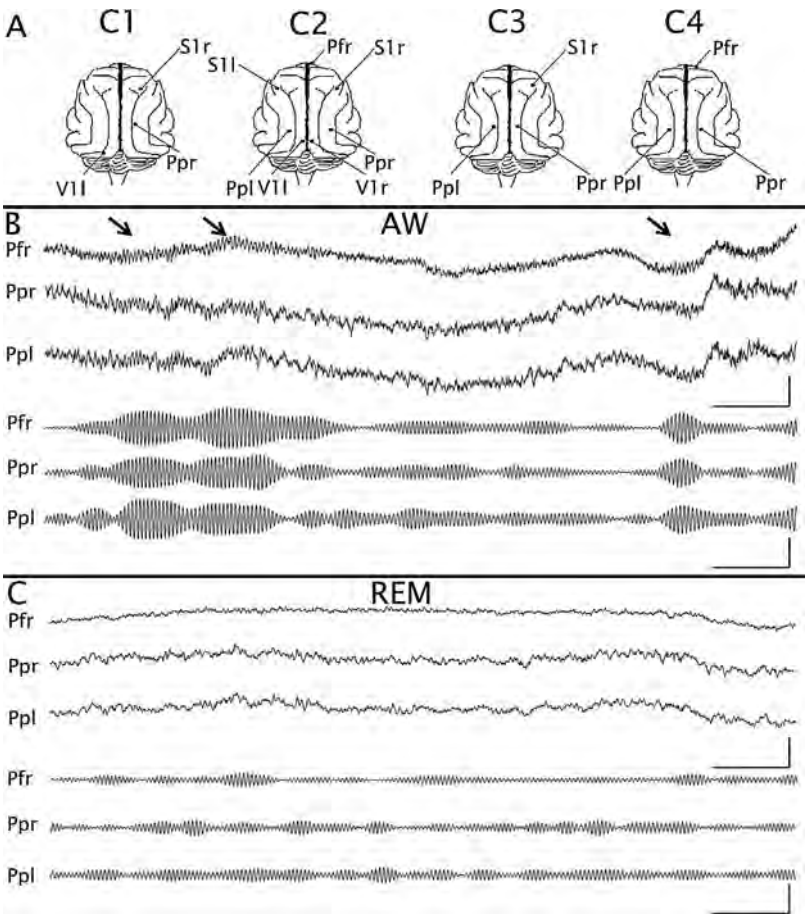

Fig. 1. Gamma oscillations during alert wakefulness and REM sleep. (A) Summary of the position of electrodes on the surface of the primary sensory, association sensory and prefrontal cerebral cortices. These electrodes were referred to a common indifferent electrode, which was located over the frontal sinus. C1–C4, are the animals' names. Pf, prefrontal cortex; Pp, posterior-parietal cortex; S1, somatosensory cortex; V1, visual primary cortex; r, right; l, left. (B) Simultaneous raw and filtered (35–40 Hz) cortical recordings from the right prefrontal (rPf), right posterior-parietal cortex (rPp) and left posterior-parietal cortex (lPp) during alert wakefulness. Gamma oscillations, which are readily observed in the raw recordings (arrows), are highlighted after filtering. Calibration bars: 1 s and 200 μV for raw recordings and 20 μV for filtered recordings. (C) Simultaneous raw and filtered (35–40 Hz) cortical recordings during REM sleep. The amplitude and duration of gamma oscillations decreased compared to alert wakefulness. Calibration bars, as in B.

processing of external percepts or internally generated thoughts and images in humans, and during attentive wakefulness in animals [8,28,29].

The degree of EEG coherence between two cortical regions is believed to reflect the strength of the functional interconnections that occur between them [7]. Coherent EEG activity in the gamma frequency band increases during different behaviors and cognitive functions in both animals and humans [5,6]. In this regard, both gamma activity and gamma coherence between different brain areas has been viewed as a possible neural correlate of consciousness [22].

In the cat, EEG "bursts" of 35–40 Hz oscillations of 200–500 ms and approximately 25 μV can be easily observed in raw EEG recordings ([10] and Fig. 1). Furthermore, EEG intra-hemispheric coherence at 35–40 Hz is greater during alert (AW) than quiet (QW) wakefulness [10]. In addition, intra-hemispheric coherence in the low (35–40 Hz) and high (60–100 Hz) gamma bands decrease to a lower level during non-REM (NREM) sleep, but reaches its nadir during REM sleep. Therefore, during REM sleep, the coupling of high frequency neuronal activity among different cortical areas of the same hemisphere is practically eliminated [10]; comparable results were obtained by other authors utilizing different experimental approaches [9,25,31]. Note that cognitive activities not only occur during wakefulness; dreams, that occur more prominently during rapid eye movement (REM) sleep, are considered a special kind of cognitive activity or proto-consciousness [19].

How is the functional interaction in the gamma frequency band between both hemispheres? Interestingly, a recent study showed that in the condition of corpus callosum agenesia, the gamma coherence (30–55 Hz) did not change during the resting state [18]. However, a subtle increase in gamma band (up to 50 Hz) coherence during REM sleep has been observed in EEG recordings in humans between anterior inter-hemispheric homotopic (equivalent areas of both cerebral hemispheres) leads [2,3]. Consequently, the present study was conducted to determine the interhemispheric coherence in the low (30–45 Hz) and high (60–100 Hz) gamma band between homotopic and heterotopic (different areas of both cerebral hemispheres) cortical areas, during sleep and wakefulness, utilizing the cat as the animal model.

2. Materials and methods

2.1. Experimental animals

Four adult cats (the same as in [10]) were used in this study. The animals were obtained from, and determined to be in good health, by the Institutional Animal Care Facility. All experimental procedures were conducted in accord with the *Guide for the Care and Use of Laboratory Animals* (8th edition, National Academy Press, Washington, DC, 2011) and approved by the Institutional Animal Care Commission. Adequate measures were taken to minimize pain, discomfort or stress of the animals. In addition, all efforts were made in

order to use the minimum number of animals necessary to produce reliable scientific data.

For details regarding the surgical and experimental procedures see [10]. Briefly, the animals were implanted with electrodes to monitor the states of sleep and wakefulness. Stainless steel screw electrodes (1.4 mm diameter) were placed on the surface (above the dura matter) of different cortical areas. Fig. 1A shows the place of the recording electrodes used in this study. The electrodes were connected to a Winchester plug that together with two plastic tubes, were bonded to the skull with acrylic cement in order to maintain the animal's head fixed in stereotaxic position without pain or pressure [10]. After the animals had recovered from the preceding surgical procedures, they were adapted to the recording environment for a period of at least two weeks.

Experimental sessions of 4 h in duration were conducted between 11 A.M. and 3 P.M. in a temperature-controlled environment (21–23 °C). During these sessions (as well as during the adaptation sessions), the animal's head was held in a stereotaxic position by four steel bars that were placed into the chronically implanted plastic tubes, while the body rested in a sleeping bag.

The simultaneous activity of three cortical areas from the same cerebral hemisphere was recorded with monopolar electrodes, utilizing a common reference electrode located in the left frontal sinus. The electromyogram (EMG) of the nuchal muscle, which was recorded by means of acutely placed bipolar electrode, was also monitored. Each cat was recorded daily for a period of approximately 30 days in order to obtain complete data sets.

Bioelectric signals were amplified (×1000), filtered (0.1–100 Hz), sampled (512 Hz, 2^{16} bits) and stored in a PC using the Spike 2 software (Cambridge Electronic Design). Data were obtained during spontaneously occurring quiet wakefulness (QW), REM sleep and non-REM sleep (NREM). Alert wakefulness (AW) was induced for a period of 300 s by a sound stimulus, which was introduced approximately 30 min after the beginning of the recording [10]. The sound stimulus consisted of clicks (0.1 ms in duration) of 60–100 dB SPL in intensity with a variable frequency of presentation (1–500 Hz, modified at random by the operator) in order to avoid habituation [10].

Sleep and waking states were quantified in epochs of 10 s. Selected recordings were filtered (band pass 30–45 Hz) and were processed by means of spectrograms (Fig. 2).

In order to analyze coherence between pairs of EEG channels, 12 manually selected artifact-free periods of 100 s were examined during each behavioral state (1200 s for each behavioral state). For each pair of recordings, data were obtained during four recording sessions.

For each 100 s period, the Magnitude Squared Coherence was analyzed by means of Spike 2 script COHER 1S (Cambridge Electronic Design) (see [10] for details in coherence definition).

The coherence between two EEG channels that were recorded simultaneously during 100 s periods was analyzed. This period of analysis was divided into 100 time-blocks with a sample rate of 512 Hz, a bin size of 1024 samples and a resolution of 0.5 Hz. Coherence between two waveforms is a function of frequency and ranges

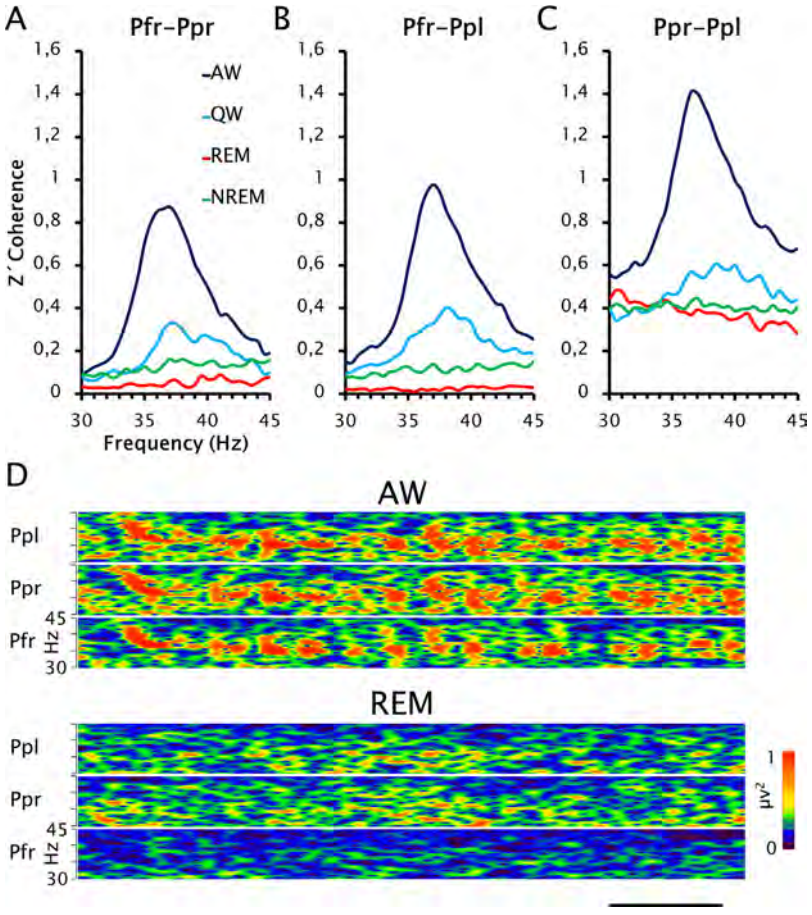

Fig. 2. Graphics that show the averaged z′-coherences profiles between representative intra-hemispheric (A), inter-hemispheric heterotopic (B) and inter-hemispheric homotopic (C) cortical areas during alert wakefulness (AW), quiet wakefulness (QW), non-REM sleep (NREM) and REM sleep in cat 4. (D) Spectrogram of the EEG gamma band of left posterior parietal (Ppl), right posterior parietal (Ppr) and right prefrontal cortex (Pfr). The dynamic of the gamma power during alert wakefulness is very similar in the recorded cortices. On the contrary, during REM sleep the gamma power coupling was reduced. However, the dynamic of the gamma power have some similarities between left and right parietal posterior cortices, but is very different between any of them and the prefrontal cortex. Calibration bar: 5 s.

Table 1
Gamma (35–40 Hz) z′-coherence values during sleep and wakefulness.

Animal	Derivates	AW	QW	NREM	REM	Statistical significance	*F*
C1	S1r-V1l	0.76 ± 0.03	0.35 ± 0.01	0.22 ± 0.02	0.18 ± 0.01	+AW vs. all; +QW vs. REM and NREM; +NREM vs. REM	202
	Ppr-V1l	1.31 ± 0.06	0.89 ± 0.06	0.92 ± 0.06	0.75 ± 0.06	+AW vs. all; +QW vs. REM; +NREM vs. REM	46
C2	Pfr-Ppl	0.49 ± 0.01	0.26 ± 0.02	0.16 ± 0.01	0.09 ± 0.01	++AW vs. all; +QW vs. NREM and REM; +NREM vs. REM	55
	Ppr-Ppl	0.95 ± 0.04	0.46 ± 0.05	0.27 ± 0.04	0.20 ± 0.03	++AW vs. all; +QW vs. NREM and REM	73
	V1r-V1l	1.70 ± 0.02	1.48 ± 0.01	1.42 ± 0.01	1.35 ± 0.01	+AW vs. all; +QW vs. REM; +NREM vs. REM	40
	S1r-S1l	0.64 ± 0.02	0.46 ± 0.01	0.45 ± 0.02	0.38 ± 0.01	++AW vs. all; +QW vs. REM	107
C3	S1r-Ppl	0.23 ± 0.01	0.08 ± 0.01	0.04 ± 0.01	0.02 ± 0.01	++AW vs. all; +QW vs. NREM and REM; +NREM vs. REM	111
	Ppr-Ppl	0.43 ± 0.01	0.34 ± 0.04	0.05 ± 0.01	0.05 ± 0.01	+AW vs. all; +QW vs. NREM and REM	31
C4	Pfr-Ppl	0.78 ± 0.02	0.33 ± 0.02	0.12 ± 0.01	0.02 ± 0.01	++AW vs. all; +QW vs. NREM and REM; +NREM vs. REM	120
	Ppr-Ppl	1.20 ± 0.03	0.55 ± 0.07	0.41 ± 0.02	0.37 ± 0.01	++AW vs. all; +QW vs. NREM and REM	90

The values represent mean ± standard error. +$P < 0.05$. ++$P < 0.0001$, ANOVA with Tamhane tests. The degrees of freedom were 3 (between groups) and 44 (within groups) for all the derivates that were analyzed. A1, auditory primary cortex; Pf, prefrontal cortex; Pp, posterior-parietal cortex; S1, somatosensory cortex; V1, visual primary cortex; r, right; l, left. The underlined derivates correspond to homotopic cortices.

from 0 for totally incoherent waveforms to 1 for maximal coherence; in order for two waveforms to be completely coherent at a particular frequency over a given time range, the phase shift between the waveforms must be constant and the amplitudes of the waves must have a constant ratio. We established that the random level of coherence was approximately 0.1 [10].

In order to normalize the data and conduct parametric statistical tests, we applied the Fisher z′ transform to the gamma coherence values. Thereafter, the profile of the z′-coherence of the gamma band in 100 s epochs for each pair of EEG recordings as well as the average of twelve epochs was analyzed, and the results were presented in a graphic form (Fig. 2). The z′-coherence of the gamma band for each pair of EEG channels was also averaged across behavioral states independently for each cat, and was expressed as the mean ± standard error. The significance of the differences among behavioral states was evaluated with the ANOVA and Tamhane post hoc tests. The criterion used to reject the null hypotheses was $P < 0.05$.

3. Results

Examples of representative EEG recordings from cortical areas of the same and different hemispheres (right prefrontal, right posterior parietal and left posterior parietal) are shown in Fig. 1B and C. “Bursts” of 35–40 Hz oscillations can be readily observed in raw recordings during AW (Fig. 1B, arrows). On the contrary, they are difficult to perceive during REM sleep (Fig. 1C). After digital filtering of the recordings to include only the low gamma band, these oscillations were unmasked.

A strong coupling of EEG gamma oscillations recorded in different cortical sites, was present during AW (even between channels within different brain hemispheres), but not during REM sleep (Fig. 1B and C). However, during REM sleep filtered records of the right and left posterior parietal cortices (Ppr and Ppl, homotopic cortices) appeared to be more coupled than were recordings between them and the right prefrontal cortex (Pfr) (Fig. 1C).

The “coherence” algorithm was applied in order to conduct an in-depth analysis of different pairs of EEG signals that were simultaneously recorded during sleep and wakefulness. Examples of representative averaged low (30–45 Hz) gamma band z′-coherence profiles for intra-hemispheric, homotopic inter-hemispheric and heterotopic inter-hemispheric combinations of EEG recordings are shown in Fig. 2A–C. A narrow peak of coherence at 35–40 Hz is readily observed in all derivations during AW. Both for intra-hemispheric and heterotopic inter-hemispheric combinations, the z′-coherence was drastically reduced during REM sleep. For homotopic inter-hemispheric combinations, the z′-coherence was similar between NREM and REM sleep.

A visual form to represent the gamma power as well as the coupling among different cortices during AW is shown in Fig. 2D; note the presence of “gamma bursts” in the form of red “clouds” that were correlated in all the recordings. Compared to AW, during REM sleep, gamma power was reduced and the correlation of the “bursts” was almost absent. However, note that during REM sleep the dynamic of the gamma power have some similarities between left and right posterior parietal cortex but is very different between any of them and the prefrontal cortex. Similar pattern can be observed in the filtered recordings of Fig. 1C.

The averaged inter-hemispheric z′-coherence in the 35–40 Hz band across behavioral states for all combinations of cortical recordings is presented in Table 1. As it is shown in the representative examples of Figs. 1 and 2, during AW z′-coherence was significantly larger in both inter-hemispheric combinations (homotopic and heterotopic). During QW and NREM sleep, z′-coherence values were intermediate, and in some combinations they were larger during QW than during NREM sleep. z′-coherence decreased during REM sleep between pairs of non-correspondent (heterotopic) cortices of both hemispheres. In contrast, in most of the derivations

Table 2
Gamma (60–100 Hz) z′-coherence values during sleep and wakefulness.

Animal	Derivates	AW	QW	NREM	REM	Statistical significance	*F*
C1	S1r-V1l	0.35 ± 0.02	0.31 ± 0.02	0.17 ± 0.02	0.04 ± 0.01	+All vs. all	81
	Ppr-V1l	0.46 ± 0.02	0.41 ± 0.01	0.28 ± 0.01	0.13 ± 0.01	+All vs. all	144
C2	Pfr-Ppl	0.39 ± 0.05	0.24 ± 0.04	0.15 ± 0.01	0.08 ± 0.01	+AW vs. NREM and REM; +QW vs. REM; +NREM vs. REM	18
	Ppr-Ppl	0.75 ± 0.05	0.39 ± 0.06	0.24 ± 0.03	0.14 ± 0.02	+AW vs. all; +QW vs. NREM and REM	36
	V1r-V1l	1.69 ± 0.02	1.59 ± 0.01	1.51 ± 0.01	1.32 ± 0.03	+All vs. all	20
	S1r-S1l	0.80 ± 0.02	0.72 ± 0.01	0.73 ± 0.02	0.65 ± 0.03	+AW vs. NREM and REM; +QW vs. REM; +NREM vs. REM.	59
C3	S1r-Ppl	0.21 ± 0.01	0.17 ± 0.02	0.09 ± 0.01	0.02 ± 0.01	+AW vs. all; +QW vs. NREM and REM; +NREM vs. REM.	38
	Ppr-Ppl	0.21 ± 0.04	0.34 ± 0.01	0.05 ± 0.01	0.03 ± 0.01	+AW vs. NREM and REM; +QW vs. REM	13
C4	Pfr-Ppl	0.49 ± 0.03	0.43 ± 0.03	0.37 ± 0.02	0.04 ± 0.01	+All vs. all	81
	Ppr-Ppl	0.82 ± 0.01	0.56 ± 0.07	0.52 ± 0.03	0.18 ± 0.01	+AW vs. all; +QW vs. REM; +NREM vs. REM	45

The values represent mean ± standard error. +$P < 0.05$, ANOVA with Tamhane tests. The degrees of freedom were 3 (between groups) and 44 (within groups) for all the derivates that were analyzed. A1, auditory primary cortex; Pf, prefrontal cortex; Pp, posterior-parietal cortex; S1, somatosensory cortex; V1, visual primary cortex; r, right; l, left. The underlined derivates correspond to homotopic cortices.

(4 out of 5), the z′-coherence between inter-hemispheric homotopic regions was similar during NREM and REM sleep.

Table 2 presents an analysis of the inter-hemispheric z′-coherence for the 60–100 Hz frequency band. The z′-coherence during AW was larger than QW in most but not all derivations. During REM sleep, there was a significant decrease in z′-coherence for both inter-hemispheric and intra-hemispheric (homotopic and heterotopic) combinations.

4. Discussion

A gamma frequency band (30–45 Hz) in the EEG was originally described by Jasper and Andrews [20], and corresponds to the 40 Hz cognitive rhythm introduced by Das and Gastaut [11]. Several seminal studies then confirmed that this frequency band plays a critically important role in cognitive functions [22].

From a methodological point of view, our animal model have the advantage that by utilizing cortical surface electrodes, ≈40 Hz oscillations can be clearly observed directly in the raw EEG recordings. Therefore, the result of the coherence analysis can also be confirmed by direct observation of the recordings; e.g., the tracing of Fig. 1 corresponds to the analysis, which is presented in Fig. 2.

In the present study, we demonstrated that the EEG inter-hemispheric coherence in the low gamma (30–45 Hz) frequency band is greater during AW than QW. In this regard, callosal-dependent inter-hemispheric synchrony has been observed during visual stimulation in the cat [15]; and in humans, synchronized activity in ≈40 Hz has been found to spread across the hemispheres during a visual recognition task [26]. Gamma-band rhythmogenesis has been systematically studied and is considered to be inextricably tied to the presence of perisomatic inhibition of cortical neurons that occurs due to $GABA_A$-receptor mediated inhibition [8]. However, the locally generated gamma rhythms can become coupled over surprisingly long distances, i.e. between hemispheres or remote regions of the cerebral cortex [8,17,23]. Interestingly, recent studies suggest that coherent gamma activity that is present in several subregions of the ascending reticular activating system may function to stabilize EEG gamma coherence during arousal [30].

Gamma coherence decreased to a lower level during NREM and REM sleep compared to QW. Although between homotopic inter-hemispheric areas z′-coherence was similar during NREM and REM sleep, between non-symmetrical inter-hemispheric areas, gamma coherence reached its nadir during REM sleep, as we found for low gamma coherence concerning intra-hemispheric regions [10].

Interestingly, low gamma coupling during REM sleep between homotopic cortices of both hemispheres is of intermediate strength compared with the lack of coupling for intra-hemispheric remote cortical areas and the high degree of local coupling (within a column or among closely cortical sites) that produce high values of gamma power [10,27]. In the cat, as in other mammals, there is a great number of callosal fibers that connect between homotopic inter-hemispheric cortical areas [24]; these connections may facilitate functional coupling between these cortical sites.

Research in oscillations of higher frequencies than 40 Hz (up to 600 Hz) has been undertaken recently [29], and the role of these higher frequency bands in cognitive function is still unknown. Nevertheless, we included an investigation of frequencies from 60 up to 100 Hz in the present study and in our previous paper [10]. We found that inter-hemispheric and intra-hemispheric high gamma coherence shares the same characteristics. Alert wakefulness produced only a small increase in coherence in some derivations compared to QW, and there was significant reduction of coherence during REM sleep for both inter-hemispheric combinations (homotopic and heterotopic cortices). It is interesting to note that even though high gamma coherence is reduced during REM sleep, the power or potency (and sign of local synchronization) in this frequency band is similar than waking levels [10]. Unfortunately, the mechanisms that are responsible for these high frequency oscillations are still unclear [29]. However, it is important to note that the possibility that artifacts induced either by muscle or saccadic activity affected the data has been previously discussed and discarded [10].

In addition to the results of EEG coherence during REM sleep of Achermann and Borbely [2,3] (see Section 1), Leveille et al. demonstrated that although intra-hemispheric EEG coherence (up to beta band) during REM sleep is altered in autism, inter-hemispheric coherence did not change [21]. Inter-hemispheric communication during REM sleep was also assessed by means of paired-pulse transcranial magnetic stimulation [4,12]. The authors demonstrated a drastic decrease in callosal inhibition, and a significant increase in intra-cortical facilitation 10 and 15 ms after awakenings that followed REM sleep, suggesting that inter-hemispheric connectivity is modified during REM sleep. However, more studies are needed to understand the functional role of inter-hemispheric interaction during REM sleep.

5. Conclusions

Functional interactions among different cortical areas, including inter-hemispheric communication, are critical for cognitive functions [14]. In the present and a previous paper we demonstrated an uncoupling of gamma frequency activity during REM sleep between intra and inter-hemispheric cortices. This fact may contribute to the uniqueness of cognitive functions that take place during REM sleep, where most dreams occur [19].

Acknowledgments

The “Programa de Desarrollo de Ciencias Básicas” (PEDECIBA), and the “Agencia Nacional de Investigacion e Innovación” (ANII), Uruguay, partially supported this work.

References

[1] F. Aboitiz, J. Montiel, One hundred million years of interhemispheric communication: the history of the corpus callosum, Braz. J. Med. Biol. Res. 36 (2003) 409–420.
[2] P. Achermann, A.A. Borbely, Coherence analysis of the human sleep electroencephalogram, Neuroscience 85 (1998) 1195–1208.
[3] P. Achermann, A.A. Borbely, Temporal evolution of coherence and power in the human sleep electroencephalogram, J. Sleep Res. 7 (Suppl. 1) (1998) 36–41.
[4] M. Bertini, L. De Gennaro, M. Ferrara, G. Curcio, V. Romei, F. Fratello, R. Cristiani, F. Pauri, P.M. Rossini, Reduction of transcallosal inhibition upon awakening from REM sleep in humans as assessed by transcranial magnetic stimulation, Sleep 27 (2004) 875–882.
[5] J.J. Bouyer, M.F. Montaron, A. Rougeul, Fast fronto-parietal rhythms during combined focused attentive behaviour and immobility in cat: cortical and thalamic localizations, Electroencephalogr. Clin. Neurophysiol. 51 (1981) 244–252.
[6] S.L. Bressler, R. Coppola, R. Nakamura, Episodic multiregional cortical coherence at multiple frequencies during visual task performance, Nature 366 (1993) 153–156.
[7] T.H. Bullock, M.C. McClune, J.T. Enright, Are the electroencephalograms mainly rhythmic? Assessment of periodicity in wide-band time series, Neuroscience 121 (2003) 233–252.
[8] G. Buzsaki, X.J. Wang, Mechanisms of gamma oscillations, Annu. Rev. Neurosci. 35 (2012) 203–225.
[9] J.L. Cantero, M. Atienza, J.R. Madsen, R. Stickgold, Gamma EEG dynamics in neocortex and hippocampus during human wakefulness and sleep, Neuroimage 22 (2004) 1271–1280.
[10] S. Castro, A. Falconi, M.H. Chase, P. Torterolo, Coherent neocortical 40-Hz oscillations are not present during REM sleep, Eur. J. Neurosci. 37 (2013) 1330–1339.
[11] N.N. Das, H. Gastaut, Variations de l'activite electrique du cerveau, du coeur et des muscles squellettiques au cours de la meditation et de l'extase yoguique, Electroencephalogr. Clin. Neurophysiol. 6 (1955) 211.
[12] L. De Gennaro, M. Bertini, M. Ferrara, G. Curcio, R. Cristiani, V. Romei, F. Fratello, F. Pauri, P.M. Rossini, Intracortical inhibition and facilitation upon awakening from different sleep stages: a transcranial magnetic stimulation study, Eur. J. Neurosci. 19 (2004) 3099–3104.

[13] K.W. Doron, D.S. Bassett, M.S. Gazzaniga, Dynamic network structure of interhemispheric coordination, Proc. Natl. Acad. Sci. U.S.A. 109 (2012) 18661–18668.
[14] G.M. Edelman, G. Tononi, A Universe of Consciousness, Basic Books, New York, 2000.
[15] A.K. Engel, P. Konig, A.K. Kreiter, W. Singer, Interhemispheric synchronization of oscillatory neuronal responses in cat visual cortex, Science 252 (1991) 1177–1179.
[16] M.S. Gazzaniga, Shifting gears: seeking new approaches for mind/brain mechanisms, Annu. Rev. Psychol. 64 (2012) 1–20.
[17] G.G. Gregoriou, S.J. Gotts, H. Zhou, R. Desimone, High-frequency, long-range coupling between prefrontal and visual cortex during attention, Science 324 (2009) 1207–1210.
[18] L.B. Hinkley, E.J. Marco, A.M. Findlay, S. Honma, R.J. Jeremy, Z. Strominger, P. Bukshpun, M. Wakahiro, W.S. Brown, L.K. Paul, A.J. Barkovich, P. Mukherjee, S.S. Nagarajan, E.H. Sherr, The role of corpus callosum development in functional connectivity and cognitive processing, PLOS ONE 7 (2012) e39804.
[19] J.A. Hobson, REM sleep and dreaming: towards a theory of protoconsciousness, Nat. Rev. Neurosci. 10 (2009) 803–813.
[20] H.H. Jasper, H.L. Andrews, Brain potentials and voluntary muscle activity in man, J. Neurophysiol. 1 (1938) 87–100.
[21] C. Leveille, E.B. Barbeau, C. Bolduc, E. Limoges, C. Berthiaume, E. Chevrier, L. Mottron, R. Godbout, Enhanced connectivity between visual cortex and other regions of the brain in autism: a REM sleep EEG coherence study, Autism Res. 3 (2010) 280–285.
[22] R. Llinas, U. Ribary, D. Contreras, C. Pedroarena, The neuronal basis for consciousness, Philos. Trans. R. Soc. Lond. B: Biol. Sci. 353 (1998) 1841–1849.
[23] L. Melloni, C. Molina, M. Pena, D. Torres, W. Singer, E. Rodriguez, Synchronization of neural activity across cortical areas correlates with conscious perception, J. Neurosci. 27 (2007) 2858–2865.
[24] H. Nakamura, T. Kanaseki, Topography of the corpus callosum in the cat, Brain Res. 485 (1989) 171–175.
[25] E. Perez-Garci, Y. del-Rio-Portilla, M.A. Guevara, C. Arce, M. Corsi-Cabrera, Paradoxical sleep is characterized by uncoupled gamma activity between frontal and perceptual cortical regions, Sleep 24 (2001) 118–126.
[26] E. Rodriguez, N. George, J.P. Lachaux, J. Martinerie, B. Renault, F.J. Varela, Perception's shadow: long-distance synchronization of human brain activity, Nature 397 (1999) 430–433.
[27] M. Steriade, F. Amzica, D. Contreras, Synchronization of fast (30–40 Hz) spontaneous cortical rhythms during brain activation, J. Neurosci. 16 (1996) 392–417.
[28] P.J. Uhlhaas, G. Pipa, B. Lima, L. Melloni, S. Neuenschwander, D. Nikolic, W. Singer, Neural synchrony in cortical networks: history, concept and current status, Front. Integr. Neurosci. 3 (2009) 17.
[29] P.J. Uhlhaas, G. Pipa, S. Neuenschwander, M. Wibral, W. Singer, A new look at gamma? High- (>60 Hz) gamma-band activity in cortical networks: function, mechanisms and impairment, Prog. Biophys. Mol. Biol. 105 (2011) 14–28.
[30] F.J. Urbano, N. Kezunovic, J. Hyde, C. Simon, P. Beck, E. Garcia-Rill, Gamma band activity in the reticular activating system, Front. Neurol. 3 (2012) 6.
[31] U. Voss, R. Holzmann, I. Tuin, J.A. Hobson, Lucid dreaming: a state of consciousness with features of both waking and non-lucid dreaming, Sleep 32 (2009) 1191–1200.

Anexo 2

(Torterolo et al., 2016a)

EJN European Journal of Neuroscience

FENS Federation of European Neuroscience Societies

European Journal of Neuroscience, Vol. 43, pp. 580–589, 2016 doi:10.1111/ejn.13151

NEUROSYSTEMS

Neocortical 40 Hz oscillations during carbachol-induced rapid eye movement sleep and cataplexy

Pablo Torterolo,[1] Santiago Castro-Zaballa,[1] Matías Cavelli,[1] Michael H. Chase[2] and Atilio Falconi[1]
[1]Laboratorio de Neurobiología del Sueño, Facultad de Medicina, Departamento de Fisiología, Universidad de la República, General Flores 2125, 11800 Montevideo, Uruguay
[2]WebSciences International and UCLA School of Medicine, Los Angeles, CA, USA

Keywords: cat, electroencephalogram, gamma, narcolepsy, nucleus pontis oralis, reticular formation

Edited by Thomas Klausberger
Received 18 July 2015, revised 3 December 2015, accepted 4 December 2015

Abstract

Higher cognitive functions require the integration and coordination of large populations of neurons in cortical and subcortical regions. Oscillations in the gamma band (30–45 Hz) of the electroencephalogram (EEG) have been involved in these cognitive functions. In previous studies, we analysed the extent of functional connectivity between cortical areas employing the 'mean squared coherence' analysis of the EEG gamma band. We demonstrated that gamma coherence is maximal during alert wakefulness and is almost absent during rapid eye movement (REM) sleep. The nucleus pontis oralis (NPO) is critical for REM sleep generation. The NPO is considered to exert executive control over the initiation and maintenance of REM sleep. In the cat, depending on the previous state of the animal, a single microinjection of carbachol (a cholinergic agonist) into the NPO can produce either REM sleep [REM sleep induced by carbachol (REMc)] or a waking state with muscle atonia, i.e. cataplexy [cataplexy induced by carbachol (CA)]. In the present study, in cats that were implanted with electrodes in different cortical areas to record polysomnographic activity, we compared the degree of gamma (30–45 Hz) coherence during REMc, CA and naturally-occurring behavioural states. Gamma coherence was maximal during CA and alert wakefulness. In contrast, gamma coherence was almost absent during REMc as in naturally-occurring REM sleep. We conclude that, in spite of the presence of somatic muscle paralysis, there are remarkable differences in cortical activity between REMc and CA, which confirm that EEG gamma (≈40 Hz) coherence is a trait that differentiates wakefulness from REM sleep.

Introduction

During wakefulness (W) there is awareness (consciousness) of the environment and internal stimuli such as hunger, thirst, etc. In contrast, during quiet or non-rapid eye movement (NREM) sleep, especially during the deep phase (N3) that occurs during the first half of the night, cognition is almost absent (Tononi, 2009). During rapid eye movement (REM) sleep there is a different cognitive state, which is when most dreams occur (Hobson, 2009; Tononi, 2009). However, the electroencephalogram (EEG) activity appears similar to that which takes place during W. Because of this fact, Jouvet (1965) called this state the 'paradoxical phase' of sleep. However, a detailed analysis of the EEG in cats and rats revealed that there is a high level of neocortical gamma (30–100 Hz) band coherence during alert W (AW), which decreases during quiet W (QW) and NREM sleep, and is almost absent during REM sleep (Castro *et al.*, 2013, 2014; Cavelli *et al.*, 2015). As EEG coherence between two cortical regions reflects the strength of the functional interconnections that occur between them (Edelman & Tononi, 2000; Bullock *et al.*, 2003), the differences in gamma band coherence indicate that the functional integration among separate cortical areas is not the same during W and REM sleep.

In order to confirm and expand knowledge about the dynamics of gamma neocortical activity during the activated behavioural states (W and REM sleep), we took advantage of the fact that microinjections of carbachol, a mixed cholinergic (muscarinic and nicotinic) agonist, into the nucleus pontis oralis (NPO) of the cat switch the behavioural state from W or NREM to REM sleep. Thus, a single microinjection of carbachol during NREM sleep induces the generation of REM sleep [REM sleep induced by carbachol (REMc)] with short latency (approximately 30 s). Interestingly, depending on the previous behavioural state of the animal, microinjections of carbachol within the NPO may also induce muscle atonia during W or cataplexy, which is similar to atonia during naturally-occurring REM sleep and REMc (Lopez-Rodriguez *et al.*, 1994). Cataplexy, which is a cardinal sign of the sleep pathology narcolepsy, consists of a sudden loss in muscle tone during W, which is most commonly elicited by an emotional response (Guilleminault & Fromherz, 2011; Mignot, 2011; Chase, 2013; Dauvilliers *et al.*, 2014).

Cataplexy induced by carbachol (CA) occurs most readily when carbachol is microinjected during AW (Lopez-Rodriguez *et al.*,

Correspondence: Pablo Torterolo, as above.
E-mail: ptortero@fmed.edu.uy

1994). In addition, transitions from REMc to CA are common, and CA can be induced from REMc by sensory stimulation (Torterolo *et al.*, 2015). Hence, in the present study we compared EEG gamma coherence during REMc and CA, which are two different states that present essentially the same somato-motor atonia. The direct transition of these carbachol-induced states from one to another allows a direct observation of the differences of the gamma activity between the activated states; W to REM sleep transitions do not take place during the natural sleep–W cycle. Because 40 Hz activity is prominent and readily observable in raw EEG recordings and is highly reactive to the level of alertness [which is not the case for higher frequency gamma activity (Castro *et al.*, 2013)], in the present report we only examined the 30–45 Hz frequency band of the gamma spectrum.

Materials and methods

Four adult cats were used in this study; these animals were also employed in a previous report (Torterolo *et al.*, 2015). The animals were determined to be in good health by veterinarians of the Department of Laboratory Medicine (Facultad de Medicina, Universidad de la República, Montevideo, Uruguay). All experimental procedures were conducted in accordance with the National Animal Care Law (no. 18611) and the Guide to the Care and Use of Laboratory Animals (8th Edn, National Academy Press, Washington D.C., 2010), and were approved by the Institutional Animal Care Committee (Comisión de Experimentación Animal). Efforts were made to use the minimal number of animals necessary to produce reliable data.

Surgical procedures were the same as those previously employed (Castro *et al.*, 2013; Torterolo *et al.*, 2015). The animals were chronically implanted with electrodes to monitor the states of sleep and W. Prior to being anaesthetized, each cat was premedicated with xylazine (2.2 mg/kg, i.m.), atropine (0.04 mg/kg, i.m.) and antibiotics (Tribrissen®, 30 mg/kg, i.m.). Anaesthesia, which was initially induced with ketamine (15 mg/kg, i.m.), was maintained with a gas mixture of isoflourane in oxygen (1–3%). Following anaesthesia, the head was positioned in a stereotaxic frame and stainless steel screw electrodes were placed in the skull to record the EEG. The position of the recording electrodes is illustrated in Fig. 1A. In addition, bipolar electrodes were implanted in both lateral geniculate nuclei in order to monitor ponto-geniculo-occipital (PGO) waves, and in the orbital portion of the the electro-oculogram. A Winchester plug (connected to the electrodes) and a chronic head- restraining bone to record restraining device were bonded to the skull with acrylic cement. A hole (5 mm diameter), which was drilled in the skull overlying the cerebellar cortex, was filled with bone-wax, and this hole was subsequently used to provide access to the pons for drug administration.

Experimental sessions

After the animals recovered from surgery and were adapted to the recording environment, polysomnographic recordings were conducted from 11:00 to 15:00 h in a temperature-controlled environment (21–23 °C). During these sessions, the head of the cat was held in a stereotaxic position by a head-restraining device. The EEG activity of three cortical areas was recorded with monopolar electrodes, utilizing a common reference electrode located in the left frontal sinus. Electro-oculogram, lateral geniculate nuclei, neck electromyogram (electrodes were placed acutely on the skin over neck muscles), ECG (electrodes were placed acutely on the skin over the precordial region) and respiratory activity (by means of a microeffort piezo crystal infant sensor) were also recorded. Each cat was recorded daily for a period of approximately 30 days in order to obtain complete data sets.

Bioelectric signals were amplified (×1000), filtered (0.1–100 Hz), sampled (512 Hz, 2^{16} bits) and stored on a PC using SPIKE 2 software (Cambridge Electronic Design). Data were obtained during QW, REM sleep and NREM sleep. AW was induced for a period of 300 s by a sound stimulus, which was introduced at approximately 30 min after the beginning of the recording (Castro *et al.*, 2013). The sound stimulus consisted of clicks (0.1 ms in duration) of 60–100 dB sound pressure level in intensity with a variable frequency of presentation (1–500 Hz) in order to avoid habituation (Castro *et al.*, 2013).

The eyes of the animals were examined throughout the recording sessions in order to determine if they were closed or open, and if the pupils were mydriatic or miotic. We also monitored the degree of relaxation of the nictitating membrane and whether the animals were able to track visual or auditory stimuli.

In order to induce REMc or CA, carbachol (0.8 μg in 0.2 μL of saline) was microinjected unilaterally for a period of 1 min into the NPO with a Hamilton syringe (Torterolo *et al.*, 2013, 2015). The coordinates were: AP, −2 to −3; L, 1.5–2.5; and H, −3.5 to −5, according to Berman (1968). Carbachol microinjections were performed either during NREM sleep or W (Lopez-Rodriguez *et al.*, 1994). Two successful carbachol microinjections (i.e. in these experiments REMc and CA episodes were generated) were carried out for each cat on different days. Mild auditory or somato-sensory stimuli were occasionally applied to the animals in order to induce CA from an ongoing state of REMc (see Results).

Sleep and coherence analyses

The states of AW, QW, NREM sleep, REM sleep, REMc and CA were determined on the basis of polysomnographic records that were divided into 10 s epochs and analysed according to standard criteria (Ursin & Sterman, 1981). The identification of REMc and CA is explained in the Results. Only well-defined periods of REMc and CA were analysed, and transitions between states were excluded.

Selected recordings were filtered (band pass 30–45 Hz) and processed by means of spectrograms. In order to analyse coherence between pairs of EEG recordings, 12 artefact-free periods of 100 s were examined during each behavioural state (1200 s for each behavioural state). For each pair of recordings, data were obtained during four separate recording sessions.

For each 100 s period, the magnitude squared coherence was analysed by means of SPIKE 2 script COHER 1S (Cambridge Electronic Design) (for details, see Castro *et al.*, 2013). The coherence between two EEG channels that were recorded simultaneously during 100 s periods was analysed. This period of analysis was divided into 100 time blocks with a sample rate of 512 Hz, bin size of 1024 and resolution of 0.5 Hz. We previously established that the random level of coherence was approximately 0.1 (Castro *et al.*, 2013).

Statistical analysis

In order to normalize the data and conduct parametric statistical tests, the Fisher z′ transform to the gamma coherence values was applied. Thereafter, the profile of the z′-coherence of the gamma band in 100 s epochs for each pair of EEG recordings, as well as the average of 12 epochs, was analysed, and the results were presented in a graphic form. In addition, for each cat, the z′-coherence

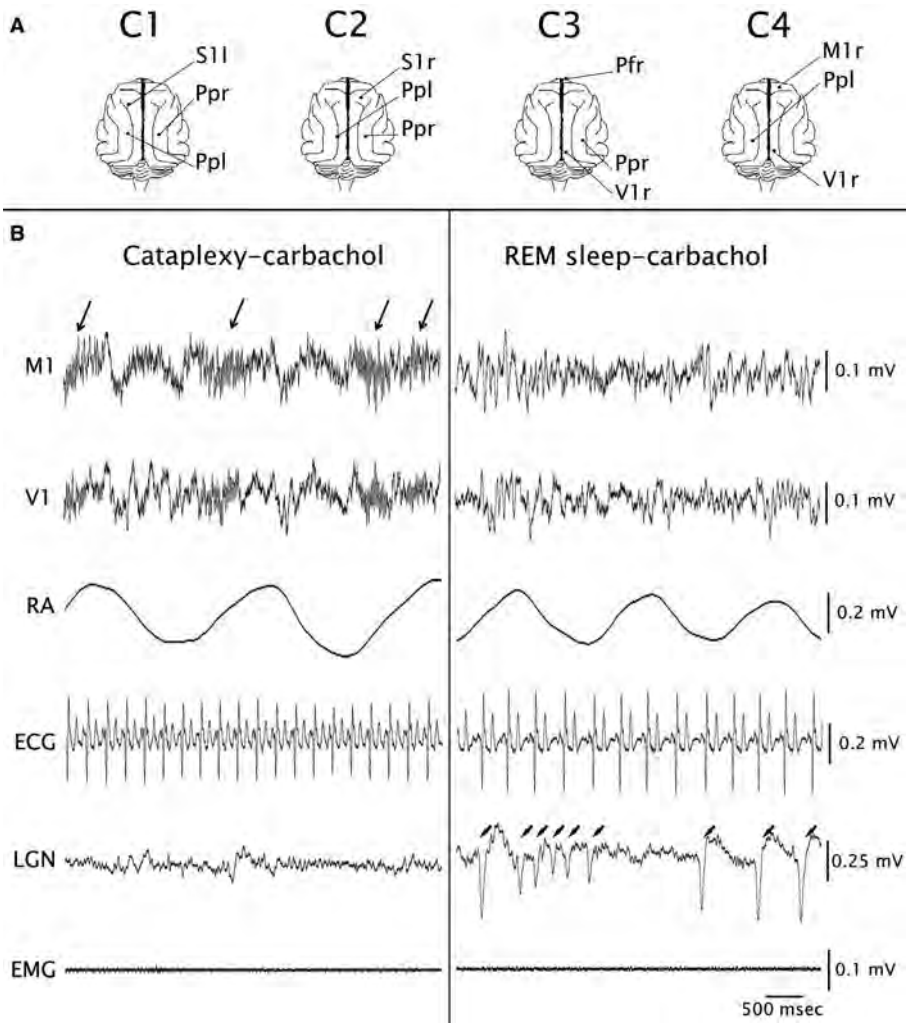

FIG. 1. (A) Location of recording electrodes. Recordings from these electrodes were referred to a common electrode, which was located over the frontal sinus. G1–G4, individual animals; M1, primary motor cortex; Pf, prefrontal cortex; Pp, posterior parietal cortex; S1, somato-sensory primary cortex; V1, visual primary cortex; r, right; l, left. (B) Polysomnographic recordings during Cataplexy induced by carbachol (CA). M1, V1 and lateral geniculate nuclei (LGN), electrogram, electromyogram (EMG), respiratory activity (RA) and electrocardiogram (ECG) during CA. Arrows indicate gamma oscillations. (C) Polysomnographic recordings during REMc. Arrowheads indicate PGO waves.

of the gamma band for all pairs of EEG channels was averaged across behavioural states and expressed as the mean ± SE. The significance of the differences between behavioural states was evaluated with the ANOVA and Tamhane *post hoc* tests. The criterion used to reject the null hypotheses was $P < 0.05$.

Results

Behavioural states induced by carbachol

As we have previously reported (Torterolo *et al.*, 2015), the microinjection of carbachol into the NPO induces either CA or REMc. The carbachol-induced states had a latency of 266 ± 29 s (mean ± SE). In addition, transitions from REMc to CA and vice versa were also observed spontaneously or provoked by sensory stimulation; the carbachol-induced states lasted 39–160 min. Figure 1B presents a representative recording during CA, and bursts of gamma oscillations are readily observed (at approximately 40 Hz, shown by arrows in Fig. 1B) in the primary motor cortex and primary visual cortex, as well as muscle atonia. In previous reports it has been established that this type of gamma activity is prominent during AW (Castro *et al.*, 2013, 2014). In addition, PGO waves were rarely observed during CA; the eyes were open with moderate pupillary dilatation and auditory and visual stimuli were tracked as during natural W (not shown). In contrast, as in naturally-occurring REM sleep, during REMc there were no clear gamma bursts in most of the animals (Fig. 1C) (Castro *et al.*, 2013, 2014). Furthermore, during REMc, PGO waves (shown by arrowheads in Fig. 1C) and muscle atonia were present. Additionally, the eyes were closed and the nictitating membrane was relaxed (not shown). Heart rate during REMc tended to be lower (Fig. 2A and B) (Torterolo *et al.*, 2015) and respiratory activity was more regular than during CA.

As previously reported (Torterolo *et al.*, 2015), mild auditory or somatic sensory stimulation during REMc aroused the animal even though atonia was maintained, i.e. CA was induced. There were also transitions from REMc to CA, which were triggered by spontaneous or uncontrolled environmental sounds. Spontaneous CA to REMc transitions were also observed. Interestingly, when the carbachol effect was diminishing and the animal aroused from REMc, it usually spent a few minutes in CA prior to entering into complete W.

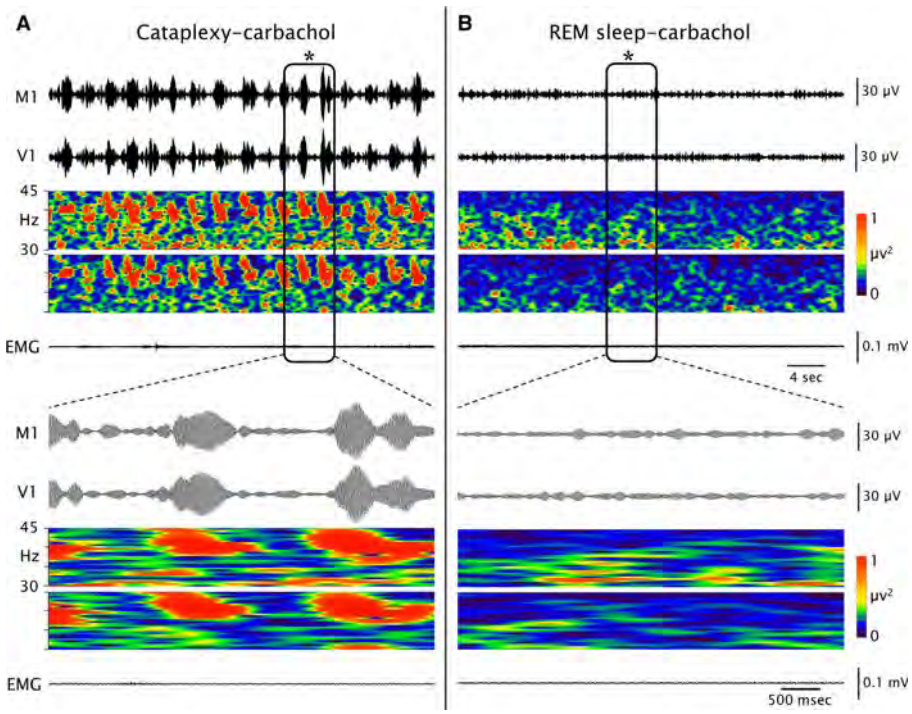

FIG. 2. Gamma band (30–45 Hz) oscillations and power during rapid eye movement (REM) sleep and Cataplexy induced by carbachol (CA). Simultaneous filtered (35–40 Hz) recordings and gamma power spectrograms from the primary motor cortex (M1) and primary visual cortex (V1) are shown together with electromyographic activity. Recordings are presented in a 40 s time window; below are shown recordings from the insets (*) with a 5 s time window. (A) CA. (B) REMc. Compared with REMc, gamma activity during cataplexy was larger and more strongly coupled between different areas.

This behaviour is similar to sleep paralysis, a clinical sign that often occurs in patients with narcolepsy (Guilleminault & Fromherz, 2011; Mignot, 2011).

Coherent gamma activity during cataplexy induced by carbachol and rapid eye movement sleep induced by carbachol

Gamma activity was unmasked after digital filtering, which included only 30–45 Hz oscillations. Filtered recordings and their spectrograms are shown during CA and REMc in Fig. 2. Note that, during CA, there was a strong coupling of EEG signals between the recorded cortices (Fig. 2A), as was demonstrated for AW (Castro *et al.*, 2013). This coherent gamma activity was present during CA in all of the animals studied. However, during REMc, gamma power was reduced and coupling was not present in three out of four animals (Fig. 2B). In one animal (labelled G1), coherent gamma activity was present during REMc; this special case will be analysed at the end of this section.

Coherence profiles for representative pairs of EEG leads are shown in Fig. 3A and B. The profile of twelve 100 s periods and their average during CA and REMc are shown in Fig. 3A. z′-coherence profiles for all 100 s periods as well as their average were larger during CA (with a restricted peak at 35–40 Hz), and were virtually absent during REMc. The average z′-coherence profile for a representative combination of cortices is shown for all naturally-occurring and carbachol-induced behavioural states in Fig. 3B. In spite of the presence of muscle atonia, the average gamma coherence profile during CA was similar to AW. However, gamma coherence during REMc was similar to naturally-occurring REM sleep. Intermediate values were present during QW and NREM sleep. The dynamic of gamma z′-coherence following carbachol microinjection into the NPO is shown in Fig. 3C and D; a high level of gamma coherence was present during CA but not during REMc.

The average z′-coherence in the 35–40 Hz band across behavioural states for all combinations of cortical recordings is presented in Table 1. In these independent analyses from different cortices from all cats, the results were consistent for CA, i.e. gamma z′-coherence was large and similar to AW. However, gamma coherence was minimal during REMc in most animals, and the values were similar to that present during naturally-occurring REM sleep.

Gamma power, which is shown in Fig. 4 and Table 2, was maximal during AW and CA. However, the gamma power during REMc was similar to that present during naturally-occurring REM sleep and QW. Gamma power values were minimal during NREM sleep.

In the animal G1, gamma power and coherence during naturally-occurring NREM and REM sleep, W and CA were similar to those present in the other animals (Tables 1 and 2). However, gamma activity during REMc was different. G1 showed long-duration bursts of high-amplitude coherent gamma oscillations during REMc, even though the classic features of REM sleep (atonia, PGO waves and relaxed nictitating membrane) were present. Values of gamma coherence and power were high in this animal (Tables 1 and 2).

Discussion

In the present report, we demonstrate that gamma coherence is significantly different during REMc and CA even though both states were induced by microinjections of carbachol into the NPO. The NPO of the cat (also called the medial pontine reticular formation or perilocus coeruleus α) and its corresponding nucleus in the rat, which is called the sublaterodorsal nucleus, is considered to exert

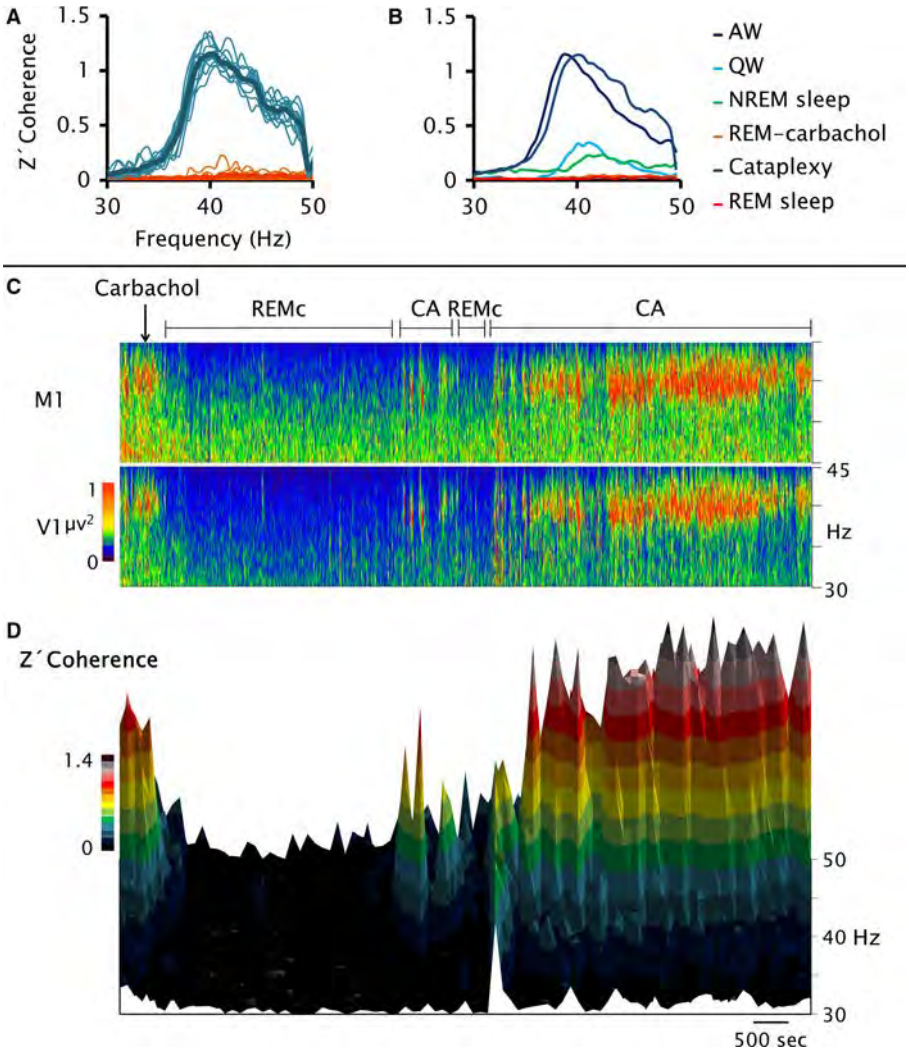

FIG. 3. Profile of electroencephalogram (EEG) gamma (30–45 Hz) coherence during rapid eye movement (REM) sleep and cataplexy induced by carbachol (CA). (A) Twelve profiles of z′-coherences (thin lines) of a representative pair of recordings (prefrontal and posterior parietal cortices of the same hemisphere) and averages of these 12 profiles (thick lines) are shown for REMc and CA. The profiles were constructed from periods of 100 s with a resolution of 0.5 Hz. Gamma coherence was maximal during CA and practically absent during REMc. (B) Averaged profiles during CA, REMc and naturally-occurring behavioural states. (C) Spectrograms of recordings from the primary motor cortex (M1) and primary visual cortex (V1) of the same hemisphere, following the microinjection of carbachol into the NPO. Episodes of REMc and CA are indicated. (D) Dynamic evolution of EEG coherence following the microinjection of carbachol into the NPO. Three-dimensional spectrogram of z′-coherence of the EEG (30–45 Hz) from simultaneous recordings from the M1 and V1. Time and frequency are shown on the horizontal and vertical (depth) axes, respectively; z′-coherence is represented by a colour code. z′-coherence was drastically reduced during REMc and was maximal during CA.

executive control over the initiation and maintenance of REM sleep (reviewed in Baghdoyan, 1997; Kubin, 2001; Reinoso-Suarez *et al.*, 2001; Luppi *et al.*, 2007; Siegel, 2011; Chase, 2013).

Gamma coherence

The EEG oscillations in the gamma frequency band (30–100 Hz) are involved in the integration or binding of spatially separated but temporally correlated neural events (Uhlhaas *et al.*, 2009, 2011; Rieder *et al.*, 2010). An increase in gamma power typically appears during states/behaviours that are characterized by active cognitive processing of external percepts or internally generated thoughts and images in humans, and during AW in animals (Llinas & Ribary, 1993; Tiitinen *et al.*, 1993; Castro *et al.*, 2013, 2014). Furthermore, gamma coherence between different brain areas, which is greatest during W, has been viewed as a neural correlate of consciousness (Llinas *et al.*, 1998); coherence in the gamma frequency band decreases during narcosis (unconsciousness) induced by anaesthesia (John, 2002; Mashour, 2006).

Gamma coherence during rapid eye movement sleep induced by carbachol

A single microinjection of carbachol into the NPO induces a state that is similar to naturally-occurring REM sleep, i.e. EEG desynchronization, PGO waves, rapid eye movements, muscle atonia, postsynaptic inhibition of motoneurons, hippocampal theta rhythm, respiratory depression and the absence of the 40 Hz rhythm of the olfactory bulb that occurs during W (Morales *et al.*, 1987; Lydic & Baghdoyan, 1989; Lopez-Rodriguez *et al.*, 1994; Garzon *et al.*, 1997).

In the present study, we demonstrated that, during REMc, coherent 40 Hz oscillations were practically absent in most animals, as in naturally-occurring REM sleep. However, although gamma coherence is strongly reduced during REMc and REM sleep, gamma

TABLE 1. Gamma (35–40 Hz) z′-coherence

	AW	QW	NREM	REM	REMc	CA	Statistical significances	F
G1								
Ppr-Ppl	1.13 ± 0.03	0.84 ± 0.07	0.77 ± 0.03	0.55 ± 0.03	1.50 ± 0.04	1.10 ± 0.04	REMc vs. ALL; CA vs. NREM, REM; AW vs. QW, NREM, REM; QW vs. REM; NREM vs. REM	61
S1 l-Ppl	0.98 ± 0.04	0.41 ± 0.03	0.53 ± 0.03	0.33 ± 0.01	1.36 ± 0.06	0.78 ± 0.02	REMc vs. ALL; CA vs. AW, QW, NREM, REM; AW vs. QW, NREM, REM; NREM vs. REM	114
G2								
Ppr-Ppl	0.43 ± 0.01	0.34 ± 0.04	0.05 ± 0.01	0.05 ± 0.01	0.03 ± 0.01	0.25 ± 0.02	REMc vs. CA, AW, QW, NREM; CA vs. AW, NREM, REM; AW vs. NREM, REM; QW vs. NREM, REM	101
S1r-Ppr	0.97 ± 0.02	0.60 ± 0.04	0.48 ± 0.01	0.48 ± 0.01	0.67 ± 0.01	0.82 ± 0.01	REMc vs. CA, AW, NREM, REM; CA vs. AW, QW, NREM, REM; AW vs. QW, NREM, REM	101
G3								
Pfr-Ppr	0.72 ± 0.05	0.27 ± 0.04	0.16 ± 0.01	0.10 ± 0.01	0.10 ± 0.01	0.84 ± 0.05	REMc vs. CA, AW, QW, NREM; CA vs. QW, NREM, REM; AW vs. QW, NREM, REM; QW vs. NREM, REM; NREM vs. REM	96
Pfr-V1r	0.88 ± 0.03	0.44 ± 0.01	0.37 ± 0.01	0.12 ± 0.01	0.19 ± 0.01	0.70 ± 0.03	REMc vs. CA, AW, QW, NREM; CA vs. QW, NREM, REM; AW vs. QW, NREM, REM; QW vs. NREM, REM; NREM vs. REM	210
Ppr-V1r	1.92 ± 0.03	1.47 ± 0.01	1.38 ± 0.01	1.05 ± 0.02	1.18 ± 0.01	1.92 ± 0.05	REMc vs. CA, AW, QW, NREM; CA vs. QW, NREM, REM; AW vs. QW, NREM REM; QW vs. NREM, REM; NREM vs. REM	208
G4								
M1r-V1r	0.91 ± 0.02	0.18 ± 0.01	0.15 ± 0.01	0.02 ± 0.01	0.02 ± 0.01	0.76 ± 0.05	REMc vs. CA, AW, QW, NREM; CA vs. QW, NREM, REM; AW vs. QW, NREM, REM; QW vs. NREM, REM; NREM vs. REM.	301
M1r-Ppl	0.77 ± 0.02	0.36 ± 0.04	0.18 ± 0.01	0.02 ± 0.01	0.01 ± 0.01	0.36 ± 0.04	REMc vs. CA, AW, QW, NREM; CA vs. AW, NREM, REM; AW vs. QW, NREM, REM; QW vs. NREM, REM; NREM vs. REM.	121

The values represent mean ± standard error. $P < 0.05$, ANOVA with Tamhane tests. All derivates have the same degrees of freedom (five between groups, 66 within groups). M1, primary motor cortex; Pf, prefrontal cortex; Pp, posterior-parietal cortex; S1, somato-sensory primary cortex; V1, visual primary cortex; r, right; l, left.

ALL, the rest of the behavioral states. AW, alert wakefulness; CA, cataplexy induced by carbachol; EEG, electroencephalogram; NPO, nucleus pontis oralis; NREM, non-rapid eye movement; PGO, ponto-geniculo-occipital; QW, quiet wakefulness; REM, rapid eye movement; REMc, rapid eye movement sleep induced by carbachol; W, wakefulness.

power during these states was similar to gamma power during QW and larger compared with NREM sleep.

A robust reduction of gamma coherence during naturally-occurring REM sleep has been previously demonstrated in the cat (Castro *et al.*, 2013, 2014), rat (Cavelli *et al.*, 2015) and humans (Perez-Garci *et al.*, 2001; Cantero *et al.*, 2004; Voss *et al.*, 2009). This significant diminution in gamma coherence strongly suggests that, during REM sleep, there is a decrease in the capacity for high-frequency integration among different neocortical areas. This phenomenon may underlie the distinctive pattern of REM sleep mentation, i.e. dreams (Hobson, 2009; Nir & Tononi, 2010).

In one animal there was coherent gamma activity during REMc. Interestingly, coherent gamma activity has been observed during REM sleep solely during lucid dreaming (Voss *et al.*, 2009). In fact, externally-imposed resonance at 40 Hz by means of electrical stimulation produces self-awareness (lucidity) during REM sleep (Voss *et al.*, 2014).

We do not have an explanation as to why gamma coherence during REMc in G1 differed from that in the other animals. However, it is possible that a small difference in the site of carbachol microinjection was responsible for the atypical electrocortical pattern of activity that was present during REMc in G1. As in our previous studies, the microinjection could spread into neighbouring areas, such as the locus coeruleus or the laterodorsal tegmental nucleus, that are critical in the promotion of W (Torterolo *et al.*, 2013). Recruiting mesopontine neurons with inherent gamma activity (Urbano *et al.*, 2012) could have induced a different pattern of gamma activity in the EEG.

Gamma coherence during cataplexy induced by carbachol

Emotionally-triggered cataplexy is observed in 60–70% of patients with narcolepsy; during cataplexy, REM sleep atonia emerges during W (Guilleminault & Fromherz, 2011; Mignot, 2011). Sleep

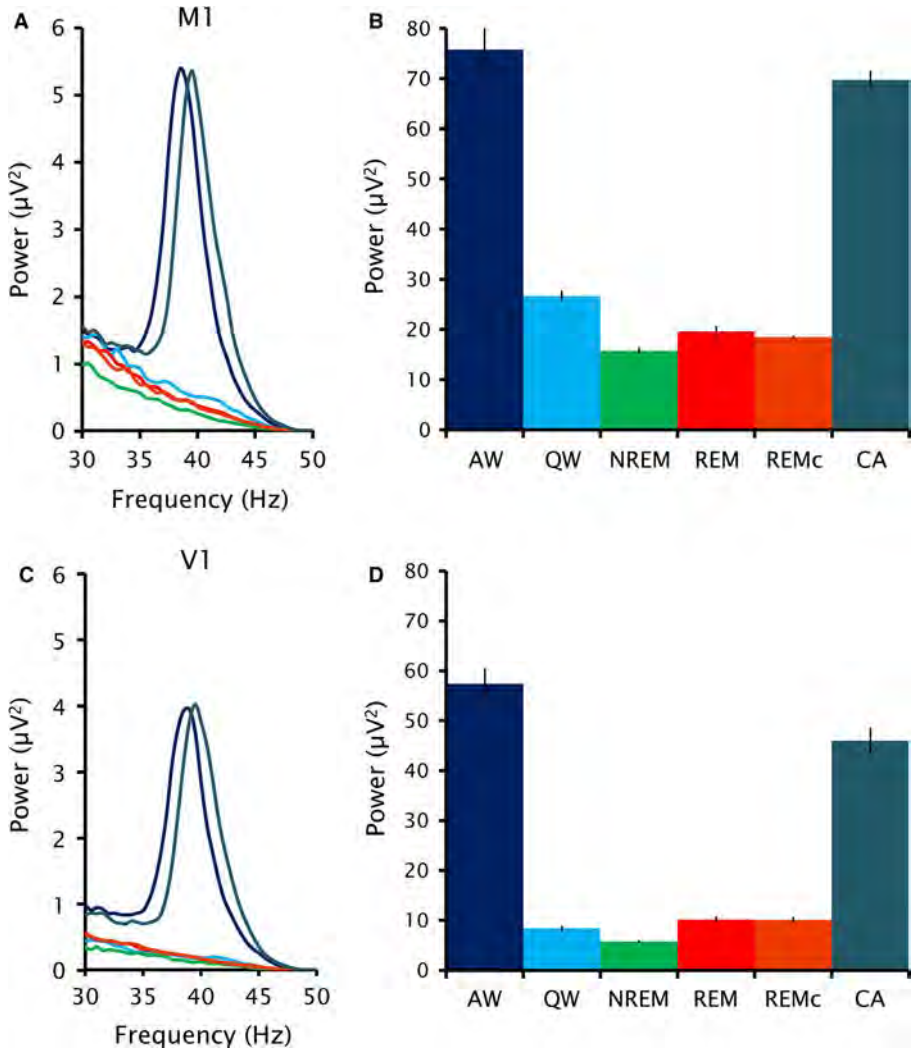

FIG. 4. Gamma band (30–45 Hz) power during naturally-occurring sleep, W and carbachol-induced states. (A) Averaged power profiles from primary motor cortex (M1) gamma activity (colours correspond to the colours of the bars in B). (B) Mean + SE of power values from the M1. (C) Averaged power profiles of gamma activity from the primary visual cortex (V1) (colours correspond to the colours of the bars in D). (D) Mean + SE of the power values from the V1. This example was obtained from animal G4 (see Table 2 for statistics).

paralysis is another condition in which REM sleep atonia takes place during W; this condition occurs in patients with narcolepsy but also as isolated periods of sleep paralysis in normal individuals (Sharpless & Grom, 2014). During sleep paralysis, the atonia is still maintained when individuals are aroused from REM sleep; fear is a common emotion during these periods (Sharpless & Grom, 2014). Interestingly, although we did not observe differences in somatomotor activity between CA and REMc, the gamma coherence during CA was high as in AW, suggesting that the animal was attentive and fully alert. However, as in naturally-occurring REM sleep, gamma coherence was absent during REMc.

Modulatory systems during rapid eye movement sleep and cataplexy

Cortical GABAergic neurons as well as glutamatergic thalamocortical neurons are critical for the generation of gamma band oscillations in the EEG (Llinas *et al.*, 1998; Buzsaki & Wang, 2012). Thalamocortical activity is modulated by regulatory systems that are comprised of small groups of neurons with a common neurotransmitter that project to various regions of the central nervous system (Jones, 2005). Cholinergic, monoaminergic and hypocretinergic neurons that integrate these systems play a critical role in the control of behavioural states (Torterolo & Vanini, 2010). By modulating the activity of the thalamocortical system, regulatory systems may control gamma oscillations and coherence.

The activity of regulatory neuronal systems has been studied during natural W and sleep states as well as during REMc by means of unit recordings or c-fos expression in different species (Yamuy *et al.*, 1995, 1998; Maloney *et al.*, 1999; Torterolo *et al.*, 2001, 2006; Lee *et al.*, 2005a,b; Lu *et al.*, 2006; Hassani *et al.*, 2009, 2010). In addition, the role of some of these systems has been assessed during cataplectic attacks in a canine model of narcolepsy (Wu *et al.*, 1999, 2004). Interestingly, as in naturally-occurring REM sleep, both serotonergic and noradrenergic neurons are inhibited during cataplectic attacks (Wu *et al.*, 1999, 2004). In contrast, although histaminergic neurons of the tuberomammillary nucleus of the hypothalamus are inhibited during naturally-occurring REM sleep, they are active during cataplexy (John *et al.*, 2004).

The activity of histaminergic neurons during cataplexy may also determine the presence and degree of gamma coherence during CA. However, as in naturally-occurring REM sleep, it is expected that,

TABLE 2. Gamma (35–40 Hz) power (μV^2)

	AW	QW	NREM	REM	REMc	CA	Statistical significance	F
G1								
Ppl	64.4 ± 2.4	18.3 ± 4.7	8.9 ± 0.3	15.1 ± 0.5	115.0 ± 12.6	32.3 ± 0.8	REMc vs. ALL; CA vs., NREM, REM; AW vs. QW, NREM, REM; NREM vs. REM	53
S1 l	15.3 ± 0.6	13.1 ± 0.9	7.6 ± 0.3	13.0 ± 0.6	28.5 ± 3.5	30.2 ± 0.7	REMc vs. ALL; CA vs. AW, QW, NREM, REM; AW vs. QW, NREM; QW vs. NREM; NREM vs. REM	27
G2								
Ppr	14.0 ± 0.8	10.8 ± 0.9	6.5 ± 0.6	9.7 ± 1.3	14.8 ± 0.6	25.3 ± 2.5	REMc vs. CA, QW, NREM, REM; CA vs. AW, QW, NREM, REM; AW vs. NREM; QW vs. NREM	26
S1r	26.2 ± 1.5	13.1 ± 0.9	6.1 ± 0.4	7.7 ± 0.5	10.2 ± 0.3	24.5 ± 2.5	REMc vs. CA, AW, NREM, REM; CA vs. QW, NREM, REM; AW vs. QW, NREM, REM; QW vs. NREM, REM	47
G3								
Pfr	60.9 ± 3.1	23.8 ± 3.6	12.5 ± 0.3	20.9 ± 0.4	20.3 ± 0.2	67.7 ± 4.7	REMc vs. CA, AW, NREM; CA vs. QW, NREM, REM; AW vs. QW, NREM, REM; NREM vs. REM	76
Ppr	57.6 ± 2.6	21.1 ± 3.9	10.3 ± 0.3	18.5 ± 0.5	12.0 ± 0.4	44.5 ± 3.8	REMc vs. CA, AW, NREM, REM; CA vs. QW, NREM, REM; AW vs. QW, NREM, REM; QW vs. NREM; NREM vs. REM	61
G4								
M1r	75.8 ± 4.3	26.7 ± 0.9	15.8 ± 0.5	19.6 ± 0.9	18.5 ± 0.2	69.8 ± 1.6	REMc vs. CA, AW, QW, NREM; CA vs. QW, NREM, REM; AW vs. QW, NREM, REM; QW vs. NREM, REM; NREM vs. REM.	195
V1r	57.4 ± 3.0	8.4 ± 0.3	5.8 ± 0.1	10.2 ± 0.5	10.1 ± 0.4	46.0 ± 2.6	REMc vs. CA, AW, NREM; CA vs. QW, NREM, REM; AW vs. QW, NREM, REM; QW vs. NREM; NREM vs. REM	195

The values represent mean ± standard error. $P < 0.05$. ANOVA with Tamhane tests. All derivates have the same degrees of freedom (five between groups, 66 within groups). The power unit is μV^2. M1, primary motor cortex; Pf, prefrontal cortex; Pp, posterior-parietal cortex; S1, somato-sensory primary cortex; V1, visual primary cortex; r, right; l, left.
ALL, the rest of the behavioral states. AW, alert wakefulness; CA, cataplexy induced by carbachol; EEG, electroencephalogram; NPO, nucleus pontis oralis; NREM, non-rapid eye movement; PGO, ponto-geniculo-occipital; QW, quiet wakefulness; REM, rapid eye movement; REMc, rapid eye movement sleep induced by carbachol; W, wakefulness.

during REMc, histaminergic neurons will drastically decrease their firing rate. Therefore, the activity of this neuronal group may be critically involved in promoting the alertness during cataplexy. Suppression of the activity of histaminergic neurons during REM sleep may be permissive for the induction of cognitive activities that are characteristic of this behavioural state, i.e. dreams.

A recent study highlighted the role of cortical-projecting GABAergic neurons of the basal forebrain in the generation of gamma oscillations in the EEG (Kim *et al.*, 2015). In addition, the authors suggested that cholinergic neurons within this area are not critical for the generation of these oscillations. The role of other wake-promoting neurons, such as dopaminergic and hypocretinergic neurons, in the generation of gamma power and coherence remains to be determined.

Gamma coherence in a paralysed body

During REM sleep, when dreams mainly occur, the networks that generate somato-motor atonia are activated. During pathological conditions such as cataplexy and sleep paralysis, REM sleep atonia is present in association with AW. Our data revealed that, when this type of paralysis is pharmacologically-induced, it is associated with a high degree of gamma power and coherence. In other words, high gamma coherence seems to be associated with alertness. Therefore, it is expected that in conditions such as the locked-in syndrome, which is mainly produced by lesions of descending motor pathways (Gosseries *et al.*, 2009) as well as during intraoperative awareness (Mashour & Avidan, 2015), gamma coherence would be high. Consequently, the present data suggest that measures of gamma power and coherence will be of assistance in diagnosing the presence of consciousness when communication with patients is not possible (Owens *et al.*, 2009).

Conclusions

In the present report, we conducted a comprehensive analysis of gamma coherence in cats during REMc, CA and naturally-occurring behavioural states. We determined that there are remarkable differences in cortical activity during REMc compared with CA, in spite of the presence of somatic muscle paralysis during both states. We conclude that EEG gamma (≈40 Hz) coherence is a trait that differentiates W from REM sleep.

Acknowledgements

This study was supported by the Programa de Desarrollo de Ciencias Básicas, PEDECIBA and by the Agencia Nacional de Investigación en Innovación (ANII) (FCE-2-2011-1-7030 grant) from Uruguay. S.C.-Z. and M.C.

currently have a postgraduate fellowship from the ANII. The authors are grateful to Giancarlo Vanini for his critical comments of the manuscript.

Abbreviations

AW, alert wakefulness; CA, cataplexy induced by carbachol; EEG, electroencephalogram; NPO, nucleus pontis oralis; NREM, non-rapid eye movement; PGO, ponto-geniculo-occipital; QW, quiet wakefulness; REM, rapid eye movement; REMc, rapid eye movement sleep induced by carbachol; W, wakefulness.

References

Baghdoyan, H.A. (1997) Cholinergic mechanism regulating REM sleep. In Schwartz, W.J. (Ed.), *Sleep Science: Integrating Basic Research and Clinical Practice. Monographs in clinical neuroscience*. Karger, Basel, pp. 88–116.

Berman, A.L. (1968) *The Brain Stem of the cat. A Cytoarchitectonic Atlas with Stereotaxic Coordinates*. University of Wisconsin, Madison.

Bullock, T.H., McClune, M.C. & Enright, J.T. (2003) Are the electroencephalograms mainly rhythmic? Assessment of periodicity in wide-band time series. *Neuroscience*, **121**, 233–252.

Buzsaki, G. & Wang, X.J. (2012) Mechanisms of gamma oscillations. *Annu. Rev. Neurosci.*, **35**, 203–225.

Cantero, J.L., Atienza, M., Madsen, J.R. & Stickgold, R. (2004) Gamma EEG dynamics in neocortex and hippocampus during human wakefulness and sleep. *NeuroImage*, **22**, 1271–1280.

Castro, S., Falconi, A., Chase, M.H. & Torterolo, P. (2013) Coherent neocortical 40-Hz oscillations are not present during REM sleep. *Eur. J. Neurosci.*, **37**, 1330–1339.

Castro, S., Cavelli, M., Vollono, P., Chase, M.H., Falconi, A. & Torterolo, P. (2014) Inter-hemispheric coherence of neocortical gamma oscillations during sleep and wakefulness. *Neurosci. Lett.*, **578**, 197–202.

Cavelli, M., Castro, S., Schwarzkopf, N., Chase, M.H., Falconi, A. & Torterolo, P. (2015) Coherent neocortical gamma oscillations decrease during REM sleep in the rat. *Behav. Brain Res.*, **281**, 318–325.

Chase, M.H. (2013) Motor control during sleep and wakefulness: clarifying controversies and resolving paradoxes. *Sleep Med. Rev.*, **17**, 299–312.

Dauvilliers, Y., Siegel, J.M., Lopez, R., Torontali, Z.A. & Peever, J.H. (2014) Cataplexy – clinical aspects, pathophysiology and management strategy. *Nat. Rev. Neurol.*, **10**, 386–395.

Edelman, G.M. & Tononi, G. (2000) *A Universe of Consciousness*. Basic Books, New York.

Garzon, M., de Andres, I. & Reinoso-Suarez, F. (1997) Neocortical and hippocampal electrical activities are similar in spontaneous and cholinergic-induced REM sleep. *Brain Res.*, **766**, 266–270.

Gosseries, O., Bruno, M., Vanhaudenhuyse, A., Laureys, S. & Schnakers, C. (2009) Consciousness in the locked-in syndrome. In Laureys, S. & Tononi, G. (Eds), *The Neurology of Consciousness: Cognitive Neuroscience and Neuropathology*. Elsevier, San Diego, pp. 191–203.

Guilleminault, C. & Fromherz, S. (2011) Narcolepsy: diagnosis and management. In Kryger, M.H., Roth, T. & Dement, W.C. (Eds), *Principles and Practices of Sleep Medicine*. Saunders, Philadelphia, pp. 957–968.

Hassani, O.K., Lee, M.G. & Jones, B.E. (2009) Melanin-concentrating hormone neurons discharge in a reciprocal manner to orexin neurons across the sleep-wake cycle. *Proc. Natl. Acad. Sci. USA.*, **106**, 2418–2422.

Hassani, O.K., Henny, P., Lee, M.G. & Jones, B.E. (2010) GABAergic neurons intermingled with orexin and MCH neurons in the lateral hypothalamus discharge maximally during sleep. *Eur. J. Neurosci.*, **32**, 448–457.

Hobson, J.A. (2009) REM sleep and dreaming: towards a theory of protoconsciousness. *Nat. Rev. Neurosci.*, **10**, 803–813.

John, E.R. (2002) The neurophysics of consciousness. *Brain Res. Brain Res. Rev.*, **39**, 1–28.

John, J., Wu, M.F., Boehmer, L.N. & Siegel, J.M. (2004) Cataplexy-active neurons in the hypothalamus: implications for the role of histamine in sleep and waking behavior. *Neuron*, **42**, 619–634.

Jones, B.E. (2005) From waking to sleeping: neuronal and chemical substrates. *Trends Pharmacol. Sci.*, **26**, 578–586.

Jouvet, M. (1965) The paradoxical phase of sleep. *Int. J. Neurol.*, **5**, 131–150.

Kim, T., Thankachan, S., McKenna, J.T., McNally, J.M., Yang, C., Choi, J.H., Chen, L., Kocsis, B., Deisseroth, K., Strecker, R.E., Basheer, R., Brown, R.E. & McCarley, R.W. (2015) Cortically projecting basal forebrain parvalbumin neurons regulate cortical gamma band oscillations. *Proc. Natl. Acad. Sci. USA.*, **112**, 3535–3540.

Kubin, L. (2001) Carbachol models of REM sleep: recent developments and new directions. *Arch. Ital. Biol.*, **139**, 147–168.

Lee, M.G., Hassani, O.K., Alonso, A. & Jones, B.E. (2005a) Cholinergic basal forebrain neurons burst with theta during waking and paradoxical sleep. *J. Neurosci.*, **25**, 4365–4369.

Lee, M.G., Hassani, O.K. & Jones, B.E. (2005b) Discharge of identified orexin/hypocretin neurons across the sleep-waking cycle. *J. Neurosci.*, **25**, 6716–6720.

Llinas, R. & Ribary, U. (1993) Coherent 40-Hz oscillation characterizes dream state in humans. *Proc. Natl. Acad. Sci. USA.*, **90**, 2078–2081.

Llinas, R., Ribary, U., Contreras, D. & Pedroarena, C. (1998) The neuronal basis for consciousness. *Philos. T. Roy. Soc. B.*, **353**, 1841–1849.

Lopez-Rodriguez, F., Kohlmeier, K., Morales, F.R. & Chase, M.H. (1994) State dependency of the effects of microinjection of cholinergic drugs into the nucleus pontis oralis. *Brain Res.*, **649**, 271–281.

Lu, J., Jhou, T.C. & Saper, C.B. (2006) Identification of wake-active dopaminergic neurons in the ventral periaqueductal gray matter. *J. Neurosci.*, **26**, 193–202.

Luppi, P.H., Gervasoni, D., Verret, L., Goutagny, R., Peyron, C., Salvert, D., Leger, L. & Fort, P. (2007) Paradoxical (REM) sleep genesis: The switch from an aminergic-cholinergic to a GABAergic-glutamatergic hypothesis. *J. Physiology-Paris*, **100**, 271–283.

Lydic, R. & Baghdoyan, H.A. (1989) Cholinoceptive pontine reticular mechanisms cause state-dependent respiratory changes in the cat. *Neurosci. Lett.*, **102**, 211–216.

Maloney, K.J., Mainville, L. & Jones, B.E. (1999) Differential c-Fos expression in cholinergic, monoaminergic, and GABAergic cell groups of the pontomesencephalic tegmentum after paradoxical sleep deprivation and recovery. *J. Neurosci.*, **19**, 3057–3072.

Mashour, G.A. (2006) Integrating the science of consciousness and anesthesia. *Anesth. Analg.*, **103**, 975–982.

Mashour, G.A. & Avidan, M.S. (2015) Intraoperative awareness: controversies and non-controversies. *Brit. J. Anaesth.*, **115**(Suppl 1), i20–i26.

Mignot, E. (2011) Narcolepsy: pathophysiology and genetic predisposition. In Krieger, M.H., Roth, T. & Dement, W. (Eds), *Principles and Practices of Sleep Medicine*. Saunders, Philadelphia, pp. 938–956.

Morales, F.R., Engelhardt, J.K., Soja, P.J., Pereda, A.E. & Chase, M.H. (1987) Motoneuron properties during motor inhibition produced by microinjection of carbachol into the pontine reticular formation of the decerebrate cat. *J. Neurophysiol.*, **57**, 1118–1129.

Nir, Y. & Tononi, G. (2010) Dreaming and the brain: from phenomenology to neurophysiology. *Trends Cogn. Sci.*, **14**, 88–100.

Owens, A., Schiff, N.D. & Laureys, S. (2009) The assessment of conscious awareness in the vegetative state. In Laureys, S. & Tononi, G. (Eds), *The Neurology of Consciousness: Cognitive Neuroscience and Neuropathology*. Elsevier, San Diego, pp. 163–172.

Perez-Garci, E., del-Rio-Portilla, Y., Guevara, M.A., Arce, C. & Corsi-Cabrera, M. (2001) Paradoxical sleep is characterized by uncoupled gamma activity between frontal and perceptual cortical regions. *Sleep*, **24**, 118–126.

Reinoso-Suarez, F., de Andres, I., Rodrigo-Angulo, M.L. & Garzon, M. (2001) Brain structures and mechanisms involved in the generation of REM sleep. *Sleep Med. Rev.*, **5**, 63–77.

Rieder, M.K., Rahm, B., Williams, J.D. & Kaiser, J. (2010) Human gamma-band activity and behavior. *Int. J. Psychophysiol.*, **79**, 39–48.

Sharpless, B.A. & Grom, J.L. (2014) Isolated sleep paralysis: fear, prevention, and disruption. *Behav. Sleep Med.*, 1–6.

Siegel, J.M. (2011) REM sleep. In Kryger, M.H., Roth, T. & Dement, W.C. (Eds), *Principles and Practices of Sleep Medicine*. Elsevier-Saunders, Philadelphia, pp. 92–111.

Tiitinen, H., Sinkkonen, J., Reinikainen, K., Alho, K., Lavikainen, J. & Naatanen, R. (1993) Selective attention enhances the auditory 40-Hz transient response in humans. *Nature*, **364**, 59–60.

Tononi, G. (2009) Sleep and dreaming. In Laureys, S. & Tononi, G. (Eds), *The Neurology of Consciousness: Cognitive Neuroscience and Neuropathology*. Elsevier, San Diego, pp. 89–107.

Torterolo, P. & Vanini, G. (2010) Nuevos conceptos sobre la generación y el mantenimiento de la vigilia. *Revista Neurología*, **50**, 747–758.

Torterolo, P., Yamuy, J., Sampogna, S., Morales, F.R. & Chase, M.H. (2001) Hypothalamic neurons that contain hypocretin (orexin) express c-fos during active wakefulness and carbachol-induced active sleep. *Sleep Res. Online*, **4**, 25–32.

Torterolo, P., Sampogna, S., Morales, F.R. & Chase, M.H. (2006) MCH-containing neurons in the hypothalamus of the cat: searching for a role in the control of sleep and wakefulness. *Brain Res.*, **1119**, 101–114.

Torterolo, P., Sampogna, S. & Chase, M.H. (2013) Hypocretinergic and non-hypocretinergic projections from the hypothalamus to the REM sleep executive area of the pons. *Brain Res.*, **1491**, 68–77.

Torterolo, P., Castro-Zaballa, S., Cavelli, M., Velasquez, N., Brando, V., Falconi, A., Chase, M.H. & Migliaro, E.R. (2015) Heart rate variability during carbachol-induced REM sleep and cataplexy. *Behav. Brain Res.*, **291**, 72–79.

Uhlhaas, P.J., Pipa, G., Lima, B., Melloni, L., Neuenschwander, S., Nikolic, D. & Singer, W. (2009) Neural synchrony in cortical networks: history, concept and current status. *Front. Integr. Neurosci.*, **3**, 17.

Uhlhaas, P.J., Pipa, G., Neuenschwander, S., Wibral, M. & Singer, W. (2011) A new look at gamma? High- (>60 Hz) gamma-band activity in cortical networks: function, mechanisms and impairment. *Prog. Biophys. Mol. Biol.*, **105**, 14–28.

Urbano, F.J., Kezunovic, N., Hyde, J., Simon, C., Beck, P. & Garcia-Rill, E. (2012) Gamma band activity in the reticular activating system. *Front. Neurol.*, **3**, 6.

Ursin, R. & Sterman, M. (1981) *Manual for Standardized Scoring of Sleep and Waking States in Adult Cats*. BIS/BRI, University of California, Los Angeles.

Voss, U., Holzmann, R., Tuin, I. & Hobson, J.A. (2009) Lucid dreaming: a state of consciousness with features of both waking and non-lucid dreaming. *Sleep*, **32**, 1191–1200.

Voss, U., Holzmann, R., Hobson, A., Paulus, W., Koppehele-Gossel, J., Klimke, A. & Nitsche, M.A. (2014) Induction of self awareness in dreams through frontal low current stimulation of gamma activity. *Nat. Neurosci.*, **17**, 810–812.

Wu, M.F., Gulyani, S.A., Yau, E., Mignot, E., Phan, B. & Siegel, J.M. (1999) Locus coeruleus neurons: cessation of activity during cataplexy. *Neuroscience*, **91**, 1389–1399.

Wu, M.F., John, J., Boehmer, L.N., Yau, D., Nguyen, G.B. & Siegel, J.M. (2004) Activity of dorsal raphe cells across the sleep-waking cycle and during cataplexy in narcoleptic dogs. *J. Physiol.*, **554**, 202–215.

Yamuy, J., Sampogna, S., Lopez-Rodriguez, F., Luppi, P.H., Morales, F.R. & Chase, M.H. (1995) Fos and serotonin immunoreactivity in the raphe nuclei of the cat during carbachol-induced active sleep: a double-labeling study. *Neuroscience*, **67**, 211–223.

Yamuy, J., Sampogna, S., Morales, F.R. & Chase, M.H. (1998) c-fos expression in mesopontine noradrenergic and cholinergic neurons of the cat during carbachol-induced active sleep: a double labeling study. *Sleep Res. Online*, **1**, 28–40.

Anexo 3

(Castro-Zaballa et al., 2018)

frontiers in Psychiatry

ORIGINAL RESEARCH
published: 17 January 2019
doi: 10.3389/fpsyt.2018.00766

EEG 40 Hz Coherence Decreases in REM Sleep and Ketamine Model of Psychosis

Santiago Castro-Zaballa[1], *Matías Lorenzo Cavelli*[1], *Joaquin Gonzalez*[1], *Antonio Egidio Nardi*[2,3], *Sergio Machado*[2,3,4], *Cecilia Scorza*[5] *and Pablo Torterolo*[1,4*]

[1] *Laboratorio de Neurobiología del Sueño, Departamento de Fisiología, Facultad de Medicina, Universidad de la República, Montevideo, Uruguay,* [2] *Laboratório de Pânico e Respiração, Instituto de Psiquiatria da Universidade Federal do Rio de Janeiro, Rio de Janeiro, Brazil,* [3] *Laboratório de Neurociência da Atividade Física, Universidade Salgado de Oliveira, Rio de Janeiro, Brazil,* [4] *The Intercontinental Neuroscience Research Group, Merida, Mexico,* [5] *Departamento de Neurofarmacología Experimental, Instituto de Investigaciones Biológicas Clemente Estable, Montevideo, Uruguay*

Cognitive processes are carried out during wakefulness by means of extensive interactions between cortical and subcortical areas. In psychiatric conditions, such as psychosis, these processes are altered. Interestingly, REM sleep where most dreams occurs, shares electrophysiological, pharmacological, and neurochemical features with psychosis. Because of this fact, REM sleep is considered a natural model of psychosis. Ketamine is a non-competitive N-methyl-D-aspartate (NMDA) receptor antagonist that at sub-anesthetic dose induces psychotomimetic-like effects in humans and animals, and is employed as a pharmacological model of psychosis. Oscillations in the gamma frequency band of the electroencephalogram (EEG), mainly at about 40 Hz, have been involved in cognitive functions. Hence, the present study was conducted to analyze the EEG low gamma (30–45 Hz) band power and coherence of the cat, in natural (REM sleep) and pharmacological (sub-anesthetic doses of ketamine) models of psychosis. These results were compared with the gamma activity during alert (AW) and quiet wakefulness (QW), as well as during non-REM (NREM) sleep. Five cats were chronically prepared for polysomnographic recordings, with electrodes in different cortical areas. Basal recordings were obtained and ketamine (5, 10, and 15 mg/kg, i.m.) was administrated. Gamma activity (power and coherence) was analyzed in the abovementioned conditions. Compared to wakefulness and NREM sleep, following ketamine administration gamma coherence decreased among all cortical regions studied; the same coherence profile was observed during REM sleep. On the contrary, gamma power was relatively high under ketamine, and similar to QW and REM sleep. We conclude that functional interactions between cortical areas in the gamma frequency band decrease in both experimental models of psychosis. This uncoupling of gamma frequency activity may be involved in the cognitive features shared by dreaming and psychosis.

Keywords: gamma, schizophrenia, electroencephalogram, NMDA, cognition, dreams

OPEN ACCESS

Edited by:
Diogo Telles-Correia, Universidade de Lisboa, Portugal

Reviewed by:
Armando D'Agostino, University of Milan, Italy
Dinesh Pal, University of Michigan, United States

****Correspondence:***
Pablo Torterolo
ptortero@fmed.edu.uy

Specialty section:
This article was submitted to Psychopathology, a section of the journal Frontiers in Psychiatry

Received: *06 August 2018*
Accepted: *21 December 2018*
Published: *17 January 2019*

Citation:
Castro-Zaballa S, Cavelli ML, Gonzalez J, Nardi AE, Machado S, Scorza C and Torterolo P (2019) EEG 40 Hz Coherence Decreases in REM Sleep and Ketamine Model of Psychosis. Front. Psychiatry 9:766. doi: 10.3389/fpsyt.2018.00766

INTRODUCTION

The word psychosis (from Greek: "disorder of the mind") is used in psychiatry to define a mental state in which there is a loss of contact with reality. The "Diagnostic and Statistical Manual of Mental Disorders (DSM), 5th Edition (2013)" classifies psychotic disorders in a chapter entitled "Schizophrenia spectrum and other psychotic disorders." Schizophrenia is the most prevalent and studied among these disorders (1). This pathology is characterized by the presence of positive symptoms (such as delusions and visual and/or auditory hallucinations, as well as disorganized behavior due to reduced ability of reality testing), negatives symptoms (apathy, loss of motivation and serious social isolation), as well as memory and executive function disorders (2–5).

Several hypotheses that attempt to explain the pathophysiology of psychotic disorders have been postulated (6, 7). One accepted hypothesis holds that glutamatergic hypofunction mediated by the N-Methyl-D-Aspartate receptor (NMDA-R) is a key mechanism contributing to positive, negative and cognitive symptoms observed in this condition (6, 8–17). This is based on clinical reports showing that the consumption of phencyclidine (PCP) or ketamine (both non-competitive antagonists of NMDA-R) induces, in healthy individuals, the characteristic alterations of the psychotic disorders, and exacerbates symptoms in patients with schizophrenia (14, 18). Therefore, the use of models involving NMDA-R hypofunction is considered a valid pharmacological model for the study of the neurobiological bases of psychotic disorders (16, 19, 20). In animals, the systemic administration of NMDA-R antagonists, such as PCP, ketamine or dizocilpine/MK-801, induce a motor behavioral syndrome, characterized by hyperlocomotion with a disorganized pattern, stereotypies, and signs of ataxia (20–22). This syndrome has been linked to the positive symptomatology of schizophrenia (12, 23). In addition, NMDA-R antagonists also produce sensory deficits and alterations in cognitive function (working and associative memory, attention) that mimic the disorders observed in psychosis; antipsychotic drugs prevent these behaviors (20–22, 24).

REM sleep is a behavioral state that has been implicated in several functions, such as brain development, learning and memory as well as in facilitating cortical plasticity. It has also been involved in increasing general creativity, and is considered critical for the well-being of the individuals (25).

Most vivid and articulate dreams occur during REM sleep (26, 27). REM sleep dreams and psychosis share important characteristics, such as internal perceptions independent of external stimulation, with a lack of criticism about the reality of the experience (28–32). REM sleep also shares neurophysiological, and neurochemical characteristics with psychosis; because of this fact, it is considered a natural model of this condition (28–30).

There are several experimental results showing that neocortical oscillations at the gamma frequency (30–100 Hz) band, mainly around 40 Hz, are involved in cognitive functions (33–35). An increase in gamma power typically appears during behaviors that are characterized by the cognitive processing of external percepts or internally generated thoughts and images (34, 36, 37). Gamma activity has been also observed during alert or attentive wakefulness (W), not only in humans, but also in animals (38–42).

The degree of electroencephalogram (EEG) coherence between two cortical regions is believed to reflect the strength of the functional interconnections that occur between them (43, 44). Recently, Cavelli et al. have proposed that the absence of EEG gamma coherence in a local activated cortical state is a conserved trait of REM sleep in mammals (45). In fact, although gamma power is relatively high, gamma coherence is lost during REM sleep in cats, rats and humans (46–49). Interestingly, gamma coherence values during lucid dreaming are between wakefulness and REM sleep (47), and self-awareness in dreams can be induced through frontal low current stimulation at gamma frequency (50).

The similarities of the cognitive functions during REM sleep and under the effect of ketamine, highlights the importance of comparing the EEG gamma activity in both experimental models of psychosis. Hence, the aim of the present study is to compare gamma (30–45 Hz) power and coherence that reflect short and long-range gamma synchronization, respectively (45, 46), during REM sleep with the effect induced by subanesthetic doses of ketamine.

MATERIALS AND METHODS

Five adult cats were used in this study; four of them were also utilized in a previous report (51). The animals were obtained from and determined to be in good health by the Institutional Animal Care Facility. All experimental procedures were conducted in accord with the *Guide for the Care and Use of Laboratory Animals* (8th edition, National Academy Press, Washington DC, 2011) and were approved by Institutional and National Animal Care Commissions (Protocol N° 070153-000089-17). Adequate measures were taken to minimize pain, discomfort or stress of the animals. In addition, all efforts were made to use the minimum number of animals necessary to produce reliable scientific data.

The surgical procedures were the same as in previous studies (48, 51, 52); hence, only a brief description of the surgical procedures will be done. Following general anesthesia, the head was positioned in a stereotaxic frame and the skull was exposed. Stainless steel screw electrodes (1.4 mm diameter) were placed on the surface (above the dura matter) of different cortical areas. **Figure 1A** shows the sites of the recording electrodes used in this study. Note that because the animals were not prepared specifically for this work, we did not analyze exactly the same cortices in all of them. The electrodes were connected to a Winchester plug, which together with two plastic tubes were bonded to the skull with acrylic cement in order to maintain the animals' head in fixed position without pain or pressure. After recovery from surgical procedures, they were adapted to the recording environment for a period of at least 2 weeks.

Experimental sessions of 4 h were conducted between 11 a.m. and 3 p.m. in a temperature-controlled environment (21–23°C).

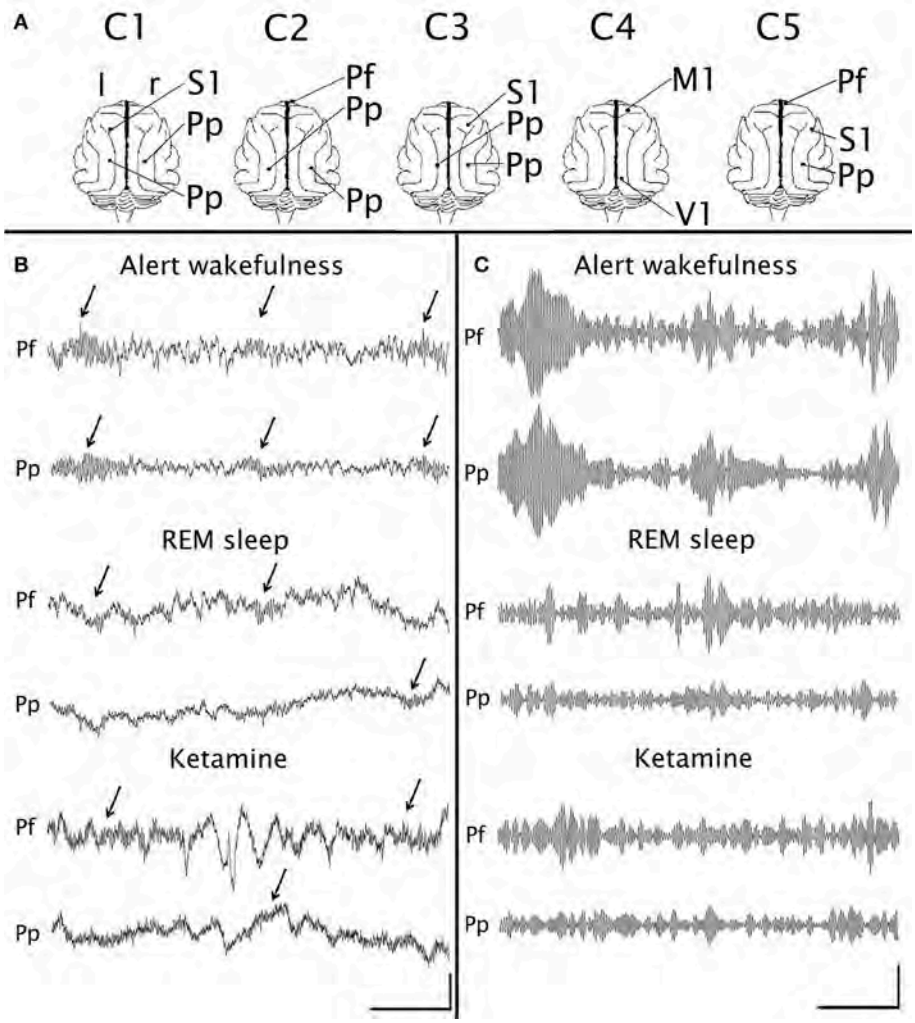

FIGURE 1 | Gamma EEG oscillations under the effect of ketamine. **(A)** Position of the recording electrodes on the surface of the cerebral cortex. The recordings were referenced to an indifferent common inactive electrode located on the frontal sinus. C1-C5, identification name of the animals. M1, primary motor cortex; Pf, prefrontal cortex; Pp, posterior-parietal cortex; S1, primary somato-sensory cortex; V1, primary visual cortex; r, right; l, left. **(B)** Simultaneous raw recordings from a representative animal of the prefrontal (Pf) and parietal posterior (Pp) cortices during alert wakefulness, REM sleep and under the administration of ketamine (15 mg/kg). The arrows indicate the gamma "bursts." **(C)** Filtered recordings (bandpass 30–45 Hz) of the same recordings as in **(B)**. Calibration bars: 1 s, 200 μV for **(B)**; 1 s, 20 μV for **(C)**.

During these sessions (as well as during the adaptation sessions), the animals' head was held in a stereotaxic position by four steel bars that were placed into the chronically implanted plastic tubes, while the body rested in a sleeping bag (semi-restricted condition).

The EEG activity was recorded with a monopolar (referential) configuration, utilizing a common reference electrode located in the left frontal sinus. The electromyogram (EMG) of the nuchal muscles, which was recorded by means of acutely placed bipolar electrode, was also monitored. The electrocardiogram (ECG), by electrodes acutely placed on the skin over the pre-cordial region, and respiratory activity by means of a micro-effort piezo crystal infant sensor were also recorded. Each cat was recorded daily for ∼30 days in order to obtain complete basal and treatment data sets.

Bioelectric signals were amplified (×1,000), filtered (0.1–500 Hz), sampled (1,024 Hz, 2^{16} bits) and stored in a PC using the Spike 2 software (Cambridge Electronic Design).

Data were obtained after ketamine administration as well as during spontaneously occurring quiet wakefulness (QW), non-REM (NREM) sleep and REM sleep. Alert wakefulness (AW) was induced for a period of 300 s by sound stimuli; in drug-free recordings, the stimuli were introduced ∼30 min after the beginning of the recording sessions. The sound consisted of clicks (0.1 ms in duration) of 60–100 dB SPL with a variable frequency of presentation (1–500 Hz, modified at random) in order to avoid habituation (48, 53). In occasions, AW was induced by visual stimulation, by means of placing a mirror in front of the animal for 300 s (48). It is important to note that in one animal (C4), the sleep and W data was the same as the one used in Torterolo et al.

(51). In other three animals, data were obtained from recordings performed specifically for the present study, but from animals that were also utilized in Torterolo et al. (51). The fifth animal was not used in previous studies.

Five, 10, and 15 mg/kg i.m. of ketamine (Ketonal®, Richmond Veterinaria S.A.) were administered to five animals. These three doses were administered four times in each animal in different experimental sessions in a counterbalanced order (each animal received 16 doses of ketamine). The recovery time between consecutive ketamine experiments was 72 h.

Ketamine (50 mg/ml) was diluted in benzethonium chloride, hydrochloric acid, and water (solution for veterinary use). In pilot experiments, saline was injected (to rule out that the effect obtained was due to the pain caused by the injection) and the EEG analysis showed similar results to those observed in baseline recordings; therefore, basal recordings (without injections) were used as control.

Sound stimuli during 300 s were applied 10 min after ketamine injection (**Supplementary Figure 1**). These sound stimuli had the same characteristics as those used to induce AW (48).

Data were analyzed as in our previous studies (48, 51, 52). Sleep and W were quantified in epochs of 10 s. In order to analyze coherence between pairs of EEG electrodes, 12 artifact-free periods of 100 s were examined during each behavioral state (1,200 s for each behavioral state). For each pair of recordings, data were obtained during four recording sessions following ketamine administration, and from four basal (without injections) recording sessions for AW, QW, NREM, and REM sleep. Gamma activity following ketamine administration was evaluated in windows taken during the stimulus, and temporarily moved away 300 s from it (see **Supplementary Figure 1**). These windows were chosen during the maximum effect of ketamine (between 5 and 20 min after the injection, see **Figures 2**, **3**).

For each selected period of 100 s, Magnitude Squared Coherence was analyzed for the low gamma frequency band (30–45 Hz) by means of Spike 2 script COHER 1S (Cambridge Electronic Design) (see (48), for details in the definition of coherence). This period of analysis was divided into 100 time-blocks with a sample rate of 1,024 Hz, a bin size of 2,048 samples and a resolution of 0.5 Hz. We employed the same time-windows as for the coherence analysis, to process gamma power (by means of the Spike 2 script COHER 1S). Recordings were also filtered (band pass 30–45 Hz) using Spike 2 digital finite impulse response filters. Averages of the signals were also performed.

In order to improve the quality of the Figures, in **Figures 2**, **4** two different approaches were used in order to display the EEG power. In **Figure 2** a multitaper method was used as described by Babadi and Brown (54). This method utilized a series of discrete prolate spheroidal sequences (Slepian) for the Fast Fourier Transform. The procedure reduces the variance of the power spectrum estimate, offering a better power estimation. On **Figure 4**, a wavelet transformed was applied in order to improve time and frequency localization. Morlet wavelet was utilized because of its proven suitability for EEG analysis (55). Both of these analyses were performed employing the Chronux Toolbox and the ND Tools Toolbox, running on self-built MATLAB routines.

The mean power and z′-coherence of the gamma band in each EEG channel or derivative (pair of EEG channels) were calculated for every behavioral state and drug treatments. The significance of the differences among conditions was evaluated for each cat with one-way ANOVA and Tamhane *post-hoc* test. In order to analyze the gamma coherence averaged in the whole group of animals, the mean intra-hemispheric z′-coherence of the gamma band between anterior (S1 for C1 and C3, Pf for C2 and C5, and M1 for C4; see **Figure 1A**) and posterior (V1 for C4, and Pp for the rest of the animals) cortices was evaluated. For this purpose, we utilized the repeated measures ANOVA (rmANOVA) and Bonferroni *post-hoc* test. The criterion used to reject null hypotheses was $p < 0.05$.

RESULTS

Following the administration of the different doses of ketamine, the animals were awake with their eyes wide open; hence the doses employed were below anesthesia threshold. However, especially with higher doses, after 5 min they stopped tracking the experimenters with their eyes. When the animals were put back in freely moving condition (at the end of the experiments, 3–4 h after the injection of ketamine), they were able to ambulate.

The results will be described in the following way. First, the different effects of the highest dose (15 mg/kg) will be presented. Thereafter, a dose-response curve will be shown.

Raw and Filtered Recordings

Figures 1B,C show raw and filtered (band pass 30–45 Hz) simultaneous recordings of the prefrontal and posterior parietal cortices, during AW, REM sleep and following ketamine administration (15 mg/kg). In AW, "bursts" of gamma oscillations appear simultaneously in both channels (arrows in **Figure 1B**), while during REM sleep these oscillations have lower amplitude and duration, and do not occur simultaneously in both channels. Under the effect of ketamine administration, gamma oscillations have very similar characteristics to those observed during REM sleep. As was described before (56, 57), some slow waves were also present after the injection of ketamine (**Figure 1B**); the analysis of these waves was out of the scope of the present study.

DYNAMIC OF THE GAMMA POWER AND COHERENCE FOLLOWING KETAMINE ADMINISTRATION

In **Figure 2**, the power and coherence analyses of a representative recording of C5 are shown after ketamine administration (15 mg/kg). **Figure 2A** shows the dynamic evolution of the power. First, there was a brief period of high gamma activity in the narrow 30–45 band triggered by the injection pinch; thereafter, the gamma power was first reduced and then increased to encompass a much wider range of frequencies (between 30 and 60 Hz). After 2 h, large values of 30–45 Hz power begins to

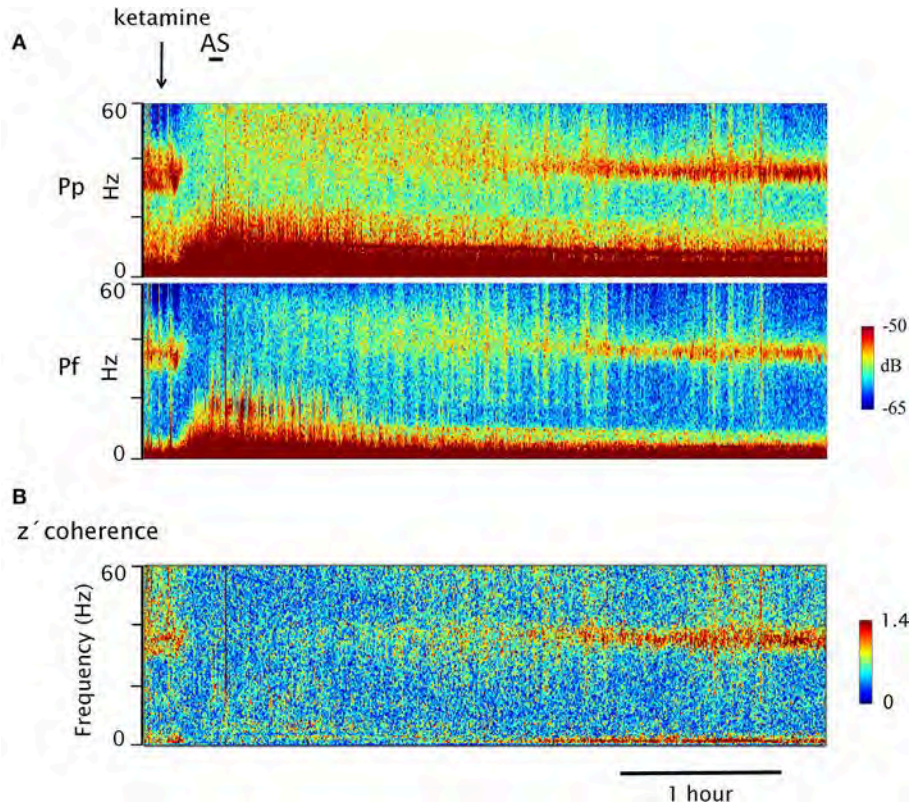

FIGURE 2 | Dynamic evolution of EEG gamma power and z′ coherence following the injection of ketamine. **(A)** Gamma power spectrograms of prefrontal (Pf) and posterior parietal (Pp) cortices following ketamine injection (arrow) in a representative animal (C5). The horizontal bar represents sound stimulation (AS). Power is represented in a color code. **(B)** Coherogram of the gamma z′-coherence between Pf and Pp cortices (same recordings as in **A**). Time and the frequency are displayed on the horizontal and vertical axes (depth), respectively; the z-coherence is represented in a color code.

reappear. **Figure 2B** exhibits the dynamic evolution of the z′-coherence between the prefrontal and parietal-posterior cortices. Following a brief increase in gamma coherence (post-injection alertness), it decreased to very low levels. The sound stimulus (labeled as AS in **Figure 2A**) had no effect, neither on the power nor on the gamma coherence. Approximately 2 h following the administration of the drug, gamma coherence began to increase, and reach values similar to AW about 3 h after the injection.

Figure 3 shows the dynamic evolution of the z′-coherence between prefrontal and posterior-parietal cortices in two representative recordings of C2 (basal recording in **Figure 3A**, and following the administration of ketamine in **Figure 3B**). In the recording shown in **Figure 3A**, sound (AS) and visual (VS) stimulation were performed. After that, the animal had periods of sleep (an episode of REM sleep is indicated). Both the AS and VS caused an increase in gamma coherence; during REM sleep the coherence decreases to a minimum level. In **Figure 3B**, the effect of ketamine (15 mg/kg) is shown. After a brief increase in gamma coherence due to the injection pinch, it decreased down to REM sleep level. The sound stimulation also had no effect on gamma coherence. The changes in gamma power and coherence induced by ketamine displayed in **Figures 2**, **3** were observed in all the animals; C5 and C2 had the longest and shortest duration of the effect, respectively.

In order to analyze more deeply the characteristics of the gamma activity during AW, REM sleep and under the effect of ketamine, gamma envelopes and spectrograms are displayed in **Figure 4**. In this Figure, it is visually simple to compare the dynamics of the "gamma bursts" among conditions. A marked coupling can be observed between the cortices during AW, whereas this coupling disappears both during REM sleep and under ketamine. Also, the average waveforms of the gamma bursts during REM sleep and under the effect of ketamine are similar (**Figure 4**, insets); these "bursts" are different from those of AW.

Mean Gamma Power and Coherence

Under ketamine, when contrasting the values of power and gamma coherence during the windows affected by the sound stimulus and not affected by it, there were no significant differences (**Figures 2**, **3**; quantitative data not shown). Therefore, to simplify, only the analysis of the windows not affected by the sound stimulus will be described.

Figure 5A shows the analysis of the power spectrum of the prefrontal cortex of C5 during W, sleep and under ketamine. Ketamine generates alterations in the low frequency bands and a small peak in the beta band (arrows). Focusing on gamma band, we observed that 30–45 Hz gamma band power under

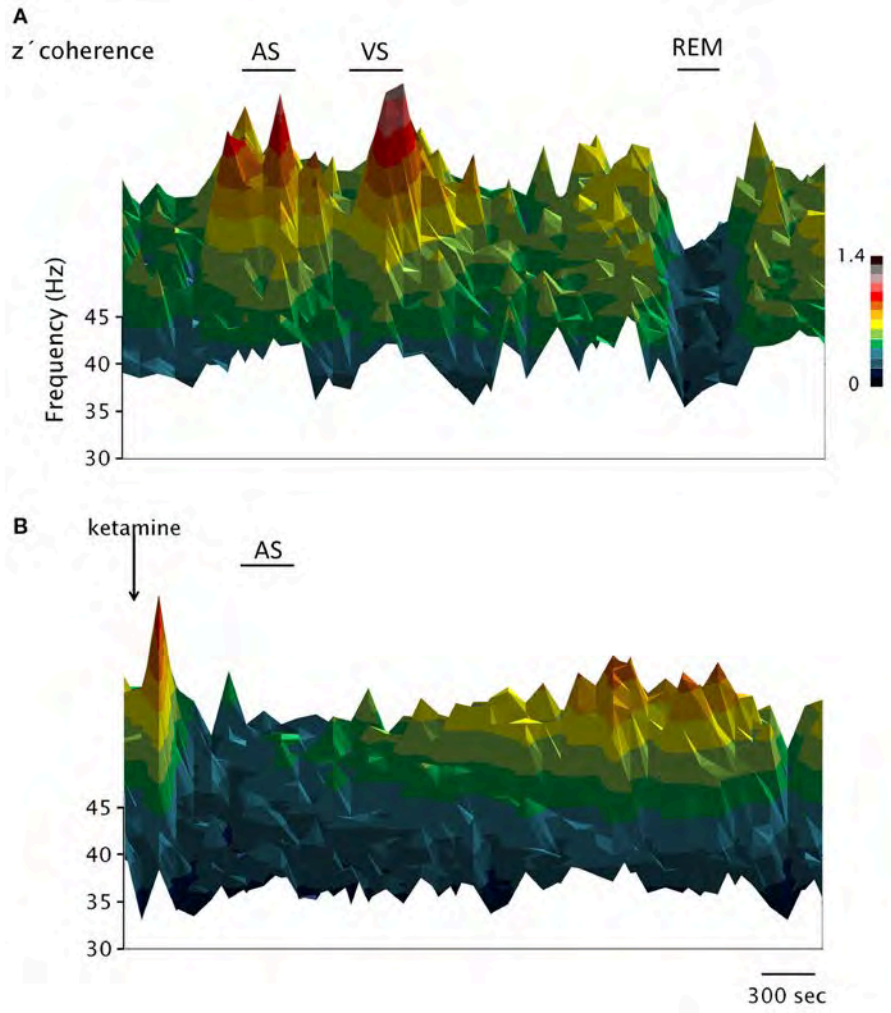

FIGURE 3 | Dynamic evolution of the EEG gamma z′-coherence during wakefulness, sleep and under the effect of ketamine. 3D coherograms of the gamma z′-coherence of simultaneous recordings of the prefrontal and posterior-parietal cortices of C2. The horizontal axis indicates the time, the vertical (depth) axis indicates frequency while the z′-coherence is represented by color code. **(A,B)** Represent the coherograms of a basal recording and following the administration of ketamine (15 mg/kg), respectively. AS, sound stimulus; VS, visual stimulus.

ketamine is lower than AW, but comparable to QW or REM sleep. However, the gamma power at frequencies above 45 Hz (high gamma, arrowhead) is greater than in physiological states.

Gamma power values for each cat and cortex are shown in **Table 1**. The power under ketamine (15 mg/kg) are comparable to QW and REM sleep; in most cases, are minor than AW and larger than NREM sleep.

Figure 5B illustrates the z′-coherence profiles between prefrontal and posterior- parietal cortices of C5 during AW, REM sleep and under the effect of ketamine (15 mg/kg). The z′-coherence profiles under ketamine were similar to those during REM sleep. **Figure 5C** shows the average coherence profiles of the gamma band for all physiological and pharmacological states in this representative animal (C5). Gamma z′-coherence under the effect of ketamine was as low as during REM sleep; gamma z′-coherence in these conditions was lower compared to the others behavioral states.

Figure 6 shows, for all animals, the gamma coherence between the anterior and posterior cortices for all behavioral states and ketamine. The level of z′-coherence under ketamine was similar to REM sleep. Although the rmANOVA only distinguished between ketamine and AW, when we analyzed each animal individually there were significant differences between all the states. **Table 2** displays the z′-coherence for all the combinations of cortices and for all the animals. Ketamine decreases gamma coherence down to REM sleep levels (or even lower) for all the combinations of cortices studied of the five animals.

Dose-Response Curve

Figure 7 shows the average gamma z′-coherence values for AW and ketamine at doses of 5, 10, and 15 mg/kg for the 5 animals. In some animals, the doses of 5 and 10 mg/kg had intermediate coherence values between AW and the dose of 15 mg/kg. In

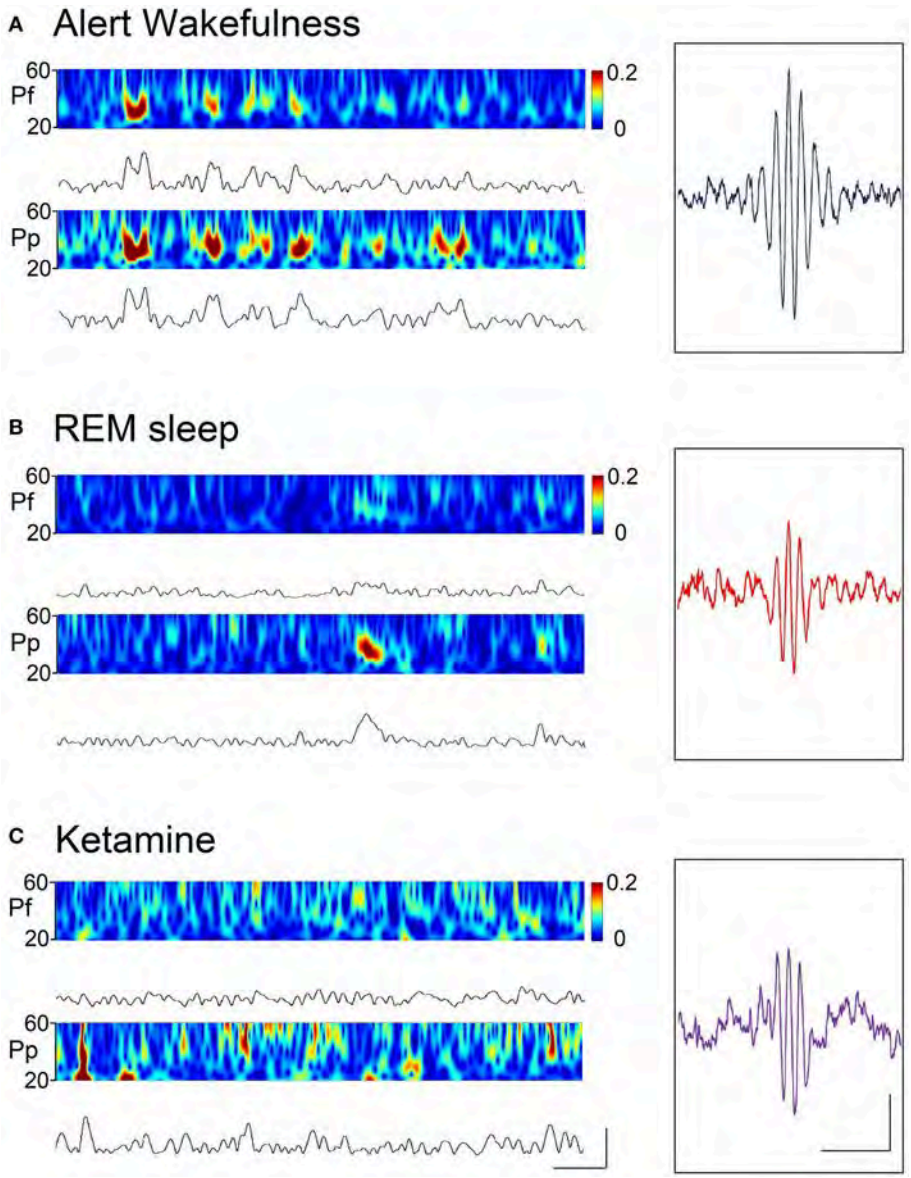

FIGURE 4 | Spectrograms (by means of the wavelet function) and rectified gamma (30–45 Hz) band or envelopes, during alert wakefulness **(A)**, REM sleep **(B)**, and following the administration of ketamine (15 mg/kg) **(C)** of a representative animal. Calibration bars; 400 ms and 30 μV. Insets. Gamma "bursts" averaged from a filtered recording (high-pass 3 Hz) selected from the prefrontal cortex. Hundred random bursts were selected and averaged; the "trigger" was the peak of the wave with greater amplitude of the "burst." Calibration bars: 200 ms and 10 μV.

others, the doses of 5 and 10 mg/kg had similar gamma z′-coherence than 15 mg/kg.

DISCUSSION

We have shown that ketamine in sub-anesthetic doses produces a decrease in z′-coherence in the low gamma frequency band (30–45 Hz). This decrease in gamma z′-coherence was similar to that occurring during REM sleep. Furthermore, gamma coherence under ketamine was not affected by novel stimuli, which in basal conditions alert the animal causing a large increase in gamma coherence. On the contrary, 30–45 Hz gamma power remained at a level similar to that observed in QW and REM sleep, but greater than during NREM sleep.

Technical Considerations

We used the cat as the animal model because it has well-defined, consolidated sleep and waking states. The recordings were obtained in semi-restricted conditions, which has the advantage that differences among states are the states *per se*; postures or movements did not influence the recordings. Furthermore, this condition reduces the possibility of artifacts. This animal model

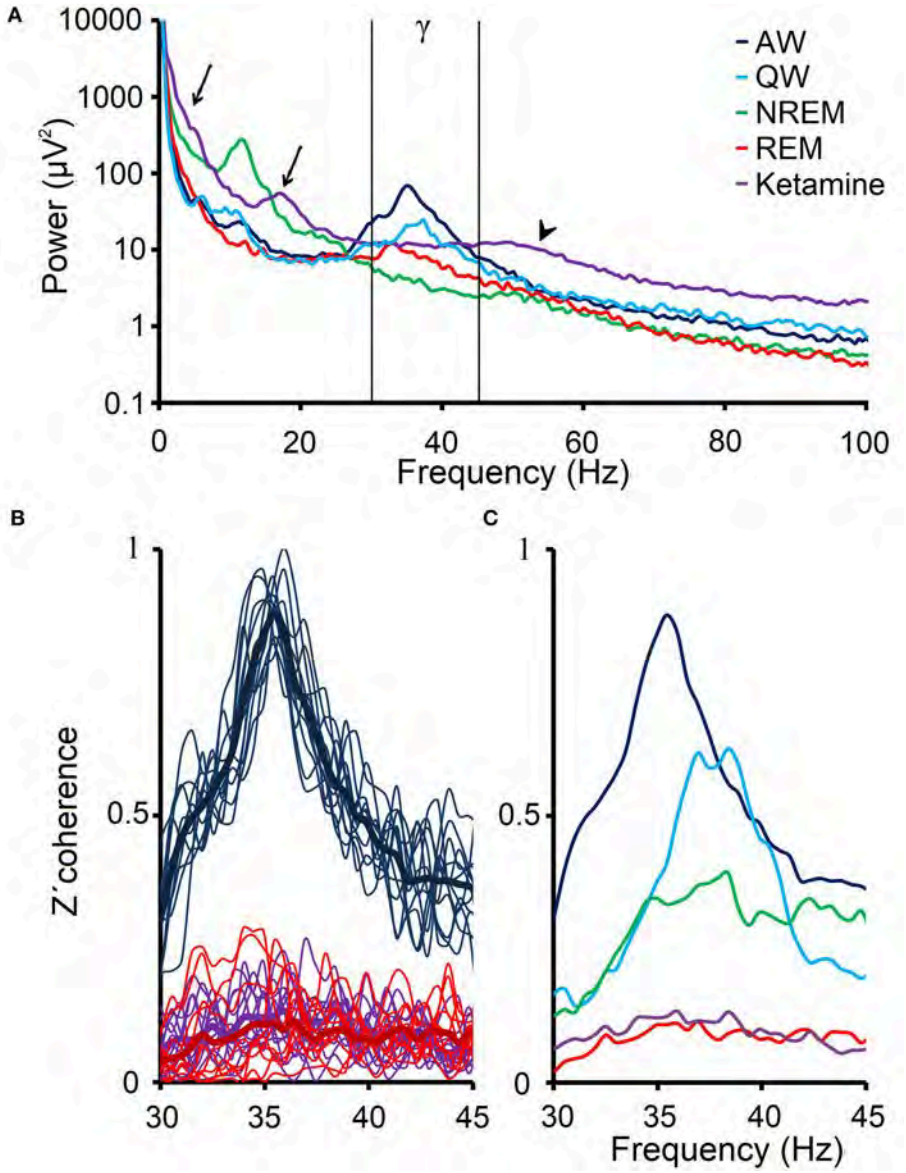

FIGURE 5 | EEG gamma power and coherence under the effect of ketamine. **(A)** Power spectrum (0.5–100 Hz) that was obtained from the average of ten 100 s windows, from the prefrontal cortex EEG of C5 during alert (AW), quiet wakefulness (QW), NREM and REM sleep as well as following the administration of ketamine (15 mg/kg). The arrows show the delta and beta power peaks under ketamine, and the arrowhead shows the high gamma power under the drug. Low gamma band is shown between vertical lines. **(B)** 12 profiles of the z′-coherence (thin lines) between the prefrontal and posterior-parietal cortical areas of the C5, as well as the averages (thick lines) of these 12 profiles for AW, REM sleep and following administration of ketamine. **(C)** Average gamma z′-coherence profiles for the same conditions as in **(A)**.

has also the advantage that 30–45 Hz EEG "bursts" of 200–500 ms and ∼25 μV, can be observed directly in the raw recordings (38, 48). It is important to highlight that in the cat, low (30–45 Hz) gamma oscillations are highly reactive to alertness and behavioral states (38, 48, 51, 52). On the contrary, high (50–100 Hz) gamma does not respond to stimuli that alert the animals (48, 52). Because of its importance, in the present study we focused in this narrow (30–45 Hz) gamma band. However, we are carrying out new studies analyzing not only on high gamma, but also the high frequency band (110–160 Hz) that is known as high frequency oscillations (HFO). HFO may have a role in psychosis, because experiments in rats have shown that ketamine increases HFO in all depths of the CA1-dentate axis (58), and HFO coherence increases between perceptual cortices of the same hemisphere during REM sleep (59).

In previous studies of our group we discarded the presence of possible artifactual signals that may bias the quantification of the gamma coherence (48, 51). In addition, as it is shown in

TABLE 1 | Gamma (35–40 Hz) power values during sleep, and wakefulness and 10 min following ketamine administration.

Animal/Cx		AW	QW	NREM	REM	*K*	*F*
C1	**Pp**	64.4 ± 2.4	18.3 ± 4.7	8.9 ± 0.3	15.1 ± 0.5	28.0 ± 0.7^{abcd}	66
	S1	15.3 ± 0.6	13.1 ± 0.9	7.6 ± 0.3	13.0 ± 0.6	6.8 ± 0.1^{abd}	7
C2	**Pf**	60.9 ± 3.1	23.8 ± 3.6	12.5 ± 0.3	20.9 ± 0.4	14.5 ± 2.6^{abd}	50
	Pp	57.6 ± 2.6	21.1 ± 3.9	10.3 ± 0.3	18.5 ± 0.5	24.7 ± 1.4^{ac}	37
C3	**Pp**	14.0 ± 0.8	10.8 ± 0.9	6.5 ± 0.6	9.7 ± 1.3	10.7 ± 0.3^{ac}	26
	S1	26.2 ± 1.5	13.1 ± 0.9	6.1 ± 0.4	7.7 ± 0.5	15.4 ± 0.5^{acd}	131
C4	**M1**	75.8 ± 4.3	26.7 ± 0.9	15.8 ± 0.5	19.6 ± 0.9	25.5 ± 0.9^{ac}	73
	V1	57.4 ± 3.0	8.4 ± 0.6	5.8 ± 0.91	10.2 ± 0.5	9.8 ± 0.2	55
C5	**Pf**	132.0 ± 4.0	57.2 ± 5	20.5 ± 1.3	18.3 ± 1.1	33.4 ± 1.8^{abcd}	113
	S1	121.2 ± 4.9	69.8 ± 4.4	18.6 ± 1.8	37.0 ± 2.4	45.6 ± 2.8^{abcd}	121
	Pp	174.0 ± 11.2	79.8 ± 4.4	35.3 ± 3.2	39.9 ± 2.5	64.8 ± 3.4^{acd}	85

The values represent mean ± standard error. The letters a, b, c, and d show the significance ($p < 0.05$, ANOVA followed by Tamhane tests) compared to ketamine (K); a vs. AW, b vs. QW, c vs. NREM, and d vs. REM sleep. All the analyses have the same degrees of freedom (4 between groups, 55 within groups). Right cortices are shown for C2–C5, while left cortices are exhibited for C1. C1–C5 identification name of the animals. M1, primary motor cortex; Pf, prefrontal cortex; Pp, posterior-parietal cortex; S1, somatosensory cortex; V1, primary visual cortex; Cx, cortex.

TABLE 2 | Gamma (35–40 Hz) z′-coherence values during sleep, wakefulness and 10 min following ketamine administration.

Animal/Cx		AW	QW	NREM	REM	*K*	*F*
C1	**Ppr-Ppl**	1.13 ± 0.03	0.84 ± 0.07	0.77 ± 0.03	0.55 ± 0.03	0.6 ± 0.03^{abc}	28
	S1l-Ppl	0.98 ± 0.04	0.41 ± 0.03	0.53 ± 0.03	0.33 ± 0.01	0.28 ± 0.01^{abc}	87
C2	**Pfr-Ppr**	0.90 ± 0.06	0.34 ± 0.05	0.16 ± 0.01	0.10 ± 0.01	0.11 ± 0.01^{abc}	78
	Ppr-Ppl	0.95 ± 0.04	0.46 ± 0.05	0.27 ± 0.04	0.20 ± 0.03	0.51 ± 0.03^{abc}	60
C3	**Ppr-Ppl**	0.43 ± 0.01	0.34 ± 0.04	0.05 ± 0.01	0.05 ± 0.01	0.04 ± 0.01^{abc}	98
	S1r-Ppr	0.97 ± 0.02	0.60 ± 0.04	0.48 ± 0.01	0.48 ± 0.01	0.42 ± 0.03^{abcd}	88
C4	**M1r-V1r**	0.91 ± 0.02	0.18 ± 0.01	0.15 ± 0.01	0.02 ± 0.01	0.01 ± 0.01^{abc}	857
C5	**Pfr-Ppr**	0.73 ± 0.04	0.59 ± 0.04	0.42 ± 0.07	0.14 ± 0.06	0.12 ± 0.03^{abc}	368
	S1r-Ppr	0.91 ± 0.04	0.82 ± 0.06	0.62 ± 0.06	0.42 ± 0.03	0.47 ± 0.03^{abc}	28

The values represent mean ± standard error. The letters a, b, c, and d show the significance ($p < 0.05$, ANOVA followed by Tamhane tests) compared to ketamine (K); a vs. AW, b vs. QW, c vs. NREM, and d vs. REM sleep. All the analyses have the same degrees of freedom (4 between groups, 55 within groups). Right cortices are shown for C2–C5, while left cortices are exhibited for C1. C1–C5 identification name of the animals. M1, primary motor cortex; Pf, prefrontal cortex; Pp, posterior-parietal cortex; S1, somatosensory cortex; V1, primary visual cortex; Cx, cortex.

Supplementary Figure 2, gamma coherence was almost 0 during AW following the subrogation (shuffling) of one channel, while the spectral component of the shuffled channel remained similar to the original one.

From the pharmacological point of view, the maximal dose of ketamine that we used was 15 mg/kg. Hence, it is important to highlight that when it is administered as a single agent, the anesthetic dose of ketamine in cats is ≥25 mg/kg (60–62).

In pilot studies in 3 cats, we administered ketamine (15 mg/kg) and analyzed the behavior in freely-moving conditions. In rodents, NMDA-R antagonists generate a behavioral syndrome characterized by hyperlocomotion, ataxia signs and stereotypies (21, 22). Hyperlocomotion was not observed in our experiments, nor in previous studies in cat (63, 64). Moreover, an increase in motor activity was neither detected in semi-restricted condition. On the contrary, ∼5 min following the injection of ketamine, the animals lay down on the floor unable to stand up (i.e., an ataxia-like effect), but responded to sound stimulus directing the gaze toward the sound source. In the absence of stimuli, the cats moved their head from one side to the other (i.e., a head-weavings like behavior, described in rodents, and defined as stereotypies characterized as lateral side-to-side movement of the head without locomotion). The animal also retained muscular tone, showed hyper-salivation and dilated pupils. Three to four hours following ketamine administration, the cats recovered completely.

REM Sleep as a Natural Model of Psychosis

Hobson (28) considers that dream experiences (the cognitive counterpart of REM sleep) have the following similarities with psychosis (28). I. The intense visual images of dream experiences, which are like the visual hallucinations that frequently occur in toxic states caused by substances that alter the chemistry of the brain (toxic psychosis). II. The conviction that the events of physically impossible dream experiences are real, which is like the delusional belief that is the hallmark of all psychosis. III. The inability to recognize that we are dreaming, which is similar to

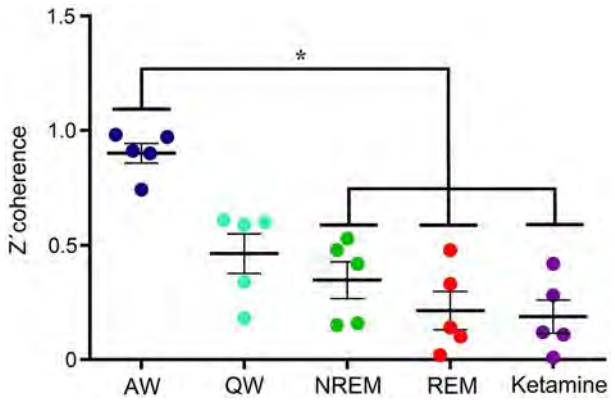

FIGURE 6 | Gamma z′-coherence between anterior and posterior cortical areas for the five animals during alert (AW) and quiet (QW) wakefulness, NREM and REM sleep, as well as following 15 mg/kg of ketamine. Error bars indicate standard error. $^{*}F_{(4,24)} = 75.4$, $p < 0.001$.

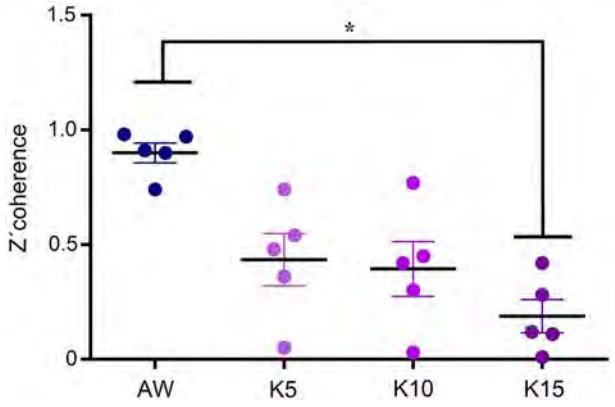

FIGURE 7 | Dose-response curve of gamma z′-coherence. Mean gamma z′-coherence between anterior and posterior cortical areas for the 5 animals during alert wakefulness (AW) and following treatments with 5, 10, and 15 mg/kg (K5, K10, and K15, respectively) of ketamine. Error bars indicate standard error. $^{*}F_{(3,19)} = 40.4$, $p < 0.003$.

the tenacity that paranoids cling to false belief. IV. The stories we invent to explain improbable and impossible imaginary events during dreams, which are like the confabulations of Korsakoff's syndrome. Hobson concludes, that "dreaming is, by definition, a psychosis."

It has been proposed that dreams characteristics, such as the violation of physical laws, inconsistencies in time, space and characters, come from the decrease in dorsolateral prefrontal brain activity that characterizes both psychosis and REM sleep (31, 65–69).

From the electrophysiological point of view, wakefulness in psychotic patients and REM sleep in normal subjects show a similar strong activation of the EEG (30).

Regarding neurochemical aspects, there are two main hypotheses relating psychosis and dreams; these hypotheses involve dopamine and glutamate neurotransmission (30). As abovementioned, NMDA-R antagonists induce psychotic symptoms but at the same time generate vivid (mostly unpleasant) dreams (70). On the other hand, the excess of dopamine in the nucleus accumbens can be considered partially responsible for the positive symptoms of the psychosis (71). In addition, indirect dopamine agonists, such as amphetamine induce both psychotic symptoms and vivid (nightmares) dreams (72, 73). Consistent with this, it was determined that dopamine release in the nucleus accumbens is maximal during REM sleep (74). Antipsychotics drugs, which antagonize the action of dopamine, suppress both psychotic symptoms and dream experiences (75, 76).

Finally, the neurobiological characteristics of REM sleep are candidates endophenotypes of psychosis, and REM sleep is considered a neurobiological model of this mental disorder (28–30).

Ketamine as a Pharmacological Model of Psychosis

The glutamatergic NMDA-R is expressed ubiquitously in the central nervous system. Clinical and preclinical studies suggest that the NMDA-R is involved in the pathophysiology of the psychotic disorders (77–79). Post-mortem studies of patients with schizophrenia found a decrease in NMDA-R in dorsolateral prefrontal cortex and hippocampus (80). Furthermore, as mentioned in the Introduction, sub-anesthetic doses of NMDA-R antagonists, including ketamine, are widely used to mimic some of the symptoms of psychosis.

Power and Gamma Coherence During REM Sleep (Natural Model of Psychosis)

Previous studies of our group have shown that the gamma power during REM sleep of the cat is similar to that of QW. On the contrary, gamma coherence is almost absent during REM sleep (45, 48, 51, 52). Similar results have been observed in rats (45, 49, 81), and humans (46, 47). In this regards, the uncoupling of the EEG activity between executive and perceptual regions during REM sleep has been related to the bizarre characteristics of dreams (69).

Power and Gamma Coherence Under Sub-anesthetic Doses of Ketamine (Pharmacological Model of Psychosis)

Our results demonstrated that sub-anesthetic doses of ketamine reduce gamma coherence between different neocortical areas at a similar level to that of REM sleep, although the gamma power remains comparable to QW.

In agreement with our results, Pinault (82) demonstrated in rats a dose-dependent increase in fronto-parietal gamma power that occurs even at relatively low doses of ketamine (2.5 mg/kg) and MK801 (0.06 mg/kg, the most potent NMDA-R antagonist) (82). Other authors obtained similar results (17, 83–86).

With respect to gamma coherence, and also in harmony with our results, Pal et al. (87) identified in the rat a decrease in coherence with an anesthetic (150 mg/kg) dose of ketamine. They demonstrated that ketamine-induced unconsciousness was

associated with reduction of power in high gamma bandwidths (>65 Hz), and in coherence in the whole gamma range. This fact was accompanied by a significant increase in acetylcholine (ACh) concentrations in the prefrontal cortex. Compared with the unconscious state, recovery of righting reflex was marked by a further increase in ACh concentrations, increases in low gamma band (25–55 Hz) power, and an increment in power and coherence in high gamma frequencies (>65 Hz). On the contrary, Akeju et al. (88) found an increase in gamma power and coherence in the anesthetic induction with ketamine in humans, probably because the coherence analysis was performed in standard EEG recordings (scalp electrodes) between frontal electrodes located at a short distance.

Ketamine seems to block NMDA-Rs (that are excitatory) in GABAergic cortical interneurons more efficiently than in pyramidal neurons. This reduction in the excitatory inputs onto the interneurons would lead to a decrease in the release of GABA at the synapses between interneurons and pyramidal neurons (89, 90), and a disinhibition of pyramidal neurons (91). This may explain why ketamine is associated with a greater use of cerebral glucose and blood flow (92, 93), and with an increase in gamma power (see above). However, it is probable that coupling between different cortical areas would be mediated by glutamate acting through NMDA-R. So, when these receptors are blocked by ketamine, the coupling between different distant cortical areas decreases, but without decreasing local synchronization.

Ketamine induces psychotic symptoms during the first 40–60 min after its administration (94). The temporal dynamics of these symptoms coincides with the dynamic evolution of the decrease in gamma coherence observed in our experiments. This lack of coupling of gamma frequency activity during the maximum effect of ketamine could be involved in the peculiarities of cognitive operations that occur under the effect of ketamine.

Do patients suffering of psychotic disorders present dysfunctions in the EEG gamma activity? Altered gamma oscillations have been observed in psychosis (95–97). In fact, schizophrenia has dysfunction of GABAergic cortical interneurons that express the calcium-binding protein parvalbumin, particularly in the prefrontal cortex (98, 99). These neurons have been involved in the generation of gamma oscillations (100).

White and Siegel (101) showed that in psychosis, gamma power is increased during QW (101). Moreover, during sleep there is a decrease in beta and gamma coherence between the right frontal and central right areas (102). In addition, under visual or auditory sensory stimulation there is an increase in gamma activity (30–50 Hz), while the phase coherence is reduced in psychotic patients (103–108). These findings agree with lack of increment in gamma coherence in response to sensory stimuli following the administration of ketamine (**Figures 2**, **3**).

CONCLUSIONS

Functional interactions between cortical areas in the gamma frequency band decrease in a similar way in both experimental models of psychosis: ketamine and REM sleep. This decoupling of gamma frequency activity may be involved in the cognitive characteristics shared by dream experiences and psychosis.

DATA AVAILABILITY STATEMENT

The data that supported the findings of this study are available from the corresponding author upon reasonable request.

AUTHOR CONTRIBUTIONS

PT provided the financial support. PT and SC-Z performed the experimental design. SC-Z, MC, JG, and PT performed the experimental procedures and were involved in the discussion and interpretation of the data. SC-Z, MC, and JG analyzed the data. SC-Z, MC, and PT wrote the manuscript. CS, AN, and SM critically revised the manuscript and added important intellectual content to it. All the authors reviewed and approved the definitive version of the manuscript.

FUNDING

This study was supported by the "Programa de Desarrollo de Ciencias Básicas, PEDECIBA" and the "Comisión Sectorial de Investigación Científica" (CSIC) I + D-2016-589 grant from Uruguay.

SUPPLEMENTARY MATERIAL

The Supplementary Material for this article can be found online at: https://www.frontiersin.org/articles/10.3389/fpsyt.2018.00766/full#supplementary-material

REFERENCES

1. Bhati MT. Defining psychosis: the evolution of DSM-5 schizophrenia spectrum disorders. *Curr Psychiatry Rep.* (2013) 15:409. doi: 10.1007/s11920-013-0409-9
2. Lewis DA, Lieberman JA. Catching up on schizophrenia: natural history and neurobiology. *Neuron* (2000) 28:325–34. doi: 10.1016/S0896-6273(00)00111-2
3. Saha S, Chant D, Welham J, McGrath J. A systematic review of the prevalence of schizophrenia. *PLoS Med.* (2005) 2:413–33. doi: 10.1371/journal.pmed.0020141
4. Kesby JP, Eyles DW, McGrath JJ, Scott JG. Dopamine, psychosis and schizophrenia: the widening gap between basic and clinical neuroscience. *Transl Psychiatry* (2018) 8:30. doi: 10.1038/s41398-017-0071-9
5. Kircher T, Brohl H, Meier F, Engelen J. Formal thought disorders: from phenomenology to neurobiology. *Lancet Psychiatry* (2018) 5:515–26. doi: 10.1016/S2215-0366(18)30059-2
6. Javitt DC, Zukin SR. Recent advances in the phencyclidine model of schizophrenia. *Am J Psychiatry* (1991) 148:1301–8. doi: 10.1176/ajp.148.10.1301
7. Carlsson A, Waters N, Holm-Waters S, Tedroff J, Nilsson M, Carlsson ML. Interactions between monoamines, glutamate, and GABA in

schizophrenia: new evidence. *Annu Rev Pharmacol Toxicol.* (2001) 41:237–60. doi: 10.1146/annurev.pharmtox.41.1.237
8. Krystal JH, Karper LP, Seibyl JP, Freeman GK, Delaney R, Bremner JD, et al. Subanesthetic effects of the noncompetitive NMDA antagonist, ketamine, in humans. Psychotomimetic, perceptual, cognitive, and neuroendocrine responses. *Arch Gen Psychiatry* (1994) 51:199–214. doi: 10.1001/archpsyc.1994.03950030035004
9. Malhotra AK, Pinals DA, Weingartner H, Sirocco K, Missar CD, Pickar D, et al. NMDA receptor function and human cognition: the effects of ketamine in healthy volunteers. *Neuropsychopharmacology* (1996) 14:301–7. doi: 10.1016/0893-133X(95)00137-3
10. Duncan EJ, Madonick SH, Parwani A, Angrist B, Rajan R, Chakravorty S, et al. Clinical and sensorimotor gating effects of ketamine in normals. *Neuropsychopharmacology* (2001) 25:72–83. doi: 10.1016/S0893-133X(00)00240-2
11. Lahti AC, Weiler MA, Tamara Michaelidis BA, Parwani A, Tamminga CA. Effects of ketamine in normal and schizophrenic volunteers. *Neuropsychopharmacology* (2001) 25:455–67. doi: 10.1016/S0893-133X(01)00243-3
12. Moghaddam B, Jackson ME. Glutamatergic animal models of schizophrenia. *Ann N Y Acad Sci.* (2003) 1003:131–7. doi: 10.1196/annals.1300.065
13. Honey GD, O'Loughlin C, Turner DC, Pomarol-Clotet E, Corlett PR, Fletcher PC. The effects of a subpsychotic dose of ketamine on recognition and source memory for agency: implications for pharmacological modelling of core symptoms of schizophrenia. *Neuropsychopharmacology* (2006) 31:413–23. doi: 10.1038/sj.npp.1300846
14. Pomarol-Clotet E, Honey GD, Murray GK, Corlett PR, Absalom AR, Lee M, et al. Psychological effects of ketamine in healthy volunteers. *Phenomenological study Br J Psychiatry* (2006) 189:173–9. doi: 10.1192/bjp.bp.105.015263
15. Stone JM, Pilowsky LS. Psychopathological consequences of ketamine. *Br J Psychiatry* (2006) 189:565–6. doi: 10.1192/bjp.189.6.565b
16. Javitt DC. Glutamatergic theories of schizophrenia. *Isr J Psychiatry Relat Sci.* (2010) 47:4–16.
17. Lee J, Hudson MR, O'Brien TJ, Nithianantharajah J, Jones NC. Local NMDA receptor hypofunction evokes generalized effects on gamma and high-frequency oscillations and behavior. *Neuroscience* (2017) 358:124–36. doi: 10.1016/j.neuroscience.2017.06.039
18. Krystal JH, D'Souza DC, Mathalon D, Perry E, Belger A, Hoffman R. NMDA receptor antagonist effects, cortical glutamatergic function, and schizophrenia: toward a paradigm shift in medication development. *Psychopharmacology* (2003) 169:215–33. doi: 10.1007/s00213-003-1582-z
19. Corlett PR, Honey GD, Fletcher PC. From prediction error to psychosis: ketamine as a pharmacological model of delusions. *J Psychopharmacol.* (2007) 21:238–52. doi: 10.1177/0269881107077716
20. Scorza MC, Meikle MN, Hill XL, Richeri A, Lorenzo D, Artigas F. Prefrontal cortex lesions cause only minor effects on the hyperlocomotion induced by MK-801 and its reversal by clozapine. *Int J Neuropsychopharmacol.* (2008) 11:519–32. doi: 10.1017/S1461145708008432
21. Geyer MA, Ellenbroek B. Animal behavior models of the mechanisms underlying antipsychotic atypicality. *Prog Neuropsychopharmacol Biol Psychiatry* (2003) 27:1071–9. doi: 10.1016/j.pnpbp.2003.09.003
22. Scorza MC, Castane A, Bortolozzi A, Artigas F. Clozapine does not require 5-HT1A receptors to block the locomotor hyperactivity induced by MK-801 Clz and MK-801 in KO1A mice. *Neuropharmacology* (2010) 59:112–20. doi: 10.1016/j.neuropharm.2010.04.012
23. Rung JP, Carlsson A, Ryden Markinhuhta K, Carlsson ML. (+)-MK-801 induced social withdrawal in rats; a model for negative symptoms of schizophrenia. *Prog Neuropsychopharmacol Biol Psychiatry* (2005) 29:827–32. doi: 10.1016/j.pnpbp.2005.03.004
24. Hill XL, Richeri A, Scorza C. Measure of anxiety-related behaviors and hippocampal BDNF levels associated to the amnesic effect induced by MK-801 evaluated in the modified elevated plus-maze in rats. *Physiol Behav.* (2015) 147:359–63. doi: 10.1016/j.physbeh.2015.05.013
25. Peever J, Fuller PM. The biology of REM sleep. *Curr Biol.* (2017) 27:R1237–48. doi: 10.1016/j.cub.2017.10.026
26. Dement W, Kleitman N. The relation of eye movements during sleep to dream activity: an objective method for the study of dreaming. *J Exp Psychol.* (1957) 53:339–46. doi: 10.1037/h0048189
27. Pace-Schott E. The neurobiology of dreaming. In: Kryger MH, Roth T, and Dement WC, editors. *Principles and Practices of Sleep Medicine.* Philadelphia: Elsevier-Saunders (2011). p. 563–75. doi: 10.1016/B978-1-4160-6645-3.00048-7
28. Hobson JA. Dreaming as delirium: a mental status analysis of our nightly madness. *Semin Neurol.* (1997) 17:121–8. doi: 10.1055/s-2008-1040921
29. Gottesmann C. The dreaming sleep stage: a new neurobiological model of schizophrenia? *Neuroscience* (2006) 140:1105–15. doi: 10.1016/j.neuroscience.2006.02.082
30. Gottesmann C, Gottesman I. The neurobiological characteristics of rapid eye movement (REM) sleep are candidate endophenotypes of depression, schizophrenia, mental retardation and dementia. *Prog Neurobiol.* (2007) 81:237–50. doi: 10.1016/j.pneurobio.2007.01.004
31. Dresler M, Wehrle R, Spoormaker VI, Steiger A, Holsboer F, Czisch M, et al. Neural correlates of insight in dreaming and psychosis. *Sleep Med Rev.* (2015) 20:92–9. doi: 10.1016/j.smrv.2014.06.004
32. Mota NB, Resende A, Mota-Rolim SA, Copelli M, Ribeiro S. Psychosis and the control of lucid dreaming. *Front Psychol.* (2016) 7:294. doi: 10.3389/fpsyg.2016.00294
33. Llinas R, Ribary U, Contreras D, Pedroarena C. The neuronal basis for consciousness. *Philos Trans R Soc Lond B Biol Sci.* (1998) 353:1841–9. doi: 10.1098/rstb.1998.0336
34. Uhlhaas PJ, Pipa G, Neuenschwander S, Wibral M, Singer W. A new look at gamma? High- (>60 Hz) gamma-band activity in cortical networks: function, mechanisms and impairment. *Prog Biophys Mol Biol.* (2011) 105:14–28. doi: 10.1016/j.pbiomolbio.2010.10.004
35. Bosman CA, Lansink CS, Pennartz CM. Functions of gamma-band synchronization in cognition: from single circuits to functional diversity across cortical and subcortical systems. *Eur J Neurosci.* (2014) 39:1982–99. doi: 10.1111/ejn.12606
36. Uhlhaas PJ, Pipa G, Lima B, Melloni L, Neuenschwander S, Nikolic D, et al. Neural synchrony in cortical networks: history, concept and current status. *Front Integr Neurosci.* (2009) 3:17. doi: 10.3389/neuro.07.017.2009
37. Rieder MK, Rahm B, Williams JD, Kaiser J. Human gamma-band activity and behavior. *Int J Psychophysiol.* (2010) 79:39–48. doi: 10.1016/j.ijpsycho.2010.08.010
38. Bouyer JJ, Montaron MF, Rougeul A. Fast fronto-parietal rhythms during combined focused attentive behaviour and immobility in cat: cortical and thalamic localizations. *Electroencephalogr Clin.* (1981) 51:244–52. doi: 10.1016/0013-4694(81)90138-3
39. Llinas R, Ribary U. Coherent 40-Hz oscillation characterizes dream state in humans. *Proc Natl Acad Sci USA.* (1993) 90:2078–81. doi: 10.1073/pnas.90.5.2078
40. Tiitinen H, Sinkkonen J, Reinikainen K, Alho K, Lavikainen J, Naatanen R. Selective attention enhances the auditory 40-Hz transient response in humans. *Nature* (1993) 364:59–60. doi: 10.1038/364059a0
41. Steriade M, Amzica F, Contreras D. Synchronization of fast (30-40 Hz) spontaneous cortical rhythms during brain activation. *J Neurosci.* (1996) 16:392–417. doi: 10.1523/JNEUROSCI.16-01-00392.1996
42. Maloney KJ, Cape EG, Gotman J, Jones BE. High-frequency gamma electroencephalogram activity in association with sleep-wake states and spontaneous behaviors in the rat. *Neuroscience* (1997) 76:541–55. doi: 10.1016/S0306-4522(96)00298-9
43. Edelman GM, Tononi G. *A Universe of Consciousness*. New York, NY: Basic Books (2000).
44. Bullock TH, McClune MC, Enright JT. Are the electroencephalograms mainly rhythmic? Assessment of periodicity in wide-band time series. *Neuroscience* (2003) 121:233–52. doi: 10.1016/S0306-4522(03)00208-2
45. Cavelli M, Castro-Zaballa S, Mondino A, Gonzalez J, Falconi A, Torterolo P. Absence of EEG gamma coherence in a local activated neocortical state: a conserved trait of REM sleep. *Transl Brain Rhytmicity* (2017) 2:1–13. doi: 10.15761/TBR.1000115
46. Cantero JL, Atienza M, Madsen JR, Stickgold R. Gamma EEG dynamics in neocortex and hippocampus during human wakefulness and sleep. *Neuroimage* (2004) 22:1271–80. doi: 10.1016/j.neuroimage.2004.03.014

47. Voss U, Holzmann R, Tuin I, Hobson JA. Lucid dreaming: a state of consciousness with features of both waking and non-lucid dreaming. *Sleep* (2009) 32:1191–200. doi: 10.1093/sleep/32.9.1191
48. Castro S, Falconi A, Chase MH, Torterolo P. Coherent neocortical 40-Hz oscillations are not present during REM sleep. *Eur J Neurosci.* (2013) 37:1330–9. doi: 10.1111/ejn.12143
49. Cavelli M, Castro S, Schwarzkopf N, Chase MH, Falconi A, Torterolo P. Coherent neocortical gamma oscillations decrease during REM sleep in the rat. *Behav Brain Res.* (2015) 281:318–25. doi: 10.1016/j.bbr.2014.12.050
50. Voss U, Holzmann R, Hobson A, Paulus W, Koppehele-Gossel J, Klimke A, et al. Induction of self awareness in dreams through frontal low current stimulation of gamma activity. *Nat Neurosci.* (2014) 17:810–2. doi: 10.1038/nn.3719
51. Torterolo P, Castro-Zaballa S, Cavelli M, Chase MH, Falconi A. Neocortical 40 Hz oscillations during carbachol-induced rapid eye movement sleep and cataplexy. *Eur J Neurosci.* (2016) 43:580–9. doi: 10.1111/ejn.13151
52. Castro S, Cavelli M, Vollono P, Chase MH, Falconi A, Torterolo P. Inter-hemispheric coherence of neocortical gamma oscillations during sleep and wakefulness. *Neurosci Lett.* (2014) 578:197–202. doi: 10.1016/j.neulet.2014.06.044
53. Torterolo P, Yamuy J, Sampogna S, Morales FR, Chase MH. Hypocretinergic neurons are primarily involved in activation of the somatomotor system. *Sleep* (2003) 1:25–8. doi: 10.1093/sleep/26.1.25
54. Babadi B, Brown EN. A review of multitaper spectral analysis. *IEEE Trans Biomed Eng.* (2014) 61:1555–64. doi: 10.1109/TBME.2014.2311996
55. Roach BJ, Mathalon DH. Event-related EEG time-frequency analysis: an overview of measures and an analysis of early gamma band phase locking in schizophrenia. *Schizophr Bull.* (2008) 34:907–26. doi: 10.1093/schbul/sbn093
56. Dworak M, McCarley RW, Kim T, Basheer R. Delta oscillations induced by ketamine increase energy levels in sleep-wake related brain regions. *Neuroscience* (2011) 197:72–9. doi: 10.1016/j.neuroscience.2011.09.027
57. Ruiz-Mejias M, Ciria-Suarez L, Mattia M, Sanchez-Vives MV. Slow and fast rhythms generated in the cerebral cortex of the anesthetized mouse. *J Neurophysiol.* (2011) 106:2910–21. doi: 10.1152/jn.00440.2011
58. Caixeta FV, Cornelio AM, Scheffer-Teixeira R, Ribeiro S, Tort AB. Ketamine alters oscillatory coupling in the hippocampus. *Sci Rep.* (2013) 3:2348. doi: 10.1038/srep02348
59. Cavelli M, Rojas-Libano D, Schwarzkopf N, Castro-Zaballa S, Gonzalez J, Mondino A, et al. Power and coherence of cortical high-frequency oscillations during wakefulness and sleep. *Eur J Neurosci.* (2017) 48:2728–37. doi: 10.1111/ejn.13718
60. Arnbjerg J. Clinical manifestations of overdose of ketamine-xylazine in the cat. *Nord Vet Med.* (1979) 31:155–61.
61. Arnbjerg J. [Clinical use of ketamine-xylazine for anaesthesia in the cat (author's transl)]. *Nord Vet Med.* (1979) 31:145–54.
62. Hanna RM, Borchard RE, Schmidt SL. Pharmacokinetics of ketamine HCl and metabolite I in the cat: a comparison of i.v., i.m., and rectal administration. *J Vet Pharmacol Ther.* (1988) 11:84–93. doi: 10.1111/j.1365-2885.1988.tb00125.x
63. Issabeagloo E, Gharachorlou AA, Ghalahkandi JG. Comparison of sedative effects of oral ketamine and chlorpheniramine in the manner of single and concomitant administration in cat. *Adv Environ Biol.* (2011) 5:784–9.
64. Ambros B, Duke T. Effect of low dose rate ketamine infusions on thermal and mechanical thresholds in conscious cats. *Vet Anaesth Analg.* (2013) 40:e76–82. doi: 10.1111/vaa.12057
65. Berman KF, Zec RF, Weinberger DR. Physiologic dysfunction of dorsolateral prefrontal cortex in schizophrenia. II Role of neuroleptic treatment, attention, and mental effort. *Arch Gen Psychiatry* (1986) 43:126–35. doi: 10.1001/archpsyc.1986.01800020032005
66. Weinberger DR, Berman KF, Zec RF. Physiologic dysfunction of dorsolateral prefrontal cortex in schizophrenia. I Regional cerebral blood flow evidence. *Arch Gen Psychiatry* (1986) 43:114–24. doi: 10.1001/archpsyc.1986.01800020020004
67. Braun AR, Balkin TJ, Wesenten NJ, Carson RE., Varga M, Baldwin P, et al. Regional cerebral blood flow throughout the sleep-wake cycle. An H2(15)O PET study. *Brain* (1997) 120 (Pt 7):1173–97.
68. Fletcher PC, McKenna PJ, Frith CD, Grasby PM, Friston KJ, Dolan RJ. Brain activations in schizophrenia during a graded memory task studied with functional neuroimaging. *Arch Gen Psychiatry* (1998) 55:1001–8. doi: 10.1001/archpsyc.55.11.1001
69. Corsi-Cabrera M, Miro E, del-Rio-Portilla Y, Perez-Garci E, Villanueva Y, Guevara MA. Rapid eye movement sleep dreaming is characterized by uncoupled EEG activity between frontal and perceptual cortical regions. *Brain Cogn.* (2003) 51:337–45. doi: 10.1016/S0278-2626(03)00037-X
70. Blagrove M, Morgan CJ, Curran HV, Bromley L, Brandner B. The incidence of unpleasant dreams after sub-anaesthetic ketamine. *Psychopharmacology* (2009) 203:109–20. doi: 10.1007/s00213-008-1377-3
71. Mackay AV, Iversen LL, Rossor M, Spokes E, Bird E, Arregui A, et al. Increased brain dopamine and dopamine receptors in schizophrenia. *Arch Gen Psychiatry* (1982) 39:991–7. doi: 10.1001/archpsyc.1982.04290090001001
72. Buffenstein A, Heaster J, Ko P. Chronic psychotic illness from methamphetamine. *Am J Psychiatry* (1999) 156:662.
73. Thompson DF, Pierce DR. Drug-induced nightmares. *Ann Pharmacother.* (1999) 33:93–8. doi: 10.1345/aph.18150
74. Lena I, Parrot S, Deschaux O, Muffat-Joly S, Sauvinet V, Renaud B, et al. Variations in extracellular levels of dopamine, noradrenaline, glutamate, and aspartate across the sleep–wake cycle in the medial prefrontal cortex and nucleus accumbens of freely moving rats. *J Neurosci Res.* (2005) 81:891–9. doi: 10.1002/jnr.20602
75. Solms M. Dreaming and REM sleep are controlled by different brain mechanisms. *Behav Brain Sci.* (2000) 23:843–50. Discussion 904–1121. doi: 10.1017/S0140525X00003988
76. Jakovljevic M, Sagud M, Mihaljevic-Peles A. Olanzapine in the treatment-resistant, combat-related PTSD–a series of case reports. *Acta Psychiatr Scand.* (2003) 107(2003). 394–6. Discussion 396. doi: 10.1034/j.1600-0447.2003.00065.x
77. Kantrowitz J, Javitt DC. Glutamatergic transmission in schizophrenia: from basic research to clinical practice. *Curr Opin Psychiatry* (2012) 25:96–102. doi: 10.1097/YCO.0b013e32835035b2
78. Schwartz TL, Sachdeva S, Stahl SM. Glutamate neurocircuitry: theoretical underpinnings in schizophrenia. *Front Pharmacol.* (2012) 3:195. doi: 10.3389/fphar.2012.00195
79. Schwartz TL, Sachdeva S, Stahl SM. Genetic data supporting the NMDA glutamate receptor hypothesis for schizophrenia. *Curr Pharm Des.* (2012) 18:1580–92. doi: 10.2174/138161212799958594
80. Konradi C, Heckers S. Molecular aspects of glutamate dysregulation: implications for schizophrenia and its treatment. *Pharmacol Ther.* (2003) 97:153–79. doi: 10.1016/S0163-7258(02)00328-5
81. Pal D, Silverstein BH, Lee H, Mashour GA. Neural correlates of wakefulness, sleep, and general anesthesia: an experimental study in rat. *Anesthesiology* (2016) 125:929–42. doi: 10.1097/ALN.0000000000001342
82. Pinault D. N-methyl d-aspartate receptor antagonists ketamine and MK-801 induce wake-related aberrant gamma oscillations in the rat neocortex. *Biol Psychiatry* (2008) 63:730–5. doi: 10.1016/j.biopsych.2007.10.006
83. Palenicek T, Fujakova M, Brunovsky M, Balikova M, Horacek J, Gorman I, et al. Electroencephalographic spectral and coherence analysis of ketamine in rats: correlation with behavioral effects and pharmacokinetics. *Neuropsychobiology* (2011) 63:202–18. doi: 10.1159/000321803
84. Phillips KG, Cotel MC, McCarthy AP, Edgar DM, Tricklebank M, O'Neill MJ, et al. Differential effects of NMDA antagonists on high frequency and gamma EEG oscillations in a neurodevelopmental model of schizophrenia. *Neuropharmacology* (2012) 62:1359–70. doi: 10.1016/j.neuropharm.2011.04.006
85. Muthukumaraswamy SD, Shaw AD, Jackson LE, Hall J, Moran R, Saxena N. Evidence that subanesthetic doses of ketamine cause sustained disruptions of NMDA and AMPA-mediated frontoparietal connectivity in humans. *J Neurosci.* (2015) 35:11694–706. doi: 10.1523/JNEUROSCI.0903-15.2015
86. Shaw AD, Saxena N, L, E Jackson L, Hall JE, Singh KD, Muthukumaraswamy SD. Ketamine amplifies induced gamma frequency oscillations in the human cerebral cortex. *Eur Neuropsychopharmacol.* (2015) 25:1136–46. doi: 10.1016/j.euroneuro.2015.04.012
87. Pal D, Hambrecht-Wiedbusch VS, Silverstein BH, Mashour GA. Electroencephalographic coherence and cortical acetylcholine during

ketamine-induced unconsciousness. *Br J Anaesth.* (2015) 114:979–89. doi: 10.1093/bja/aev095
88. Akeju O, Song AH, Hamilos AE, Pavone KJ, Flores FJ, Brown EN, et al. Electroencephalogram signatures of ketamine anesthesia-induced unconsciousness. *Clin Neurophysiol.* (2016) 127:2414–22. doi: 10.1016/j.clinph.2016.03.005
89. Homayoun H, Moghaddam B. NMDA receptor hypofunction produces opposite effects on prefrontal cortex interneurons and pyramidal neurons. *J Neurosci.* (2007) 27:11496–500. doi: 10.1523/JNEUROSCI.2213-07.2007
90. Seamans J. Losing inhibition with ketamine. *Nat Chem Biol.* (2008) 4:91–3. doi: 10.1038/nchembio0208-91
91. Jackson ME, Homayoun H, Moghaddam B. NMDA receptor hypofunction produces concomitant firing rate potentiation and burst activity reduction in the prefrontal cortex. *Proc Natl Acad Sci USA.* (2004) 101:8467–72. doi: 10.1073/pnas.0308455101
92. Langsjo JW, Salmi E, Kaisti KK, Aalto S, Hinkka S, Aantaa R, et al. Effects of subanesthetic ketamine on regional cerebral glucose metabolism in humans. *Anesthesiology* (2004) 100:1065–71. doi: 10.1097/00000542-200405000-00006
93. Langsjo JW, Maksimow A, Salmi E, Kaisti K, Aalto S, Oikonen V, et al. S-ketamine anesthesia increases cerebral blood flow in excess of the metabolic needs in humans. *Anesthesiology* (2005) 103:258–68. doi: 10.1097/00000542-200508000-00008
94. Krystal JH, Perry EB Jr, Gueorguieva R, Belger A, Madonick SH, et al. Comparative and interactive human psychopharmacologic effects of ketamine and amphetamine: implications for glutamatergic and dopaminergic model psychoses and cognitive function. *Arch Gen Psychiatry* (2005) 62:985–94. doi: 10.1001/archpsyc.62.9.985
95. Kornmayer L, Leicht G, Mulert C. Attentional capture by physically salient stimuli in the gamma frequency is associated with schizophrenia symptoms. *World J Biol Psychiatry* (2018) 19:S52–62. doi: 10.1080/15622975.2016.1258491
96. Leicht G, Vauth S, Polomac N, Andreou C, Rauh J, Mussmann M, et al. EEG-informed fMRI reveals a disturbed gamma-band-specific network in subjects at high risk for psychosis. *Schizophr Bull.* (2016) 42:239–49. doi: 10.1093/schbul/sbv092
97. Suazo V, Lubeiro A, Jurado-Barba R, Moreno-Ortega M, Dompablo M, Morales-Munoz I, et al. Elevated midline-parietal gamma band noise power in schizophrenia but not in bipolar patients. *Eur Arch Psychiatry Clin Neurosci.* (2016) 266:743–53. doi: 10.1007/s00406-016-0673-x
98. Lewis DA, Volk DW, Hashimoto T. Selective alterations in prefrontal cortical GABA neurotransmission in schizophrenia: a novel target for the treatment of working memory dysfunction. *Psychopharmacology* (2004) 174:143–50. doi: 10.1007/s00213-003-1673-x
99. Lewis DA, Hashimoto T, Volk DW. Cortical inhibitory neurons and schizophrenia. *Nat Rev Neurosci.* (2005) 6:312–24. doi: 10.1038/nrn1648
100. Mann EO, Suckling JM, Hajos N, Greenfield SA, Paulsen O. Perisomatic feedback inhibition underlies cholinergically induced fast network oscillations in the rat hippocampus *in vitro*. *Neuron* (2005) 45:105–17. doi: 10.1016/j.neuron.2004.12.016
101. White RS, Siegel SJ. Cellular and circuit models of increased resting-state network gamma activity in schizophrenia. *Neuroscience* (2016) 321:66–76. doi: 10.1016/j.neuroscience.2015.11.011
102. Yeragani VK, Cashmere D, Miewald J, Tancer M, Keshavan MS. Decreased coherence in higher frequency ranges (beta and gamma) between central and frontal EEG in patients with schizophrenia: a preliminary report. *Psychiatry Res.* (2006) 141:53–60. doi: 10.1016/j.psychres.2005.07.016
103. Kwon JS, O'Donnell BF, Wallenstein GV, Greene RW, Hirayasu Y, Nestor PG, et al. Gamma frequency-range abnormalities to auditory stimulation in schizophrenia. *Arch Gen Psychiatry* (1999) 56:1001–5. doi: 10.1001/archpsyc.56.11.1001
104. Lee KH, Williams LM, Haig A, Gordon E. "Gamma (40 Hz) phase synchronicity" and symptom dimensions in schizophrenia. *Cogn Neuropsychiatry* (2003) 8:57–71. doi: 10.1080/713752240
105. Light GA, Hsu JL, Hsieh MH, Meyer-Gomes K, Sprock J, Swerdlow NR, et al. Gamma band oscillations reveal neural network cortical coherence dysfunction in schizophrenia patients. *Biol Psychiatry* (2006) 60:1231–40. doi: 10.1016/j.biopsych.2006.03.055
106. Spencer KM, Niznikiewicz MA, Shenton ME, McCarley RW. Sensory-evoked gamma oscillations in chronic schizophrenia. *Biol Psychiatry* (2008) 63:744–7. doi: 10.1016/j.biopsych.2007.10.017
107. Uhlhaas PJ, Singer W. Abnormal neural oscillations and synchrony in schizophrenia. *Nat Rev Neurosci.* (2010) 11:100–13. doi: 10.1038/nrn2774
108. Sun Y, Farzan F, Barr MS, Kirihara K, Fitzgerald PB, Light GA, et al. γ oscillations in schizophrenia: mechanisms and clinical significance. *Brain Res.* (2011) 1413:98–114. doi: 10.1016/j.brainres.2011.06.065

Conflict of Interest Statement: The authors declare that the research was conducted in the absence of any commercial or financial relationships that could be construed as a potential conflict of interest.

Anexo 4

(Castro-Zaballa et al., 2019)

Behavioural Brain Research 359 (2019) 28–37

Contents lists available at ScienceDirect

Behavioural Brain Research

journal homepage: www.elsevier.com/locate/bbr

Research report

EEG dissociation induced by muscarinic receptor antagonists: Coherent 40 Hz oscillations in a background of slow waves and spindles

Santiago Castro-Zaballa[a], Matías Cavelli[a], Joaquín González[a], Jaime Monti[b], Atilio Falconi[a], Pablo Torterolo[a,*]

[a] Laboratorio de Neurobiología del Sueño, Departamento de Fisiología, Facultad de Medicina, Universidad de la República, Montevideo, Uruguay
[b] Departamento de Farmacología y Terapéutica, Facultad de Medicina, Hospital de Clínicas, Universidad de la República, Montevideo, Uruguay

GRAPHICAL ABSTRACT

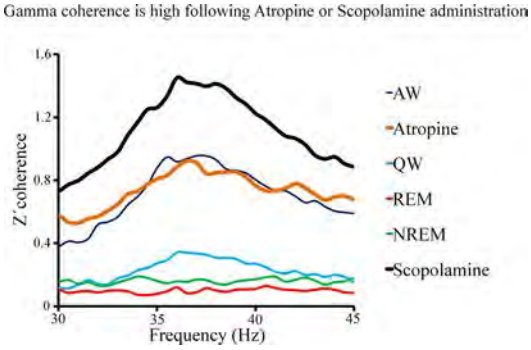

ARTICLE INFO

Keywords:
Sleep
gamma
Atropine
Scopolamine
Cat

ABSTRACT

Mesopontine and basal forebrain cholinergic neurons are involved in the control of behavioral states and cognitive functions. Animals treated with cholinergic muscarinic receptor antagonists display a dissociated state characterized by behavioral wakefulness (W) associated with high amplitude slow oscillations and spindles in the electroencephalogram (EEG), similar to those that occur during non-REM (NREM) sleep.

Oscillations in the gamma frequency band (≈ 40 Hz) of the EEG also play a critical role during W and cognition. Hence, the present study was conducted to determine the effect of muscarinic antagonists on the EEG gamma band power and coherence.

Five cats were implanted with electrodes in different cortices to monitor the EEG. The effects of atropine and scopolamine on power and coherence within the low gamma frequency band (30–45 Hz) from pairs of EEG recordings were analyzed and compared to gamma activity during sleep and W.

Muscarinic antagonists induced a NREM sleep-like EEG profile that was accompanied by a large increase in gamma power and coherence. The values of gamma coherence were similar to that occurring during alert W (AW), and greater than in quiet W, NREM and REM sleep.

We conclude that under atropine or scopolamine, functional interactions between cortical areas in the gamma frequency band remain high, as they are during AW. This significant functional connectivity at high frequency may explain why the animals remain awake in spite of the presence of slow waves and spindles.

* Corresponding author at: Departamento de Fisiología, Facultad de Medicina, Universidad de la República, General Flores 2125, 11800, Montevideo, Uruguay.
E-mail address: ptortero@fmed.edu.uy (P. Torterolo).

https://doi.org/10.1016/j.bbr.2018.10.016
Received 16 July 2018; Received in revised form 3 October 2018; Accepted 10 October 2018
Available online 12 October 2018
0166-4328/

1. Introduction

Mesopontine and basal forebrain cholinergic neurons are critically involved in the generation and maintenance of wakefulness (W) and rapid-eye-movements (REM) sleep [1,2]. In this regard, animals treated with atropine, a muscarinic receptor antagonist, display high voltage slow waves and spindles in the electroencephalogram (EEG) that resembles non-rapid eyes movement (NREM) sleep; however, they remain behaviorally awake and active [3]. Furthermore, atropine decreases the electrocortical arousal response elicited either by sensory or midbrain reticular formation stimulation, but the gross behavior in response to such stimuli is not affected [4,5]. This “dissociation” in which waking behavior coexists with NREM sleep-like EEG was observed in cats, dogs, rats and rabbits [3,6–9].

The brain integrates fragmentary neural events that occur at different times and locations into a unified perceptual experience. EEG oscillations in the gamma frequency band (mainly around 40 Hz) are involved in the integration or binding of spatially separated but temporally correlated neural events [10,11]. An increase in gamma power typically appears during behaviors that are characterized by cognitive processing of external percepts or internally generated thoughts and images [12–14]. High gamma power has been observed during attentive W not only in humans, but also in animals [15–19]. Furthermore, gamma coherence between different brain areas have been viewed as a possible neural correlate of consciousness [20,21]; the degree of EEG coherence between two cortical regions is believed to reflect the strength of the functional interconnections that occur between them [22,23].

In the cat, EEG "bursts" of 35–40 Hz oscillations of 200–500 ms and approximately 25 μV are readily observed in raw EEG recordings during alert wakefulness (AW) [24]. The EEG coherence in this frequency band is greater during AW than quiet wakefulness (QW); it decreases to a lower level during NREM sleep, and reaches its nadir during REM sleep [24–26]. Additionally, high gamma coherence has been observed during cataplexy induced by microinjections of carbachol into the nucleus pontis oralis (when the animal is fully awake but with complete muscle atonia), but not during REM sleep induced by the same procedure [27].

In order to find clues that account for the lack of correspondence between gross behavior and EEG patterns induced by muscarinic receptor antagonists, in the present report we studied the power and coherence in the EEG low gamma frequency band (30–45 Hz) of the cat treated with atropine and scopolamine, two commonly employed non-selective competitive muscarinic antagonists. We compared these results with the EEG gamma power and coherence that is present during naturally-occurring W and sleep.

2. Material and methods

Five adult cats were used in this study. The animals were obtained from the Institutional Animal Care Facility and determined to be in good health by veterinarians of the institution. All experimental procedures were conducted in accordance with the *Guide for the Care and Use of Laboratory Animals* (8th edition, National Academy Press, Washington DC, 2011) and were approved by the Institutional Animal Care Commission. Adequate measures were taken to minimize pain, discomfort or stress of the animals. In addition, all efforts were made to use the minimum number of animals necessary to produce reliable scientific data.

The animals were also employed in previous studies [24,25,27]. These animals were chronically implanted with electrodes to monitor the states of sleep and wakefulness. Prior to being anesthetized, each cat was premedicated with xylazine (2.2 mg/kg, i.m.), atropine (0.04 mg/ kg, i.m.) and antibiotics (Tribrissen®, 30 mg/kg, i.m.). Anesthesia, which was initially induced with ketamine (15 mg/kg, i.m.), was maintained with a gas mixture of isoflurane in oxygen (1–3%). The

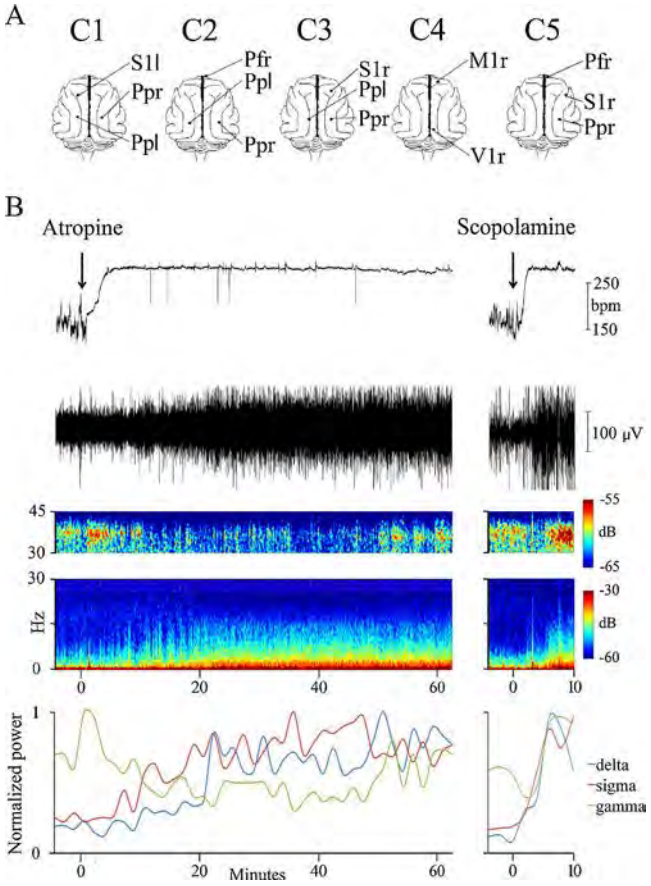

Fig. 1. A. Position of the recording electrodes. Recordings from these electrodes were referred to a common referential electrode, which was located over the frontal sinus. C1–C5, individual animals. M1, primary motor cortex; Pf, prefrontal cortex; Pp, posterior-parietal cortex; S1, somato-sensory primary cortex; V1, visual primary cortex; r, right; l, left. B. The tachogram, the EEG of the posterior parietal cortex, and its spectrogram (0–30 Hz and 30–45 Hz have different power scale) are shown following atropine or scopolamine injections (arrows). Delta, sigma and gamma normalized power are also shown. bpm, beats per minute; EEG, electroencephalogram.

head was positioned in a stereotaxic frame and the skull was exposed. Stainless steel screw electrodes (1.4 mm diameter) were placed on the surface (above the dura matter) of different cortical areas. Fig. 1A shows the sites of the recording electrodes whose signals were analyzed in the present study. The electrodes were connected to a Winchester plug, which together with two plastic tubes (used to fix the animal's head position without pain or pressure) were bonded to the skull with acrylic cement. After the animals recovered from the preceding surgical procedures (that usually takes three weeks), they were adapted to the recording environment for a period of at least two weeks.

Experimental sessions of 4 h were conducted between 11 A.M. and 3 P.M. in a temperature-controlled environment (21–23 °C). During these sessions (as well as during the adaptation sessions), the animal's head was held in a stereotaxic position by four steel bars that were placed into the chronically-implanted plastic tubes, while the body rested in a sleeping bag.

The simultaneous activity of 3 cortical areas (two in C4) was recorded with a monopolar (referential) configuration, utilizing a common reference electrode located in the left frontal sinus. The electromyogram (EMG) of the nuchal muscles, which was recorded by means of acutely placed bipolar electrode, was also monitored. The electrocardiogram (ECG), by electrodes acutely placed on the skin over the pre-cordial region, and respiratory activity by means of a micro-effort piezo-crystal infant sensor, were also recorded [28]. Each cat was

recorded daily for approximately 30 days in order to obtain complete basal and treatment data sets.

Bioelectric signals were amplified (×1000), filtered (0.1–500 Hz), sampled (1024 Hz, 2^{16} bits) and stored in a PC using the Spike 2 software (Cambridge Electronic Design).

Data were obtained after atropine or scopolamine administration as well as during spontaneously-occurring QW, NREM sleep and REM sleep. AW was induced for a period of 300 s by a sound stimulus, which was introduced approximately 30 min after the beginning of the recording session. The sound stimulus consisted of clicks (0.1 ms in duration) of 60–80 dB SPL in intensity with a variable frequency of presentation (1–500 Hz, modified at random) in order to avoid habituation [24,27,29]. Atropine (0.2 and 0.4 mg/kg s/c, Sigma) or scopolamine (1 mg/kg s/c., Sigma) were administrated in 4 experimental sessions to 5 and 3 animals, respectively; the doses were similar than in previous studies [30–32]. In pilot experiments where vehicle (saline) was administered, the EEG analysis during W and sleep showed results similar to those of the baseline condition; therefore, baseline experiments (without saline administration) were used for the analysis.

Data was analyzed as in our previous studies [24,25,27]. Sleep and W were quantified in epochs of 10 s. In order to analyze gamma coherence between pairs of EEG electrodes, 12 artifact-free periods of 100 s were examined during each behavioral state (1200 s for each behavioral state). The data of the drug administration experiments were obtained in four recording sessions for each drug and dose. Quantitative analyses were performed in time windows between 50 and 60 min following atropine, and between 5 and 15 min following scopolamine administration; these time periods correspond with the peaks of the EEG effects induced by these drugs (Fig. 1B). Furthermore, control data were obtained from four recording sessions during AW, QW, NREM and REM sleep.

For each selected period of 100 s, the Magnitude Squared Coherence was analyzed by means of Spike 2 script COHER 1S (Cambridge Electronic Design) (see Castro et al. 2013, for details in the definition of coherence). Coherence between two EEG channels that were recorded simultaneously during 100 s periods was analyzed. This period of analysis was divided into 100 time-blocks with a sample rate of 1024 Hz, a bin size of 2048 samples and a resolution of 0.5 Hz. The random level of coherence was approximately 0.1 [24]. In order to normalize the data and conduct parametric statistical tests, the Fisher z' transform to the gamma coherence values was utilized. In order to process the power spectrum of the EEG (by means of the Spike 2 script COHER 1S), we employed the same time-windows as for the coherence analysis.

Recordings were also filtered (band pass 30–45 Hz) using Spike 2 digital finite impulse response filters. The amplitude of simultaneously recorded pairs of filtered EEG signals was also analyzed by means of auto-correlation (ACF) cross-correlation (CCF) functions. Averages, and spectrograms were also performed. In addition, the RR intervals of the ECG signal was also analyzed and plotted against time (tachogram) [28,33] (see Fig. 1B).

In Figs. 1 and 4, two different approaches were used in order to estimate EEG power. In Fig. 1 a multitaper method was used as described by [34]. This method utilized a series of discrete prolate spheroidal sequences (Slepian) for the Fast Fourier Transform. The procedure reduces the variance of the power spectrum estimate, offering a better power estimation. In Fig. 4 wavelet transform was applied in order to improve time and frequency localization. We used Morlet wavelet because of its proven suitability for EEG analysis [35]. Both analyses were performed employing Chronux and ND Toolbox running on self-built MATLAB routines.

Power and z'-coherence of the gamma band for each EEG channel or derivative (pair of EEG channels) were also averaged across behavioral states and drug treatments. Data were expressed as the mean ± standard error. The significance of the differences among behavioral states was evaluated for each cat with one-way ANOVA and Tamhane test. Because the electrodes positions were not the same in all the animals (Fig. 1A), in order to analyze the effect of the drugs in the whole group of animals, the mean intra-hemispheric z'-coherence of the gamma band between anterior (S1 for C1 and C2, Pf for C3 and C5, and M1 for C4; see Fig. 1A) and posterior (V1 for C4, and Pp for the rest of the animals) cortices was evaluated (Fig. 6). For this purpose, we utilized the repeated measures ANOVA (rmANOVA) and Bonferroni *post hoc* test. The criterion used to reject null hypotheses was $p < 0.05$.

3. Results

3.1. Behavior

Following atropine (0.2 and 0.4 mg/kg) or scopolamine (0.1 mg/kg) administration, the animals were awake and were able to track the experimenters with their eyes; they were also capable of vocalization. When the animals, still under the effects of the drugs, were reintroduced to freely-moving condition (at the end of the experiments, 3–4 h after drug injection), they were able to ambulate.

3.2. Analysis of the EEG recordings

As expected, both doses of atropine increased heart rate and eliminated its variability (an example is shown in the tachogram of Fig. 1B); however, the agent produced clear central effects only at 0.4 mg/kg. Hence, we only analyzed the effects of the higher dose.

Atropine (0.4 mg/kg) produced high amplitude slow waves and spindles; i.e., a NREM sleep-like EEG (Fig. 1B); however, the animals continued in behavioral W. Cardiovascular effects reached their greatest values with a latency of 3–5 min, whereas EEG slow waves and spindles were fully developed after 30–40 min. These electrographic events are readily observed in the EEG and spectrogram of Fig. 1B.

In contrast to NREM sleep, but similar to AW, intense gamma activity (30–45 Hz) was present under atropine. In the spectrogram of Fig. 1B, following the atropine injection there was an intense gamma activity due to the high alertness induced by the puncture. Thereafter, there was a relative decrease in gamma power (to the level of QW), and after 50 min, gamma power was very high again. This increase in gamma power was accompanied by an increase in delta (0.5–3 Hz) and sigma (11–14 Hz) power (Fig. 1B).

The heart rate and EEG effect induced by scopolamine is also shown in Fig. 1B. The main difference with atropine is that the latency of the EEG effects is only about 3 min.

In raw recordings, it can be readily observed that gamma activity following atropine administration was present in the form of gamma "bursts", as was previously described for AW [24,25,27] (Fig. 2); these gamma “burst” seemed to be coupled between cortices. Similar results were obtained following scopolamine administration (Fig. 3). In 30–45 Hz filtered (band pass) recordings, it is readily apparent that after scopolamine, gamma activity and gamma coupling between cortices is very similar to during AW, but different compared to NREM sleep (Fig. 3). On the contrary, under scopolamine, slow waves and spindles were very similar compared to NREM sleep.

In summary, following either atropine or scopolamine administration, the EEG consisted of coupled gamma oscillations in a background of slow waves and spindles. Because these NREM sleep-like phenomena (delta waves and spindles) have been already described [36], we did not analyze them in detail.

3.3. Characterization of the gamma “bursts” following atropine/scopolamine treatment

The characteristics of the gamma “bursts” present following muscarinic antagonist treatment were analyzed. The gamma activity during these conditions was compared with the activity present in AW and NREM sleep. Because (disregarding the latency, Fig. 1B) the central

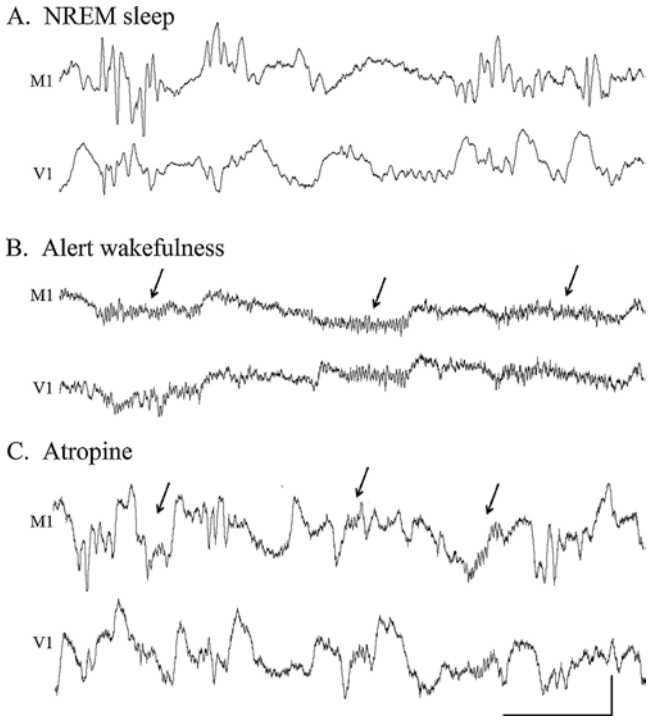

Fig. 2. Effects of atropine. Simultaneous raw EEG recordings from the primary motor cortex (M1) and primary visual cortex (V1) during: NREM sleep (A), alert wakefulness (B) and atropine administration (C). Arrows indicate gamma "burst" oscillations. Calibration bars: 1 s and 200 μV.

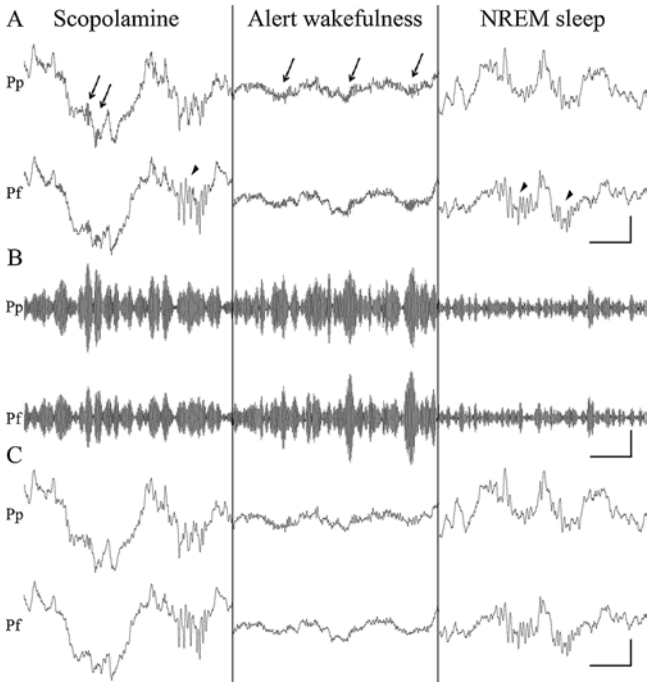

Fig. 3. Effects of scopolamine. The activity of the prefrontal (Pf) and posterior parietal cortex (Pp) during NREM sleep, alert wakefulness and following scopolamine administration are shown in: (A) simultaneous raw recordings, (B) 30–45 Hz and (C) 0.5–30 Hz band-pass filtered EEG recordings. Arrows and arrowheads indicate gamma "burst" and sleep spindles, respectively. Calibration bars: 1 s, 200 μV for A and C; 20 μV for B.

effects of scopolamine and atropine were similar, in this section we will do an overall description of gamma "bursts" under the effect of both muscarinic antagonists.

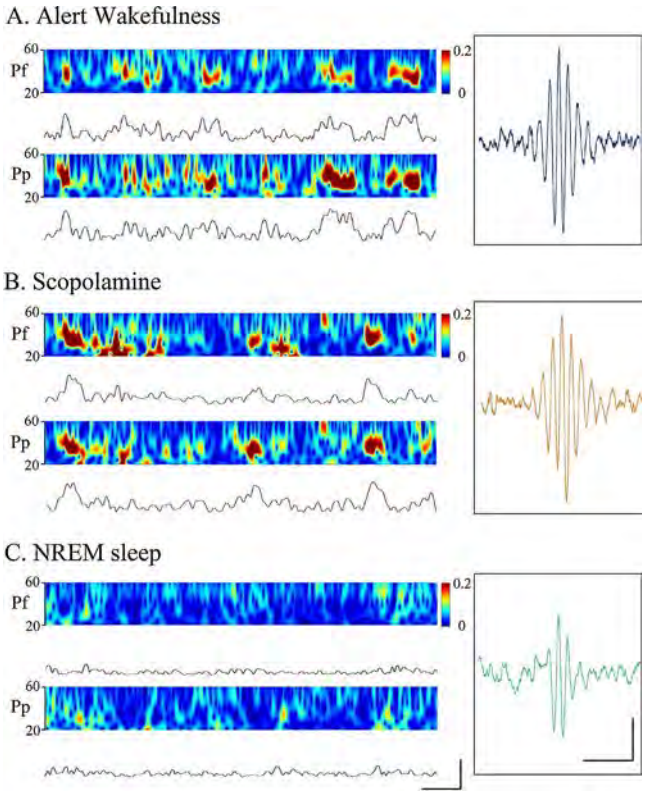

Fig. 4. Spectrograms (by means of wavelet function) and rectified gamma band (30–45 Hz) or gamma envelopes, during AW (A), under scopolamine (B) and during NREM sleep (C). For the spectrograms, frequency is represented in the ordinates, while the color code shows a wavelet coefficient that represent in relative units the energy of the signal. Calibration bars: 400 ms and 30 μV (for the envelopes). Insets. Average gamma "bursts" from a selected and filtered (high pass 3 Hz) recording of the prefrontal cortex. 100 random bursts were selected and averaged; the trigger was the peak of the higher amplitude wave of the "burst". Calibration bars: 10 μV and 200 ms.

In Fig. 4, gamma spectrograms and gamma envelopes were used to compare the dynamics of the "bursts" among AW, scopolamine and NREM sleep. While there is a marked coupling between cortices during AW and following scopolamine, this coupling is decreased during NREM sleep. The gamma burst waveforms were also similar (both in amplitude and duration) during AW and following muscarinic antagonists' treatment (Fig. 4, insets). Dominant frequency analysis revealed not significant differences between AW, atropine, and NREM sleep (37 ± 2 Hz, 36 ± 2 Hz and 35 ± 2 Hz, respectively; ANOVA). During NREM sleep although the dominant frequency is the same, Fig. 4 clearly shows that NREM sleep bursts have lower amplitude and duration.

Fig. 5A shows examples of the ACF of the gamma burst during AW and following atropine administration in the prefrontal cortex of a representative animal. CCF functions between filtered recordings (30–45 Hz) of prefrontal and posterior parietal cortices during AW and following atropine are also shown. ACFs and CCFs were similar during AW and following this pharmacological treatment.

In Fig. 5B the average of gamma bursts was shown. The gamma "bursts" under scopolamine (as well as under atropine, not shown) were associated with the slow waves negativity; similar association with the slow waves can be observed during NREM sleep.

3.4. Gamma power and coherence

The power spectrum analysis of the EEG on a representative animal and cortical site is shown in Fig. 6A. Power is similar in the recordings during NREM sleep, atropine and scopolamine for frequencies under

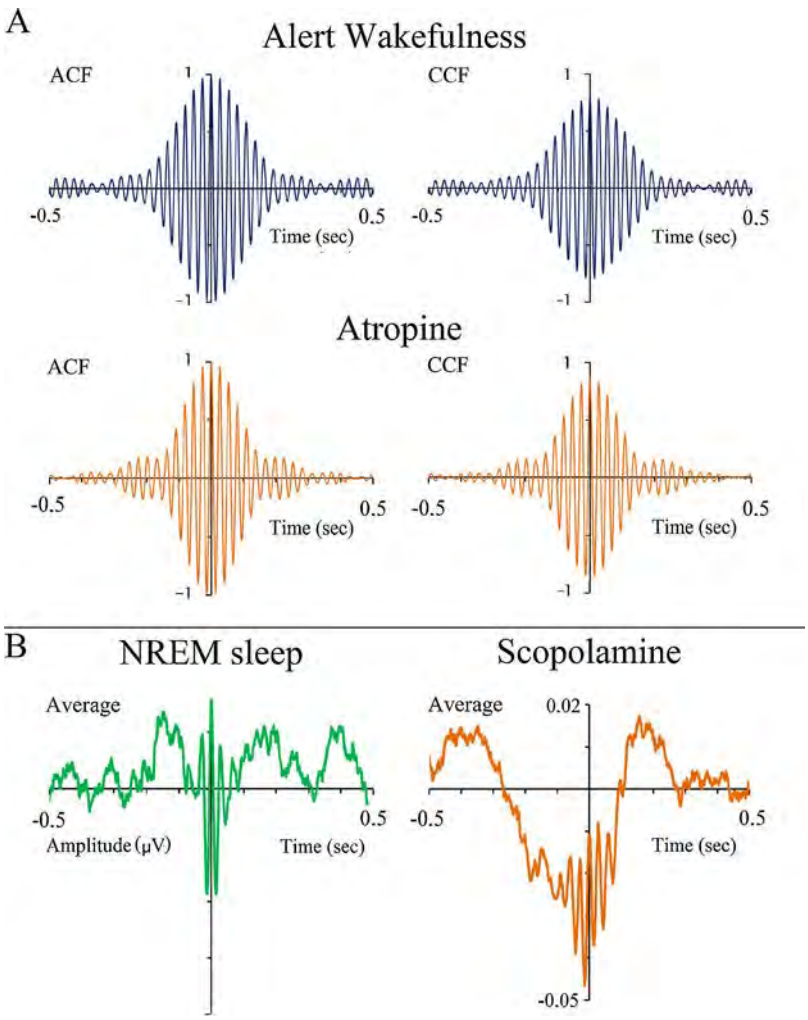

Fig. 5. A. Autocorrelation (ACF) and cross-correlation functions (CCF) from filtered (30–45 Hz) recordings. The functions were processed from 300 s EEG recording windows of the prefrontal cortex (ACF) and from simultaneous EEG recordings from the prefrontal cortex and posterior parietal cortex (CCF). The ACF and CCF are shown during alert wakefulness and following atropine administration. B. Averaged gamma "burst" of a selected raw recording of the prefrontal cortex. 100 random bursts were selected and averaged; the trigger was the peak of the higher amplitude wave of the "burst". The averages are shown during NREM sleep and following scopolamine administration.

30 Hz. In contrast, gamma band (30–45 Hz) power is larger following atropine and scopolamine administration compared to that present during NREM sleep (Fig. 6A, inset). Tables 1 and 2 present the results of a statistical analysis of gamma power for all animals (and recorded cortices). Gamma power under atropine (Table 1) or scopolamine (Table 2) was greater than during NREM sleep for all animals and most of the cortices (Table 1).

The coherence function was utilized to conduct an in-depth analysis of the 'coupling' between the gamma oscillations that were simultaneously recorded in different cortices during W and sleep, as well as under the effect of atropine and scopolamine. The z'-coherence profiles for a representative pair of EEG leads of one cat, of twelve 100-second periods and their average for AW as well as for atropine and scopolamine-induced states are exhibited in Fig. 6B1 and B2, respectively. z'-coherence profiles under atropine were similar to those during AW whereas following scopolamine, the z'-coherence profiles were still greater. The z-coherence average profiles for the different physiological and drug-induced states are displayed in Fig. 6C.

Fig. 7 shows the z-coherence between the "anterior" and "posterior" cortices for all animals treated with atropine. Following atropine administration, gamma coherence was larger than during QW, NREM and REM sleep.

Statistical analyses for z´-coherence are also shown for each animal (and cortical pairs) treated with atropine and scopolamine (Tables 3 and 4). In all the cats and derivatives analyzed, z'-coherence under atropine or scopolamine was greater than during NREM and REM sleep. Depending of the cat or derivative the z-coherence values were similar to AW (in most of the cases) or to QW.

4. Discussion

It is well known that muscarinic receptor antagonists induce behavioral W associated with slow waves and sleep spindles in the EEG (the EEG markers of NREM sleep). In the present report, we demonstrated that under the effect of atropine or scopolamine, coherent gamma (≈ 40 Hz) oscillations are also conspicuous.

Coherent gamma oscillations are a distinctive characteristic of attentive or alert W in the cat [24–27]. Therefore, this new finding has two important conceptual insights. First, acetylcholine, acting through muscarinic receptors, is not necessary to generate neocortical 40-Hz EEG oscillations. Second, the large and coherent gamma oscillations are likely the electrocortical footprints of the behavioral W that is present under the muscarinic cholinergic antagonists' treatment. In other words, this "dissociated" EEG with slow waves and sleep spindles, but also with coherent 40 Hz-oscillations (a trait of AW), may be the neurophysiologic basis of the "classic" EEG and behavior dissociation that is produced by these drugs.

4.1. Technical considerations

We used the cat as the animal model because it has well-defined, consolidated sleep and waking states. In addition, this animal model has the advantage that ≈40 Hz oscillations can be clearly observed directly in the raw EEG recordings [16,24]. Finally, the recordings were obtained in a semi-restricted condition, which has the advantage that the differences among states are the states *per se*; postures or movements did not influence the recordings, and movements' artifacts are

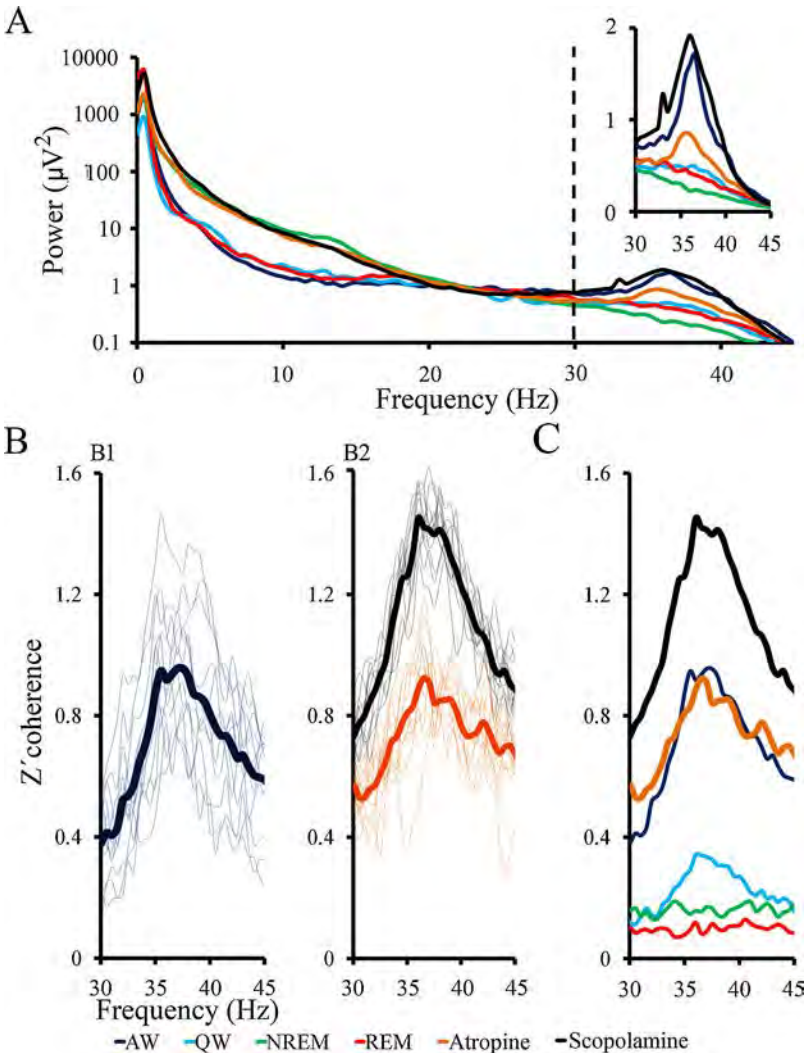

Fig. 6. A. Power spectrum (0–45 Hz) of the posterior-parietal cortex during alert (AW) and quiet (QW) wakefulness, sleep, atropine and scopolamine administration. The inset highlight the low gamma band. B. Twelve profiles of the z´-coherences (thin lines) of a representative pair of recordings (prefrontal and posterior-parietal cortices) as well as the averages of these 12 profiles (thick lines) are shown for AW (B1), and following atropine and scopolamine administration (B2). C. Average gamma z'-coherence profiles' during AW, QW, NREM sleep, REM sleep, atropine and scopolamine administration. Statistical analyses are presented in the Tables. All the analyses are from the same representative animal.

Table 1
Gamma (30–45 Hz) power values during sleep, wakefulness and following atropine administration.

		AW	QW	NREM	REM	A	F
C1	Pp	64.4 ± 2.4*	18.3 ± 4.7*	8.9 ± 0.3*	15.1 ± 0.5*	81.1 ± 3.7	66
	S1	15.3 ± 0.6	13.1 ± 0.9*	7.6 ± 0.3*	13.0 ± 0.6*	17.8 ± 0.8	7
C2	Pf	60.9 ± 3.1*	23.8 ± 3.6	12.5 ± 0.3	20.9 ± 0.4	18.6 ± 1.6	50
	Pp	57.6 ± 2.6*	21.1 ± 3.9	10.3 ± 0.3*	18.5 ± 0.5	23.1 ± 1.3	37
C3	Pp	14.0 ± 0.8*	10.8 ± 0.9	6.5 ± 0.6*	9.7 ± 1.3	9.9 ± 0.8	26
	S1	26.2 ± 1.5*	13.1 ± 0.9*	6.1 ± 0.4	7.7 ± 0.5	8.4 ± 0.8	131
C4	M1	75.8 ± 4.3*	26.7 ± 0.9*	15.8 ± 0.5*	19.6 ± 0.9*	34.3 ± 1.2	73
	V1	57.4 ± 3.0*	8.4 ± 0.6*	5.8 ± 0.91*	10.2 ± 0.5*	28.2 ± 3.6	55
C5	Pf	132.0 ± 4.0*	57.2 ± 5	20.5 ± 1.3*	18.3 ± 1.1*	51.2 ± 7,7	113
	S1	121.2 ± 4.9*	69.8 ± 4.4*	18.6 ± 1.8*	37.0 ± 2.4	38.9 ± 3.9	121
	Pp	174.0 ± 11.2*	79.8 ± 4.4	35.3 ± 3.2*	39.9 ± 2.5*	63.8 ± 5.0	85

The values represent mean ± standard error. The asterisks indicate statistical significance ($p < 0.05$) compared to atropine (A). ANOVA with Tamhane tests. All the analyses have the same degrees of freedom (4 between groups, 55 within groups). Right cortices are shown for C2 to C5, while left cortices are exhibited for C1.

also reduced.

In previous studies, we analyzed the gamma band in the cat up to 100 Hz [24–26]. In these studies, we demonstrated that the narrow 30–45 Hz band is highly modified by alertness or attention. This is not the case for higher gamma band (50–100 Hz), since we only observed that coherence decreased during REM sleep, without significant differences between AW, QW or NREM sleep. Hence, as we did before [27], in the present report we focused in low gamma (30–45 Hz) band. However, we noticed that high gamma coherence under scopolamine/atropine was similar than during AW, QW or NREM sleep (data not shown).

At random sound stimulation produces a large increase in gamma coherence ([24], and Fig. 6B and C). However, in pilot experiments we observed that under atropine/scopolamine the alertness induced by this stimulation did not further increase the gamma coherence (data not shown). Moreover, it is important to comment that in the present report we did not design experiments to explore the sensory evoked/induced potentials in the gamma range, neither in basal nor in drug-induced

Table 2
Gamma (30–45 Hz) power values during sleep, wakefulness and following scopolamine administration.

		AW	QW	NREM	REM	S	F
C1	Pp	64.4 ± 2.4	18.3 ± 4.7*	8.9 ± 0.3*	15.1 ± 0.5*	61.1 ± 5.3	6
	S1	15.3 ± 0.6	13.1 ± 0.9	7.6 ± 0.3*	13.0 ± 0.6	14.8 ± 2.4	64
C2	Pf	60.9 ± 3.1*	23.8 ± 3.6	12.5 ± 0.3*	20.9 ± 0.4	24.8 ± 1.2	71
	Pp	57.6 ± 2.6*	21.1 ± 3.9	10.3 ± 0.3*	18.5 ± 0.5	35.3 ± 1.4	71
C5	Pf	132.0 ± 4.0	57.2 ± 5*	20.5 ± 1.3*	18.3 ± 1.1*	69.1 ± 3.0	187
	S1	121.2 ± 4.9*	69.8 ± 4.4*	18.6 ± 1.8*	37.0 ± 2.4*	38.9 ± 3.9	116
	Pp	174.0 ± 11.2*	79.8 ± 4.4	35.3 ± 3.2*	39.9 ± 2.5*	112.0 ± 5.2	86

The values represent mean ± standard error. The asterisks indicate statistical significance ($p < 0.05$) compared to scopolamine (S). ANOVA with Tamhane tests. All the analyses have the same degrees of freedom (4 between groups, 55 within groups). Right cortices are shown for C2 and C5, while left cortices are exhibited for C1.

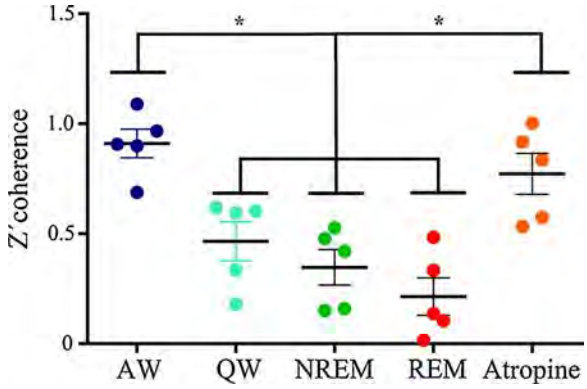

Fig. 7. The plot shows the z'-coherence from intra-hemispheric (Anterior-Posterior), combinations of electrodes during alert (AW) and quiet (QW) wakefulness, NREM and REM sleep, and following the administration of atropine. * $p < 0.0001$, $F_{4,24} = 31.4$, n = 5; rmANOVA and Bonferroni tests.

states.

Acetylcholine produces its biological effects by acting on nicotinic and muscarinic receptors. Five muscarinic receptors (M1–M5) have been cloned [37]. Atropine and scopolamine are non-selective competitive muscarinic antagonists that differ in their pharmacokinetics; the latter has a short half-life and easily permeates the blood-brain barrier, whereas atropine does not [38,39]. Hence, scopolamine has more pronounced and rapid central effects compared to atropine; this property may explain that the differences between both drugs were mainly in quantity, but not in quality.

4.2. Electrocortical and behavior dissociation

As shown in the present and several other studies (see Introduction), behavioral W is present following treatment with muscarinic receptor antagonists. However, subtle cognitive effects have been described in the cat [30]. In fact, scopolamine disrupts the executive phase of predation (i.e., the killing grip) and the consumption of prey without disturbing the preparatory (motivational) phase of predation (usually expressed in interest in the mouse and approaching it by means of crouching, running or jumping) [30].

Classic pharmacological studies have also shown cognitive disturbances in humans treated with atropine [40]. This drug produces a decrease in spontaneous speech and movement, impairment in memory and attention, and drowsiness. However, subjects are able to answer simple questions and perform tasks without the requirement of prolonged attention or memory. They can sit, stand, open or close their eyes or extend their extremities on request, although they move more slowly than in the pre-drug period. Scopolamine also produces sedation, impairment of coordinative and reactive skills, visual disturbances and diminution of short-term memory [41]. Furthermore, the drug affects simple and choice reaction time, number matching and memory scanning tasks. On the contrary, it does not modify word recognition and delayed word recall [39]. Sahakian (1988) suggested that the most prominent effects of scopolamine are those that involve discrimination processes, vigilance, selective attention, as well as consolidation and retrieval of memories [42].

Strikingly, following atropine or scopolamine treatment, the above-mentioned waking behavior in animals and humans is accompanied by sleep spindles and slow waves in the EEG [3,5,6,8,40,43–46]. The present results also demonstrate this fact. However, although we did not perform an in-depth analysis of slow waves and spindles, these waves are similar to those present during NREM sleep.

4.3. Gamma activity nested in slow waves

Figs. 3–5 clearly show that gamma activity is present during NREM sleep. Previous reports have already demonstrated that gamma activity can be observed nested in the slow waves “up states” during anesthesia and NREM sleep [47–51]. In our recordings, gamma oscillations both during atropine/scopolamine and NREM sleep, are associated with the negative component of the slow waves, which probably is associated with the “up states”. Hence, it is likely that atropine and scopolamine enhance these oscillations.

Table 3
Gamma (30–45 Hz) z'-coherence values during sleep, wakefulness and following atropine administration.

		AW	QW	NREM	REM	A	F
C1	Ppr-Ppl	1.13 ± 0.03	0.84 ± 0.07	0.77 ± 0.03*	0.55 ± 0.03*	1.52 ± 0.02	11
	S1l-Ppl	0.98 ± 0.04	0.41 ± 0.03*	0.53 ± 0.03*	0.33 ± 0.01*	1.00 ± 0.08	31
C2	Pfr-Ppr	0.90 ± 0.06	0.34 ± 0.05*	0.16 ± 0.01*	0.10 ± 0.01*	0.84 ± 0.03	38
	Ppr-Ppl	0.95 ± 0.04	0.46 ± 0.05*	0.27 ± 0.04*	0.20 ± 0.03*	0.96 ± 0.02	67
C3	Ppr-Ppl	0.43 ± 0.01	0.34 ± 0.04	0.05 ± 0.01*	0.05 ± 0.01*	0.47 ± 0.08	12
	S1r-Ppr	0.97 ± 0.02	0.60 ± 0.04*	0.48 ± 0.01*	0.48 ± 0.01*	0.92 ± 0.08	22
C4	M1r-V1r	0.91 ± 0.02*	0.18 ± 0.01*	0.15 ± 0.01*	0.02 ± 0.01*	0.53 ± 0.05	88
C5	Pfr-Ppr	0.69 ± 0.04*	0.59 ± 0.04*	0.42 ± 0.07	0.14 ± 0.06*	0.57 ± 0.04	215
	S1r-Ppr	0.91 ± 0.04*	0.82 ± 0.06	0.62 ± 0.06*	0.42 ± 0.03*	0.83 ± 0.03	190

The values represent mean ± standard error. The asterisks indicate statistical significance ($p < 0.05$) compared to atropine (A). ANOVA with Tamhane tests. All the analyses have the same degrees of freedom (4 between groups, 55 within groups).

Table 4
Gamma (30–45 Hz) z'-coherence values during sleep, wakefulness and following scopolamine administration.

		AW	QW	NREM	REM	S	F
C1	Ppr-Ppl	1.13 ± 0.03*	0.84 ± 0.07*	0.77 ± 0.03*	0.55 ± 0.03*	1.43 ± 0.02	70
	S1l-Ppl	0.98 ± 0.04*	0.41 ± 0.03*	0.53 ± 0.03*	0.33 ± 0.01*	1.26 ± 0.06	172
C2	Pfr-Ppr	0.90 ± 0.06*	0.34 ± 0.05*	0.16 ± 0.01*	0.10 ± 0.01*	1.30 ± 0.03	179
	Ppr-Ppl	0.95 ± 0.04*	0.46 ± 0.05*	0.27 ± 0.04*	0.20 ± 0.03*	1.09 ± 0.01	200
C5	Pfr-Ppr	0.69 ± 0.04*	0.59 ± 0.04	0.42 ± 0.07*	0.14 ± 0.06*	0.56 ± 0.01	184
	S1r-Ppr	0.91 ± 0.0*4	0.82 ± 0.06	0.62 ± 0.06*	0.42 ± 0.03*	0.92 ± 0.03	178

The values represent mean ± standard error. The asterisks indicate statistical significance ($p < 0.05$) compared to scopolamine (S). ANOVA with Tamhane tests. All the analyses have the same degrees of freedom (4 between groups, 55 within groups).

4.4. Lessons for cognitive functions

The present results strongly suggest that the presence of spindles and delta waves oscillations in the EEG, by their own, are not responsible for the total loss of consciousness that occurs during deep NREM sleep [52]. Nevertheless, although behavioral W is present under atropine/scopolamine, cognition is affected.

Slow waves. It has been hypothesized that the brain's capacity to generate conscious experiences is reduced in the presence of slow waves [23,52,53]. In this regard, thalamo-cortical neurons become hyperpolarized and fire in a burst mode during the slow waves of NREM sleep. This hyperpolarization reduces the transmission of sensory information through the thalamus, which results in the cortex being, at least partially, functionally disconnected from outside sensory experiences [54]. Furthermore, because the level of consciousness depends on the brain's capacity to integrate large amount of information [55], the intracortical reduction of communication during NREM sleep is likely to be directly involved in the loss of consciousness [56].

Gamma activity. In spite of the presence of gamma activity during sleep, recordings with macroelectrodes in the present and previous studies in animals [15,24,57], and humans [58], have shown that during NREM sleep there is a decrease in gamma power compared to W (AW and QW) and REM sleep. In addition, compared to W, long-range gamma coherence or functional connectivity is reduced during NREM sleep [24,57–59]. In contrast, high gamma power and coherence in the EEG are present following muscarinic receptor antagonists' treatment.

Hence, gamma power, which is related to local synchronization at that frequency, and gamma coherent activity, that reflects functional interactions between "distant" cortical areas, may contribute in a significant way to the maintenance of a functional cognitive state during W; i.e. it is likely critical for consciousness. In fact, studies utilizing general anesthetics as an "off-switch" for consciousness, have shown that a strong reduction in gamma coherence (mainly between far cortical regions) is correlated with the loss of awareness [60–62]. Therefore, it is possible that in order to lose consciousness, as in deep NREM sleep, both slow waves and a decrease in gamma coherence are required.

Based on experiment in rats, Vanderwolf (2000) showed that while during W there is a continuous cortical gamma activity, during anesthesia as well as under scopolamine, predominates an interrupted pattern of gamma waves [51]. The author suggested that this last profile may not support a normal cognitive function. A detailed analysis of the temporal patterns of the gamma "bursts" during W, sleep, and under different drugs that affect cognition is still lacking.

4.5. The activation of muscarinic receptors is not needed for gamma activity

Gamma-band rhythmogenesis is inextricably tied to perisomatic inhibition in the cerebral cortex, wherein the key ingredient is $GABA_A$-receptor mediated inhibition [63]. GABAergic cortical neurons, glutamatergic cortico-cortical neurons as well as glutamatergic thalamo-cortical neurons have been suggested as the anatomical substrate for gamma band oscillations and coherence in the EEG [20,63]. Intrinsic neuronal properties of cortical neurons that determine that when activated by subthreshold current injection produce membrane potential oscillations at or near 40 Hz may be also involved [64]. In addition, thalamo-cortical activity is modulated by regulatory systems that consist of small groups of neurons that, with a common neurotransmitter, project to many regions of the central nervous system [1,2]. Cholinergic, monoaminergic and hypocretinergic neurons are part of these systems. By acting through the thalamus and/or cortex, these systems promote W and may regulate the appearance of gamma oscillations and coherence (and therefore cognitive functions). In fact, activation of the mesencephalic reticular formation, where part of the activating systems are located, was shown to facilitate oscillatory activity in the gamma frequency range and to enhance the stimulus-specific synchronization of neuronal spike responses in the visual cortex of cats [65].

Cholinergic neurons of the laterodorsal and pedunculo-pontine tegmental nucleus (LDT and PPT) project to the non-specific thalamo-cortical system where they promote cortical activation [1,2]. Cholinergic neurons discharge at high rates during W and REM sleep [66]. In addition, Garcia-Rill and co-workers sustain that neurons within the PPT generate beta/gamma band activity during waking [67,68]. These neurons have low-gamma membrane oscillations that are mediated by voltage-dependent high-threshold N- and P/Q-type calcium channels modulated by G proteins. In anesthetized animals, cholinergic projection neurons in the PPT fire rhythmically during cortical slow oscillations, and predominantly discharge in time with the phase of the slow oscillations supporting nested gamma oscillations (30–60 Hz) [49]. Also, cholinergic neurons of the basal forebrain have long been known to have an important role in cortical activation [69]. However, we found that atropine and scopolamine are unable to prevent coherent gamma oscillation. Then, this result suggests that the acetylcholine, acting through muscarinic receptors, is not critical to generate coherent gamma activity. In agreement with these findings, the role of cholinergic basal forebrain neurons in the generation of gamma oscillations in the EEG has been negated [70]; however, basal forebrain GABAergic neurons that project to the cortex play an important role in the generation of gamma activity [70]. The fact that cholinergic neurons are active during REM sleep [66], and gamma coherence in virtually absent during this behavioral state [24,26,27,57,58,71,72], is in total agreement with the present results. However, following antimuscarinic treatment, ensembles of cholinergic (through nicotinic receptors), glutamatergic and GABAergic neurons of the PPT may still transfer gamma actitity to the cortex through the intalaminar thalamic nuclei, or by the regulation of non-cholinergic neurons of the basal forebrain [73,74]. Finally, also in accordance with our results, systemic atropine administration in exploring mice increases the amplitude of gamma oscillations of the CA1 region of the dorsal hippocampus [75].

Monoaminergic and hypocretinergic systems, that may remain active following the administration of muscarinic receptor antagonists, might induce gamma power and gamma coherence acting through the thalamus and/or cortex despite the presence of sleep spindles and slow waves. New sets of experiments are needed to test this hypothesis.

4.6. Pathology, toxicology and drug abuse

A decrease in cortical cholinergic activity is present in Alzheimer disease (AD); this illnesses involve a failure to focus on the most relevant information, and difficulty in maintaining an appropriate stream of awareness [76]. Interestingly, AD patients increased sensory-evoked and event-related gamma coherence values compared to healthy controls [77].

Anticholinergic drugs have been used for recreational or ritualistic purposes. One of the most widely described religious or magical experiences dating back to ancient times is the alteration of consciousness with the induction of hallucinations by a member of the Solanaceae family of plants (Belladonna, Henbane or Datura), which contain scopolamine, atropine and other closely related alkaloids [76]. Similar effects occur with the intoxication either with prescribed anti-muscarinic medical drugs [76]. Perhaps the most extraordinary example of cognitive dysfunction is the criminal use of anticholinergic substances that are present in Datura extracts (called "burundanga"), to induce amnesia and submissive behavior or "obedience" in victims [78,79]. Our results that demonstrate the presence of coherent gamma activity following anti-muscarinic receptor treatment; this result is important to advance our understanding of the syndromes that occur when the central cholinergic system is dysfunctional.

Finally, psychosis is associated with disturbances in gamma coherence [80–82]. Interestingly, second generation antipsychotic drugs such as clozapine and olanzapine have an important antagonism on M1 receptors [83]. Hence, due to antimuscarinic antagonists conserve gamma coherence (present results), it would be interesting to know if the benefits of clozapine and olanzapine is in part associated with their impact on gamma activity.

5. Conclusions

Although atropine and scopolamine produced an EEG with slow waves and sleep spindles that resemble NREM sleep, functional interactions between cortical areas in the gamma band remained high, similar to AW. This phenomenon could explain the dissociation between the EEG and behavior that is elicited by muscarinic receptor antagonist drugs.

Acknowledgements

This work is dedicated to the memory of our dear mentor Dr. Michael Chase, that regretfully passed away this year. Dr. Chase collaborated with an early version of this work.

This study was supported by the "Programa de Desarrollo de Ciencias Básicas", PEDECIBA, by the "Agencia Nacional de Investigación e Innovación"(ANII)-FCE-2-2011-1-7030, and by the "Comisión Sectorial de Investigación Científica"(CSIC) I+D-2016-589 grants from Uruguay.

References

[1] P. Torterolo, G. Vanini, New concepts in relation to generating and maintaining arousal, Rev. Neurol. 50 (12) (2010) 747–758.
[2] P. Torterolo, J.M. Monti, S.R. Pandi-Perumal, Neuroanatomy and neuropharmacology of sleep and wakefulness, in: S.R. Pandi-Perumal (Ed.), Synopsis of Sleep Medicine, Apple Academic Press, Oakville, Canada, 2016.
[3] A. Wikler, Pharmacologic dissociation of behavior and EEG "sleep patterns" in dogs; morphine, n-allylnormorphine, and atropine, Proc. Soc. Exp. Biol. Med. 79 (2) (1952) 261–265.
[4] F. Rinaldi, H.E. Himwich, Alerting responses and actions of atropine and cholinergic drugs, AMA Arch. Neurol. Psychiatry 73 (4) (1955) 387–395.
[5] P.B. Bradley, B.J. Key, The effect of drugs on arousal responses produced by electrical stimulation of the reticular formation of the brain, Electroencephalogr. Clin. Neurophysiol. 10 (1) (1958) 97–110.
[6] V.G. Longo, Effects of scopolamine and atropine electroencephalographic and behavioral reactions due to hypothalamic stimulation, J. Pharmacol. Exp. Ther. 116 (2) (1956) 198–208.
[7] K.L. Chow, E.R. John, Acetylcholine metabolism and behavior of rats, Science 129 (3340) (1959) 64.
[8] J. Yamamoto, Roles of cholinergic, dopaminergic, noradrenergic, serotonergic and GABAergic systems in changes of the EEG power spectra and behavioral states in rabbits, Jpn. J. Pharmacol. 47 (2) (1988) 123–134.
[9] D.F. Lindsley, R.S. Carpenter, E.K. Killam, K.F. Killam, EEG correlates of behavior in the cat. I. Pattern discrimination and its alteration by atropine and LSD-25, Electroencephalogr. Clin. Neurophysiol. 24 (6) (1968) 497–513.
[10] C. von der Malsburg, Binding in models of perception and brain function, Curr. Opin. Neurobiol. 5 (4) (1995) 520–526.
[11] R. Velik, From single neuron-firing to consciousness, towards the true solution of the binding problem, Neurosci. Biobehav. Rev. 34 (7) (2009) 993–1001.
[12] M.K. Rieder, B. Rahm, J.D. Williams, J. Kaiser, Human gamma-band activity and behavior, Int. J. Psychophysiol. 79 (1) (2010) 39–48.
[13] P.J. Uhlhaas, G. Pipa, B. Lima, L. Melloni, S. Neuenschwander, D. Nikolic, W. Singer, Neural synchrony in cortical networks: history, concept and current status, Front. Integr. Neurosci. 3 (2009) 17.
[14] P.J. Uhlhaas, G. Pipa, S. Neuenschwander, M. Wibral, W. Singer, A new look at gamma? High- (&60 Hz) gamma-band activity in cortical networks: function, mechanisms and impairment, Prog. Biophys. Mol. Biol. 105 (1–2) (2011) 14–28.
[15] K.J. Maloney, E.G. Cape, J. Gotman, B.E. Jones, High-frequency gamma electroencephalogram activity in association with sleep-wake states and spontaneous behaviors in the rat, Neuroscience 76 (2) (1997) 541–555.
[16] J.J. Bouyer, M.F. Montaron, A. Rougeul, Fast fronto-parietal rhythms during combined focused attentive behaviour and immobility in cat: cortical and thalamic localizations, Electroencephalogr. Clin. Neurophysiol. 51 (3) (1981) 244–252.
[17] R. Llinas, U. Ribary, Coherent 40-Hz oscillation characterizes dream state in humans, Proc. Natl. Acad. Sci. U. S. A. 90 (5) (1993) 2078–2081.
[18] H. Tiitinen, J. Sinkkonen, K. Reinikainen, K. Alho, J. Lavikainen, R. Naatanen, Selective attention enhances the auditory 40-Hz transient response in humans, Nature 364 (6432) (1993) 59–60.
[19] M. Steriade, F. Amzica, D. Contreras, Synchronization of fast (30-40 Hz) spontaneous cortical rhythms during brain activation, J. Neurosci. 16 (1) (1996) 392–417.
[20] R. Llinas, U. Ribary, D. Contreras, C. Pedroarena, The neuronal basis for consciousness, Philos. Trans. R. Soc. Lond. B Biol. Sci. 353 (1377) (1998) 1841–1849.
[21] E. Rodriguez, N. George, J.P. Lachaux, J. Martinerie, B. Renault, F.J. Varela, Perception's shadow: long-distance synchronization of human brain activity, Nature 397 (6718) (1999) 430–433.
[22] T.H. Bullock, M.C. McClune, J.T. Enright, Are the electroencephalograms mainly rhythmic? Assessment of periodicity in wide-band time series, Neuroscience 121 (1) (2003) 233–252.
[23] G.M. Edelman, G. Tononi, A Universe of Consciousness, Basic Books, 2000 New York.
[24] S. Castro, A. Falconi, M.H. Chase, P. Torterolo, Coherent neocortical 40-Hz oscillations are not present during REM sleep, Eur. J. Neurosci. 37 (8) (2013) 1330–1339.
[25] S. Castro, M. Cavelli, P. Vollono, M.H. Chase, A. Falconi, P. Torterolo, Inter-hemispheric coherence of neocortical gamma oscillations during sleep and wakefulness, Neurosci. Lett. 578 (2014) 197–202.
[26] M. Cavelli, S. Castro-Zaballa, A. Mondino, J. Gonzalez, A. Falconi, P. Torterolo, Absence of EEG gamma coherence in a local activated neocortical state: a conserved trait of REM sleep, Transl. Brain Rhytmicity 2 (1) (2017) 1–13.
[27] P. Torterolo, S. Castro-Zaballa, M. Cavelli, M.H. Chase, A. Falconi, Neocortical 40 Hz oscillations during carbachol-induced rapid eye movement sleep and cataplexy, Eur. J. Neurosci. 43 (4) (2016) 580–589.
[28] V. Brando, S. Castro-Zaballa, A. Falconi, P. Torterolo, E.R. Migliaro, Statistical, spectral and non-linear analysis of the heart rate variability during wakefulness and sleep, Arch. Ital. Biol. 152 (1) (2014) 32–46.
[29] P. Torterolo, J. Yamuy, S. Sampogna, F.R. Morales, M.H. Chase, Hypocretinergic neurons are primarily involved in activation of the somatomotor system, Sleep 1 (2003) 25–28.
[30] J. Zagrodzka, P. Kubiak, Scopolamine-induced alterations in predatory behaviour pattern in cats, Acta Neurobiol. Exp. (Wars.) 51 (1–2) (1991) 29–36.
[31] W.R. Martin, C.G. Eades, A comparative study of the effect of drugs on activating and vasomotor responses evoked by midbrain stimulation: atropine, pentobarbital, chlorpromazine and chlorpromazine sulfoxide, Psychopharmacologia 1 (1960) 303–335.
[32] G.H. Hall, Effects of nicotine and tobacco smoke on the electrical activity of the cerebral cortex and olfactory bulb, Br. J. Pharmacol. 38 (2) (1970) 271–286.
[33] P. Torterolo, S. Castro-Zaballa, M. Cavelli, N. Velasquez, V. Brando, A. Falconi, M.H. Chase, E.R. Migliaro, Heart rate variability during carbachol-induced REM sleep and cataplexy, Behav. Brain Res. 291 (2015) 72–79.
[34] B. Babadi, E.N. Brown, A review of multitaper spectral analysis, IEEE Trans. Biomed. Eng. 61 (5) (2014) 1555–1564.
[35] B.J. Roach, D.H. Mathalon, Event-related EEG time-frequency analysis: an overview of measures and an analysis of early gamma band phase locking in schizophrenia, Schizophr. Bull. 34 (5) (2008) 907–926.
[36] V. Santucci, A. Glatt, H. Demieville, H.R. Olpe, Quantification of slow-wave EEG induced by atropine: effects of physostigmine, amphetamine and haloperidol, Eur. J. Pharmacol. 73 (2–3) (1981) 113–122.
[37] C.J. Langmead, J. Watson, C. Reavill, Muscarinic acetylcholine receptors as CNS drug targets, Pharmacol. Ther. 117 (2) (2008) 232–243.
[38] L. Brunton, K. Parker, Goodman and Gilman's Manual of Pharmacology and Therapeutics, McGraw Hill Medical, New York, 2008.
[39] U. Ebert, M. Siepmann, R. Oertel, K.A. Wesnes, W. Kirch, Pharmacokinetics and pharmacodynamics of scopolamine after subcutaneous administration, J. Clin.

Pharmacol. 38 (8) (1998) 720–726.
[40] A.M. Ostfeld, X. Machne, K.R. Unna, The effects of atropine on the electroencephalogram and behavior in man, J. Pharmacol. Exp. Ther. 128 (1960) 265–272.
[41] E. Nuotto, Psychomotor, physiological and cognitive effects of scopolamine and ephedrine in healthy man, Eur. J. Clin. Pharmacol. 24 (5) (1983) 603–609.
[42] B. Sahakian, Cholinergic drugs and human cognitive performance, Handbook of Psychopharmcology, (1988), pp. 393–424.
[43] P.B. Bradley, J. Elkes, The effects of some drugs on the electrical activity of the brain, Brain 80 (1) (1957) 77–117.
[44] W.G. Sannita, M. Fioretto, L. Maggi, G. Rosadini, Effects of scopolamine parenteral administration on the electroretinogram, visual evoked potentials, and quantitative electroencephalogram of healthy volunteers, Doc. Ophthalmol. 67 (4) (1987) 379–388.
[45] W.G. Sannita, L. Maggi, G. Rosadini, Effects of scopolamine (0.25–0.75 mg i.m.) on the quantitative EEG and the neuropsychological status of healthy volunteers, Neuropsychobiology 17 (4) (1987) 199–205.
[46] T.M. Itil, Anticholinergic drug-induced sleep-like EEG pattern in man, Psychopharmacologia 14 (5) (1969) 383–393.
[47] M. Valencia, J. Artieda, J.P. Bolam, J. Mena-Segovia, Dynamic interaction of spindles and gamma activity during cortical slow oscillations and its modulation by subcortical afferents, PLoS One 8 (7) (2013) e67540.
[48] M. Le Van Quyen, R. Staba, A. Bragin, C. Dickson, M. Valderrama, I. Fried, J. Engel, Large-scale microelectrode recordings of high-frequency gamma oscillations in human cortex during sleep, J. Neurosci. 30 (23) (2010) 7770–7782.
[49] J. Mena-Segovia, H.M. Sims, P.J. Magill, J.P. Bolam, Cholinergic brainstem neurons modulate cortical gamma activity during slow oscillations, J. Physiol. 586 (Pt 12) (2008) 2947–2960.
[50] M. Valderrama, B. Crepon, V. Botella-Soler, J. Martinerie, D. Hasboun, C. Alvarado-Rojas, M. Baulac, C. Adam, V. Navarro, M. Le Van Quyen, Human gamma oscillations during slow wave sleep, PLoS One 7 (4) (2012) e33477.
[51] C.H. Vanderwolf, Are neocortical gamma waves related to consciousness? Brain Res. 855 (2) (2000) 217–224.
[52] G. Tononi, Sleep and dreaming, in: S. Laureys, G. Tononi (Eds.), The Neurology of Consciousness: Cognitive Neuroscience and Neuropathology, Elsevier, San Diego, 2009, pp. 89–107.
[53] F. Siclari, G. Tononi, Local aspects of sleep and wakefulness, Curr. Opin. Neurobiol. 44 (2017) 222–227.
[54] M. Steriade, D.A. McCormick, T.J. Sejnowski, Thalamocortical oscillations in the sleeping and aroused brain, Science 262 (5134) (1993) 679–685.
[55] G. Tononi, Information integration: its relevance to brain function and consciousness, Arch. Ital. Biol. 148 (3) (2010) 299–322.
[56] M. Massimini, F. Ferrarelli, R. Huber, S.K. Esser, H. Singh, G. Tononi, Breakdown of cortical effective connectivity during sleep, Science 309 (5744) (2005) 2228–2232.
[57] M. Cavelli, S. Castro, N. Schwarzkopf, M.H. Chase, A. Falconi, P. Torterolo, Coherent neocortical gamma oscillations decrease during REM sleep in the rat, Behav. Brain Res. 281 (2015) 318–325.
[58] J.L. Cantero, M. Atienza, J.R. Madsen, R. Stickgold, Gamma EEG dynamics in neocortex and hippocampus during human wakefulness and sleep, Neuroimage 22 (3) (2004) 1271–1280.
[59] E. Mikulan, E. Hesse, L. Sedeno, T. Bekinschtein, M. Sigman, M.D.C. Garcia, W. Silva, C. Ciraolo, A.M. Garcia, A. Ibanez, Intracranial high-gamma connectivity distinguishes wakefulness from sleep, Neuroimage 169 (2018) 265–277.
[60] G.A. Mashour, Integrating the science of consciousness and anesthesia, Anesth. Analg. 103 (4) (2006) 975–982.
[61] E.R. John, The neurophysics of consciousness, Brain Res. Brain Res. Rev. 39 (1) (2002) 1–28.
[62] D. Pal, B.H. Silverstein, H. Lee, G.A. Mashour, Neural correlates of wakefulness, sleep, and general anesthesia: an experimental study in rat, Anesthesiology 125 (5) (2016) 929–942.
[63] G. Buzsaki, X.J. Wang, Mechanisms of gamma oscillations, Annu. Rev. Neurosci. 35 (2012) 203–225.
[64] R.R. Llinas, A.A. Grace, Y. Yarom, In vitro neurons in mammalian cortical layer 4 exhibit intrinsic oscillatory activity in the 10- to 50-Hz frequency range, Proc. Natl. Acad. Sci. U. S. A. 88 (3) (1991) 897–901.
[65] M.H. Munk, P.R. Roelfsema, P. Konig, A.K. Engel, W. Singer, Role of reticular activation in the modulation of intracortical synchronization, Science 272 (5259) (1996) 271–274.
[66] S. Boucetta, Y. Cisse, L. Mainville, M. Morales, B.E. Jones, Discharge profiles across the sleep-waking cycle of identified cholinergic, GABAergic, and glutamatergic neurons in the pontomesencephalic tegmentum of the rat, J. Neurosci. 34 (13) (2014) 4708–4727.
[67] E. Garcia-Rill, B. Luster, S. D'Onofrio, S. Mahaffey, V. Bisagno, F.J. Urbano, Implications of gamma band activity in the pedunculopontine nucleus, J. Neural Transm. (Vienna) 123 (7) (2015) 655–665.
[68] E. Garcia-Rill, Bottom-up gamma and stages of waking, Med. Hypotheses 104 (2017) 58–62.
[69] B.E. Jones, Activity, modulation and role of basal forebrain cholinergic neurons innervating the cerebral cortex, Prog. Brain Res. 145 (2004) 157–169.
[70] T. Kim, S. Thankachan, J.T. McKenna, J.M. McNally, C. Yang, J.H. Choi, L. Chen, B. Kocsis, K. Deisseroth, R.E. Strecker, R. Basheer, R.E. Brown, R.W. McCarley, Cortically projecting basal forebrain parvalbumin neurons regulate cortical gamma band oscillations, Proc. Natl. Acad. Sci. U. S. A. 112 (11) (2015) 3535–3540.
[71] E. Perez-Garci, Y. del-Rio-Portilla, M.A. Guevara, C. Arce, M. Corsi-Cabrera, Paradoxical sleep is characterized by uncoupled gamma activity between frontal and perceptual cortical regions, Sleep 24 (1) (2001) 118–126.
[72] U. Voss, R. Holzmann, I. Tuin, J.A. Hobson, Lucid dreaming: a state of consciousness with features of both waking and non-lucid dreaming, Sleep 32 (9) (2009) 1191–1200.
[73] E. Garcia-Rill, B. Luster, S. Mahaffey, M. MacNicol, J.R. Hyde, S.M. D'Onofrio, C. Phillips, Pedunculopontine gamma band activity and development, Brain Sci. 5 (4) (2015) 546–567.
[74] R. Szymusiak, Magnocellular nuclei of the basal forebrain: substrates of sleep and arousal regulation, Sleep 18 (6) (1995) 478–500.
[75] S. Balakrishnan, R.A. Pearce, Spatiotemporal characteristics and pharmacological modulation of multiple gamma oscillations in the CA1 region of the hippocampus, Front. Neural Circuits 8 (2014) 150.
[76] E.K. Perry, R.H. Perry, Acetylcholine and hallucinations: disease-related compared to drug-induced alterations in human consciousness, Brain Cogn. 28 (3) (1995) 240–258.
[77] E. Basar, B. Femir, D.D. Emek-Savas, B. Guntekin, G.G. Yener, Increased long distance event-related gamma band connectivity in Alzheimer's disease, Neuroimage Clin. 14 (2017) 580–590.
[78] A. Ardila-Ardila, C.B. Moreno, S.E. Ardila-Gomez, Scopolamine poisoning ('burundanga'): loss of the ability to make decisions, Rev. Neurol. 42 (2) (2006) 125–128.
[79] A. Ardila, C. Moreno, Scopolamine intoxication as a model of transient global amnesia, Brain Cogn. 15 (2) (1991) 236–245.
[80] L. Kornmayer, G. Leicht, C. Mulert, Attentional capture by physically salient stimuli in the gamma frequency is associated with schizophrenia symptoms, World J. Biol. Psychiatry (2016) 1–11.
[81] V. Suazo, A. Lubeiro, R. Jurado-Barba, M. Moreno-Ortega, M. Dompablo, I. Morales-Munoz, R. Rodriguez-Jimenez, T. Palomo, V. Molina, Elevated midline-parietal gamma band noise power in schizophrenia but not in bipolar patients, Eur. Arch. Psychiatry Clin. Neurosci. 266 (8) (2016) 743–753.
[82] G. Leicht, S. Vauth, N. Polomac, C. Andreou, J. Rauh, M. Mussmann, A. Karow, C. Mulert, EEG-informed fMRI reveals a disturbed gamma-band-Specific network in subjects at high risk for psychosis, Schizophr. Bull. 42 (1) (2016) 239–249.
[83] J.M. Monti, P. Torterolo, S.R. Pandi Perumal, The effects of second generation antipsychotic drugs on sleep variables in healthy subjects and patients with schizophrenia, Sleep Med. Rev. 33 (2017) 51–57.

Anexo 5

(Torterolo et al., 2019)

Chapter 1

Arousal and normal conscious cognition

Pablo Torterolo, Santiago Castro-Zaballa, Matías Cavelli, Joaquín Gonzalez

Laboratory of Sleep Neurobiology, Department of Physiology, School of Medicine, Republic University, Montevideo, Uruguay

Introduction

The knowledge of the neurophysiological processes that generates and maintains consciousness provides the clinician the foundations to understand its absence and alterations. Consciousness is probably the main feature of human wakefulness (W), which is lost in the falling asleep process. However, we have a hint that during our night sleep, our mind is very active and fly without control during our dreams. Dreams are a different type of cognitive state, with its own rules. Neurological syndromes such as comma or vegetative state suppress consciousness. Psychiatric conditions such as psychosis generate an alteration of consciousness. Furthermore, while general anesthetic drugs suppress consciousness, several drugs, such as hallucinogens, alter it.

Which are the neuronal networks involved in the generation consciousness? How do they work? What are the adjustments in these networks that determine that consciousness is not supported during sleep? In the present chapter, focusing on the information provided by the electroencephalogram (EEG), we reviewed the most relevant concepts of the electrocortical correlates of normal conscious cognition and the physiological and drug-induced network modification that are involved in its absence or alteration.

Arousal and consciousness

Arousal is the physiological and psychological state of being awoken from sleep and the increase in vigilance or alertness during W. It involves the function of the activating system (AS) in the brain; one of its main components is the reticular activating system (RAS) whose soma is located in the mesopontine brain stem. The RAS is a phylogenetically conserved system that modulates fight-or-flight responses (Yates and Garcia-Rill, 2015). An increase in the firing

Arousal in Neurological and Psychiatric Diseases. https://doi.org/10.1016/B978-0-12-817992-5.00001-5

rate of the RAS neurons mediates the activation of the thalamocortical system (i.e., the main neuroanatomical structure associated with consciousness), the sympathetic autonomic nervous system, and the motor and the endocrine systems (Yates and Garcia-Rill, 2015). This increase in the firing rate of RAS neurons generates sensory alertness, mobility, and readiness to respond, that is, accompanied by an increase in heart rate and blood pressure, respiratory activity, and other phenomena related with fight-or-flight responses. Hence, during W, there are periods with low level of arousal (quiet or relaxed W) and periods with high level of arousal. A novel, painful, or motivational stimuli can induce high level of arousal; in any case, the result is alertness or full attention status. In humans (and supposedly in animals with high cognitive abilities), arousal is accompanied by consciousness.

"There is nothing we know more intimately than consciousness, but there is nothing harder to explain," stated the mind philosopher David Chalmers (Chalmers, 2005). Dictionaries usually define consciousness as the ability to be aware of surroundings and ourselves. Although this is a circular definition (because awareness and consciousness are synonyms), it captures the essence: consciousness allows us to know about ourselves and the existence of objects and events (Damasio and Meyer, 2009). In the present work, following the directives of Edelman and Tononi, we define consciousness in practical terms: "Everyone knows what consciousness is: it is what abandons you every evening when you fall asleep and reappears the next morning when you wake up" (Edelman and Tononi, 2000). This definition suggests that for normal W, consciousness is a sine qua non condition. However, we must keep in mind that dreams are considered a special (or altered) type of consciousness (see succeeding text).

The concept of "neural correlates of consciousness" (NCC) represents the smallest set of neural events and structures sufficient for a given conscious percept, explicit memory, or cognitive function. Where is the structural (neural) basis of consciousness? The thalamocortical system is the ultimate responsible for the generation of consciousness, and the associative cortices play a major role (Llinas and Pare, 1991; Tononi and Laureys, 2009).

Due to fact that the thalamocortical system is also the main responsible for the electric activity recorded in the EEG, in this chapter, we will focus in the EEG phenomena related to arousal and normal conscious condition and in its physiological and nonphysiological suppression or alteration.

Electroencephalogram

The EEG is produced by the summed electric activities of populations of neurons, with a modest contribution from glial cells (Lopes da Silva, 2010). Pyramidal neurons of the cortex are the main contributor of the EEG signal, since they are arranged in palisades with the apical dendrites aligned perpendicularly to the cortical surface. The electric fields generated by these neurons can be recorded by means of

electrodes located at a short distance from the source (local field potentials, LFPs), from the cortical surface (electrocorticogram or ECoG), or at longer distances such as from the scalp (standard EEG). In the standard EEG, oscillations higher than 30 Hz are difficult to observe because they are filtered out by the skull and scalp and there is more distance from the source and worse spatial resolution. On the contrary, oscillations up to 200 Hz can be recorded with LFPs or ECoG.

Several oscillatory rhythms can be observed in the EEG. These rhythms are generated in the thalamus and/or at cortical levels and are modified according to the behavioral state (W and sleep).

Wakefulness

In humans (and mammals in general), three behavioral states can be distinguished: W, nonrapid eye movement (NREM) sleep (also called slow-wave sleep), and rapid eye movement (REM) sleep. These behavioral states can be recognized by means of polysomnography, which consists of the simultaneous recording of various physiological parameters such as EEG, electromyogram (EMG), and electrooculogram.

The EEG recording during W is characterized by the presence of high-frequency and low-voltage oscillations (cortical activation). The EEG (ECoG in sensu stricto) during W (alert wakefulness, AW; quite wakefulness, QW) of a cat is shown in Fig. 1.1. EEG recordings during W show relatively low-amplitude and high-frequency oscillations (active EEG). As it is shown in Fig. 1.2, the analysis of the frequency content of the EEG signal (i.e., the power spectrum) shows that in comparison with other behavioral states the power of the low-frequency bands (delta, theta, and sigma bands) during AW is low, while there is an increment in high-frequency bands, especially the low gamma band (30–45 Hz).

High EEG gamma activity during W has been described in several species, including humans (Maloney et al., 1997; Cantero et al., 2004; Cavelli et al., 2017a). In the ECoG of the cat, gamma activity is readily observed in the raw recordings during W (indicated with "a" in Fig. 1.1). As is displayed in Fig. 1.3, low gamma (30–45 Hz) oscillations take place as "bursts" of approximately 25 μV of amplitude and 200–500 ms of duration; these "bursts" are enhanced (in frequency of appearance, amplitude, and duration) during arousal produced by a stimulus that produces alertness (sound and light) or motivation (smell of food). In Figs. 1.3 and 1.4A, AW was produced with random sound stimulation, and gamma bursts seem to be coupled among several cortices. As it is shown in Fig. 1.5, when this intercortical gamma coupling is analyzed by the magnitude square coherence function, gamma coherence increases during AW in comparison with QW and sleep (see Castro et al., 2013, 2014). Another clear example of gamma coherence increment during AW is exhibited in Fig. 1.6. In this case, a person unknown to the animal entered in the recording room, and there was a large increase in gamma power (Fig. 1.6A) and coherence (Fig. 1.6B). A large gamma coherence between two cortical areas strongly suggests that there is a

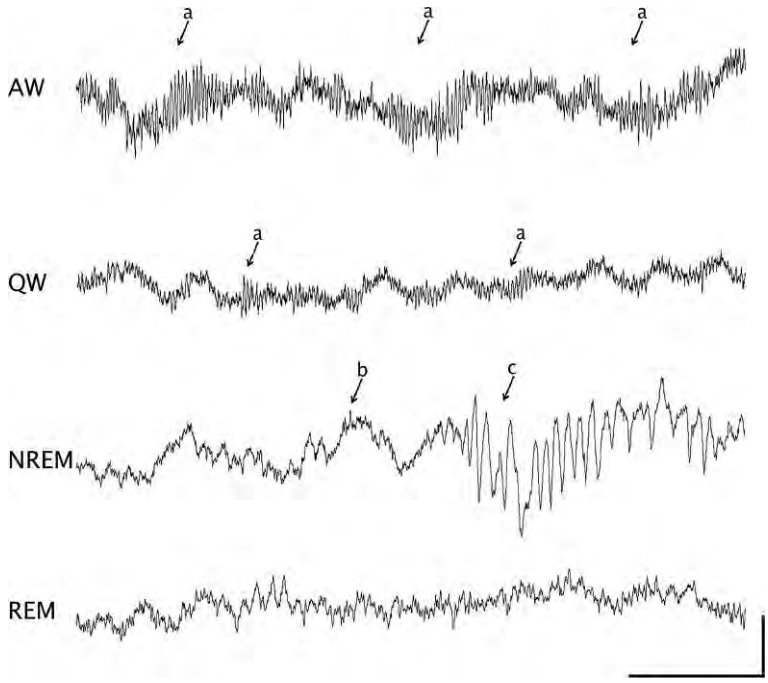

FIG. 1.1 EEG raw recordings of the dorsolateral prefrontal cortex of the cat during alert wakefulness (AW), quiet wakefulness (QW), and NREM and REM sleep. *a*, gamma (30–45 Hz) oscillations; *b*, slow waves; *c*, sleep spindles. Calibration bars, 1 s and 200 µV.

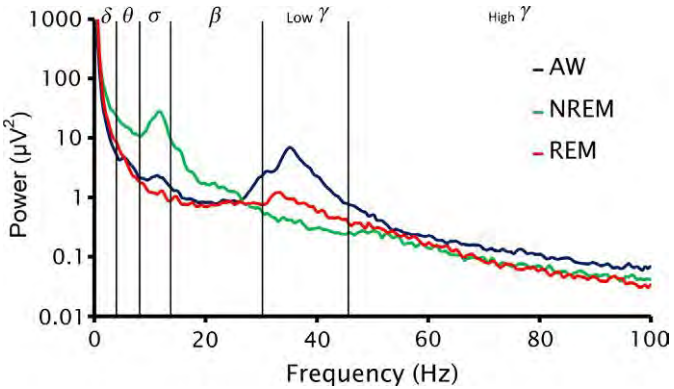

FIG. 1.2 Power spectrum (0.5–100 Hz) during wakefulness and sleep. The figure shows the average profile of 10,100 s' windows from the prefrontal cortex EEG of a cat during alert wakefulness (AW), NREM sleep, and REM sleep. Delta (0.5–4 Hz), theta (5–9 Hz), sigma (10–15 Hz), beta (16–30 Hz), and low (31–45 Hz) and high gamma (46–100 Hz) bands are shown between vertical lines.

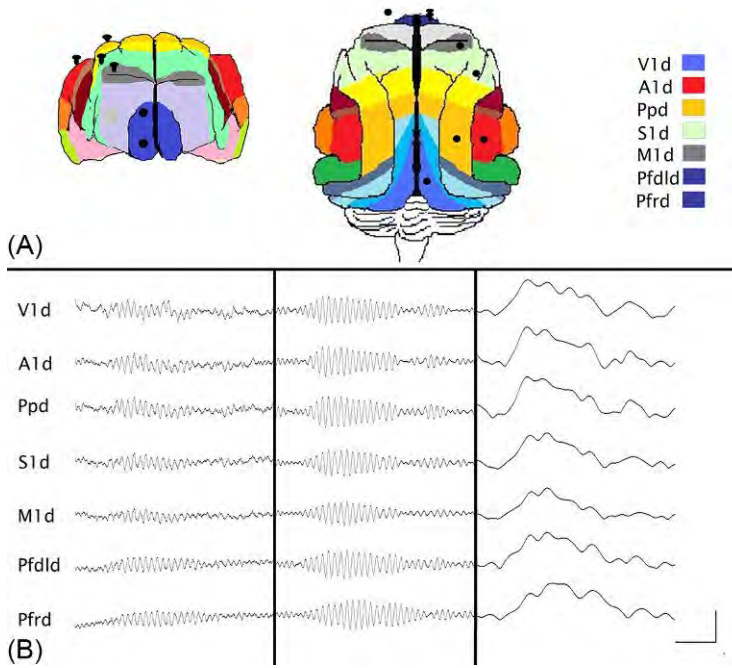

FIG. 1.3 Gamma oscillations during alert wakefulness. (A) Anterior and top view of the cat brain. The position of the cortical recording electrodes on the right cerebral hemisphere is displayed. The recordings were monopolar and referenced to an electrode located in the left frontal sinus. (B) The simultaneous recordings of the cortical gamma oscillation are exhibited. Raw recordings are shown on the left, filtered recordings (band pass 30–45 Hz) are on the middle, and the envelope of the gamma oscillations is displayed on the right. There is a large coupling in the gamma oscillations among cortical areas. Horizontal calibration bar, 200 ms. Vertical calibration bar: raw recording, 200 μV; filtered recording, 100 μV; envelopes, 50 μV. *Pfrd*, right rostral prefrontal cortex; *Pfdld*, right dorsolateral prefrontal cortex; *M1d*, right primary motor cortex; *S1d*, right primary somatosensory cortex; *Ppd*, right posterior parietal cortex; *A1d*, right auditory cortex; *V1d*, right visual cortex.

high degree of communication between these areas at the gamma band. This gamma coupling during aroused W has been also observed in rodents and humans (Llinas and Ribary, 1993; Cantero et al., 2004; Voss et al., 2009; Cavelli et al., 2015, 2017a).

During relaxed or QW, gamma activity decrease, and oscillations at lower frequencies begin to appear. This fact is readily observed in humans; during relaxed W with eyes closed, a high-amplitude alpha (8–12 Hz) oscillation appears mainly in the occipital (visual) cortex. The frequency of these oscillations is considered the basic idle (resting) speed of the brain during W (Garcia-Rill, 2015a).

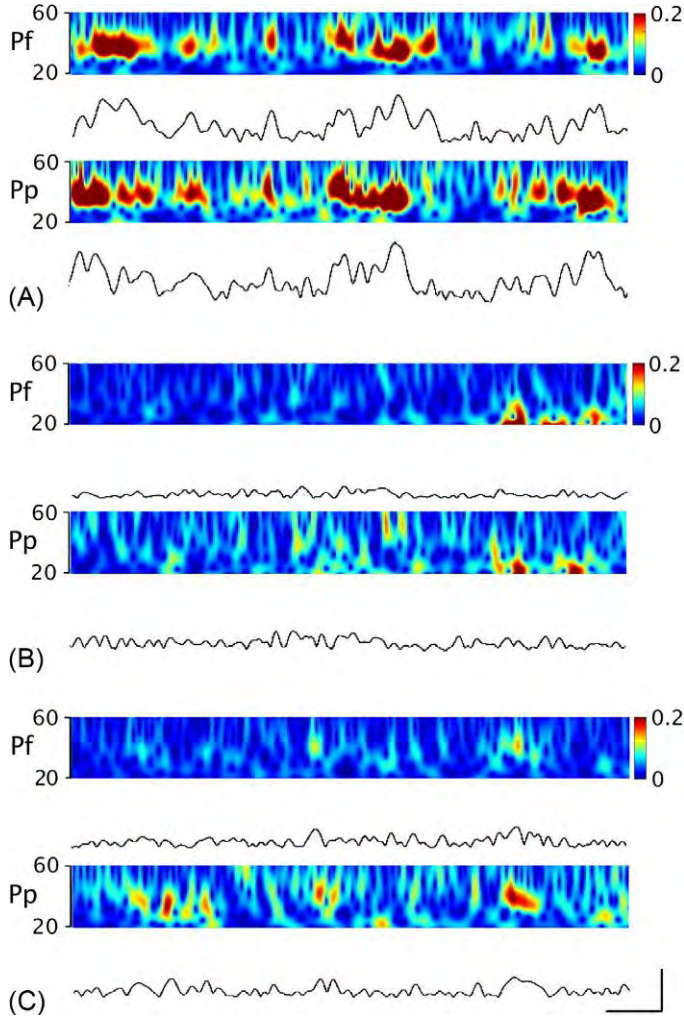

FIG. 1.4 Spectrograms (by means of wavelet function) and rectified gamma band (30–45 Hz) or gamma envelopes, during alert (A) wakefulness (AW) and (B and C) NREM and REM sleep. Calibration bars, 30 μV and 400 ms. The color code of the spectrograms shows a wavelet coefficient that represents in relative units the energy of the signal.

In summary, during W, the EEG activity transits from slower EEG rhythms such as alpha during relaxed W to higher-frequency rhythms during aroused W (especially at frequencies around 40 Hz in humans and cats). Both cortical gamma power (associated with synchronized neuronal oscillations within a cortical area) and long-range gamma coherence (associated with gamma coupling between distant cortical areas) tend to increase in correlation with the level of arousal.

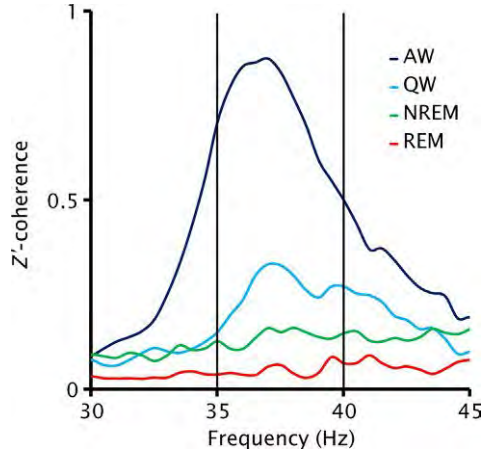

FIG. 1.5 Gamma coherence. Average EEG gamma z'-coherence profiles (between prefrontal and posterior parietal cortices) of 12,100 s' windows during alert (AW) and quiet wakefulness (QW) and NREM and REM sleep. The gamma coherence peak is between 35 and 40 Hz and is shown between vertical lines.

EEG correlates of wakefulness and arousal

As previously mentioned, consciousness (awareness) is the cognitive counterpart of normal W. It is considered that two "components" are needed to support consciousness (Posner et al., 2007; Garcia-Rill, 2015b). One is the "content" of consciousness. In spite of the fact that several neural networks contribute to the cognitive well-being (such as the basal ganglia, neocerebellum, hippocampus, and reticular formation), the thalamocortical system constitutes its main anatomical site where the "content" is processed; the associative cortical areas and related thalamic nuclei are considered to play the major role. These areas are fed with information provided by sensory pathways. The other component that supports consciousness is activation or arousal, which is also supposed to provide the "context" of sensory experience. This function is supported by the AS, in which the RAS and nonspecific thalamic nuclei play a critical role. A disturbance in the "content" of W is characteristic of diffuse cortical lesions and metabolic or toxic disorders that affect the cortex or thalamic nuclei; these injuries may produce what it is known as vegetative state. On the other hand, subtle injuries or deficits of the AS may produce comma, usually accompanied by an increase in the EEG slow activity (Posner et al., 2007).

Which are the electrocortical correlates of waking consciousness? In a very schematic way, the main EEG correlates of W consciousness are listed in Table 1.1. As commented before, an active EEG is needed to support W. In other words, widespread slow waves (delta waves) and sleep spindles that are features of NREM sleep do not support W.

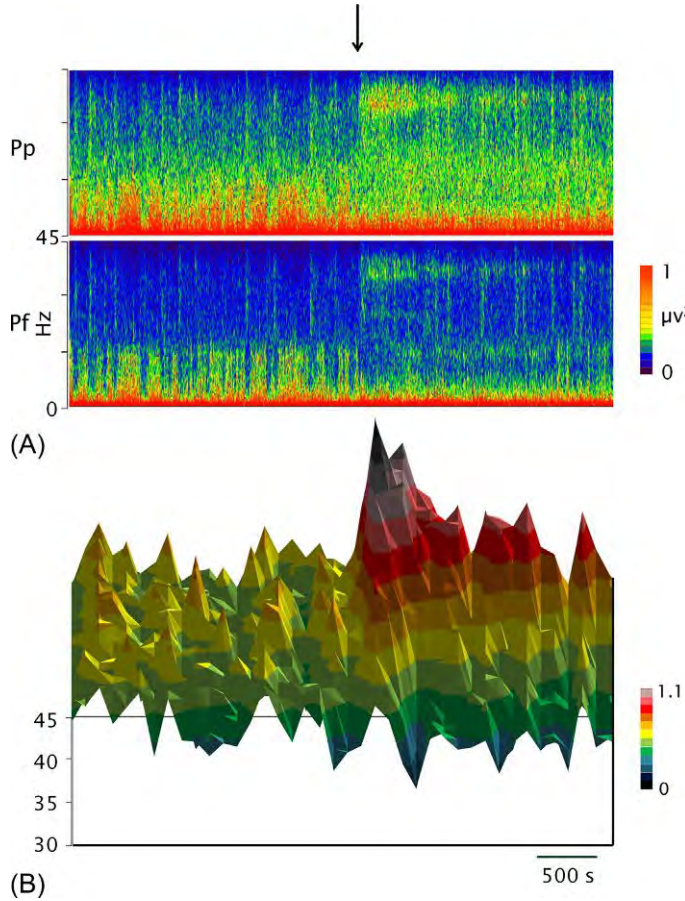

FIG. 1.6 Dynamic evolution of the EEG gamma z'-coherence when the animal is aroused. (A) Gamma power spectrograms of prefrontal (Pf) and posterior parietal (Pp) cortices when the animal is alerted by a stimulus that consisted on unknown people entering to the recording room *(arrow)*. (B) Three-dimensional spectrogram of the gamma z'-coherence between Pf and Pp cortices (same recordings as in A). Time and frequency are displayed on the horizontal and vertical axes (depth), respectively; the z'-coherence is represented in a color code.

For unified perceptual experiences, the brain integrates fragmentary neural events that occur at different times and locations. Synchronization of neuronal activity by phase locking of network oscillations has been proposed for integration or binding mechanism ("binding by synchrony") (Singer, 1999). Gamma activity, especially gamma coherence, has been involved in the explanation of this "binding problem" (Varela et al., 2001; Uhlhaas et al., 2009; Buzsaki et al., 2013; Buzsaki and Schomburg, 2015) and is one of the most studied neural correlates of consciousness (Noreika, 2015). In this regard, gamma coherence is lost during general anesthesia (see succeeding text). Higher-frequency

TABLE 1.1 Main EEG features across physiological and nonphysiological states

	W	NREM	REM	Isoflurane	Ketamine	S/A
Slow waves	–	+	–	+	–	+
Sleep spindles	–	+	–	+	–	+
Gamma power	+	–	+	–	+	+
Gamma coherence	+	–	–	–	–	+

Main electrographic features during wakefulness (W), NREM sleep, REM sleep, isoflurane general anesthesia, ketamine (subanesthetic dose), and scopolamine or atropine treatment (S/A). These profiles could explain the cognitive differences between these physiological and pharmacological conditions. Positive symbols indicate the presence of these features in the EEG; negative signs indicate absence.

oscillations, known as HFO (up to 160 Hz), may also play a role in this function (Cavelli et al., 2017b).

Wakefulness-promoting neuronal networks

Thalamocortical, premotor/motor, autonomic, and hypothalamic neuroendocrine neuronal networks modify their function during the waking-sleep cycle. However, the "primary engine" that determines changes in these neuronal networks during W is the AS. This system is composed of neurons that utilize different neurotransmitters (such as acetylcholine, noradrenaline, serotonin, dopamine, histamine, and hypocretins) and have widespread projections (Torterolo and Vanini, 2010; Torterolo et al., 2016b). The firing rate of the W-promoting neurons and the release of their neurotransmitters into the synaptic cleft tend to be maximal during W and decrease during NREM sleep.

NREM sleep

In the falling asleep process, adults enter into NREM sleep. In addition to the quiescent behavior and deep modification of autonomic and endocrine activity that regulate visceral functions, NREM sleep is associated with impressive cognitive alterations. The manifestation of the changes in thalamocortical activity on passing from W to NREM sleep can be partially appreciated in the EEG.

In humans, three NREM sleep phases are recognized: N1, N2, and N3, according to the depth of the state. N1 is the transitional stage from W, where hypnagogic imaginary (dreamlike activity) is common. This transition into NREM sleep is complex and heterogeneous from the EEG point of view. In fact, Tanaka et al. (1996) divided the transition in nine "hypnagogic states" (from relaxed W with alpha activity to N2). N2 is characterized by the presence of sleep spindles (11–15 Hz oscillatory events with a duration

of 0.5–2 s) and K-complexes. K-complex, which is often associated with sleep spindles, consists of a brief negative sharp high-voltage peak (usually greater than 100 μV), followed by a slower positive complex and a final negative peak.

The presence of high-amplitude (approximately 70 μV), low-frequency (0.5–4 Hz, delta) oscillations characterizes N3 (Carskadon and Dement, 2011). Fig. 1.1 shows the EEG activity during NREM sleep in the cat; slow-wave oscillations and sleep spindles are indicated (indicated with "b" and "c," respectively). Fig. 1.2 depicts the power spectrum during NREM sleep. Large values of delta and sigma power produced by slow waves and spindles, respectively, are distinctive features of NREM sleep. Also, the decrease in the gamma band power and coherence is another remarkable feature of NREM sleep (Figs. 1.2, 1.4B, and 1.5).

Somnambulism or sleepwalking is an NREM sleep parasomnia that can be explained as a dissociated state, with both waking and NREM sleep features (Mahowald and Schneck, 2011; Canclini et al., 2018). In other words, part of the brain is active (i.e., as in waking state, with probable activation of motor cortical and subcortical regions), while other cortical regions present slow waves (as in NREM sleep) in the EEG. As a result, the individual is awake enough to carry out complex motor acts but is unconscious and irresponsible for these actions (because is partially asleep). It is likely that slow waves during these events are mainly present in associative cortical areas that are critical for awareness (Tononi and Laureys, 2009). The slow cortical activity during somnambulism is a pathological manifestation of what is known as local sleep. Nowadays, it is accepted that during W, part of the cortical columns behaves as they were asleep, especially when there is high sleep pressure, that is, during sleep deprivation or prolonged W (Vyazovskiy et al., 2011).

The presence of slow waves and/or sleep spindles during NREM sleep is against the generation of consciousness (Table 1.1). The high-amplitude slow waves of NREM sleep are widespread throughout the cortex and are produced by the synchronization of a large number of pyramidal neurons. This electrocortical condition suggests that large groups of neurons are doing quite the same at the same time; this reduction in the degree of freedom would wane consciousness. On the contrary, a feature of cortical activity during W is regional "functional differentiation," and according to Tononi's information integration theory, functional differentiation between different areas is critical for consciousness (Tononi, 2010). This feature is lost during NREM sleep. A similar circumstance occurs in generalized seizures such as "petit mal," where unconsciousness of the event is associated with widespread stereotyped slow waves. In addition, functions such as cortical lateral inhibition that is critical for perception are lost when pyramidal neurons behave in an homogeneous manner such as in deep NREM sleep (Garcia-Rill, 2015c).

Oneiric activity is scarce or absent during deep NREM sleep (N3) (Dement and Kleitman, 1957; Pace-Schott, 2011; Siclari et al., 2017). As previously

mentioned, widespread slow waves and spindles, as well as low gamma power and coherence in the EEG, do not support cognitive activity (neither W consciousness nor dreams) (Table 1.1). However, oneiric activity may appear by local REM sleep–like activation of critical areas in a background of light NREM sleep (N1 and N2 at the end of a nocturnal sleep period). In fact, both during NREM and REM sleep, dream reports were associated with local decrease in low-frequency activity in posterior cortical regions, while an increase in high-frequency activity within these regions is correlated with specific dream contents (Siclari et al., 2017).

NREM sleep-promoting system

Cognitive activity (waking consciousness and dreams) and the different EEG rhythms that support these functions are mainly generated by the activity of cortical and thalamic neuronal networks, which are mutually interconnected. Thalamic neurons have a complex electrophysiology that allows them to operate differently according to their level of polarization (Steriade et al., 1993). When hyperpolarized, the thalamic neurons that project to the cortex (thalamocortical neurons) oscillate at low frequency (0.5–4 Hz) and tend to block the sensory information that travels toward the cortex. This "oscillatory mode" of function synchronizes cortical neurons and, accompanied by other phenomena of cortical origin, generates the slow waves of NREM sleep (Huguenard and McCormick, 2007; Crunelli et al., 2015). Moreover, the reticular nucleus of the thalamus is the site of generation of the sleep spindles that characterize N2 (Fuentealba and Steriade, 2005; Huguenard and McCormick, 2007). On the contrary, when thalamic neurons are relatively depolarized, they enter in the "tonic mode" of function. In this condition, the thalamocortical neurons transmit sensory information toward the cortex in a reliable way. This mode of function occurs during W and REM sleep because the AS maintains a depolarized membrane potential in these neurons.

Neurons from the preoptic area (POA) of the hypothalamus are critical in the generation and maintenance of NREM sleep (Torterolo and Vanini, 2010; Torterolo et al., 2016b). Most of these neurons are GABAergic; these inhibitory neurons project in monosynaptic form toward the activating nuclei. On the other hand, experimental evidence suggests that W-promoting neurons inhibit NREM sleep–promoting POA neurons (Gallopin et al., 2000; Williams et al., 2014). This reciprocal inhibition between activating and hypnogenic neurons is critical for the transition between sleep and W and the basis of the flip-flop state switch model (Saper et al., 2010).

Other neuronal networks also seem to play a role in NREM sleep generation, such as neurons located in the medullary reticular formation (Anaclet et al., 2012) and the melanin-concentrating hormone (MCH)-containing neurons of the lateral hypothalamus and incertohypothalamic area (Torterolo et al., 2011; Monti et al., 2013).

REM sleep

REM sleep (also called stage R) is a deep sleep stage even though it exhibits similar electrographic characteristics to that of W, that is, has an active EEG. Hence it is also called "paradoxical" sleep. REM sleep is also characterized by REM, muscle atony, and phasic changes in autonomic activity.

REM sleep EEG in rodents and cats is similar to W (Fig. 1.1) (Torterolo et al., 2016b). However, the EEG during REM sleep in humans has more similarities to N1; in both states, the EEG is described as low-voltage, mixed-frequency activity (Keenan and Hirshkowitz, 2011).

In humans, during nighttime sleep, REM sleep episodes occur with a period of approximately 90 min; in fact, there are four to five "sleep cycles" per night. The "sleep cycles" are the period between the onset of sleep until the end of the first episode of REM sleep or the period from the end of an episode of REM sleep to the end of the subsequent REM sleep episode (Carskadon and Dement, 2011).

Dreams occur mainly during REM sleep and are considered a special kind of cognitive activity or protoconsciousness (Hobson, 2009). REM sleep dreams are characterized by their vividness, single-mindedness, bizarreness, and the loss of voluntary control over the plot. Attention is unstable and rigidly focused, facts and reality are not checked, violation of physical laws and bizarreness are passively accepted, contextual congruence is distorted, time is altered, and memories become labile (Rechtschaffen, 1978; Hobson, 2009; Nir and Tononi, 2010). Interestingly, some authors have suggested that cognition during REM sleep resembles psychosis (Gottesmann and Gottesman, 2007). In fact, Hobson stands that "dreaming is, by definition, a psychosis" (Hobson, 1997).

High local cortical gamma activity (and hence relatively large gamma power) is present during REM sleep (Fig. 1.2), both in humans and animals (Maloney et al., 1997; Cantero et al., 2004; Cavelli et al., 2017a). However, long-range gamma coherence is almost absent during REM sleep (Figs. 1.4C and 1.5). High gamma power accompanied by minimal gamma coherence is a trait that characterizes REM sleep (Fig. 1.7 and Table 1.1), which is conserved in rodents, felines, and humans (Cantero et al., 2004; Voss et al., 2009; Castro et al., 2013, 2014; Cavelli et al., 2015, 2017a; Torterolo et al., 2016a).

Coherent EEG gamma activity has been observed during REM sleep solely during lucid REM sleep dreaming; the level of gamma coherence during lucid dreaming is intermediate between W and nonlucid REM sleep (Voss et al., 2009). Lucid dreams are a relatively infrequent phenomenon, whereby the "sleeper" reports being aware that he/she is dreaming and, in some cases, is able to deliberately modify the events of the ongoing dream. Interestingly, externally imposed resonance at 40 Hz by means of electric stimulation produces self-awareness (lucidity) during REM sleep (Voss et al., 2014). From the electrocortical point of view, lucid dreams share features for both W and REM sleep; hence it could be considered a type of dissociate state.

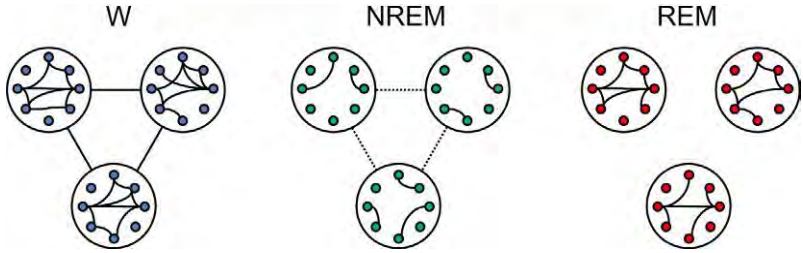

FIG. 1.7 Schematic representation of the short- and long-range gamma synchronization during wakefulness (W), NREM sleep, and REM sleep. The *small circles* represent neurons, while *large circles* represent the areas of the cortex where these neurons are located. Colors in neurons represent the behavioral states (*blue*, W; *green*, NREM sleep; *red*, REM sleep) and connecting lines between the circles represent the gamma synchronization between distant cortical areas. Short-range (local) and long-range (distant) gamma synchronization occurs during W. During NREM sleep, both short- and long-range gamma synchronization decrease. During REM sleep, while gamma synchronization is present at local level, distant gamma coupling is absent.

Neural systems that promote the generation of REM sleep

The neural networks necessary and sufficient for the generation and maintenance of REM sleep are found in the mesopontine reticular formation (Siegel, 2011). In fact, most of the mesopontine neurons that play a role in the maintenance of W coincide with the neurons that are responsible for the generation of REM sleep.

Within these areas, monoaminergic (noradrenergic and serotonergic) neurons that are active during W turn off during REM sleep (REM-off neurons). On the other hand, cholinergic neurons increase their firing rate both during W and REM sleep (REM-ON neurons) (McCarley, 2007). Mesopontine GABAergic and glutamatergic neurons (Luppi et al., 2007) and hypothalamic MCH-containing neurons also play a critical role in REM sleep generation (Torterolo et al., 2011, 2015; Monti et al., 2013).

Drug-induced loss of consciousness: General anesthesia

Comma, vegetative state, and seizures are the more salient conditions related to pathological loss of consciousness. Since the variety and complexity of these conditions, they will not be analyzed in the present report. However, we will focus in drug-induced loss and alteration of consciousness.

General anesthesia is a drug-induced state, characterized by a relatively safe and reversible loss of consciousness. The ability to render a patient unconscious (hypnosis) and insensible to pain made modern surgery possible, and general anesthetics have become one of the most widely used class of drug (Franks, 2006). Sleep and anesthesia share many behavioral and electroencephalographic characteristics (Vanini et al., 2011). In addition, several authors suggest that sleep and anesthesia (induced by most anesthetic) share an underlying mechanism. In fact, several studies showed that most anesthetics suppress consciousness by recruiting or inhibiting regions that regulate sleep and W (Vanini et al., 2011).

When the anesthetic plane is reached, NREM sleep–like slow waves are present during this drug-induced state (Lydic and Baghdoyan, 2005). In addition, as it is shown in Fig. 1.8, isoflurane decreases EEG gamma power and coherence activity in the cat. Similar effects were observed for long-range gamma coherence in humans and rats (John, 2002; Mashour, 2006; Pal et al., 2016). Hence both the presence of slow waves and the decrease in gamma power and coherence are associated with the absence of consciousness induced by anesthesia (Table 1.1).

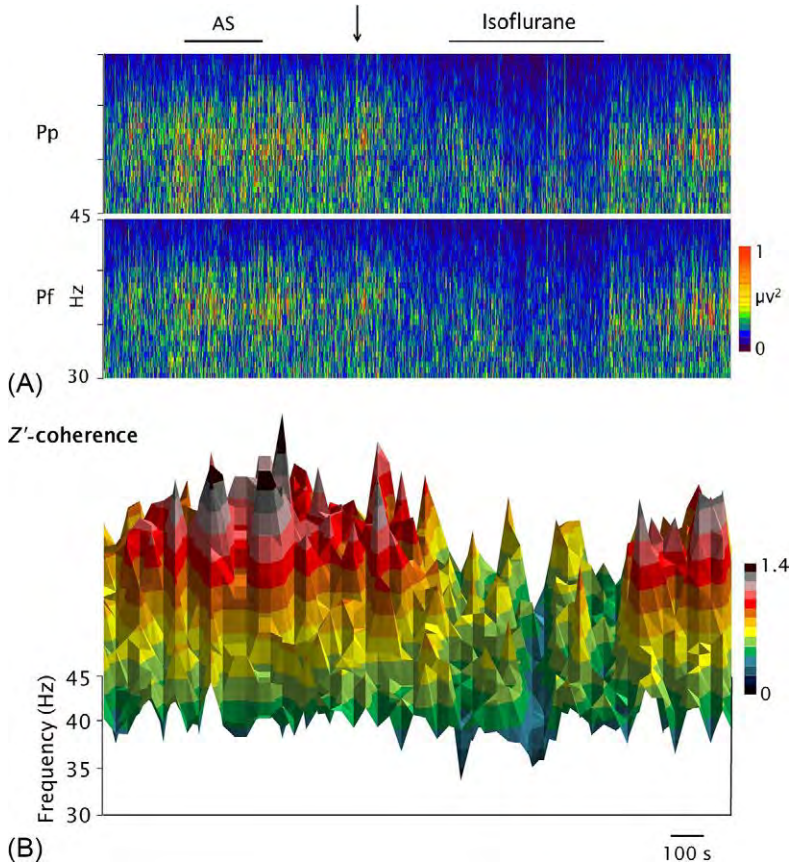

FIG. 1.8 Dynamic evolution of the EEG gamma z'-coherence following isoflurane administration (bar). (A) Gamma power spectrograms of prefrontal (Pf) and posterior parietal (Pp) cortices. The first bar (AS) shows when the animal is alerted by a stimulus that consisted of unknown people entering the recording room during wakefulness. The *arrow* indicates an auditory stimulus. The time during the administration of an anesthetic dose of isoflurane is also displayed. (B) Three-dimensional spectrogram of the gamma z'-coherence between Pf and Pp cortices (same recordings as in A). Time and frequency are displayed on the horizontal and vertical axes (depth), respectively; the z'-coherence is represented in a color code. The decrease in gamma power and coherence is readily observed.

Drug-induced alteration of consciousness

Ketamine, a pharmacological model of psychosis

The word psychosis (from Greek "disorder of the mind") is used in psychiatry to define a mental state in which there is a loss of contact with reality. The *Diagnostic and Statistical Manual of Mental Disorders (DSM), 5th Edition (2013)* classifies psychotic disorders in a chapter entitled "Schizophrenia Spectrum and Other Psychotic Disorders," highlighting among them schizophrenia (Bhati, 2013). This pathology is characterized by the presence of positive or psychotic (visual and auditory hallucinations, delusions, and paranoia) and negatives symptoms (apathy, the loss of motivation, and serious social isolation) and memory and executive function disorders.

Several hypotheses that attempt to explain the pathophysiology of psychotic disorders have been postulated. Among them, it is widely accepted that glutamatergic hypofunction mediated by the *N*-methyl-D-aspartate receptor (NMDA-R) is a key mechanism contributing to the positive, negative, and cognitive symptoms observed in this condition (Krystal et al., 1994; Pomarol-Clotet et al., 2006; Javitt, 2010). This is based on clinical reports showing that the consumption of noncompetitive antagonists of NMDA-R, such as ketamine, induces in healthy individuals the characteristic alterations of the psychotic disorders and exacerbates the symptoms in schizophrenic patients (Krystal et al., 2003; Pomarol-Clotet et al., 2006). Therefore models involving NMDA-R hypofunction is considered a valid pharmacological approach for the study of the psychotic disorders (Corlett et al., 2007; Scorza et al., 2008; Javitt, 2010).

Ketamine in subanesthetic doses produces an activated state, with relatively high gamma power (Fig. 1.9); however, it also produces a deep decrease in gamma (30–45 Hz) band coherence (Fig. 1.10). This decrease was similar to that occurring during REM sleep, which is considered a natural model of psychosis (Hobson, 1997; Gottesmann, 2006; Gottesmann and Gottesman, 2007). Furthermore, under ketamine, the gamma coherence was not affected by novel stimuli (Fig. 1.10), which in basal conditions alert the animal causing a large increase in gamma coherence (Castro-Zaballa et al., 2019b).

Disruptions in gamma activity similar to the induced by ketamine, have been described in psychosis (Lee et al., 2003; Light et al., 2006; Yeragani et al., 2006; Uhlhaas and Singer, 2010; Sun et al., 2011; White and Siegel, 2016).

In summary, it is possible that an active state with high local gamma band synchronization (i.e., high gamma power), accompanied with low long-range gamma coherence, is associated to the cognitive features shared by REM sleep and psychosis (Table 1.1).

Dissociative state induced by atropine and scopolamine

Mesopontine and basal forebrain cholinergic neurons are critically involved in the EEG activation during W and REM sleep (Torterolo and Vanini, 2010;

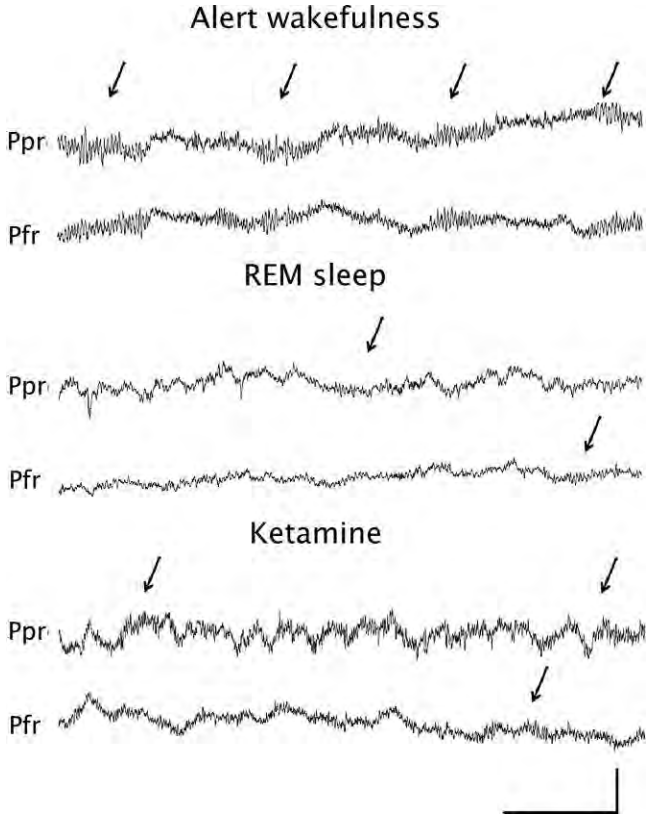

FIG. 1.9 Simultaneous raw recordings of the prefrontal (Pf) and parietal posterior (Pp) cortices during alert wakefulness and REM sleep and under the administration of ketamine (15 mg/kg). The *arrows* indicate the gamma "bursts." Calibration bars, 1 s and 200 μV. Gamma activity is present under ketamine; however, this gamma activity is not coupled between cortical areas.

Torterolo et al., 2016b). In this regard, animals treated with muscarinic antagonists (atropine or scopolamine) display high-voltage slow waves and spindles in EEG that resembles NREM sleep; however, they remain behaviorally awake and active (Wikler, 1952). Furthermore, these drugs decrease the electrocortical arousal response elicited by either sensory or midbrain reticular formation stimulation, but the gross behavior in response to such stimuli is not affected (Rinaldi and Himwich, 1955; Bradley and Key, 1958). This "dissociation" in which waking behavior coexists with NREM sleep–like EEG was observed in different animals and humans (Wikler, 1952; Longo, 1956; Chow and John, 1959; Lindsley et al., 1968; Yamamoto, 1988).

Classic pharmacological studies have also shown cognitive disturbances in humans treated with muscarinic antagonists (Ostfeld et al., 1960). They produce

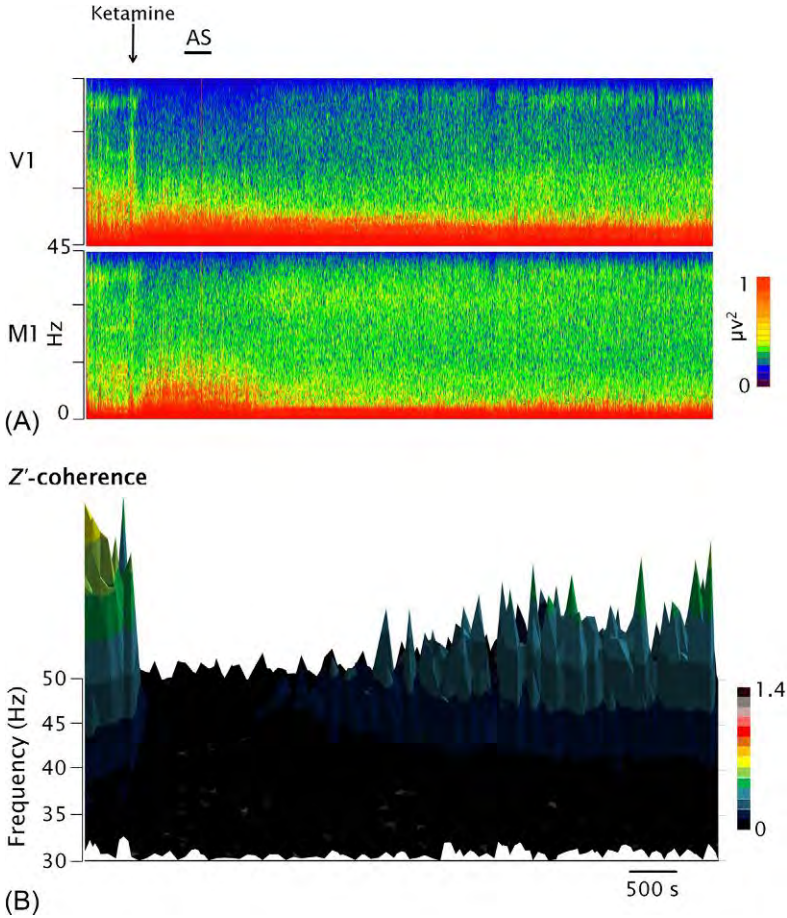

FIG. 1.10 Dynamic evolution of EEG gamma power and z'-coherence following the administration of subanesthetic dose of ketamine. (A) Gamma power spectrograms of primary motor (M1) and primary visual (V1) cortices following ketamine administration (*arrow*). The horizontal bar represents at random sound stimulation (AS) in order to arouse the animal. (B) Three-dimensional spectrogram of the gamma z'-coherence between M1 and V1 cortices (same recordings as in A). Time and frequency are displayed on the horizontal and vertical axes (depth), respectively; the z'-coherence is represented in a color code. Ketamine produced a large decrement in gamma coherence that was not affected by sensory stimulation.

a decrease in spontaneous speech and movement, impairment in memory and attention, and drowsiness. However, subjects are able to answer simple questions and perform tasks without the requirement of prolonged attention or memory. They can sit, stand, open or close their eyes, or extend their extremities on request, although they move more slowly than in the predrug period. In addition, muscarinic antagonists produce sedation, impairment of coordinative and reactive skills, visual disturbances, and diminution of short-term memory (Nuotto, 1983).

Furthermore, these drugs affect simple and choice reaction time, number matching, and memory scanning tasks (Ebert et al., 1998). It is considered that the most prominent effects of scopolamine involve discrimination processes, vigilance, selective attention, and consolidation and retrieval of memories (Sahakian, 1988).

Anticholinergic drugs have been used for recreational or ritualistic purposes. One of the most widely described religious or magical experiences dating back to ancient times is the alteration of consciousness with the induction of hallucinations by a member of the Solanaceae family of plants (belladonna, henbane, or datura), which contain scopolamine, atropine, and other closely related alkaloids (Perry and Perry, 1995). Perhaps the most extraordinary example of cognitive dysfunction is the criminal use of anticholinergic substances that are present in datura extracts (called "burundanga"), to induce amnesia and submissive behavior or "obedience" in victims (Ardila and Moreno, 1991; Ardila-Ardila et al., 2006).

We recently demonstrated that under the effect of atropine or scopolamine, coherent gamma (≈40 Hz) oscillations are conspicuous (Castro-Zaballa et al., 2019a) (Fig. 1.11). This "dissociated" EEG not only with slow waves and sleep

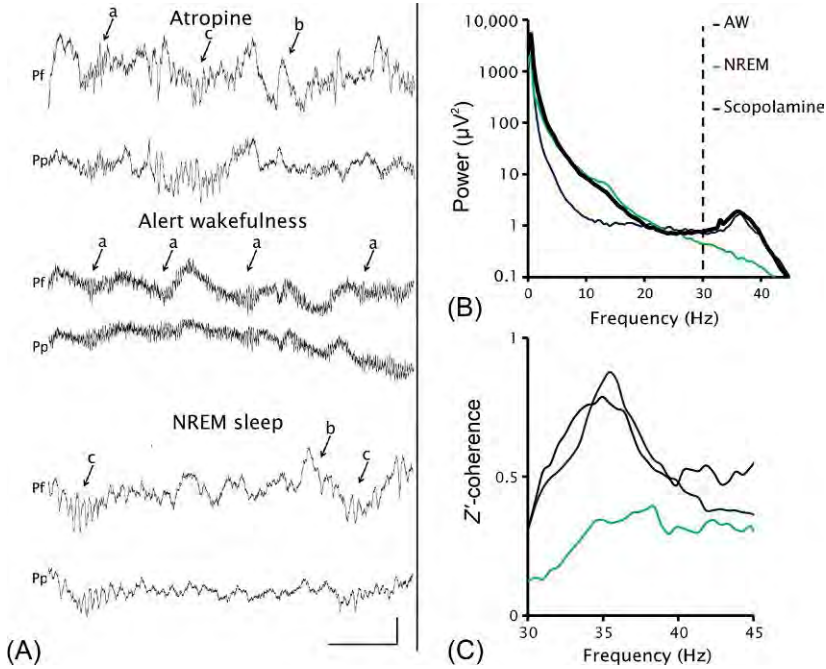

FIG. 1.11 (A) Simultaneous raw recordings of the prefrontal (Pf) and parietal posterior (Pp) cortices. Raw recordings during alert wakefulness and REM sleep and following the administration of atropine. *a*, gamma (30–45 Hz) oscillations; *b*, slow waves; *c*, sleep spindles. Calibration bars, 1 s and 200 μV. (B) Power spectrum (0–45 Hz) of the posterior parietal cortex during alert wakefulness (AW), NREM sleep, and scopolamine administration. (C) Average gamma z'-coherence profiles (30–45 Hz) in the same conditions as in B. The coherence profile during AW and scopolamine is similar.

spindles but also with coherent 40 Hz oscillations (a trait of AW) may be the neurophysiological basis of the "classic" EEG and behavior dissociation that is produced by these drugs. Hence the alteration of consciousness produced by antimuscarinic drugs is associated with slow waves and spindles (NREM sleep feature), combined with high gamma power and coherence, a trait of AW (Table 1.1).

Conclusions

Consciousness is the cognitive counterpart of normal W, at least for animals with higher cognitive abilities. W is characterized by an EEG with the absence of slow-wave (delta) activity and the presence of coherent high-frequency waves, mainly at about 40 Hz. These coherent gamma oscillations are highly dependent of the level of arousal. On the other hand, important adjustments of the delta waves and/or gamma activity (power and coherence) are associated with physiological absence or alteration of consciousness (NREM and REM sleep, respectively). An important modulation of gamma and delta activity is also associated with either the loss or alteration of consciousness induced by drugs.

Acknowledgments

This study was supported by the "Agencia Nacional de Investigación e Innovación, Fondo Clemente Estable FCE-1-2017-1-136550" grant, the "Comisión Sectorial de Investigación Científica I+D-2016-589" grant, and the "Programa de Desarrollo de las Ciencias Básicas, PEDECIBA" from Uruguay.

References

Anaclet, C., Lin, J.S., Vetrivelan, R., Krenzer, M., Vong, L., Fuller, P.M., Lu, J., 2012. Identification and characterization of a sleep-active cell group in the rostral medullary brainstem. J. Neurosci. 32, 17970–17976.

Ardila, A., Moreno, C., 1991. Scopolamine intoxication as a model of transient global amnesia. Brain Cogn. 15, 236–245.

Ardila-Ardila, A., Moreno, C.B., Ardila-Gomez, S.E., 2006. Scopolamine poisoning ('burundanga'): loss of the ability to make decisions. Rev. Neurol. 42, 125–128.

Bhati, M.T., 2013. Defining psychosis: the evolution of DSM-5 schizophrenia spectrum disorders. Curr. Psychiatry Rep. 15, 409.

Bradley, P.B., Key, B.J., 1958. The effect of drugs on arousal responses produced by electrical stimulation of the reticular formation of the brain. Electroencephalogr. Clin. Neurophysiol. 10, 97–110.

Buzsaki, G., Schomburg, E.W., 2015. What does gamma coherence tell us about inter-regional neural communication? Nat. Neurosci. 18, 484–489.

Buzsaki, G., Logothetis, N., Singer, W., 2013. Scaling brain size, keeping timing: evolutionary preservation of brain rhythms. Neuron 80, 751–764.

Canclini, M.R., Canzani, M.B., Luna, M.J., Royol, M.J., Rusiñol, M.C., Vega, M., Torterolo, P., 2018. Parasomnias: state of the art. An. Facultad Med. (Univ. Repúb. Urug.) 5, 29–43.

Cantero, J.L., Atienza, M., Madsen, J.R., Stickgold, R., 2004. Gamma EEG dynamics in neocortex and hippocampus during human wakefulness and sleep. Neuroimage 22, 1271–1280.

Carskadon, M.A., Dement, W., 2011. Normal human sleep: an overview. In: Kryger, M.H., Roth, T., Dement, W. (Eds.), Principles and Practices of Sleep Medicine. Elsevier-Saunders, Philadelphia, pp. 16–26.

Castro, S., Falconi, A., Chase, M.H., Torterolo, P., 2013. Coherent neocortical 40-Hz oscillations are not present during REM sleep. Eur. J. Neurosci. 37, 1330–1339.

Castro, S., Cavelli, M., Vollono, P., Chase, M.H., Falconi, A., Torterolo, P., 2014. Inter-hemispheric coherence of neocortical gamma oscillations during sleep and wakefulness. Neurosci. Lett. 578, 197–202.

Castro-Zaballa, S., Cavelli, M., Gonzalez, J., Monti, J., Falconi, A., Torterolo, P., 2019a. EEG dissociation induced by muscarinic receptor antagonists: coherent 40 Hz oscillations in a background of slow waves and spindles. Behav. Brain Res. 359, 27–38.

Castro-Zaballa, S., Cavelli, M., Gonzalez, J., Nardi, A.E., Machado, S., Scorza, C., Torterolo, P., 2019b. EEG 40 Hz coherence decreases in REM sleep and ketamine models of psychosis. *Front.Psychiatr*. 766, https://doi.org/10.3389/fpsyt.2018.00766.

Cavelli, M., Castro, S., Schwarzkopf, N., Chase, M.H., Falconi, A., Torterolo, P., 2015. Coherent neocortical gamma oscillations decrease during REM sleep in the rat. Behav. Brain Res. 281, 318–325.

Cavelli, M., Castro-Zaballa, S., Mondino, A., Gonzalez, J., Falconi, A., Torterolo, P., 2017a. Absence of EEG gamma coherence in a local activated neocortical state: a conserved trait of REM sleep. Transl. **Brain** Rhythm. 2, 1–13.

Cavelli, M., Rojas-Libano, D., Schwarzkopf, N., Castro-Zaballa, S., Gonzalez, J., Mondino, A., Santana, N., Benedetto, L., Falconi, A., Torterolo, P., 2017b. Power and coherence of cortical high-frequency oscillations during wakefulness and sleep. Eur. J. Neurosci. 48, 272–273, https://doi.org/10.1111/ejn.13718.

Chalmers, D.J., 2005. Facing up to the problem of consciousness. J. Conscious. Stud. 2, 200–219.

Chow, K.L., John, E.R., 1959. Acetylcholine metabolism and behavior of rats. Science 129, 64.

Corlett, P.R., Honey, G.D., Fletcher, P.C., 2007. From prediction error to psychosis: ketamine as a pharmacological model of delusions. J. Psychopharmacol. 21, 238–252.

Crunelli, V., David, F., Lorincz, M.L., Hughes, S.W., 2015. The thalamocortical network as a single slow wave-generating unit. Curr. Opin. Neurobiol. 31, 72–80.

Damasio, A., Meyer, K., 2009. Consciousness:an overview of the phenomenon and of its possible neural basis. In: Laureys, S., Tononi, G. (Eds.), The Neurology of Consciousness. Academic Press, London, pp. 3–14.

Dement, W., Kleitman, N., 1957. The relation of eye movements during sleep to dream activity: an objective method for the study of dreaming. J. Exp. Psychol. 53, 339–346.

Ebert, U., Siepmann, M., Oertel, R., Wesnes, K.A., Kirch, W., 1998. Pharmacokinetics and pharmacodynamics of scopolamine after subcutaneous administration. J. Clin. Pharmacol. 38, 720–726.

Edelman, G.M., Tononi, G., 2000. A Universe of Consciousness. Basic Books, New York.

Franks, N.P., 2006. Molecular targets underlying general anaesthesia. Br. J. Pharmacol. 147 (Suppl. 1), S72–S81.

Fuentealba, P., Steriade, M., 2005. The reticular nucleus revisited: intrinsic and network properties of a thalamic pacemaker. Prog. Neurobiol. 75, 125–141.

Gallopin, T., Fort, P., Eggermann, E., Cauli, B., Luppi, P.H., Rossier, J., Audinat, E., Muhlethaler, M., Serafin, M., 2000. Identification of sleep-promoting neurons in vitro. Nature 404, 992–995.

Garcia-Rill, E., 2015a. The 10 Hz fulcrum. In: Garcia-Rill, E. (Ed.), Waking and the Reticular Activating System in Health and Disease. Elsevier, London, pp. 157–170.

Garcia-Rill, E., 2015b. Governing principles of brain activity. In: Garcia-Rill, E. (Ed.), Waking and the Reticular Activating System in Health and Disease. Elsevier, pp. 1–16.

Garcia-Rill, E., 2015c. The science of waking and public policy. In: Garcia-Rill, E. (Ed.), Waking and the Reticular Activating System in Health and Disease. Elsevier, London, pp. 292–306.

Gottesmann, C., 2006. The dreaming sleep stage: a new neurobiological model of schizophrenia? Neuroscience 140, 1105–1115.

Gottesmann, C., Gottesman, I., 2007. The neurobiological characteristics of rapid eye movement (REM) sleep are candidate endophenotypes of depression, schizophrenia, mental retardation and dementia. Prog. Neurobiol. 81, 237–250.

Hobson, J.A., 1997. Dreaming as delirium: a mental status analysis of our nightly madness. Semin. Neurol. 17, 121–128.

Hobson, J.A., 2009. REM sleep and dreaming: towards a theory of protoconsciousness. Nat. Rev. Neurosci. 10, 803–813.

Huguenard, J.R., McCormick, D.A., 2007. Thalamic synchrony and dynamic regulation of global forebrain oscillations. Trends Neurosci. 30, 350–356.

Javitt, D.C., 2010. Glutamatergic theories of schizophrenia. Isr. J. Psychiatry Relat. Sci. 47, 4–16.

John, E.R., 2002. The neurophysics of consciousness. Brain Res. Brain Res. Rev. 39, 1–28.

Keenan, S., Hirshkowitz, M., 2011. Monitoring and staging human sleep. In: Kryger, M.H., Roth, T., Dement, W.C. (Eds.), Principles and Practices of Sleep Medicine. Elsevier-Saunders, Philadelphia, pp. 1602–1609.

Krystal, J.H., Karper, L.P., Seibyl, J.P., Freeman, G.K., Delaney, R., Bremner, J.D., Heninger, G.R., Bowers Jr., M.B., Charney, D.S., 1994. Subanesthetic effects of the noncompetitive NMDA antagonist, ketamine, in humans. Psychotomimetic, perceptual, cognitive, and neuroendocrine responses. Arch. Gen. Psychiatry 51, 199–214.

Krystal, J.H., D'Souza, D.C., Mathalon, D., Perry, E., Belger, A., Hoffman, R., 2003. NMDA receptor antagonist effects, cortical glutamatergic function, and schizophrenia: toward a paradigm shift in medication development. Psychopharmacology (Berl) 169, 215–233.

Lee, K.H., Williams, L.M., Haig, A., Gordon, E., 2003. "Gamma (40 Hz) phase synchronicity" and symptom dimensions in schizophrenia. Cogn. Neuropsychiatry 8, 57–71.

Light, G.A., Hsu, J.L., Hsieh, M.H., Meyer-Gomes, K., Sprock, J., Swerdlow, N.R., Braff, D.L., 2006. Gamma band oscillations reveal neural network cortical coherence dysfunction in schizophrenia patients. Biol. Psychiatry 60, 1231–1240.

Lindsley, D.F., Carpenter, R.S., Killam, E.K., Killam, K.F., 1968. EEG correlates of behavior in the cat. I. Pattern discrimination and its alteration by atropine and LSD-25. Electroencephalogr. Clin. Neurophysiol. 24, 497–513.

Llinas, R.R., Pare, D., 1991. Of dreaming and wakefulness. Neuroscience 44, 521–535.

Llinas, R., Ribary, U., 1993. Coherent 40-Hz oscillation characterizes dream state in humans. Proc. Natl. Acad. Sci. U. S. A. 90, 2078–2081.

Longo, V.G., 1956. Effects of scopolamine and atropine electroencephalographic and behavioral reactions due to hypothalamic stimulation. J. Pharmacol. Exp. Ther. 116, 198–208.

Lopes da Silva, F., 2010. EEG: origin and measurement. In: Mulert, C., Lemieuz, L. (Eds.), EEG-fMRI. Springer-Verlag, Berlin, pp. 19–38.

Luppi, P.H., Gervasoni, D., Verret, L., Goutagny, R., Peyron, C., Salvert, D., Leger, L., Fort, P., 2007. Paradoxical (REM) sleep genesis: the switch from an aminergic-cholinergic to a GABAergic-glutamatergic hypothesis. J. Physiol. Paris 100, 271–283.

Lydic, R., Baghdoyan, H.A., 2005. Sleep, anesthesiology, and the neurobiology of arousal state control. Anesthesiology 103, 1268–1295.

Mahowald, M.W., Schneck, C., 2011. Non-REM arousal parasomnias. In: Kryger, M.H., Roth, T., Dement, W.C. (Eds.), Principles and Practices of Sleep Medicine. Elsevier-Saunders, Philadelphia, pp. 1075–1082.

Maloney, K.J., Cape, E.G., Gotman, J., Jones, B.E., 1997. High-frequency gamma electroencephalogram activity in association with sleep-wake states and spontaneous behaviors in the rat. Neuroscience 76, 541–555.

Mashour, G.A., 2006. Integrating the science of consciousness and anesthesia. Anesth. Analg. 103, 975–982.

McCarley, R.W., 2007. Neurobiology of REM and NREM sleep. Sleep Med. 8, 302–330.

Monti, J.M., Torterolo, P., Lagos, P., 2013. Melanin-concentrating hormone control of sleep-wake behavior. Sleep Med. Rev. 17, 293–298.

Nir, Y., Tononi, G., 2010. Dreaming and the brain: from phenomenology to neurophysiology. Trends Cogn. Sci. 14, 88–100.

Noreika, V., 2015. It's not just about the contents: searching for a neural correlate of consciousness. In: Metzinger, T., Windt, J.M. (Eds.), Open Mind, pp. 1–12.doi: 10.15502/9783958570504.

Nuotto, E., 1983. Psychomotor, physiological and cognitive effects of scopolamine and ephedrine in healthy man. Eur. J. Clin. Pharmacol. 24, 603–609.

Ostfeld, A.M., Machne, X., Unna, K.R., 1960. The effects of atropine on the electroencephalogram and behavior in man. J. Pharmacol. Exp. Ther. 128, 265–272.

Pace-Schott, E., 2011. The neurobiology of dreaming. In: Kryger, M.H., Roth, T., Dement, W.C. (Eds.), Principles and Practices of Sleep Medicine. Elsevier-Saunders, Philadelphia, pp. 563–575.

Pal, D., Silverstein, B.H., Lee, H., Mashour, G.A., 2016. Neural correlates of wakefulness, sleep, and general anesthesia: an experimental study in rat. Anesthesiology 125, 929–942.

Perry, E.K., Perry, R.H., 1995. Acetylcholine and hallucinations: disease-related compared to drug-induced alterations in human consciousness. Brain Cogn. 28, 240–258.

Pomarol-Clotet, E., Honey, G.D., Murray, G.K., Corlett, P.R., Absalom, A.R., Lee, M., McKenna, P.J., Bullmore, E.T., Fletcher, P.C., 2006. Psychological effects of ketamine in healthy volunteers. Phenomenological study. Br. J. Psychiatry 189, 173–179.

Posner, J., Saper, C.B., Schiff, N.D., Plum, F., 2007. The Diagnosis of Stupor and Coma. Oxford University Press, New York.

Rechtschaffen, A., 1978. The single-mindedness and isolation of dreams. Sleep 1, 97–109.

Rinaldi, F., Himwich, H.E., 1955. Alerting responses and actions of atropine and cholinergic drugs. A.M.A. Arch. Neurol. Psychiatry 73, 387–395.

Sahakian, B., 1988. Cholinergic drugs and human cognitive performance. In: Handbook of Psychopharmcology, pp. 393–424. https://doi.org/10.1007/978-1-4613-0933-8_9.

Saper, C.B., Fuller, P.M., Pedersen, N.P., Lu, J., Scammell, T.E., 2010. Sleep state switching. Neuron 68, 1023–1042.

Scorza, M.C., Meikle, M.N., Hill, X.L., Richeri, A., Lorenzo, D., Artigas, F., 2008. Prefrontal cortex lesions cause only minor effects on the hyperlocomotion induced by MK-801 and its reversal by clozapine. Int. J. Neuropsychopharmacol. 11, 519–532.

Siclari, F., Baird, B., Perogamvros, L., Bernardi, G., LaRocque, J.J., Riedner, B., Boly, M., Postle, B.R., Tononi, G., 2017. The neural correlates of dreaming. Nat. Neurosci. 20, 872–878.

Siegel, J.M., 2011. REM sleep. In: Kryger, M.H., Roth, T., Dement, W.C. (Eds.), Principles and Practices of Sleep Medicine. Elsevier-Saunders, Philadelphia, pp. 92–111.

Singer, W., 1999. Neuronal synchrony: a versatile code for the definition of relations? Neuron 24, 49–65. 111–125.

Steriade, M., McCormick, D.A., Sejnowski, T.J., 1993. Thalamocortical oscillations in the sleeping and aroused brain. Science 262, 679–685.

Sun, Y., Farzan, F., Barr, M.S., Kirihara, K., Fitzgerald, P.B., Light, G.A., Daskalakis, Z.J., 2011. Gamma oscillations in schizophrenia: mechanisms and clinical significance. Brain Res. 1413, 98–114.

Tanaka, H., Hayashi, M., Hori, T., 1996. Statistical features of hypnagogic EEG measured by a new scoring system. Sleep 19, 731–738.

Tononi, G., 2010. Information integration: its relevance to brain function and consciousness. Arch. Ital. Biol. 148, 299–322.

Tononi, G., Laureys, S., 2009. The neurology of consciousness: an overview. In: Laureys, S., Tononi, G. (Eds.), The Neurology of Consciousness: Cognitive Neuroscience and Neuropathology. Elsevier, San Diego, pp. 375–412.

Torterolo, P., Vanini, G., 2010. New concepts in relation to generating and maintaining arousal. Rev. Neurol. 50, 747–758.

Torterolo, P., Lagos, P., Monti, J.M., 2011. Melanin-concentrating hormone (MCH): a new sleep factor? Front. Neurol. 2, 1–12.

Torterolo, P., Scorza, C., Lagos, P., Urbanavicius, J., Benedetto, L., Pascovich, C., Lopez-Hill, X., Chase, M.H., Monti, J.M., 2015. Melanin-concentrating hormone (MCH): role in REM sleep and depression. Front. Neurosci. 9, 475.

Torterolo, P., Castro-Zaballa, S., Cavelli, M., Chase, M.H., Falconi, A., 2016a. Neocortical 40 Hz oscillations during carbachol-induced rapid eye movement sleep and cataplexy. Eur. J. Neurosci. 43, 580–589.

Torterolo, P., Monti, J.M., Pandi-Perumal, S.R., 2016b. Neuroanatomy and neuropharmacology of sleep and wakefulness. In: Pandi-Perumal, S.R. (Ed.), Synopsis of Sleep Medicine. Apple Academic Press, Oakville, Canada.

Uhlhaas, P.J., Singer, W., 2010. Abnormal neural oscillations and synchrony in schizophrenia. Nat. Rev. Neurosci. 11, 100–113.

Uhlhaas, P.J., Pipa, G., Lima, B., Melloni, L., Neuenschwander, S., Nikolic, D., Singer, W., 2009. Neural synchrony in cortical networks: history, concept and current status. Front. Integr. Neurosci. 3, 17.

Vanini, G., Torterolo, P., Baghdoyan, H., Lydic, R., 2011. Effects of general anesthetics on sleep-wake centers. In: Mashour, G.A., Lydic, R. (Eds.), The Neuroscientific Foundations of Anesthesiology. Oxford University Press, Oxford.

Varela, F., Lachaux, J.P., Rodriguez, E., Martinerie, J., 2001. The brainweb: phase synchronization and large-scale integration. Nat. Rev. Neurosci. 2, 229–239.

Voss, U., Holzmann, R., Tuin, I., Hobson, J.A., 2009. Lucid dreaming: a state of consciousness with features of both waking and non-lucid dreaming. Sleep 32, 1191–1200.

Voss, U., Holzmann, R., Hobson, A., Paulus, W., Koppehele-Gossel, J., Klimke, A., Nitsche, M.A., 2014. Induction of self awareness in dreams through frontal low current stimulation of gamma activity. Nat. Neurosci. 17, 810–812.

Vyazovskiy, V.V., Olcese, U., Hanlon, E.C., Nir, Y., Cirelli, C., Tononi, G., 2011. Local sleep in awake rats. Nature 472, 443–447.

White, R.S., Siegel, S.J., 2016. Cellular and circuit models of increased resting-state network gamma activity in schizophrenia. Neuroscience 321, 66–76.

Wikler, A., 1952. Pharmacologic dissociation of behavior and EEG "sleep patterns" in dogs; morphine, n-allylnormorphine, and atropine. Proc. Soc. Exp. Biol. Med. 79, 261–265.

Williams, R.H., Chee, M.J., Kroeger, D., Ferrari, L.L., Maratos-Flier, E., Scammell, T.E., Arrigoni, E., 2014. Optogenetic-mediated release of histamine reveals distal and autoregulatory mechanisms for controlling arousal. J. Neurosci. 34, 6023–6029.

Yamamoto, J., 1988. Roles of cholinergic, dopaminergic, noradrenergic, serotonergic and GABAergic systems in changes of the EEG power spectra and behavioral states in rabbits. Jpn. J. Pharmacol. 47, 123–134.

Yates, C., Garcia-Rill, E., 2015. Descending projections of the RAS. In: Garcia-Rill, E. (Ed.), Waking and the Reticular Activating System in Health and Disease. Elsevier, London, pp. 129–156.

Yeragani, V.K., Cashmere, D., Miewald, J., Tancer, M., Keshavan, M.S., 2006. Decreased coherence in higher frequency ranges (beta and gamma) between central and frontal EEG in patients with schizophrenia: a preliminary report. Psychiatry Res. 141, 53–60.